Hybrid-state Driven Autonomous Control for Planar Bipedal Locomotion

A thesis submitted

in partial fulfilment for the award of the degree of

Doctor of Philosophy

by

Sam K. Zachariah

Department of Avionics

Indian Institute of Space Science and Technology

Thiruvananthapuram, India

1st March 2019

Certificate

This is to certify that the thesis titled **Hybrid-state Driven Autonomous Control for Planar Bipedal Locomotion** submitted by **Sam K. Zachariah**, to the Indian Institute of Space Science and Technology, Thiruvananthapuram, in partial fulfilment for the award of the degree of **Doctor of Philosophy**, is a *bona fide* record of the original research work carried out by him under my supervision. The contents of this report, in full or in parts, have not been submitted to any other Institute or University for the award of any degree or diploma.

Dr. Thomas Kurian
Supervisor
Former Dean, R & D, IIST

Prof. B.S. Manoj
Head
Department of Avionics, IIST

Place: Thiruvananthapuram
Date: 1st March 2019

Declaration

I declare that this thesis titled **Hybrid-state Driven Autonomous Control for Planar Bipedal Locomotion** submitted in partial fulfilment for the award of the degree of **Doctor of Philosophy** is a record of original research work carried out by me under the supervision of **Dr. Thomas Kurian** and has not formed the basis for the award of any degree, diploma, associateship, fellowship, or other titles in this or any other Institution or University of higher learning. In keeping with the ethical practice in reporting scientific information, due acknowledgements have been made wherever the findings of others have been cited.

Place: Thiruvananthapuram
Date: 1st March 2019

Sam K. Zachariah
(SC09D001)

Acknowledgements

First of all, I would like to express my sincere gratitude to my research supervisor, Dr. Thomas Kurian for his continuous support and providing me the right balance of autonomy and supervision. Besides my supervisor, I would like to thank the rest of my doctoral committee members: Prof. Ravi N. Banavar, Prof. K. Kurien Issac, Prof. B. S. Manoj, Dr. S. Dasgupta , Dr. N. Selvaganesan, and Dr. Priyadarshnam H. for their insightful comments and encouragement. I am much indebted to Dr. B. N. Suresh, the founder Director and Chancellor of IIST and Dr. K. Radhakrishnan, former Chairman, ISRO who have been the main source of inspiration for taking up the Doctoral research work. I am also indebted to Dr. K. S. Dasgupta, the former Director and Dr. V. K. Dadhwal, the current Director of IIST for all their encouragement and advices during the research work.

I would like to express my sincere thanks to Prof. Karsten Berns, Chief Editor, Robotics and Autonomous Systems, Elsevier for providing all the necessary technical support for publishing two of my technical articles and to the anonymous reviewers for their constructive criticisms and valuable suggestions. I gratefully acknowledge the examiners of my thesis, Dr Harish K. Pillai, IIT Bombay and Dr. Prahlad Vadakkepat, NUS, Singapore for their valuable comments and suggestions. I thank my colleagues Dr. R. V. Ramanan, Dr. Anup S., Dr. Shine S. R. and Dr. Deepu M. from the Department of Aerospace Engineering for the stimulating discussions and advices. I also thank Prof. Raju K. George, Dean (R & D) and Prof. A. Chandrasekar, & Dean (Academic) for all the institutional support for completing the doctoral research work.

I gratefully acknowledge Mr. Sarath Babu, Ph D. scholar for helping me by generating the necessary thesis templates in LaTeX. I do appreciate my UG students, Mr. Amir Iqbal and Mr. Jayakrishnan from the Department of Aerospace Engineering for generating the CAD model for the biped. Finally, my deepest gratitude for my wife, Mahima and for my children, Sneha and Sandeep and for my parents for supporting me physically, mentally and spiritually throughout the period of my doctoral research.

1st March 2019 Sam K. Zachariah

Abstract

The bipedal locomotion control is identified as a challenging problem by the control community due to its multiphase, hybrid nature and the unilateral characteristics of ground contact forces. The underactuation during heel and toe centred rolling motions and the intermittent ground impacts introduce additional complexity. The focus of this doctoral research is on the development of an autonomous control framework for a planar bipedal robot to realize human-like walking projected onto sagittal plane. In addition, a unified modelling scheme is proposed for the biped dynamics incorporating the effects of various locomotion constraints due to recurrent feet-ground contact states, unilateral ground contact force, contact friction cone, joint torque limit and due to the passive dynamics associated with floating base. The autonomous control synthesis is formulated as a two-level hierarchical control algorithm with a hybrid-state based supervisory control in outer level and an integrated set of constrained motion control primitives, called task level control, in inner level. The supervisory level control is designed based on a human inspired heuristic approach whereas the task level control is formulated as a quadratic optimization problem with linear constraints. The explicit analytic solution obtained in terms of joint acceleration and ground contact force is used in turn to generate the joint torque command based on inverse dynamics model of the biped. The proposed controller framework is named as *Hybrid-state Driven Autonomous Control (HyDAC)*. Unlike many other bipedal control schemes, HyDAC does not require any preplanned trajectory or orbit in terms of joint variables for locomotion control. Moreover, it is built upon a set of basic motion control primitives similar to those in human walk which provides a transparent and easily adaptable structure for the controller.

A control oriented stability theorem, called *Contraction stability theorem*, based on Lyapunov, Poincaré and contraction mapping theorems, is proposed to analyse the stability of bipedal walk in realistic situations. This provides two stability measures, namely, the *contraction factor* and the *radius of convergence* to quantitatively represent the stability margins applicable for both periodic gait over uniform terrain as well as for non-periodic gait over uneven terrain. The multi-phase goal seeking concept of HyDAC is justified on the basis of contraction stability theorem.

HyDAC is further extended to dynamic walking situation over ascending and descending stairs with non-uniform tread depth and riser height and having arbitrary, but bounded

distribution of tread slope. Dynamic walking over non-uniform stairs requires to control the swing foot placement at predetermined feasible foothold on each toe-impact event in addition to forward velocity regulation. HyDAC law is modified in both task level and supervisory level to meet these demands. A novel scheme for forward velocity control by direct regulation of the centre of pressure due to ground contact forces is also developed as a part of HyDAC.

The stability and agility of HyDAC for uniform terrain locomotion are demonstrated through dynamic model simulation of a 12-link planar biped having similar size and mass properties of an adult sized human projected onto sagittal plane. Simulation results show that the planar biped is able to walk for a speed range of 0.1 m/s to 2 m/s on level terrain and for a ground slope range of +/- 20 deg for 1 m/s speed. Similarly, the performance of the control algorithm for stair-walk is demonstrated for a forward velocity range of 0.1 m/s to 0.75 m/s over ascending and descending stairs with tread depth of $1.5L_f$ to $2.5L_f$, riser height up to $2L_f$ and tread slope within ± 15 deg, for a planar biped with foot-sole span of $L_f = 0.2$ m, nominal hip height of $h_{hip} = 0.98$ m, and nominal centre of mass height of, $h_{com} = 1.13$ m. Cases with wide range of torso mass perturbation, external force disturbance and with random perturbation of terrain height, slope and stair-parameters have been considered for both the cases of simulation. The simulation results demonstrate the performance robustness and postural reflex behaviour of HyDAC which are essential for unplanned realistic walking situations with unexpected environmental disturbances. The stability margins for uniform terrain walk as well as for stair-walk are analysed based on the proposed contraction stability theorem.

Thus the thesis brings out solutions for many open problems in bipedal walking with respect to modelling, online control design and postural stability analysis, all applicable in realistic walking situations. The superiority of HyDAC over current design methodologies such as Zero Moment Point (ZMP), Hybrid Zero Dynamics (HZD) etc. are also brought out in the thesis. The recommended directions for future research to extend HyDAC towards realization of human like 3D bipedal locomotion are discussed at the end.

Contents

List of Figures

List of Tables

List of Algorithms

Abbreviations

CCW	Counter clockwise
$\mathcal{CDR}$	Control design requirement
$\mathcal{CFR}$	Control functional requirement
CoM	Centre of mass
CoP	Centre of pressure
DoF	Degree of freedom
EPS	Event periodic stability
FF	Flat foot
FVCA	Forward velocity control algorithm
GCC	Ground clearance control
GC	Gait Cycle
GCoM	Ground projection of CoM
GCoP	Ground projection of centre of pressure
HR	Heel roll
HRRC	Heel roll reset control
HyDAC	Hybrid-state driven autonomous control
HZD	Hybrid zero dynamics
IPG	Impact posture goal
MI	Moment of inertia
NJC	Neck joint control
PD	Proportional plus Derivative
RKJC	Reference knee joint control
RFSC	Reference leg floating state control
SLC	Supervisory level control
SVD	Singular value decomposition
SW	Swing
THFP	Transit heel forward positioning

TFO	Transit foot orientation
TKJC	Transit knee joint control
TLC	Task level control
TFSC	Transit leg floating state control
TOCP	Torso orientation control primitive
TR	Toe roll
TRRC	Toe roll reset control
TTOC	Transit thigh orientation control
ULC	Upper limb control
ZMP	Zero moment point

Nomenclature

C	Coriolis and Centrifugal force coefficient matrix
D	Joint space inertia matrix
D_p	Rows of D matrix corresponding to the passive joints
$\mathbb{D}_{es}$	Discrete event state corresponding to binary vector, π_m or π_c
F_c	Ground contact force vector expressed in $\{O_0\}$
F_g	Ground contact force vector expressed in $\{O_g\}$
G	Gravitational force vector expressed in generalized coordinate frame
g	Acceleration due to gravity
$\mathcal{G}$	Combined Coriolis, Centrifugal and Gravitational force vector
$\mathcal{G}_p$	Rows of $\mathcal{G}$ corresponding to the passive joints
H_{c_n}	Stacked Jacobian matrix corresponding to the set of all nonholonomic constraints
H_{c_h}	Stacked Jacobian matrix corresponding to the set of all holonomic constraints
H_{t_l}	Stacked Jacobian matrix corresponding to the set of all locomotion tasks
h_{com}	Height of biped-CoM in nominal straight knee stance posture
h_{hip}	Height of biped's hip joint in nominal straight knee stance posture
$\mathbb{H}_{es}$	Hybrid event state
J_c	Feet-ground contact Jacobian w.r.t. translational motion
J_{cp}	Columns of J_c matrix corresponding to the passive joints
J_g	Feet-ground contact Jacobian expressed w.r.t $\{O_g\}$
J_{hip}	Jacobian of hip joint expressed in $\{O_0\}$ frame
K_p	Task loop position error gain
K_v	Task loop velocity error gain
L_f	Length of foot sole
M_{bp}	Total mass of biped links
N_{stp}	Step index starting from 1

$\mathcal{N}_\epsilon(\mathbf{y})$	ϵ- neighbourhood of $\mathbf{y}$
n_c	Number of foot tips in ground contact state
n_C	Total rank of active constraints
n_{C_h}	Total rank of all holonomic type of constraints
n_{C_n}	Total rank of all nonholonomic type of constraints
n_J	Number of joints for planar biped including passive DoF at the floating base
$\{O_0\}$	Right handed inertial frame of reference fixed to the ground at the starting location and is also represented as $O_0X_0Y_0Z_0$.
$\{O_g\}$	Right handed coordinate frame attached to any foot-ground contact point with $\overrightarrow{O_gX_g}$ tangential to the ground
$\mathcal{P}(.)$	Poincaré return map
$\mathcal{P}'(.)$	Freché t derivative of $\mathcal{P}(.)$
q	Generalized position vector
q_{kr}	Regulation goal for reference foot knee joint angle
q_{kt}	Regulation goal for transit foot knee joint angle
q_{To}	Regulation goal for transit thigh joint angle
R_g	2D rotation matrix from $\{O_0\}$ frame to $\{O_g\}$ frame
$\mathcal{R}_C$	Radius of convergence
stp_{ij}	j^{th} step of i^{th} flight of stairs
$\mathcal{S}_{ei}$	i^{th} ground envelope segment over stair- steps
$\mathcal{S}_{SP}$	Strictly proper switching set
$\bar{\mathcal{S}}_{SP}$	Closure of $\mathcal{S}_{SP}$
$\mathring{\mathcal{S}}_{SP}$	Interior of $\mathcal{S}_{SP}$
$\partial\mathcal{S}_{SP}$	Boundary set of $\mathcal{S}_{SP}$
V_{fc}	Forward velocity command for biped with direction parallel to ground plane
V_{comx}	Centroidal velocity of biped along $\overrightarrow{O_0X_0}$
(x_g, y_g)	Coordinates of a point on ground expressed w.r.t ground fixed inertial frame, $\{O_gX_gY_gZ_g\}$
$\mathbf{x}$	State vector of biped given by $[q'\ \dot{q}']'$
$\mathbf{x}_P$	Postural state vector of biped with dimension $2n_P$
$\mathbf{x}_{Pc}$	Postural configuration state vector of biped with dimension n_P
$\mathbf{x}_P^o$	Goal point for $\mathbf{x}_P$ on transit foot ground impact
(x_G, y_G)	Coordinates of a point on ground expressed w.r.t reference inertial frame, $\{O_0X_0Y_0Z_0\}$
(x_{com}, y_{com})	Coordinates of biped-CoM expressed w.r.t, $\{O_0\}$

(x_{tc}, y_{tc})	Coordinates of a transit foot's sole centre expressed w.r.t, $\{O_0\}$
y_{G0}	Intercept of extended ground line with $\overrightarrow{O_0Y_0}$ axis
Γ, Γ_d	Generalized force vector acting at biped joints and the corresponding command
γ	Angle of foot triangle at toe vertex
$\Delta(.)$	Impact reset map operating on **x**
$\Delta^i(q)$	Impact map operator on **x**
$\Delta^i_{th}(q)$	$\Delta^i(q)$ for transit foot heel impact
$\Delta^i_{rt}(q)$	$\Delta^i(q)$ for reference foot toe impact
$\Delta^R(.)$	Half cycle index reset map operating on **x**
θ_{tor}	Inertial orientation of torso link
θ_{dna}	Orientation of dynamic neutral axis in inertial frame
κ	Normalized weight of biped w.r.t an adult's weight on earth given by $M_{bp}g/(830)$
μ_c	Dry friction parameter of foot-ground contact model
π_m	Physical feet-ground contact state vector
π_c	Active feet-ground contact state vector defined for control
ρ_c	Contraction factor for asymptotic convergence
ρ_C	Contraction factor for truncated convergence
ρ_{gc}	Clearance between transit foot bottom and ground
σ_G	Ground slope measured w.r.t. $\overrightarrow{O_0X_0}$ axis
σ_{Gd}	Effective ground slope including terrain step discontinuity measured w.r.t. $\overrightarrow{O_0X_0}$ axis
σ_{ge_i}	Slope of i^{th} ground envelope segment measured w.r.t. $\overrightarrow{O_0X_0}$ axis
$\rho_{ij}, \tau_{ij}, \& \sigma_{ij}$	Riser height, Tread depth and Slope of j^{th} step of i^{th} flight of stairs

Chapter 1
Background and Motivation

1.1 Introduction

Wheeled locomotion is unambigously the most efficient means of mobility over land mass. The distinct advantages of wheeled locomotion are minimum friction loss, no vertical motion during forward motion over level ground and no impact loss due to any intermittent ground contacts. However, its basic requirement is that the terrain should be continuous and smooth enough without obstacles so that wheels can easily roll over them. However, the majority of earth's land mass are not paved enough to suit for wheeled or tracked vehicles and legged locomotion like in animals is the easiest means for mobility under such situations. Legs provide better mobility than wheels over unprepared terrain as they can use isolated footholds to optimize support and traction whereas wheels requires continuous path of support [1]. Another advantage is that legs provide active suspension that isolate the body from the unevenness of the terrain. Further, relative to other mammals, humans are economical walkers, in terms of energetic efficiency [2] and reported to be more efficient than knuckle-walking or quadrupedalism [3]. Apart from its energetic efficiency, bipedalism also has the advantages of raising the head, and therefore allowing a wider range of vision in a grassland environment, and of freeing the hands for carrying items or for tool use. Hence from an architecture point of view, bipedal configuration with human-like walking philosophy is the best-suited for an autonomous robot for exploratory and rescue operations where a human cannot have direct access as in planetary surfaces and hazardous environments.

Apart from these benefits of bipedal locomotion, there are other reasons which makes the field so important. The basic understanding of the underlying biomechanical control of bipedal locomotion is of paramount importance for developing rehabilitation devices

and for diagnosing the root cause for many ambulatory disabilities. The understanding of biomechanical postural control will help in developing smart prosthetic limbs which can perform the same ambulatory tasks as the healthy parts. Another is the application in exoskeleton devices to enhance the capacity of an able bodied person or for assisting a weak bodied person.

1.2 Motivation and Research focus

The fascinating complexity and autonomous dynamicity of the nature have ignited and challenged intuitive minds across the generations to arrive at a consistent set of rules which may lay a unified foundation for its origin and survival. Out of the fascinating features, the most fundamental characteristics of Universe is its cyclic attribute [4]. The cyclic nature of Universe has been manifested right from the wave nature of its minutest particle to the cyclic motion of huge galactic systems. On the other side, the living world is sustained and multiplied by its periodic behaviour starting from the self-replicating cycle of its smallest building block, the living cell, to the biogeochemical cycles of the entire biosphere. The face of earth is renewed by the repetitive behaviour of its meteorological cycle. The animal world moves over one or another sort of recurring actuation mechanism for its forward locomotion. Hence, modelling of the cyclic phenomena is of paramount importance for understanding the systematic self organizing characteristics of the Nature and the Universe. The basic characteristic feature behind all the above mentioned natural phenomena is that, what we observe externally are the state trajectories in terms of either energy flow or mass flow emerging out of interacting multiple behaviours. Most often, a complex dynamical system is made up of multiple dynamical behaviour primitives, temporally distributed in a cyclic manner, with each behaviour activated or deactivated based on certain events such as observed in replication cycle of living cell [5]. The events are defined either based on certain thresholds with respect to state trajectories like neuron firing in brain or based on the interaction of systems states with the constraining environments of the system like recurring ground impacts in legged animal locomotion. Intuitively, such natural phenomena can be classified as an *Event driven cyclic process*. An event represents the discrete transition from one phase of the system to another phase whereas phase represents the period for which the system dynamics remain the same. The importance of cyclic process for explaining the philosophy behind complex dynamical systems has been gaining lot of attention recently [5].

The bipedal locomotion, being one of the most complex cyclic biomechanical processes

of the living world, can also be visualized as an event driven cyclic process. Initially, to start with forward acceleration from rest, the torso of the biped is inertially stabilized along an optimal orientation on single foot by the dynamically coordinated behaviour modes of support foot in a bottom-up or ascending fashion and the swing foot is commanded to ensure a stable support for the next gait. Having regulated the orientation and forward velocity to establish itself as a virtually extended inertial base from ground, the torso delivers commands[1] [6] to the swing foot in top-down or descending fashion to ensure the same status in the next walking step to repeat the entire sequence of operations as in the current step. A higher level supervisory controller, located either centrally or in distributed manner, is essential to sustain this locomotion cycle by dynamically coordinating the motion behaviours of support foot, torso along with upper body parts and swing foot. Different types of supervisory controllers will of course result in different patterns of locomotion. This has been the motivation behind the exploration of a novel hybrid-state driven autonomous cyclic control framework for capturing the essence of bipedal locomotion.

1.2.1 Research focus

The focus of the research is on the development of an autonomous control framework for a planar bipedal robot to realize human-like walking projected onto sagittal plane. The forward dynamic walking of a bipedal robot is the result of coordinated control of coupled motion dynamics belonging to three orthogonal planes, namely sagittal, frontal and transverse planes. Out of these planes, continuous forward motion takes place only in the sagittal plane requiring more attention with respect to controlled behaviours. Hence the current research concentrates only on the locomotion control restricted to sagittal plane.

1.3 Thesis Overview

The structure of the thesis for the rest of the chapters is given below.

Chapter 2 provides review of literature related to basic definitions in bipedal locomotion and review of control and stability concepts for bipedal locomotion. The deficiency of the current control schemes are clearly brought out and the need for a multi-phase autonomous control framework is projected. Finally the objectives of the present doctoral research work are provided.

Chapter 3 gives the details of the proposed unified mathematical model of planar biped.

[1]The actual computation of command can be somewhere else, but the kinetic base rests on the upper body.

The biped is modelled as a hybrid dynamical system by defining the relevant discrete event states and continuous system event states. A realistic assumption that simplifies the velocity impact map is brought out. The unified model provides a common mathematical framework to represent various locomotion related tasks, holonomic and nonholonomic constraints, all with respect to the generalized joint acceleration vector. The details of the simulation model of planar biped used for numerical study are also provided at the end of Chapter 3.

Chapter 4 provides the major contribution of the thesis, which includes the development of HyDAC for uniform terrain locomotion and the development of relevant stability theory. The justification for the structure of HyDAC in terms of its hierarchical levels are brought out in comparison with the biological counterparts. The concept of postural configuration space is introduced for developing the stability theory and locomotion control algorithm. The classical stability theorems are reviewed in the context of periodic dynamical systems and proposed a new stability theorem called, contraction stability theorem for realistic walking situations. The development of a novel control algorithm for the online regulation of biped-CoM[2] velocity is another topic of discussion. Finally, HyDAC synthesis is formulated as a quadratic optimization problem with linear equality constraints.

Chapter 5 provides the formal mathematical definition of locomotion behaviour primitives required for planar bipedal locomotion over uniform terrain. This is followed by extensive simulation studies to validate the control algorithm for wide range of forward velocities and terrain slopes.

Chapter 6 provides the extension of HyDAC for dynamic walking over non-uniform staircase by relevant modifications in both hierarchical levels of HyDAC. Detailed simulation results are provided to demonstrate the agility and robustness of Stair-HyDAC.

Chapter7 provides the inferences of the research, list of contributions of the thesis and the recommendations for future research.

Finally, the list of publications out of the current research, bibliography and the appendices are provided at the end of the thesis. The real time animation of all the simulation results reported in the thesis are provided at the video links given in Appendix B.

[2]biped-CoM refers to the centre of mass of biped.

Chapter 2

Review of Literature and Research objectives

2.1 Introduction

The quest for understanding the science behind stable human locomotion has been active ever since the time of the ancient Greek philosopher Aristotle [7]. Active research in bipedal locomotion control started with the pioneering work of Vukobratovic in the late 1960's [8, 9]. A summary of the research work happened during the last fifty years with respect to the development of various hardware prototypes and control algorithm are given by Westervelt et al. [10] and hence not repeated here. However, the current chapter provides a brief summary of the major control approaches reported in the literature for bipedal locomotion and emphasizes the need for a multiphase autonomous control framework for realistic situations of bipedal walk. Finally, the objectives of the current research work are highlighted. Prior to these, a list of basic terms relevant to bipedal locomotion and their definitions are provided.

2.2 Basic definitions in Bipedal locomotion

Since the focus of the current research is on developing human-like locomotion, various terms associated with bipedal locomotion are defined as per the standard definition of human locomotion gait available in the literature of human biomechanics [11, 12]. The definitions of various terms are given below.

2.2.1 Human locomotion gait

The gait in a legged locomotion is defined as the process of loading and unloading weight in the legs during the act of motion. The period of time starting from one event of a specific foot to the subsequent occurrence of the same event with the same foot is known as gait cycle (GC). The reference planes of the human body in the standard anatomical position is shown in Fig 2.1 and are defined as follows:

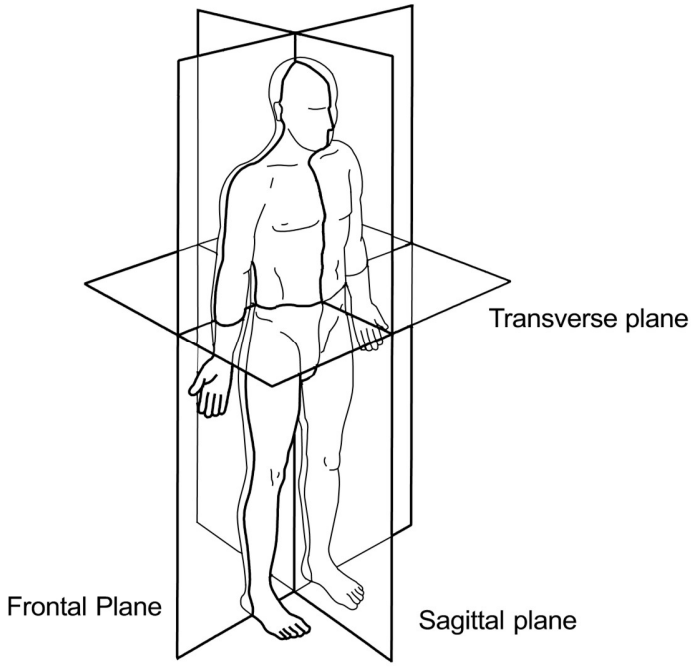

7

Figure 2.1: The reference planes of the human body in the standard anatomical position (Taken from Fig 2.1 of [11])

Frontal or Coronal plane: The plane that divides the body or body segment into anterior or ventral (front) and posterior or dorsal (back) parts.

Sagittal plane: The plane that divides the body or body segment into the right and left parts.

Transverse plane: The plane that divides the body or body segment into superior or cranial (head) and inferior or caudal (feet) parts.

The basic gait parameters are shown in Fig 2.2 with respect to the footprint of a normal person and can be defined as,

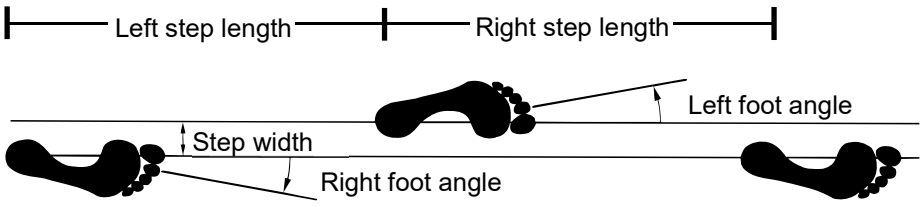

Figure 2.2: Gait parameters defined with respect to a person's footprint (Taken from Fig 2.8 of [11])

Stride length: The distance from initial contact of one foot to the following initial contact of the same foot. Sometimes referred to as cycle length, expressed in meters (m).

Step length: The distance from a point of contact with the ground of one foot to the following occurrence of the same point of contact with the other foot. The right step length is the distance from the left heel to the right heel when both feet are in contact with the ground, expressed in meters (m).

Walking base (or stride width): The side-to-side distance between the feet, which is typically measured from the ankle joint center.

The normal gait cycle of human walk can be divided into multiple phases as shown in Fig 2.3. Based on the standard definition released by North American Society for Gait and Human Movement 1993 and AAOP Gait Society 1994, the human gait can be partitioned into the following phases: [12]. The percentages given apply to the normal gait of a healthy person.

Stance phase: The period of time when the foot is in contact with the ground. Approximately 62% of the GC.

Swing phase (SW): The period of time when the foot is not in contact with the ground and is approximately 39% of GC.

Double support: The period of time when both feet are in contact with the ground. This occurs twice in the gait cycle, at the beginning and end of stance phase.

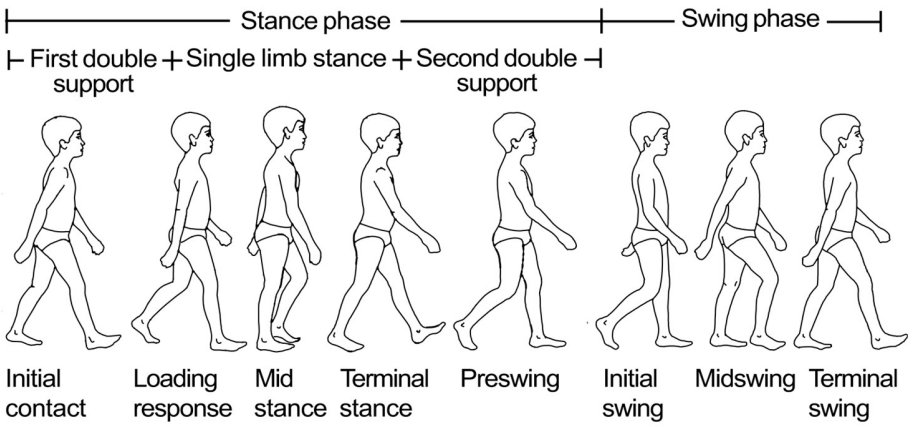

Figure 2.3: The normal gait cycle of an 8-year old boy (Taken from Fig 2.5 of [11]) Definitions given at the bottom apply to the right leg of boy

Single support: The period of time when only one foot is in contact with the ground. In walking, this is equal to the swing phase of the other limb.

Terminal contact: The point in the gait cycle when the foot leaves the ground and this represents the end of the stance phase or the beginning of swing phase. Terminal contact is also referred to as foot-off. The termination of stance and the onset of swing is defined as the point where all portions of the foot have achieved motion relative to the floor. Likewise, the termination of swing and the onset of stance may be defined as the point when the foot ends motion relative to the floor.

Toe-off: When terminal contact is made with the toe.

Foot-flat (FF): The point in time in stance phase when the foot is plantar grade.

Heel-off: The point in time in stance phase when the heel leaves the ground.

Apart from this partitioning, the gait cycle may be further divided into specific sub phases related to normal function; loading response, mid stance, terminal stance, pre-swing, initial swing, mid swing and terminal swing . This terminology is very useful for referring to specific portions of the gait cycle when describing pathological gait. The cyclic perception of human gait provided by Christopher L. Vaughan et al. [11] as given in Fig 2.4 has been one of the most important inspiration for the current research work.

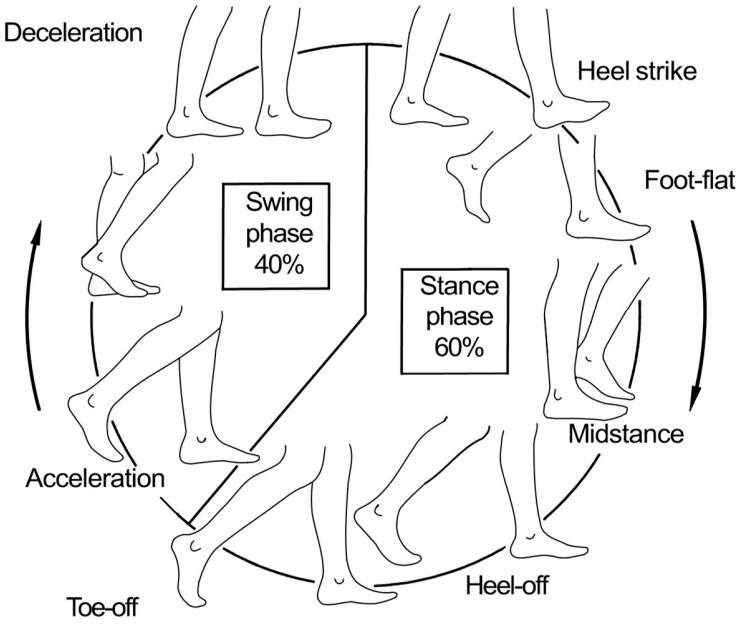

Figure 2.4: Basic event phases of human walking gait percieved as a cyclic process (Taken from Fig 2.7 of [11])

2.2.2 Planar bipedal gait

Out of the three planes associated with human locomotion, the continuous forward motion occurs only in sagittal plane. Even though, it is not possible to decouple the 3D locomotion dynamics into individual planes, the control concept for bipedal locomotion can be developed with respect to the sagittal plane as a starting point. If the control algorithm is generic enough, it can be extended to 3D-locomotion control without changing the overall control philosophy. Hence the work presented in this thesis focus only on the planar bipedal locomotion restricted to sagittal plane. All the definitions and terminologies of human gait given above hold good with respect to planar bipedal locomotion, except the step width and foot angle. Moreover, based on the joint mechanism and the associated actuation schemes, one can select different locomotion patterns without strictly following the human gait pattern.

2.3 Review of Control and Stability concepts for Bipedal locomotion

The bipedal locomotion control is identified as a challenging problem by the control community due to its multiphase, hybrid nature and the unilateral characteristics of ground contact forces. The underactuation during heel or toe centred rolling motion and the intermittent ground impacts introduce additional complexity. An underactuated robot is the one having fewer independent actuators than the total DoF for movement. The essence of bipedal walking control is to sustain near-periodic gaits with certain desired postural pattern while the biped is steered forward with the specified velocity over a fairly known terrain. There are basically four approaches reported in the literature for the design of bipedal locomotion control, viz. zero moment point (ZMP) based control methods, passive dynamic walking approach with minimal control, analytical approach based on hybrid zero dynamics (HZD), and heuristic control methods. A brief description of each of these approaches are given below.

2.3.1 Zero moment point based control

The most popular approach of bipedal control in the literature is known as *Zero Moment Point (ZMP)*[1] concept, proposed in the late 1960's by Vukobratovic et al. [8, 9]. It states that as long as the ZMP of a biped stays within the foot support polygon, the biped cannot fall by tipping over the edges of its feet. ZMP concept was later extended by A. Goswami by introducing Foot Rotation Indicator (FRI) point useful for quantifying the instability associated with foot rotation about stance toe [13]. Different variants of ZMP based controls were used in many practical humanoids such as ASIMO, WABIAN-2, LOLA, ATLAS etc. [14, 15, 16, 17]. However, it has been proved that ZMP criterion as such is neither necessary nor sufficient for bipedal gait stability [10, 18] and it leads to inefficient bent-knee type locomotion. However it can be considered as a sufficient condition for stability when used along with stiff trajectory tracking controllers for internal joint coordination [19]. The distance from the ZMP to the edge of the support polygon can be used as a measure of robustness.

The philosophy of an ZMP based bipedal walking controller can be represented as in Fig 2.5 [20]. The first step of the control scheme is to generate a sequence of footstep

[1]ZMP is the same as the centre of pressure at the foot-ground interface denoted by GCoP as long as the latter remains within the foot support polygon without reaching the boundary.

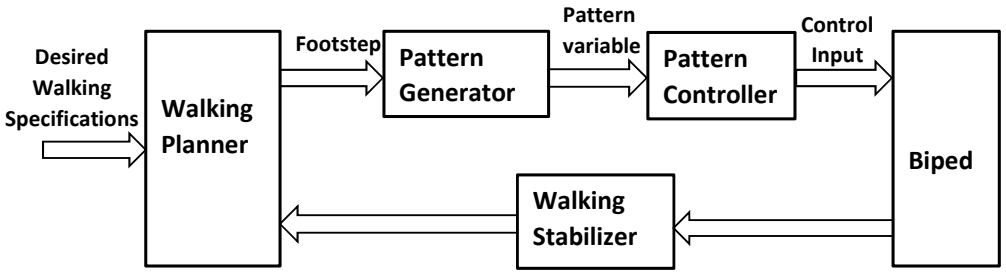

Figure 2.5: Generic scheme for ZMP based bipedal walking (Adapted from Fig.1 of [20])

locations as a part of walking planner for the specified walking speed, direction and terrain details. This is followed by generation of the desired walking pattern in terms of the pattern variables such as biped-CoM, centroidal angular momentum etc.[21, 22] consistent with the constraint that the trajectory of ZMP remains within the sequence of foot support polygons associated with the planned footsteps. The pattern controller generates the torque command for the joint drives to realize the desired walking pattern, thus derived. The ZMP preview controller [23, 20] has the additional features of planning or changing the walking pattern at least two footsteps in advance along with provision to modify ZMP position as well as foot steps to stabilize walking against the pattern tracking error, ZMP tracking error and/or walking error. Computationally efficient algorithms for the generation of ZMP and CoM trajectories developed for ATLAS and LOLA bipeds are given in [16] and [17].

2.3.2 Control based on passive dynamic walking

The second approach known as passive dynamic walking was developed by Tad McGeer in the late 1980's [24]. Unlike traditional robots, which expend energy for controlled actuation by using motors, McGeer showed that a human-like frame can walk itself down a slope without requiring powered joints. McGeer's initial configuration for passive dynamic walker relies only on the natural swinging of the limbs under gravity to move forward down a slope. Later, Steven H. Collins and his associates have demonstrated a 3D passive dynamic walker with two legs and knees by extending the concept of McGeer [24]. Extensions to passive dynamic walker have been made later on by adding minimal actuation to the joints [25, 26, 27]. Strategies for stabilizing roll motion in passive 3D walkers are

discussed in [28]. Even though passive dynamics based control approach leads to energetically efficient gaits, it lacks robustness in the presence of large disturbances [18] and control will become quite complex for real humanoids with multiple joints.

2.3.3 Hybrid zero dynamics based control

Hybrid zero dynamics (HZD) control is a rigorous analytical control approach for dynamic bipedal locomotion [29, 10, 30] based on the full order mathematical model of biped. HZD control generates a provably stable orbit for the bipedal gait prior to the current walking step followed by closed loop implementation of the same through stiff path following control [10]. The admissible gait is defined by a viable set of virtual constraints to be designed prior to each walking step using nonlinear optimizers. Each virtual constraint imposes a kinematic or holonomic relation between joint variables, q (and hence between $\dot{q}$) through the action of actuators and feedback control instead of physical contact force. Hence there can be a maximum number of virtual constraints equal to the number of actuators. If the total number virtual constraints is n_C and the joint DoF during the current ground contact state is n_J, then the joint variable, $q \in \mathcal{Q} \subset \mathbb{R}^{n_J}$ can be partitioned into a set of constrained variable, $q_c \in \mathcal{Q}_c \subset \mathbb{R}^{n_C}$ and free variable, $q_f \in \mathcal{Q}_f \subset \mathbb{R}^{n_J - n_C}$. The virtual constraints are expressed in the holonomic form,

$$y(q) = q_c - h_d(q_f) = 0 \in \mathbb{R}^{n_C} \tag{2.1}$$

which will constrain the bipedal state variable, $\mathbf{x} = (q, \dot{q})$ along a low dimensional invariant manifold, $\mathcal{Z}$. As the output function, $y(q)$ is constrained to be zero for any path of $\mathbf{x}$ $(q_f) \in \mathcal{Z}$, the constrained domain is known as zero dynamics manifold and has a dimension of $2n_f = 2(n_J - n_C)$. As the joint velocity variable, $\dot{q}$ undergoes discrete transition at the end of every walking step on swing foot impact, it is necessary to incorporate the effect of impact map also in the zero dynamics manifold. The zero dynamics manifold which is invariant under transit foot impact is called, hybrid zero dynamics manifold. Thus any path of $\mathbf{x}$ belonging to $\mathcal{Z}$ is both forward invariant and impact invariant. The virtual constraints effectively reduces the dimension of joint variables from n_J to n_f. HZD control was originally developed for a planar biped with point foot with q_f representing the passive joint rotation about the point foot [10]. Later, it has been extended to planar biped with actuated ankle by incorporating direct regulation of ZMP point [31, 32]. In this case, q_f is related to the unactuated rotation about ZMP during flat-foot (FF) phase or passive rotation about toe joint during toe-roll (TR) phase.

The HZD manifold does not specify any trajectory for $\mathbf{x}$ as a function of time, instead the required path for $\mathbf{x}$ is specified as a function of the unactuated free variable, q_f. As q_f builds up as a function of time under the influence of gravity, the joint variables q_c are virtually constrained to move along the internally coordinated path belonging to HZD manifold. To make the computation easier, the desired orbit belonging to HZD manifold as well as the HZD controller are parameterized by the coefficients of Bé zier polynomial, α. The HZD control synthesis is posed as an optimization problem with an objective to minimize the energy function of control signal subject to various constraints such as unilateral and friction cone constraints on ground contact forces, actuator torque and deflection limits and the periodic stability of the orbit in Poincaré sense. The solution of a priori optimization provides the parameters of the HZD controller as a function of optimized Bé zier polynomial coefficients, α^*.

There are two terms for HZD control torque command expressed as, $u = u^*(q, \dot{q}, \ddot{q}^d) + u_\epsilon(q, \dot{q})$. The first part, u^* is the computed torque command responsible for steering $\mathbf{x}$ along the asymptotically stable periodic orbit belonging to HZD manifold in the forward direction based on the desired reference acceleration, $\ddot{q} = \ddot{q}^d(q_f, \dot{q}_f, \ddot{q}_f)$ establishing the required internal coordination.[2] The second part, u_ϵ is the control torque responsible for inducing a stable transverse dynamics for the path, $\mathbf{x}(q_f) \in \mathcal{Z}$ to ensure rapidly exponential stabilization of any local perturbation from the periodic orbit within a finite settling time much smaller than the gait period [33].

The strong point of HZD control approach is that it provides a provably stable orbit for bipedal gait which can be shaped a priori to suit for different types of walking patterns [34] as well as for different walking situations [35, 36, 37]. However, it has certain limitations when applied to realistic walking situations. Firstly, HZD control is mathematically rigorous, and computationally intensive. The formulation of the orbit-control optimization problem with all the associated holonomic and nonholonomic constraints makes the solution for u^* quite hard to obtain. Moreover, multiple local minima exist due to the non-convexity of formulation. Secondly, there is no guarantee for the perturbation control part, u_ϵ to be consistent with physical constraints such as unilateral and friction cone unless specifically accounted during gait optimization for certain expected worst case situation [38]. Even though the periodic stability of the target orbit belonging to HZD manifold is ensured by Poincaré return map, there is no estimate for its region of attraction. In particular, the mod-

[2] $\ddot{q}^d(q_f, \dot{q}_f, \ddot{q}_f)$ is obtained by double differentiation of the virtual holonomic constraint given by (2.1) which specifies the forward traversal of q as a function of the free underactuated variable q_f in acceleration form so as to derive the computed torque command for the current biped state, $(q, \dot{q})$.

elling uncertainty of impacts in the presence of joint compliance [39] plays an important role here. If the energy lost during an impact is greater than expected, the impact invariance of the target orbit will be lost and the robot will fall backwards [40]. The gem of HZD, viz., the inherent stability associated with invariant HZD orbit is applicable only to planar case. When the degree of underactuation is more than one as in 3D- biped, there is no default stability guarantee and special care should be taken for appropriate design of virtual constraints to achieve the same. This will further complicate the HZD design procedure for a practical biped. Thirdly, in a practical sense, the control is not robust against external force disturbances [18] and unexpected changes in ground slopes or step discontinuities within a gait [41]. Finally, it is not fair to constrain the actuated variables, q_c to follow a predetermined path belonging to $\mathcal{Z}$ as a function of underactuated variables, q_f just due to the inability to ensure the gait stability in real time. If the biped has to recover from an external push or from an unexpected foot slip, the controller has to either place the transit foot at a suitable capture point or dynamically manipulate its centroidal momenta to ensure postural balance [42]. The biped should have the freedom to make use of a dynamically emergent coordination among the components of q consistent with physical constraints, rather than getting virtually constrained to an explicit coordination imposed a priori as in HZD. Hence, in the author's opinion, the suitability of HZD for realistic outdoor situation is questionable.

2.3.4 Heuristic control approaches

Drawing inspiration from locomotion control structure in vertebrates, numerous heuristic locomotion concepts have been reported, though the specific methods vary widely. There are numerous implementations of neural networks, neural oscillators, and central pattern generators [43, 44] which are regulated through various feedback mechanisms. Virtual model control is another intuitive approach proposed by Pratt et al. [45]. Heuristic methods generally make use of simplified models of biped [46, 18] to represent the interaction between CoM and GCoP[3] and lack proper analytical framework for performance analysis and design.

[3]GCoP is obtained by estimating the centre of pressure acting on the foot sole of biped exerted by the ground reaction forces assuming that there is no other contact point between biped and the ground or its any extensions.

2.3.5 Control schemes for bipedal locomotion over uneven terrain

Uneven terrain locomotion is another potential area of research [47, 48, 49] as the superiority of bipedal locomotion over wheeled locomotion is really based on this aspect. Truly speaking, the efficacy of a bipedal control scheme should be judged based on its suitability for uneven terrain condition. The stability of locomotion over uneven terrain is linked with the gait stability criterion and the means by which, the same is achieved. The parameters of terrain like slope, level difference, friction coefficients etc. will be known only for the next adjacent step. In some situations, full foothold will not be available and biped have to step over partial foothold or line contact type foothold or even point contact type foothold. There can be situations when the foothold shape cannot be judged through exterioceptive sensors like camera or lidars, rather will be known only after making contact with foot sole through pressure sensors. Hence locomotion control methods which require pre-synthesized orbit for bipedal gait are not suitable for uneven terrain.

As per the available open literature, ATLAS humanoid of Boston Dynamics is the best in this category [42] which has demonstrated its ability to walk over partial footholds such as small stepping stones and rocks with sharp surfaces. Their algorithm does not rely on prior knowledge of the foothold even though information about an expected foothold can be used to improve the stepping performance. After a step is taken, the robot explores the new contact surface by attempting to shift the center of pressure around the foot. The feasibility of the next foothold is decided by making use of the concepts of *centroidal moment pivot (CMP)* [50] and *instantaneous capture point (ICP)* [51]. When stepping is not available or is insufficient, angular momentum strategy is used to regain balance.

The extension of HZD control for planar bipedal locomotion in the presence of modestly uneven terrain is given in [52]. A single (non-switching) controller and nominal periodic gait that are insensitive to a predetermined and finite set of terrain variations are derived. However the applicability of HZD control for a generic uncertain terrain is yet to be answered. Manchester et al. has explored a more complex approach in the line of HZD for stable non-periodic dynamic locomotion over uneven terrain with experimental verification on a 2 DoF planar compass bipedal [40]. The proposed technique was to compute a transverse linearization about the desired motion: a linear impulsive system which locally represents "transversal" dynamics about a target trajectory. This system is then exponentially stabilized using a modified receding-horizon control design, providing exponential orbital stability of the target trajectory of the original nonlinear system. But the procedure to guarantee the constraints on contact force on a real time basis while traversing over

uncertain terrain is not discussed.

2.4 Need for a Multi-phase Autonomous control framework

Think about a situation, when one has to exactly plan the motion trajectories for various joints of limbs and torso prior to each walking step while going for a morning walk. As the permissible joint trajectories are too restricted, the decision cannot be left to the subconscious part of the central nervous system (CNS), rather the conscious involvement of the brain will be required. That means, the person has to be too calculative of each joint trajectory loosing all the enjoyment of a leisurely walk! This does not match with the reality and not the right strategy for walking control. What are we basically bothered while walking over a reasonably uniform terrain? There are five things that our CNS is trained to perform autonomously [21, 19]. (i) To maintain a minimum ground clearance of swing foot to avoid scuffing. (ii) To target a desired postural configuration on heel strike to minimize the impact shock and to minimize the walking effort (iii) To maintain a specific horizontal offset between body-CoM and heel impact site so as to be in a comfort zone avoiding both backward fall or forward fall for the current forward velocity. (iv) To regulate the forward lean of torso along certain comfortable orientation. (v) To regulate the forward velocity during the flat-foot phase. These objectives are satisfied by our CNS even in the presence of slight unevenness of the terrain without any conscious replanning by the brain. This is made possible by the locomotor task loops built over the neuro-muscular system to ensure postural stability and forward velocity regulation without violating the contact force constraints, all as real time dynamic behaviours so that they get automatically adapted to the terrain excursions. Thus the natural bipedal gait evolves out as an optimal trajectory out of the structured behaviour framework while we walk forward without any further need to remember the same as a reference trajectory for stiff tracking for the future gaits.

The deficiency of today's bipedal control algorithms is attributed to their limitation against few of the basic locomotion requirements as mentioned above. A realistic bipedal control should be able to ensure postural stability and forward velocity regulation without violating the contact force constraints as well as joint torque limits, all as real time behaviours. The walking gait should be allowed to evolve out of these structured behavioural framework to optimize other desirable features like energy spent, maximum toque etc. The regulation of forward velocity of biped has been classified as the "most difficult subtask"

by Pratt et al. since the degrees of freedom that contribute to the velocity vector are under-actuated from a continuous dynamics point of view [19]. Hence in ZMP as well as in HZD based methods, the forward velocity is embedded within the desired path of the joint variables. Postural stability without violation of contact force constraint is achieved in ZMP scheme by ensuring that the ZMP of biped always remains within the foot support polygon, again through trajectory pre-planning and to certain limited extend by preview control (1.6 s in advance using ZMP preview control [23, 20]). This artificial approach leads to walking pattern with bent knees, loosing the grace and efficiency of bipedal locomotion. On the other hand, HZD approach does not make use of actuated flat foot phase and hence there are no means to regulate the postural stability in real time and therefore the stability requirement is also embedded within the optimal trajectory synthesis problem.[4] Hence it is necessary to develop a control scheme which will autonomously ensure the above three basic control requirements, namely postural stability, velocity regulation and constraint consistency, while interacting with the terrain.

As mentioned earlier, the dynamics of bipedal locomotion inherently belongs to the class of hybrid dynamics systems due to the recurring set of kinematics, dynamics, constraints and control requirements as the biped proceeds forward along multiple discrete event phases associated with multiple feet-ground contact state. Added to this is the uncertainty of terrain parameters like surface geometry and soil physical properties. Hence to be realistic, the natural choice of the walking controller should be a closed loop controller with parameters and goals switched depending on the current state of system dynamics and terrain condition. Further, the controller should have its inbuilt logic to identify the current discrete event state and switch over to the appropriate controller. If it was guaranteed that the control-DoF of the biped in any discrete event phase is independent of the control actions of any other phase, we could have designed the controller for each phase exclusively by concentrating only on the dynamics of the current phase. However, the soft boundaries of unilateral and friction cone constraints make the occurrence of future discrete events and their control-DoF highly dependent on the state trajectories evolving out of the current controlled dynamics. Hence the feasibility and optimality of controller belonging to any gait phase cannot be judged locally, rather to be decided based on the evaluation over the entire gait cycle. Thus, instead of a mere automatically switching controller based on certain pre-set rules, the demand goes naturally to make use of an intelligent autonomous controller which has the capability to predict the impact of a current control law over the

[4]Even though actuated ankle strategy has been applied in HZD framework [31], it makes use of ZMP strategy for stability, again missing the real goal.

entire gait based on certain accumulated knowledge base accrued through learning based on either hardware experimentation or simulation of detailed system model. The initial selection of controller structure, parameters and goals for each discrete event phase can be arrived at based on information from the biomechanical control or by using empirical control based on reduced order model of the biped capturing the significant dynamic features relevant to the current phase. Finally to be more versatile, the controller switching is to be carried based on hybrid event phase instead of discrete event phase which have further subdivisions of phase based on continuous postural states. Hence the research presented in the thesis is focussed on the development of *Hybrid-state driven autonomous controller (HyDAC)* for controlling planar bipedal locomotion having the research objectives given below.

2.5 Research Objectives

The following are the major objectives of the present research work.

1. To develop a two-level hierarchical type control scheme for controlling planar bipedal locomotion over uniform terrain. The walking gait is to be partitioned into a finite number of hybrid event states with each state managed by a dedicated set of motion control primitives forming the lower level control called *Task Level Controller (TLC)*. The higher level controller, called *Supervisory Level Controller (SLC)* is to be designed to coordinate the control primitives of TLC in an autonomous fashion.

2. To develop online control strategies for the regulation of forward velocity of biped-CoM and the postural orientation without violation of contact force constraints and joint torque limits. These are essential for an autonomous control framework.

3. To formulate a control oriented stability criterion for ensuring the postural stability of planar biped, applicable for both periodic gait over uniform terrain as well for aperiodic gait over non-uniform terrain.

4. To extend the autonomous control scheme to a class of uneven terrain represented by non-uniform staircase with arbitrary distribution of stair parameters.

In summary, the current research is focussed on developing a suitable control framework to realize the bipedal dynamic walking as a an event driven cyclic process with guaranteed postural stability margins.

Chapter 3

Unified Mathematical model for Planar biped

3.1 Introduction

There are two standard approaches for modelling the dynamics of robotic manipulators, namely Lagrange-Euler method and Newton-Euler method [53, 54, 55]. The former gives closed form analytic expression for the dynamics whereas the latter provides recursive expression. The analytic form is preferred for control formulation as it is suitable for algebraic manipulation. Hence Lagrange-Euler type model of the biped is adopted in the present work. However, it has the drawback of high computational complexity when applied to manipulators with large DoF. The computational burden can be reduced to certain extent by using recursive algorithm to compute various coefficient matrices in the Lagrange-Euler model [56, 54]. The present chapter develops a unified mathematical model of planar biped in Lagrange-Euler framework. The bipedal dynamics belongs to the general class of underactuated floating body systems since there are fewer actuators than the DoF and the feet-ground contact constraints are unilateral in nature. Moreover, the structure of kinematics and dynamics undergo cyclic variation as the biped proceeds forward through multiple feet-ground contact states. Hence it is essential to have a unified formulation of bipedal dynamics fitting well for all discrete kinematic phases of biped and suitable for formulating the final control expression taking care of different types of constraints and tasks [41].

The following sections start with the formulation of rigid body dynamics of planar biped. The expressions for holonomic constraints due to ground contact state as well as nonholonomic constraints due to underactuation are provided. This is followed by modelling of ground impact events and leg index swapping at the end of each walking step. The planar biped is then classified as a hybrid dynamic system by defining discrete event states

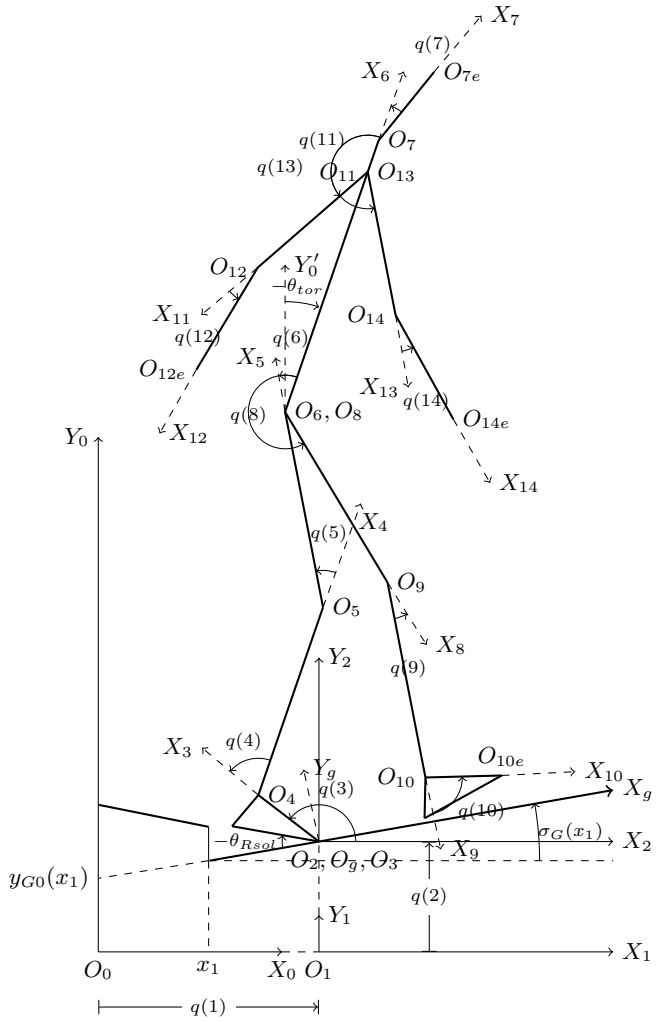

Figure 3.1: Coordinate frame assignment to planar biped

as well as continuous domain event states. Finally, the details of the simulation model are provided which is used for conducting simulation based case studies under different walking situations of planar biped.

3.2 Rigid body dynamics of Planar biped

The planar biped is modelled as a 12-link tree structured robotic manipulator with floating base having the origin of reference frame at the toe joint of stance foot as shown in Fig 3.1. To avoid confusion in double foot support phase, the stance leg is designated as *reference leg* and the swing leg is designated as *transit leg* and they are represented by

symbols 'r' and 't' respectively in different variables associated with corresponding legs. The roles of reference and transit legs get swapped immediately after the current transit foot which is in swing state strikes the ground ahead of the current reference foot which is in stance state. The precise mathematical definition in this regard is given in Section 3.4.2. The inertial reference coordinate frame is represented by the right handed Cartesian frame, $O_0X_0Y_0Z_0$ or $\{O_0\}$ with $\overrightarrow{O_0Z_0}$ pointing out of paper plane in normal direction. The origin, O_0 is assumed to be a point on ground close to the starting point of locomotion[1]. Since we are concentrating only on planar biped, the translational motion is restricted to the sagittal plane represented by $O_0X_0Y_0$ and the rotational motion of the individual links are about their respective joint axes, $\overrightarrow{O_iZ_i}$ parallel to $\overrightarrow{O_0Z_0}$. Due to space limitation, we omit $\overrightarrow{O_iZ_i}$ and $\overrightarrow{O_iY_i}$ axes from $\{O_3\}$ onwards in Fig 3.1. The ground profile is assumed to have piecewise segments having different slopes, σ_G and vertical offsets, y_{G0} which change as a function of horizontal displacement, x_G at discrete points. The floating base coordinate frame attached with the reference foot toe joint is labelled as $O_3X_3Y_3Z_3$ and its displacement with respect to $\{O_0\}$ are represented by the generalized position variables q_1 and q_2 along $\overrightarrow{O_1X_1}$ and $\overrightarrow{O_2Y_2}$ axes respectively. Including these two generalized variables, there are a total of, n_J=14 elements for the generalized position vector, q with q_3 to q_{14} representing the rotations of the biped links about the respective $\overrightarrow{O_iZ_i}$ axes attached to them. The i^{th} joint angle, q_i is measured as the CCW deflection of O_iX_i axis from $O_{p_i}X_{p_i}$ axis for $i = [3, 14]$ where p_i refers to the index of the parent link corresponding to i^{th} link. For simulation studies, each link is modelled as a point mass. The numerical values of the biped model parameters used for simulation studies are given in Table 3.1. The mass centre is measured from the joint axis about which each link is actuated when the biped is in stance posture on reference toe. The planar foot link is represented by a triangle, ATH as shown in Fig. 3.2 with the vertices A,T and H corresponding to the ankle, toe and heel tips respectively. Since there is no toe joint in the current bipedal model, the foot-sole extends from heel-tip to toe-tip and hence it appears to be longer compared to human foot. The mass centre of the planar foot link is given by a 2D coordinate vector with respect to $O_3X_3Y_3$ plane.

Assuming that the biped floating base joint, O_3 is attached to the inertial reference frame $\{O_0\}$ through two virtual links, the biped dynamics can be represented by the standard rigid multi-body dynamics equation [57] given by,

$$D(q)\ddot{q} + C(q, \dot{q})\dot{q} + G(q) = \Gamma + J_c'(q).F_c \tag{3.1}$$

[1]The modelling presented in this thesis assumes earth as a stationary inertial frame of reference.

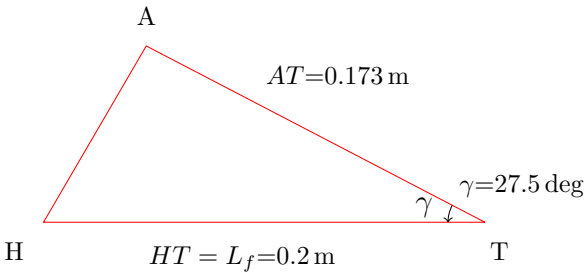

Figure 3.2: Foot link of planar biped

Table 3.1: Parameter values of planar biped model

Link name	foot	tibia	femur	torso	head	upper arm	lower arm
Mass (kg)	1.28	4.19	10.19	40.75	5.29	2.1	1.45
Length (m)	0.173	0.45	0.451	0.65	0.27	0.33	0.27
Mass centre(m)	[0.13 0.03]	0.276	0.368	0.39	0.1	0.155	0.106

subject to constraints,

$$\Gamma_j = 0 \qquad \forall\, j \in [1,3] \tag{3.2}$$

$$\text{and} \quad J_c(q)\ddot{q} = B(q,\dot{q}) \tag{3.3}$$

where $D(q) \in \mathbb{R}^{n_J \times n_J}$ is the joint space inertia matrix, $C(q,\dot{q})\dot{q} \in \mathbb{R}^{n_J}$ is the vector representing Coriolis and centrifugal force terms, $G(q) \in \mathbb{R}^{n_J}$ represents the gravity force vector, $\Gamma \in \mathbb{R}^{n_J}$ is the generalized force vector acting about joint axes and $J_c \in \mathbb{R}^{2n_c \times n_J}$ is the ground contact Jacobian for n_c number of contact points and $F_c \in \mathbb{R}^{2n_c}$ is the ground contact force vector with their x,y components along $\overrightarrow{O_0X_0}$ and $\overrightarrow{O_0Y_0}$ directions respectively. The inertia of joint drive system can be augmented to D matrix and the effect of drive viscous damping and friction can be augmented to Γ without loss of generality. The passive dynamic constraint represented by (3.2) corresponds to the underactuated floating base joint of biped and the equality constraint in (3.3) is the acceleration form representation of holonomic ground contact constraint with $B(q,\dot{q}) \in \mathbb{R}^{2n_c}$ [57].

We can simplify (3.1) by combining Coriolis, centrifugal and gravity forces into a new

vector, $\mathcal{G}(q, \dot{q}) = C(q, \dot{q})\dot{q} + G(q)$ so that

$$D(q)\ddot{q} + \mathcal{G}(q, \dot{q}) = \Gamma + J_c'(q)F_c \tag{3.4}$$

3.2.1 Ground contact states and contact forces

The ground profile for planar bipedal locomotion in sagittal plane $O_0X_0Y_0$ is approximated by piecewise line segments as shown in Fig 3.1. The ground profile can have both slope changes as well as step changes in vertical direction at finite intervals. In general, the ground line segment passing through a point, (x_G, y_G) on the ground is represented by the line equation,

$$y_G = y_{G0}(x_G) + x_G \tan\sigma_G(x_G) \tag{3.5}$$

where $y_{G0}(x_G)$ is the intercept made by the extended ground profile with $\overrightarrow{O_0Y_0}$ axis and $\sigma_G(x_G)$ is the angle made by the ground profile with $\overrightarrow{O_0X_0}$ axis measured in CCW direction. Both y_{G0} and σ_G are functions of the x-coordinate, x_G of the point on the ground. Let us represent the inertial frame with origin at (x_G, y_G) and having its x-axis directed along the ground by $\{O_gX_gY_gZ_g\}$ or $\{O_g\}$ with $\overrightarrow{O_gX_g}$ making an angle of $\sigma_G(x_G)$ with $\overrightarrow{O_0X_0}$. The planar biped with flat foot sole can have a maximum of four ground contact points namely, *Reference Heel (*rh*), Reference Toe (*rt*), Transit Heel (*th*) and Transit Toe (*tt*)* with each of these symbols taking a value of 1 if the point is in non-sliding contact with the ground and zero if the point is not in contact with the ground[2]. Based on the contact conditions at these four corner points, we can define the feet-ground contact state by the 4-dimensional binary vector,

$$\pi_m = [rh\ rt\ th\ tt] \tag{3.6}$$

Assumption 3.1. *The values of all variables and constants are assumed to be in SI units wherever not specified.*

Assumption 3.2. *The ground profile is assumed to have no surface discontinuities leading to convex projections within the span of stance foot or feet. This limits the foot-ground contact location to either foot or toe or both heel and toe.*

Remark 3.1. *In situations where Assumption 3.2 is violated, the control algorithm will proceed by assuming that the convex ground projections penetrate into the foot sole until the heel and toe of the foot intersect with the ground line. However, this is not a limitation*

[2]The sliding contact state is not considered in the current modelling framework as HyDAC avoids such a situation by explicit virtual constraints imposed during control synthesis.

of the proposed control scheme as such and can be taken care by modifying the ground contact constraint such that it is applicable to all locations on the foot sole. Proper shaping of foot sole with inward curvature as in human foot can also be attempted to avoid frequent interior contact points on foot sole.

Associated with the four ground contact points, there exist four numbers of 2D contact force vectors represented by F_{rh}, F_{rt}, F_{th}, and F_{tt} with each having x and y components directed along $\overrightarrow{O_0X_0}$ and $\overrightarrow{O_0Y_0}$ directions respectively. The components of ground contact force are represented by the following notations:

$$F_{rh} = \begin{bmatrix} f_{rhx} \\ f_{rhy} \end{bmatrix}, F_{rt} = \begin{bmatrix} f_{rtx} \\ f_{rty} \end{bmatrix}, F_{th} = \begin{bmatrix} f_{thx} \\ f_{thy} \end{bmatrix}, F_{tt} = \begin{bmatrix} f_{ttx} \\ f_{tty} \end{bmatrix} \tag{3.7}$$

The combined vector of contact force, F_c is obtained by vertically stacking all the elements of nonzero contact forces. For example, if $\pi_m = [1\,1\,1\,1]'$ then, $F_c = [F'_{rh}\ F'_{rt}\ F'_{th}\ F'_{tt}]'$. However, the ground contact forces have to be resolved parallel and perpendicular to the ground plane to verify unilateral contact force criterion as well as friction cone criterion associated with assumed contact state. The contact forces expressed with respect to inclined ground frame, $\{O_g\}$ are obtained by premultiplying with the associated rotation matrix, R_g so that

$$F_{grh} = R_g(\sigma_G)F_{rh} \text{ etc. where } R_g(\sigma_G) = \begin{bmatrix} \cos\sigma_G & \sin\sigma_G \\ -\sin\sigma_G & \cos\sigma_G \end{bmatrix} \tag{3.8}$$

with σ_G measured at the relevant ground contact point. The individual components of F_{grh} etc. are represented by f_{grh_x}, f_{grh_y} etc. The combined vector of contact forces, F_g expressed in $\{O_g\}$ is obtained by vertically stacking all the elements of nonzero contact forces. For example, if $\pi_m = [1\,1\,1\,1]'$ then, $F_g = [F'_{grh}\ F'_{grt}\ F'_{gth}\ F'_{gtt}]'$. The contact force components expressed in ground frame, $\{O_g\}$ corresponding to the current contact points have to satisfy unilateral force criterion to sustain the point in positive contact state. The unilateral force requirement can be expressed as,

$$f_{grh_y}, f_{grt_y}, f_{gth_y}, f_{gtt_y} > 0 \tag{3.9}$$

If any of the above components relevant to the current contact point crosses zero with a drooping trend, the corresponding contact state in π_m is made zero. Another requirement on the ground contact forces is that it should be within the friction cone to ensure that the contact points do not slide along the ground plane. For example, the friction cone criterion

for single point contact at reference heel can be expressed as

$$|f_{grh_x}| < \mu_c f_{grh_y} \tag{3.10}$$

where μ_c is the dry friction parameter of Amontons-Coulomb model of friction at foot-ground interface point [58]. When the support foot is in flat foot state, the friction cone criteria for heel and toe contacts can be combined as,

$$|f_{grh_x} + f_{grt_x}| < \mu_c(f_{grh_y} + f_{grt_y}) \tag{3.11}$$

since the two contact points are rigidly connected along the foot sole. If the contact force goes outside the friction cone, the corresponding contact point will slide along the ground and π_m as defined in (3.6) will become invalid. The current work assumes that the control algorithm will ensure the friction cone criterion with sufficient margin.

3.3 Modelling of Contact constraints

3.3.1 Holonomic constraint due to ground contact state

The holonomic constraint on reference heel when it is in nonsliding contact with the ground can be expressed as, $(x_{rh}; y_{rh}) = (x^c_{rh}; y^c_{rh})$, where the RHS gives the coordinates of ground contact point with respect to inertial frame $\{O_0\}$. On differentiating this expression, we get the corresponding velocity constraint,

$$\begin{bmatrix} \dot{x}_{rh} \\ \dot{y}_{rh} \end{bmatrix} = \begin{bmatrix} 0 \\ 0 \end{bmatrix} = J_{rh}.\dot{q} \tag{3.12}$$

where $J_{rh} \in \mathbb{R}^{2\times n_J}$ is the translational part of Jacobian with respect to ground contact point at reference heel. Further differentiation of (3.12) gives the acceleration form representation of ground contact constraint [59] as

$$J_{rh}\ddot{q} = -\dot{J}_{rh}\dot{q} \tag{3.13}$$

Similarly, we can define the ground contact constraints at other foot-ground contact points as,

$$J_{rt}\ddot{q} = -\dot{J}_{rt}\dot{q},\ J_{th}\ddot{q} = -\dot{J}_{th}\dot{q},\ \text{and}\ J_{tt}\ddot{q} = -\dot{J}_{tt}\dot{q} \tag{3.14}$$

The ground contact constraints given by (3.13)-(3.14) can be combined into a single expression by vertically stacking the active constraints as,

$$J_c \ddot{q} = -\dot{J}_c \dot{q} \tag{3.15}$$

For example, when $\pi_m = [1\,1\,1\,1]$, $J_c = [J'_{rh}\ J'_{rt}\ J'_{th}\ J'_{tt}]' \in \mathbb{R}^{8\times n_J}$. The contact point Jacobian can be represented in $\{O_g\}$ frame by,

$$J_{grh} = R_g(\sigma_G)J_{rh} \text{ etc.} \tag{3.16}$$

with individual elements given by ,

$$J_{grh} = \begin{bmatrix} J_{grh_x} \\ J_{grh_y} \end{bmatrix}, J_{grt} = \begin{bmatrix} J_{grt_x} \\ J_{grt_y} \end{bmatrix}, J_{gth} = \begin{bmatrix} J_{gth_x} \\ J_{gth_y} \end{bmatrix}, \text{and } J_{gtt} = \begin{bmatrix} J_{gtt_x} \\ J_{gtt_y} \end{bmatrix}. \tag{3.17}$$

The combined ground contact Jacobian, $J_g \in \mathbb{R}^{2n_c\times n_J}$ expressed with respect to $\{O_g X_g Y_g\}$ plane is obtained by vertically stacking the above Jacobian matrices corresponding to the active contact points. Since R_g is an orthogonal matrix, we have the relation, $R'_g R_g = R_g R'_g = I_2$ and hence the active ground contact points have the relation like,

$$J'_{rh}F_{rh} = J'_{rh}R'_g R_g F_{rh} = (R_g J_{rh})'(R_g F_{rh}) = J'_{grh}F_{grh} \tag{3.18}$$

which can be generalized to

$$J'_c F_c = J'_g F_g \tag{3.19}$$

By combining (3.4) and (3.19), the bipedal dynamics with respect to the local ground frame, $\{O_g\}$ can be written as,

$$D(q)\ddot{q} + \mathcal{G}(q,\dot{q}) = \Gamma + J'_g(q)F_g \tag{3.20}$$

3.3.2 Nonholonomic constraint due to underactuation

The passive dynamic constraint due to underactuation expressed by (3.2) along with the system dynamics given by (3.4) can be written as a linear equality constraint in terms of $\ddot{q}$ as,

$$\text{i.e.} \qquad D_p.\ddot{q} + \mathcal{G}_p = J'_{cp}\,F_c \tag{3.21}$$

where the subscript 'p' refers to the first three indices, 1-3 corresponding to the passive DoF of the biped and $D_p, \mathcal{G}_p$ and J'_{cp} represent the first three rows of the corresponding matrices and vectors. In other words, $D_p = D_{(p,:)}$ and $J'_{cp} = J'_{c\,(p,:)}$ or $J_{cp} = J_{c\,(:,p)}$. The generalized acceleration vector, $\ddot{q}$ of the planar biped has to satisfy a rank-1 passive dynamic constraint due to the passive rotation about the heel or toe joint of the support foot for single-point nonsliding type contact state. Even though the equality constraint (3.21), provides general statement of passive dynamics associated with floating base of biped, the presence of ground contact force provides implicit actuation in the respective directions with zero work when the same is within the unilateral and friction cone limits. Hence it is required to derive an explicit minimal row expression for unconstrained passive dynamics orthogonal to the motion subspace spanned by $J'_{cp}F_c$ which corresponds to the passive rotational motion space about the $\overrightarrow{OZ}$ axis passing through the contact point.

The required unconstrained passive dynamics can be obtained by projecting the passive dynamics in (3.21) to the orthogonal space of $J'_{cp}F_c$ similar to a procedure mentioned in [60]. The unconstrained passive DoF will increase to 2 if the contact point slides along the ground plane and the same will increase to 3 if the biped floats freely with no ground contact. On the other hand, if there are more than one ground contact point, the floating base of biped will become over-constrained and hence there will not be any unconstrained passive DoF. The dynamic constraints due to underactuation and other nonholonomic constraints are written in the general form,

$$H_{c_n}(q)\ddot{q} = B_{c_n}(q, \dot{q}) \text{ with } H_{c_n} \in \mathbb{R}^{n_{Cn} \times n_J}, B_{c_n} \in \mathbb{R}^{n_{Cn} \times 1} \tag{3.22}$$

for the subsequent use in Section. 4.9.

By combining (3.20) and (3.21), the floating base dynamics of the biped can be expressed with respect to local ground coordinates, $\{O_g X_g Y_g\}$ as

$$D_p.\ddot{q} + \mathcal{G}_p = J'_{gp}\, F_g \tag{3.23}$$

where $J'_{gp} \in \mathbb{R}^{3 \times 2n_c}$ represents the first 3 rows of $J'_g \in \mathbb{R}^{n_J \times 2n_c}$ corresponding to the passive joints of biped. The range space of J'_{gp} is the same as the row space of J_{gp}. Hence the projection operator to the orthogonal space of $J'_{gp}F_g$ can be obtained as [60],

$$P_N = I_3 - J^+_{gp} J_{gp} \tag{3.24}$$

where J^+_{gp} represents the Moore-Penrose inverse of J_{gp} and P_N is the null space projec-

tor [61]. The required unconstrained passive dynamics is obtained as,

$$P_N(D_p\ddot{q} + \mathcal{G}_p) = P_N\, J'_{gp}\, F_g = \mathbf{0}_{3\times 1} \tag{3.25}$$

$$\text{or} \quad P_N\, D_p\, \ddot{q} = -P_N \mathcal{G}_p \tag{3.26}$$

For single point nonsliding type contact state, P_N will have only rank 1 and hence the above 3-row equation can be reduced to a single row equation based on SVD approach. Let

$$H_p = P_N\, D_p \in \mathbb{R}^{3\times n_J} \tag{3.27}$$

which has rank 1. The SVD factorization of H_p is given by

$$H_p = U_p\, S_p\, V'_p \tag{3.28}$$

with $U_p \in \mathbb{R}^{3\times 3}, S_p \in \mathbb{R}^{3\times n_J}, V_p \in \mathbb{R}^{n_J\times n_J}$ and U_p and V_p are orthogonal matrices. As H_p has only rank 1, S_p will have only one nonzero singular value. Let $U_{p1} = U_{p\,(:,1)}$,$V_{p1} = V_{p\,(:,1)}$ and $S_{p1} = S_{p\,(1,1)}$. As all elements of S_p except $S_{p\,(1,1)}$ are zeros, we can write,

$$U_p\, S_p\, V'_p = U_{p1}\, S_{p1}\, V'_{p1} \tag{3.29}$$

Simplifying (3.26)-(3.29),

$$U_{p1}\, S_{p1}\, V'_{p1}\, \ddot{q} = -P_N\, \mathcal{G}_p \tag{3.30}$$

As $U'_{p1}U_{p1} = 1$, being one column of orthogonal matrix, U_p, we can premultiply both sides of (3.30) to get the single row version of the unconstrained passive dynamics as

$$S_{p1}\, V'_{p1}\, \ddot{q} = -U'_{p1}\, P_N\, \mathcal{G}_p \ \in \mathbb{R}^1 \tag{3.31}$$

which is in the general form of (3.22) with $H_{c_n} = S_{p1}\, V'_{p1}$ and $B_{c_n} = -U'_{p1}\, P_N\, \mathcal{G}_p$. See Appendix A for the detailed derivation for truncated SVD based regularization.

3.3.3 Nonholonomic constraint due to free-floating state

In free floating state, both the feet of biped will be above the ground plane and hence there will not be any ground contact force F_g. Hence the passive dynamic constraint due to underactuation can be derived from (3.23) as

$$D_p.\ddot{q} = -\mathcal{G}_p(q, \dot{q}) \tag{3.32}$$

which is also in the general form (3.22) of nonholonomic constraint.

3.4 Modelling of Ground impact

Ground impact of the transit foot is an important event of dynamic walk which terminates the current walking step interchanging the functions of reference and transit legs. Normally, the transit foot strikes the ground with its heel when the reference foot is in single point or double point contact state. However depending on various terrain conditions, it is possible to have all possible combinations of contact points when the biped impacts on ground with its transit foot. The mechanics of contacting bodies is inherently a complex topic as one has to make many assumptions regarding the mechanical properties of the contact points, locations of simultaneous contacts and their relative velocities [62, 63]. There are two basic approaches followed in literature to model the transit foot contact event with ground. One approach makes use of an elastic model whereas the other uses rigid impact model. The former method [64] has the advantage of capturing the realistic ground contact phenomena of human walk, but suffer from the disadvantage of introducing a flexible model along with a set of uncertain parameters [58]. On the other hand, the latter approach with rigid impact model gives diversified results for post-impact velocities depending on the strike point velocities and biped configuration prior to impact as well as on the local ground slope and friction coefficient between foot sole and ground [65]. The assumption of perfect inelastic impact for rigid heel strike rules out the possibility of double support phase [66] and even existence of solution in some cases [65]. These results do not match with the physical observations in natural human walk which can maintain a reasonably good repeatability on heel strike even with slight unevenness of the ground. Hence the development of a foot impact model to capture the realistic behaviour of human locomotion with “stiff” feet and limbs has been projected as an essential requirement by J. W. Grizzle et al. [58]. Our approach provides a compact expression for impact velocity map assuming that the links and joint interfaces of the lower limbs as well as the feet-ground interfaces have appropriate compliance and damping to fully absorb the impact shock from transit foot within a short duration compared to various control loop response times, without affecting the ground contact state of current support foot.

3.4.1 Velocity impact map

We make use of a realistic assumption of the invariance of the ground contact state of current support foot to ensure the possibility of finite double foot support phase for biped walk as observed in human walk. Based on the principle of conservation of generalized momentum, the dynamics of rigid impact can be derived as [58, 67],

$$D(q)(\dot{q}^+ - \dot{q}^-) = J_c(q)'F_{imp} \tag{3.33}$$

where F_{imp} is the intensity of impulsive contact force acting at the contact points over the infinitesimal impact event and J_c is the contact Jacobian corresponding to the ground contact points on impact. Assuming impact invariance of the contact state of current support foot, J_c is obtained by stacking the contact Jacobian prior to impact with the additional contact point Jacobian corresponding to the impact points. Hence the post impact velocity constraint can be written as,

$$J_c\dot{q}^+ = \mathbf{0} \in \mathbb{R}^{2n_c \times 1} \tag{3.34}$$

Combining (3.33) and (3.34), the constrained impact dynamics can be represented by,

$$\begin{bmatrix} D & -J_c' \\ J_c & \mathbf{0} \end{bmatrix} \begin{bmatrix} \dot{q}^+ \\ F_{imp} \end{bmatrix} = \begin{bmatrix} D\,\dot{q}^- \\ \mathbf{0} \end{bmatrix} \tag{3.35}$$

Assuming full row rank for J_c, (3.35) can be solved to get [58],

$$\dot{q}^+ = \left(I_{n_J} - D^{-1}J_c'\left(J_cD^{-1}J_c'\right)^{-1}J_c\right)\dot{q}^- \tag{3.36}$$

If J_c is not of full row rank, (3.36) can be modified as[3],

$$\dot{q}^+ = \left(I_{n_J} - D^{-1}J_c'\left(J_cD^{-1}J_c'\right)^{+}J_c\right)\dot{q}^- = \Delta^{iv}(q)\dot{q}^- \tag{3.37}$$

where $\Delta^{iv}(q) \in \mathbb{R}^{n_J \times n_J}$ is called the velocity impact map. Since the joint position vector, q is invariant during impact, the transition for the biped state vector, $\mathbf{x} := [q'\ \dot{q}']'$ on impact can be expressed as,

$$\mathbf{x}^+ = \Delta^i(q)\mathbf{x}^- \tag{3.38}$$

where, $\Delta^i := \text{blockdiag}(I_{n_J}, \Delta^{iv})$ is called the *impact map*.

[3]The superscript on the LHS of (3.37) refers to post-impact instant whereas the same on RHS refers to Moore-Penrose generlized inverse.

In an ideal situation with rigid impact, the components of F_{imp} obtained by solving (3.35) should be verified a posteriori with respect to unilateral and friction cone constraints for validating the assumed contact state during impact [65]. However, the observation of finite double foot support phase in human locomotion justifies the assumption of impact invariance of support contact state. It is conceptually possible to capture this physical phenomena by using elastic impact model instead of rigid impact [64], on the cost of introducing a host of additional parameters of uncertain values [58]. However to avoid such additional modelling complexity and to manage with the same configuration variables, q, we followed a simpler, but approximate route by enforcing the assumption of impact invariance of contact state as an explicit virtual constraint along with the ideal impact dynamics[4]. In uniform terrain locomotion, the proposed impact map is applied for both transit heel and the subsequent toe ground impacts. To differentiate the two events, the impact map for transit heel impact and subsequent reference toe impact are represented as $\Delta^{i}_{th}(q)$ and $\Delta^{i}_{rt}(q)$ respectively.

3.4.2 Half cycle index reset and impact reset map

Half cycle index reset marks the end of the present walking step and the beginning of a new step. It is activated when the transit foot strikes the ground with either heel or toe or with both heel and toe with the condition, $x_{th} > x_{rh}$. On the occurrence of half cycle index reset, the roles of reference leg joints and transit leg joints get swapped along with the respective numerical values of q_j's and $\dot{q}_j$'s. The swapping relation for q_j's can be given as,

$$q_1^{\tau+} = x_{tt}^{\tau-},\ q_2^{\tau+} = y_{tt}^{\tau-} \tag{3.39}$$

$$q_3^{\tau+} = \sum_{\substack{3 \leqslant j \leqslant 10 \\ j \neq 7}} q_j^{\tau-} - \pi \tag{3.40}$$

$$q_j^{\tau+} = -q_{(n_J - j)}^{\tau-} \quad \text{for } j = 4, 5, 9, 10 \tag{3.41}$$

$$q_j^{\tau+} = \pi - q_{(n_J - j)}^{\tau-} \quad \text{for } j = 6, 8 \tag{3.42}$$

[4]It is assumed that the high frequency passive dissipative dynamics associated with joints, links and foot sole contact surfaces will effectively absorb the shock energy which may otherwise cause the reference foot contact points to lift-off.

Similarly, the swapping relation for $\dot{q}(j)$'s can be given as,

$$\begin{bmatrix} \dot{q}_1 \\ \dot{q}_2 \end{bmatrix}^{\tau+} = J_{tt}^{\tau-}\dot{q}^{\tau-},\ \dot{q}_3^{\tau+} = \sum_{\substack{3\leqslant j\leqslant 10 \\ j\neq 7}} q_j^{\tau-} \tag{3.43}$$

$$\dot{q}_j^{\tau+} = -\dot{q}_{(n_j-j)}^{\tau-} \quad \text{for } j = 4,5,6,8,9,10 \tag{3.44}$$

Here the fictitious time mark, '$\tau-$' represents the instant prior to half cycle index reset which coincides with the time mark, '$+$', the instant just after the transit foot ground impact as referred in the previous subsection. Half cycle index reset is to be applied only after mapping the biped state, $\mathbf{x}$ through the impact map, Δ_q^i. In addition to the swapping of leg variables, some of the system flags are also reset to zero on the detection of half cycle index reset as described in Section 3.5.2.1. The half cycle index reset expressed by (3.39)-(3.44) can be written in a compact functional form as,

$$\mathbf{x}^{\tau+} = \Delta^R(\mathbf{x}^{\tau-}) \tag{3.45}$$

The effect of $\Delta^R(.)$ on $\mathbf{x}$ is only with respect to labelling without any discontinuity for physical variables and it occurs twice in every walking gait nullifying the net effect as $\Delta^R(\Delta^R(\mathbf{x})) = \mathbf{x}$. Combining the algebraic maps expressed by (3.38) and (3.45), the net effect of impact map and half cycle index reset map can be expressed as,

$$\mathbf{x}^{+} = \Delta(\mathbf{x}^{-}) \tag{3.46}$$

where, $\Delta(\mathbf{x}^-) := \Delta^R(\Delta^i\mathbf{x}^-)$ and is named as *Impact Reset Map*. Here we made use of the fact that, both 'τ^-' and 'τ^+' are physically equivalent to the time instant, '$+$' which refers to the instant just after the transit foot heel impact and the former notations are used only to represent the algorithmic sequence. To differentiate between impact reset maps on transit foot heel strike and transit foot toe strike[5], they are represented respectively by Δ_h and Δ_t.

3.5 Planar biped as a Hybrid dynamical system

The bipedal motion dynamics belongs to the class of discrete event system from modelling perspective due to the recurrent topological structure as the biped traverse through different feet-ground contact states during dynamic walking. However, these discrete event phases have to be further subdivided for effective control design based on certain postural state

[5]The former happens during uniform terrain walking whereas the latter happens during stair-walk.

variables in continuous time domain. The resulting partitioning is designated as hybrid event state for bipedal dynamics.

3.5.1 Discrete event states of bipedal gait

For a planar biped with flat foot sole as shown in Fig 3.2, four types of foot-ground interface contacts are possible for each foot. They are named as *Heel Roll (HR), Flat Foot (FF), Toe Roll (TR) and Swing (SW)*. In HR state, the stance foot rotates about its heel on the ground plane and it occurs normally just after the heel strike event of transit foot. In TR state, the stance foot rotates about its toe on the ground plane. The normal pattern of contact state sequence for human walk with respect to either right foot or left foot is HR→FF→TR→ SW→HR. Accordingly, the elements of contact state vector, π_{m} for a particular foot takes the sequence of values [1 0] → [1 1] → [0 1] → [0 0] → [1 0]. Let us define the *Discrete Event State* ($\mathbb{D}_{es}$) of the biped as the state of biped with its reference-transit feet pair having a specific contact state with the ground. The $\mathbb{D}_{es}$ can be represented either by π_{m} as defined in (3.6) or symbolically by pairs like FF-TR, FF-SW, TR-HR etc. There can be different patterns of bipedal walk having different $\mathbb{D}_{es}$ sequences. For example, stair-walk can be represented by the $\mathbb{D}_{es}$ sequence TR→FF→TR→ SW→TR with respect to any foot. he sequence will also change with ground slope and with other terrain properties. However, the locomotion efficiency and stability robustness will vary with walking patterns.

3.5.2 Continuous system events and associated flags

A closed loop controller designed purely on the basis of $\mathbb{D}_{es}$ cannot realize a stable dynamic walking for the biped. It also depends on the relative positions of upper body and transit foot with respect to the stance foot and also on the forward velocity of the upper body. Moreover the biped control has to satisfy various virtual constraints to prevent sliding, lift-off etc. and to avoid reaching near the kinematic and torque limits of joint actuators. Hence it is essential to recognize the current state of the continuous system against predefined thresholds along with the current $\mathbb{D}_{es}$ to execute appropriate control action . Hence a set of flags, named *Continuous System Event State Flags (C_{SF})* are defined to identify various continuous system event states relevant for control execution.

3.5.2.1 Definition of Continuous System Event State Flags (C_{SF})

Continuous System Event State Flags (C_{SF}) take discrete values of 1 or 0 when the corresponding continuous system variable or combination of variables cross the specified value

or values or depending on whether the ground contact force constraint is active or passive. The definition of various C_{SF} used for the control algorithm are given below:

MidSwgFlg: The Mid Swing Flag, *MidSwgFlg* is set when the mid-point of transit foot crosses the mid-point of reference foot in forward direction at the first time during each walking step and is reset when the transit foot strikes the ground.

MidStnFlg: The Mid Stance flag, *MidStnFlg* is set when the biped-CoM crosses the mid point of reference foot, x_{rc} in the forward direction at the first time during each walking step and is reset on the subsequent transit foot impact on ground.

FwdTDFlg:
The Forward Touch Down Flag, *FwdTDFlg* initiates the touch down phase of transit foot. During uniform terrain walk, *FwdTDFlg* is set if $\begin{pmatrix} (x_{com} \geqslant x_{rh} - L_f) \textbf{ and} \\ \min\left(\sigma_G(x_{rt}), \sigma_{Gd}\right) \leqslant -15\pi/180) \end{pmatrix}$ **or** $\left(x_{com} > x_{rt}\right)$ during the post mid-swing period. σ_{Gd} is the effective ground slope between the ground projection of transit foot heel and the ground projection of reference foot toe in the presence of step and slope discontinuities on the ground profile and is given by

$$\sigma_{Gd} = \tan^{-1} \frac{y_G(x_{th}) - y_G(x_{rt})}{x_{th} - x_{rt}} \tag{3.47}$$

FwdTDFlg will be reset on transit foot ground strike. The hybrid state for *FwdTDFlg* will be different for stair-walk and the same will be defined in Chapter.4.

TrnKneExt, RgtElbExt, LftElbExt: The Transit Knee Extension Flag, *TrnKneExt* will be set if the transit knee joint extends towards straight leg condition with $q_9 > -10\pi/180$ and will be in reset state otherwise. The Right Elbow Extension Flag, *RgtElbExt* will be set if the right elbow joint extends towards straight arm condition with $q_{12} < 12\pi/180$ and will be in reset state otherwise. Similarly, the Left Elbow Extension Flag, *LftElbExt* will be set if the left elbow joint extends towards straight arm condition with $q_{14} < 12\pi/180$ and will be in reset state otherwise. For a planar biped, we cannot however differentiate between the right and left side.

FyrFlg: *FyrFlg* is set when it is required to constrain the perpendicular component of ground contact force on reference foot, viz. $f_{gr_y} = f_{grh_y} + f_{grt_y}$, to a specified value. When the computed value of f_{gr_y} during any control synthesis iteration violates either upper or lower limit, *FyrFlg* will be set and f_{gr_y} will be constrained to the respective limit for the current control interval. The definition is applicable in single point contact state

also, for the active component of contact force.

FcrFlg: The friction cone criterion for the FF state of reference foot can be expressed as

$$|f_{grh_x} + f_{grt_x}| < \mu_c(f_{grh_y} + f_{grt_y}) \tag{3.48}$$

where μ_c is the dry friction parameter of Amontons-Coulomb model of friction at foot-ground interface point. When the computed value of contact force components violate the friction cone bounds, *FcrFlg* will be set and the control algorithm will ensure that $|f_{grh_x} + f_{grt_x}| = 0.95\mu_c(f_{grh_y} + f_{grt_y})$ for the current control instant[6]. For single point contact states like HR or TR of reference foot, above expressions are applicable with only single force element on both sides corresponding to the active ground contact point.

TdjFlg: The joint torque limit flag, *TdjFlg* will be set when the computed value of torque command of the j^{th} joint, Γ_{d_j} exceeds its upper or lower limit and Γ_{d_j} will be constrained to the respective limit by the control algorithm.

3.5.3 Hybrid event states of planar biped

Hybrid Event State ($\mathbb{H}_{es}$) of the biped can be defined as the state of biped with its reference-transit feet pair having a specific contact state with the ground (i.e. a specific $\mathbb{D}_{es}$) and the set of continuous system event state flags, C_{SF} having the specified values. Just like π_m specifies a particular $\mathbb{D}_{es}$, the hybrid event state, $\mathbb{H}_{es}$ can be specified by another binary vector, π_h having a length of $n_{cs}+4$, where n_{cs} is the number of C_{SF} flags defined for a particular locomotion pattern.

3.6 Simulation model of Planar biped

The 12-link planar biped with the parameter values given in Table 3.1 has been used for the simulation studies. Each link is modelled as a point mass and the mass centre is measured from the joint axis about which each link is actuated when the biped is in stance posture on its reference toe. For the planar foot link, mass centre is given by a 2D coordinate vector with respect to $O_3X_3Y_3$ plane. The unique solution for the ground contact force, F_g expressed in $\{O_g\}$ for a given joint torque command, Γ_d and biped state, $(q, \dot{q})$ can be

[6] The factor of 0.95 is introduced to provide a safety margin of 5% from the friction cone boundary to account for modelling errors and error due to finite control sampling interval.

obtained as [60, 68],

$$F_g = \left(J_g D^{-1}(q) J_g'\right)^+ \left(-\dot{J}_g \dot{q} - J_g D^{-1}(q)(\Gamma_d - \mathcal{G}(q, \dot{q}))\right) \tag{3.49}$$

where $J_g \in \mathbb{R}^{2n_c \times n_J}$ is the stacked contact Jacobian expressed in $\{O_g\}$. Prior to substitution in (3.49), the joint torque commands, Γ_d are subjected to the speed dependent torque limits of the joint actuator hardware to remove spikes of torque commands exceeding the respective limits. Making use of the above solution for ground contact force, F_g, the generalized joint acceleration, $\ddot{q}$ for the given joint torque command can be obtained from (3.1) as,

$$\ddot{q} = D(q)^{-1}\left(\Gamma_d - \mathcal{G}(q, \dot{q}) + J_g'(q) F_g\right) \tag{3.50}$$

The biped state trajectories for dynamic walking are obtained by integrating $(\dot{q}, \ddot{q})$ using fourth order Runge-Kutta (RK4) algorithm with a control computation interval of 0.002 s.

3.7 Chapter Summary

A unified framework for representing the rigid body dynamics of a planar biped was described in this chapter. The model presented is applicable for all phases of locomotion like single-foot single-point contact state to multi-foot multi-point contact state including even the non-contact free-floating state by using appropriate contact state Jacobian. A practical formulation of impact dynamics was provided to ensure the invariance of support-foot contact state during the ground impact. The bipedal gait was visualized as a hybrid event system dynamic process by defining various discrete event states as well as hybrid event states. Finally, a brief description of the dynamic simulation model was also provided.

Chapter 4

Hybrid-state Driven Autonomous Control for Planar bipedal locomotion

4.1 Introduction

From a hardware perspective, the biped can be visualized as an underactuated, floating base, tree-structured robotic manipulator energised by control commands to joint actuators. By judicious design of coordinated movements of the bipedal joints, it is possible to realize a coherent set of temporally distributed postural behaviours which when imparted on biped hardware, support the autonomous evolution of stable dynamic walking. This concept has led to the development of a two-level hierarchical control framework called, Hybrid-state Driven Autonomous Control (HyDAC) capable of generating bipedal gait autonomously under various walking situations. To ensure emergent type dynamic coordination among various behaviour modes consistent with active constraints, the behaviour modes as well as control constraints are all expressed in second order differential form.

To start with, it is essential to clearly define the functional requirements of bipedal dynamic walk for control design. This is followed by justification of the selected structure of HyDAC by comparing with the biological counterpart. The functions of different hierarchical levels of HyDAC are then discussed. Thereafter, the mathematical framework for HyDAC is developed in detail along with the developments of a novel forward velocity control algorithm and a control oriented stability theory based on contraction mapping. This is followed by formulation of HyDAC as a constrained optimization problem.

4.2 Control functional requirements for Dynamic walk

The following set of 10 control functional requirements ($\mathcal{CFR}$) define the human-like planar bipedal dynamic walk considered in the thesis [41].

(i) $\mathcal{CFR}1$: It is necessary to ensure that at least one point of stance foot (reference foot) is in contact with ground while walking [11].

(ii) $\mathcal{CFR}2$: The transit leg control should ensure minimum ground clearance and obstacle avoidance of the foot during the forward motion.

(iii) $\mathcal{CFR}3$: It is necessary to regulate the forward velocity of the biped-CoM as per the external command.

(iv) $\mathcal{CFR}4$: It is desirable to regulate the orientation of torso link along an optimal inertial orientation expressed as a function of forward velocity and ground slope [21, 6].

(v) $\mathcal{CFR}5$: It is necessary to have freedom for the head and upper limb segments to execute any desired tasks during walking without affecting the postural stability of biped.

(vi) $\mathcal{CFR}6$: The control law should be adaptable with respect to velocity command change including starting from stance state and stopping to stance condition.

(vii) $\mathcal{CFR}7$: It is desirable to restrain the knee and ankle joints of both the legs from reaching the neighbourhood of singular orientations[1].

(viii) $\mathcal{CFR}8$: It is necessary to have adaptability for the control law with respect to variation in ground parameters like slope and vertical offset.

(ix) $\mathcal{CFR}9$: It is necessary to have robustness for the control law against external disturbance forces and should be adaptive with the variation of payload mass.

(x) $\mathcal{CFR}10$: It is necessary to dynamically coordinate various locomotion behaviour modes designed to meet $\mathcal{CFR}1$ to $\mathcal{CFR}9$ to ensure postural stability while moving forward according to the specified pattern[2] without violating constraints with respect to joint kinematic limits as well as torque limits.

The bipedal dynamic walking considered in the present work does not incorporate toe-off phase having rolling motion about toe joint. The basic reason is the absence of an actuated toe joint in the current model of planar biped as in human being.

[1] The kinematic rank deficiency at singular orientation affects the solution of resolved acceleration based bipedal control laws. Moreover, this restriction will avoid hyper extension at these joints as in human walk.

[2] Locomotion pattern is specified as a desired sequence of hybrid event states for dynamic walking.

4.3 Hierarchical structure of Vertebrate's locomotor system

Recent studies by neurobiologists [69, 70, 6] in vertebrate locomotion reveals that the locomotion is controlled by a two-level hierarchical architecture as shown in Fig 4.1. Various parts of brain, namely the motor cortex, thalamus, basal ganglia and cerebellum constitute the supervisory level control and the central pattern generators (CPG) in the spinal column constitutes the task level control. The spinal CPG in walking mammals is a distributed network with centres at cervical and lumbar levels that control forelimbs and hindlimbs respectively [71]. It has been verified [69] that the descending signals from the brainstem, basal ganglia and cortex, control the selection and shaping of the outputs from the locomotor CPG, with further layers of modulation coming from sensory and vestibular pathways that converge on CPG neorons as shown in Fig 4.1. The sensory feedback are important for initiating and correcting the locomotor rhythm and are also responsible for changing the motor output and for regulating phase changes during stepping [69]. In control system point of view, well practised routine activities are encoded as CPG's which will be executed as an event driven cyclic process adapting with the environment based on proprioceptive sensor feedback. However, any deviation from routine activities to take care of additional constraints needs real time change in behaviour coordination. This is carried out by cerebellum by mediating sensory and internal feedback and optimizing the motor pattern to the task at hand [69]. The two level hierarchical control structure of HyDAC is tailor-made to match with the above neuroanatomical structure of vertebrates with the task level control executing the function of CPG whereas the supervisory level control does the function of brain. On the contrary, stiff path following approaches as used in many virtual constraint based approaches [58, 72], will not fit into the biological control framework since they have no provision for real time coordination of behaviour primitives with unplanned additional constraints.

4.4 Hierarchical control structure of HyDAC

HyDAC makes use of a two-level hierarchical control architecture as shown in Fig 4.2 in line with the hierarchical locomotor systems in vertebrates [6]. The outer level is called *Supervisory Level Control (SLC)* and the inner level is called *Task Level Control (TLC)*. The activated motion control primitives of TLC are combined, prioritized and kinemati-

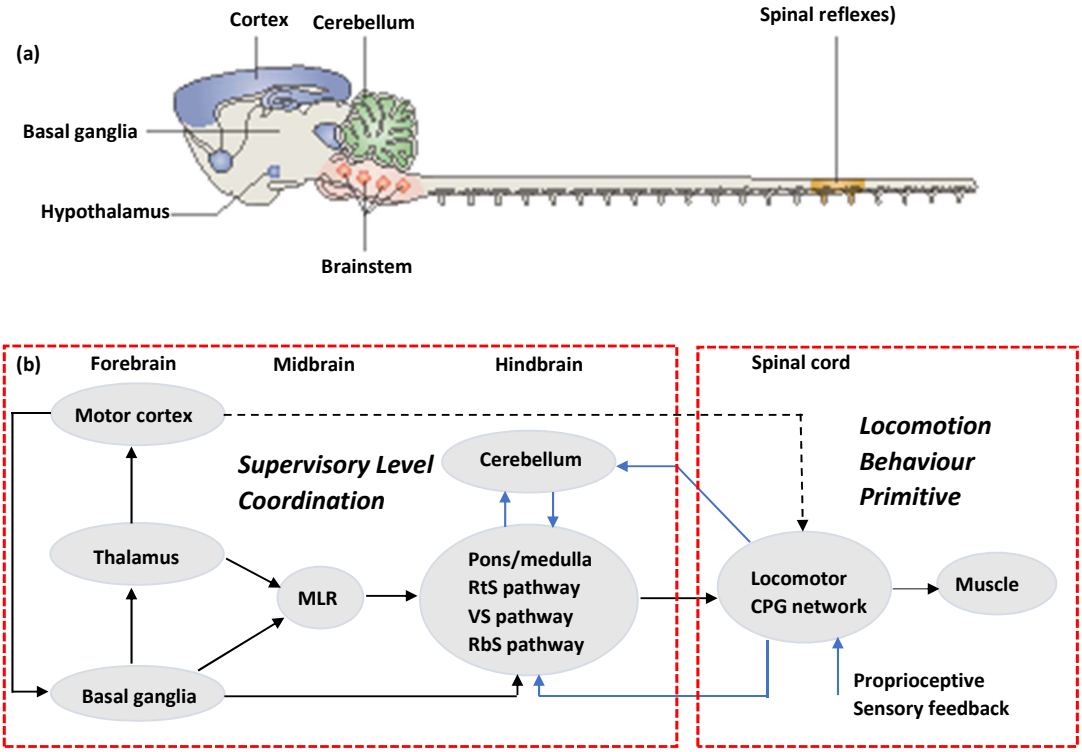

Figure 4.1: Organization of the locomotor system in vertebrates (Adapated from Figure 1 of [69] by permission from RightsLink Permissions Springer Customer Service Centre GmbH: Springer Nature Reviews Neuroscience, Copyright 2009)
(a) Schematic of the rodent central nervous system (CNS) showing the neural structures that make up the motor pathways controlling simple behaviours such as mastication, respiration and locomotion
(b) Neuroanatomical structure and motor pathways in aquatic and terrestrial vertebrates
MLR : mesencephalic locomotor region, RtS: reticulospinal, RbS: rubrospinal, VS: vestibulospinal, CPG: central pattern generator

cally inverted subject to the satisfaction of physical constraints to generate the desired joint space acceleration command, $\ddot{q}_d^*$ and the associated ground contact force vector, F_g^*. This is followed by the synthesis of equivalent joint torque command, $\Gamma_d = \Gamma_d(q, \dot{q}, \ddot{q}_d^*, F_g^*)$ based on the inverse dynamics of biped. The most suitable locomotion pattern is selected autonomously based on the class of terrain like uniform, uneven, stairways etc. sensed through exteroceptive sensors like camera as done by cortical control in vertebrates. The task level control acts just like central pattern generators in the spinal column as both are effictively local closed loop controls built over actuation system, joint level dynamics and proprioceptive feedback sensing internal and external interaction variables. The series-

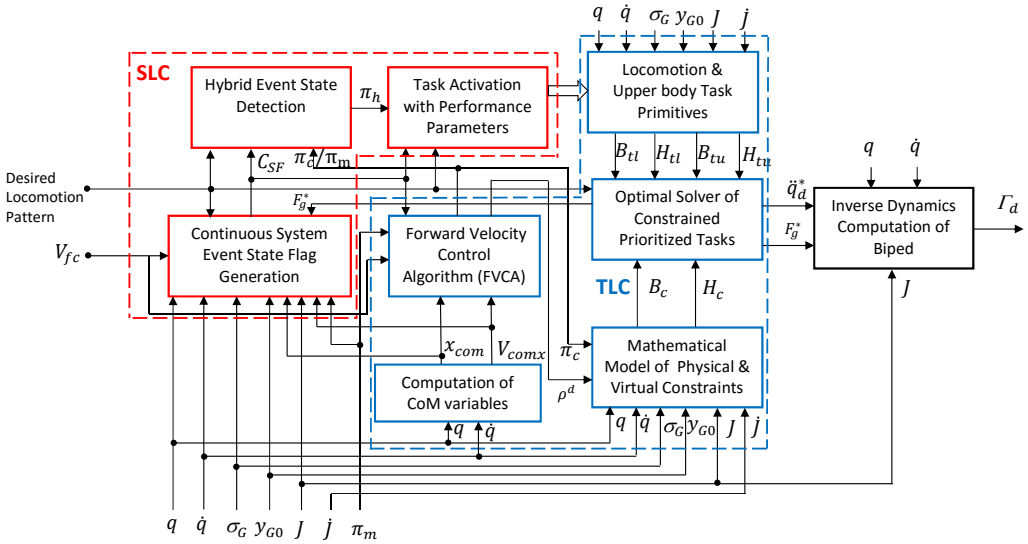

Figure 4.2: Block Schematic of HyDAC Algorithm for Bipedal Locomotion

parallel combination of multiple behaviour modes of TLC under the modulation of SLC generates rhythmic locomotor patterns as generated by CPG under the supervision of cortex control. HyDAC differs from conventional CPG controllers [70, 73] which make use of artificial neural network based oscillators to mimic biological neuromuscular oscillators. But usage of systematic ODE type[3] behaviour primitives provides a better mathematical framework with respect to adaptation and coordination and they can be easily networked by SLC to generate hybrid dynamical oscillators providing a better morphological match with neuromuscular oscillators. The autonomy of HyDAC is provided by a knowledge base in SLC encoded as the three blocks shown in Fig 4.2, which are generated by a priori learning using the data of extensive model based simulation studies. The present work does not include the real-time learning architecture of autonomous system.

The architecture of HyDAC is also suitable for a two-phase control optimization in realistic walking situations. The rules of supervisory level control (SLC) of HyDAC are generated by a priori optimization whereas the inner task level control (TLC), which is expressed in differential form, is analytically solved online as a constrained quadratic optimization algorithm. The benefit of this offline-online type partitioning for optimization is that control synthesis can be easily made terrain adaptive. The output of SLC is only a set of values or empirical rules or C_{SF} flag conditions which specifies the performance pa-

[3]ODE is the abbreviation for ordinary differential equation.

rameters and regulation goals of TLC. These SLC parameters can be easily quantized with respect to different ranges of terrain parameters and forward velocity command. As the underlying cases are finite in number, SLC can be readily optimized a priori based on analytical studies or through model based simulation studies. In the actual walking situation, SLC can easily activate the appropriate optimal rule (i.e. TLC), based on the sensed terrain parameter range. There is no need for synthesizing the actual walking trajectory, rather it evolves out as optimal online solution of TLC which makes use of real-time terrain data and takes care of all types of holonomic and nonholonomic constraints active at the current instant. Thus the benefits associated with a priori gait planning is retained to a large extent in SLC whereas all the robustness properties associated with compliant closed loop control are ensured by TLC.

The current formulation of HyDAC does not have any behaviour primitive for toe off phase as in human gait. Right at the beginning of each new gait, the rear foot is commanded to lift off assuming that the biped is able to rotate forward passively about the heel of front foot using the post-impact residual kinetic energy. For this purpose, a control oriented feet-ground contact state vector, π_c is defined by making $\pi_c(3:4) = [0\ 0]$ and $\pi_c(1:2) = \pi_m(1:2)$ provided $V_{fc} > 0$ and the reference foot is in contact state with the ground. All computations for implementing motion control primitives make use of π_c instead of the actual system's contact state, π_m. The resulting control law will effectively passivize the rear foot contact by way of not demanding any ground contact force from the same until it gets physically lifted off from the ground. However, the presence of double foot contact state under any adverse situation does not create any problem for the application of HyDAC as long as the post-impact residual kinetic energy is able to prevent backward falling of biped once the rear foot is lifted off from the ground.

4.4.1 Task level control (TLC)

The task level control (TLC) for bipedal locomotion gait is generated by a sequential combination of subtasks, TLC^i designed for each hybrid state, $\mathbb{H}^i_{es}$ of the gait. Each of these subtasks, TLC^i is synthesized out of a set of activated behaviour primitives, $\{\mathcal{B}^i_j\}$. A kinematic behaviour primitive, $\mathcal{B}^i_j$ of bipedal locomotion is defined as the regulation of the position or orientation of a specific part of the biped, θ^i_j as per the regulation goal, $\Theta^i_j(V_{fc}, \sigma_{Gd})$ during the respective $\mathbb{H}^i_{es}$. This kinematic behaviour can be executed using an equivalent desired joint space motion, $q(t)$. By differentiating, the velocity form expression for $\mathcal{B}^i_j$

can be given as,

$$\dot{\theta}^i_j = H^i_j(q)\dot{q} \tag{4.1}$$

where $H^i_j(q)$ represents the Jacobian of the behaviour primitive. On further differentiating, we get the acceleration form expression for the behaviour primitive as,

$$\text{i.e.} \quad \ddot{\theta}^i_j = H^i_j\ddot{q} + \dot{H}^i_j\dot{q} \tag{4.2}$$

Based on the approach reported in [57], the above basic task expression can be converted into an attractor type closed loop expression as,

$$H^i_j\ddot{q}^d + \dot{H}^i_j\dot{q} = k^i_{pj}\left(\Theta^i_j - \theta^i_j(q)\right) - k^i_{vj}\dot{\theta}^i_j(q,\dot{q}) \tag{4.3}$$

This can be represented as a standard PD type behaviour primitive in the form,

$$H^i_j(q)\ddot{q}^d = B^i_j(q,\dot{q}) \tag{4.4}$$

where,
$$B^i_j(q,\dot{q}) = k^i_{pj}\left(\Theta^i_j - \theta^i_j(q)\right) - k^i_{vj}\dot{\theta}^i_j(q,\dot{q}) - \dot{H}^i_j\dot{q} \tag{4.5}$$

The constants, k^i_{pj} and k^i_{vj} can be selected to assign the desired closed loop bandwidth and damping factor for the locomotion behaviour. The behaviour primitives are to be designed to generate the basic kinematic behaviour modes similar to those observed in human walk. A similar approach for modelling behaviour primitive is given in [74].

The distinguishing features of behaviour primitives when expressed in closed loop regulator form compared to stiff path tracking type behaviours can be explained based on the example of a second order behaviour primitive imparted on an inverted pendulum.

4.4.1.1 Induced and Imposed behaviours: Architecture and properties

Consider an inverted pendulum having a mass m, length l and actuator torque T_p acting in counter clockwise direction about the pivot point to produce a deflection, q with respect to horizontal direction as shown in Fig 4.3. Its dynamics can be represented by the differential equation,

$$ml^2\ddot{q} + b\dot{q} + mgl\cos q = T_p \tag{4.6}$$

where b is the pivot point damping coefficient. Let us consider a kinematic behaviour primitive possessing a second order dynamics, (ω_b, ζ_b) and a preset goal orientation, $\Theta =$

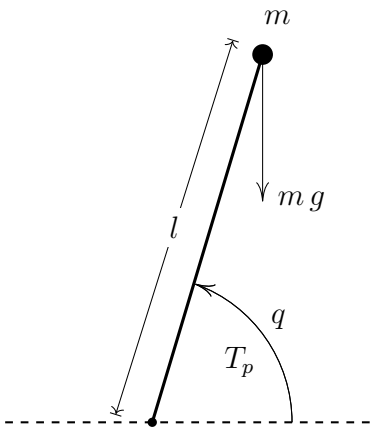

Figure 4.3: Inverted pendulum for behaviour demonstration

θ^o represented as,

$$\ddot{\theta} = \omega_b^2(\theta^o - \theta) - 2\zeta_b\omega_b\dot{\theta} \tag{4.7}$$

The behaviour response will evolve starting from any initial state, $\big(\theta(0), \dot{\theta}(0)\big)$ to reach the final goal, $(\theta^o, 0)$ according to the second order dynamics characterized by (ω_b, ζ_b). There are two ways to impart this behaviour primitive on the inverted pendulum. One approach is by direct induction of behaviour on the mechanical structure of inverted pendulum by closed loop state feedback. This is achieved by modifying (4.7) and (4.6) as follows:

$$\ddot{q}^d = \omega_b^2(\theta^o - q) - 2\zeta_b\omega_b\dot{q} \tag{4.8}$$

$$T_p^d = ml^2\ddot{q}^d + b\dot{q} + mgl\cos q \tag{4.9}$$

On substituting the computed torque command, T_p^d for T_p in (4.6), the inverted pendulum dynamics for any $m > 0$ can be derived as,

$$\ddot{q}(t) = \omega_b^2(\theta^o - q(t)) - 2\zeta_b\omega_b\dot{q}(t) \tag{4.10}$$

which makes the inverted pendulum to behave as a second order closed loop regulator with parameters (ω_b, ζ_b) to reach the final goal of $q = \theta^o$. Comparison of (4.7) and (4.10) reveals that the dynamic characteristics of the behaviour primitive is directly induced on the inverted pendulum.

The second approach for imparting the behaviour primitive is by direct imposition.

This works on the basis of enforcing the behaviour path, $\theta(\alpha)$ on the pendulum angle, $q(\alpha)$ where α is an intermediate monotonic function of time t, to express the control law in time invariant form. The required control torque to be applied on the inverted pendulum can be written in the form,

$$T_p^d = T_p^* + T_{p\epsilon} \tag{4.11}$$

where T_p^* is the feed forward computed control torque for driving the pendulum angle, $q(\alpha)$ along the behaviour path, $\theta(\alpha)$ and $T_{p\epsilon}$ is the feedback control torque responsible for inducing an attractor property for the path $\theta(\alpha)$ by way of exponentially stabilizing against local perturbations. To simplify the control law, let us assume that $\alpha(t) = t$ and the expression for the first term of the control torque can be given as,

$$T_p^* = ml^2\ddot{\theta} + b\dot{q} + mgl\cos q \tag{4.12}$$

where $\ddot{\theta}$ is given by (4.7). If we would like to induce a second order attractor dynamics for the path $\theta(\alpha)$, the expression for the second term can be given as,

$$T_{p\epsilon} = ml^2\left(\omega_a^2(\theta - q) + 2\zeta_a\omega_a(\dot{\theta} - \dot{q})\right) \tag{4.13}$$

which ensures asymptotic convergence of $q(t)$ to $\theta(t)$ as per the second order dynamics characterized by (ω_a, ζ_a). Normally, ω_a is selected much larger than ω_b to ensure rapid settling of the path error, $\theta(\alpha) - q(\alpha)$ in comparison with the transients of the path reference, $\theta(t)$. By substituting (4.11)-(4.13) in (4.6) for T_p, we get the expression for the imposed behaviour primitive on the inverted pendulum as,

$$\ddot{q} = \ddot{\theta} + \omega_a^2(\theta - q) + 2\zeta_a\omega_a(\dot{\theta} - \dot{q}) \tag{4.14}$$

which represents a stiff path tracking control imposing the reference trajectory, θ on q at any time. The expression is applicable for any reference path, θ as long as the corresponding $\dot{\theta}$ and $\ddot{\theta}$ are available for real time control. Comparison of (4.7) and (4.14) reveals that the dynamics of the imposed behaviour characterized by (ω_a, ζ_a) has no direct correlation with the intrinsic dynamics of the reference behaviour primitive.

By architecture, induced behaviour is associated with primitives having preset regulation goals whereas imposed behaviour is associated with primitives having preset reference paths for tracking. Hence imposed behaviour type task is not suitable for bipedal locomotion control, in the presence of unexpected disturbance or obstacles, where a priori path planning is not feasible. Another disadvantage is its inability to get coordinated with un-

planned upper body tasks. Moreover, the relatively large control bandwidth, ω_a needed to ensure close tracking of reference path has all the associated problems like, low compliance during environmental interaction, control-structure interaction with link flexible modes, and less immunity to sensor noise. However, a repetitive task with imposed behaviour characteristics can have provably stable periodic stability to its merit since the target orbit can be selected a priori as a stable one. Stiff path tracking type control algorithms like HZD possess the demerits and merits of imposed behaviour primitives mentioned above.

In HyDAC algorithm, the unplanned or unexpected locomotion requirements are handled locally in TLC by a set of induced behaviours without any need for changing the supervisory control logic operating in the higher level, SLC. On the other hand, the guaranteed stability of imposed type behaviours is indirectly achieved in HyDAC since it uses the preset SLC parameters obtained by optimizing over a given set of induced behaviour parameters of TLC while the biped walks over the terrain with known range of parameters. This control structure of HyDAC fits well with the locomotor behaviour architecture observed in vertebrates shown in Fig 4.1, where the behaviour primitives are embedded within the neuro-anatomic structure of locomotor system.

4.4.1.2 Joint acceleration as the basic control variable

Out of $q, \dot{q}, \ddot{q}, \Gamma$, which is the best choice as the domain variable for behaviour formulation and task level control optimization? The selection goes naturally to joint acceleration vector, $\ddot{q}$ based on the following arguments.

1. Biped can be visualized as a higher order dynamical system made out of nonlinearly coupled multiple second order subsystems driven by multiple joint torques. Both $q, \dot{q}$ are states of the biped and hence cannot be changed instantaneously by joint torquers and cannot be the independent variable for TLC optimization.

2. The biped being a floating base robot with unilateral contact force constraint, it is of paramount importance to control joint accelerations to take care of inertial forces.

3. Various contact force constraints can be equivalently transformed into joint acceleration constraints through the system dynamics equation.

4. Different task requirements in terms of position, velocity and force, all can be expressed in terms of joint acceleration variable.

5. As it is desirable to follow induced behaviour architecture, the position and velocity requirements of the behavioural modes are to be expressed in closed loop attractor

form, which generates the corresponding acceleration requirement. Behaviours expressed as stiff tracking of a predefined path for a specific position type task should be avoided as it cannot be dynamically coordinated with other tasks.

6. Another advantage of local optimization with acceleration variable is that only the active constraints are to be considered at any instant and the same can be put as equality constraints for getting direct analytic solution for HyDAC.

4.4.2 Supervisory level control (SLC)

The supervisory level control (SLC) is responsible for enforcing a specified dynamic coordination structure for the autonomous evolution of walking gait out of the dynamically interacting primitives of the task level control. The specified dynamic coordination structure is imposed on the biped hardware through the execution of the following functions:

1. Selection of a minimal set of hybrid event states, $\mathbf{H}_{es} := \{\mathbb{H}^{i}_{es}\}$ in proper sequence required for steering the bipedal locomotion as per the specified locomotion pattern while satisfying the requirements for the cyclic stability of gait.

2. C_{SF} update and detection of the current hybrid event state $\mathbb{H}^{i}_{es}$ based on the current $\mathbb{D}_{es}$ and C_{SF}.

3. Activation of the minimal set of behaviour primitives to drive the biped during the current hybrid event state, $\mathbb{H}^{i}_{es}$.

4. Assignment of regulation goals, $\Theta^{i}_{j}(V_{fc}, \sigma_{Gd})$ for each of the activated behaviour primitive.

5. Assignment of the performance parameters like bandwidth, damping factor, intermediate saturation limits etc. for each of the activated behaviour primitive for implicitly carrying out dynamic coordination among them.

6. Partitioning of the biped joint acceleration vector, $\ddot{q}$ among certain activated primitives to provide kinematic decoupling between them as discussed, for example, in Section 5.2.3.3

7. Selection of a specific group of tasks for prioritization over the rest when there is deficiency for actuated DoF under contact force constraints.

Such a SLC-TLC type hierarchical control structure is inevitable for moving machines with cyclically changing kinematic and dynamic structures. When there is a deficiency of control DoF due to the activation of virtual contact force constraints, HyDAC cannot execute all the pre-assigned behaviour primitives during the respective $\mathbb{H}^{i}_{es}$. Under such situation, SLC has to judiciously select the minimum number of behaviour primitives with proper relative weighting and prioritization.

4.4.3 Does HyDAC belong to Autonomous or Automatic Control ?

Since "automatic control" and "autonomous control" seem to have a wide range of definitions with confusing similarities, it is appropriate to state how these terms are used in the context of the thesis. Both terms refer to controlled processes that may be executed independently from start to finish without any human intervention. Both uses automatic feedback control for its basic task-level execution phase. Hence distinction is to be made only with respect to the decision making or supervisory level control and beyond. Automated processes simply replace routine manual processes with software or hardware elements, which follow a step-by-step sequence that may still include human participation. It normally uses if-then-else rules for decision making based on the values of system variables, environmental conditions and external commands. Autonomous processes, on the other hand, have higher level goal of emulating human processes rather than simply replacing them. It is able to take independent decisions based on real time events, being aware of its immediate and future effects. Table 4.1 gives definitions of the terms automatic and autonomous given by Oxford English dictionary.

Thus the adjective, "automatic" is suitable for "self-acting processes" whereas "autonomous" is suitable for "self-governing processes" having a higher level of independency. Let us look at the usage of autonomy in the context of bipedal walking control also. The domain of "walking control" for the current discussion is confined to the automation of walking over an uncertain terrain without fall and rejecting any unexpected external disturbance force. The global commands in terms of direction of walk, velocity of walk and any specific walking styles, all are assumed to be commanded by a dedicated motion planning unit which is external to walking control unit. To have a stable walk over an uneven terrain having foothold constraints, a minimum of two-step planning is essential. The decision for turning around obstacle, preparing for stepping up or down and even for stopping, all can be executed within two walking steps. The locomotion control schemes developed so far can be broadly classified into three groups in this context: One group uses pre-planned

Table 4.1: Definitions from Oxford English dictionay

Automatic
Adjective
(of a device or process) working by itself with little or no direct human control.
'an automatic kettle that switches itself off when it boils'
'calibration is fully automatic'
Origin: Mid 18th century: from Greek automatos 'acting of itself' (see automaton) + -ic
Autonomous
Adjective
Denoting or performed by a device capable of operating without direct human control.
'autonomous underwater vehicles'
'the spread of autonomous robotic weaponry'
'tests indicate that autonomous driving will cut fuel consumption by up to five per cent'
Origin: Early 19th century: from Greek autonomos 'having its own laws' + -ous

trajectory or joint space orbits proven in principle to meet the stability and performance requirements under the predicted walking situations. The other group does online correction for the locomotion control over the pre-planned control to take care of the uncertainties to certain extent.The third group employs compliant control schemes to induce suitable behaviour pattern for biped as it proceed forward interacting with the terrain under gravity pull. The last group which does not rely on any pre-planned trajectory or orbit can be classified as "autonomous control" since all the walking performance and stability related decisions are taken in a self-governing manner independent of any external influence in the form of pre-planned trajectory or control force. The ideal example of autonomous bipedal walking is passive dynamics based control [24, 75, 25, 26] and the term "autonomous biped based on passive dynamic walking" has been used in the pioneering work of Wisse [26]. As the name indicates, passive dynamics based walking in its simplest form does not use any actuators to implement any externally dictated control low, rather uses only the passive dynamics of inverted pendulum motion over a downward slope along with ground impact forces at the end of each walking gait to stabilize the trajectory. However, this lacks stability robustness and not suitable for more complex mechanisms with human-like upper body. Hybrid-state driven autonomous control (HyDAC) can be considered as an extension of the passive dynamics concept to a complex humanoid with actuation to ensure stability robustness and disturbance rejection. The behaviour primitives for each hybrid event state are embedded in the supervisory level control of HyDAC and the right set of behaviour primitives are activated as per the current hybrid event state. The task level control imple-

ments the activated set of behaviour primitives subject to various real-time constraints using multiple sensor-actuation control loops without actually tracking any offline generated gait trajectory. The actual trajectory evolves out of the interaction of the biped with the terrain and disturbance forces. HyDAC in its perfect form will have all the necessary behaviour primitives to enable the biped to walk forward over an uneven terrain assuming that the terrain parameters for the two subsequent steps are made available by the embedded sensor unit. Thus HyDAC belongs to the basic "autonomous control" class with respect to its self-governing capacity to select and implement the right structure of control for different realistic situations of walking without external interference. On the other hand, the "trajectory following type controls" belong to the "automatic control class" as they simply follow the commanded trajectory automatically without any online decision making. Higher levels of intelligence can be incorporated in HyDAC using additional hierarchical control levels to update SLC parameters using learning architecture.

4.4.4 Behaviour prioritization through null space projection

The general scheme for assigning hierarchical priority in a multibehaviour framework is by projecting the least norm solution of lower priority behaviours onto the null space of higher priority behaviours as proposed by Sentis and Khatib [76, 77]. However, a more efficient scheme is reported by Fabrizio Flacco et al. [78] and Siciliano and Slottine [79], where the lower priority behaviours are solved for least norm, least square solution from the null space of higher priority behaviours to meet the residual behaviour objective. This approach achieves what is the best possible for the lower priority behaviours once the higher priority behaviours have been executed. However, we should be careful to handle the rank deficiency of the modified Jacobian matrix of the lower priority behaviours as it may lead to unbounded solution. The major application of prioritization in HyDAC is in obtaining the constraint consistent optimal solution for the task level behaviours as will be discussed in Section 4.9.

4.5 Formulation of Virtual constraints

HyDAC makes use of nonholonomic type virtual constraints to avoid violation of limits on ground contact forces and actuator torques and also to implement highest priority behaviours such as GCoP regulation. The virtual constraints used in HyDAC has the same meaning as those used in HZD framework [10], but for a different purpose. HyDAC makes

use of nonholonomic type virtual constraints on the generalized acceleration variable, $\ddot{q}$ to ensure consistency of the executed locomotion behaviours with respect to the force limits and torque limits as mentioned. In contrast, HZD imposes holonomic type virtual constraints on the generalized position variable, q during a priori gait synthesis to execute the locomotion task as a coordinated behaviour assuming that it will hold good during the actual bipedal walk without constraint violation.

4.5.1 GCoP or ZMP constraint

HyDAC employs direct regulation of GCoP during FF state for achieving important control objectives like regulation of forward velocity (Section 4.6) during dynamic walking or stabilizing the biped posture during stance condition. The direct online regulation of GCoP

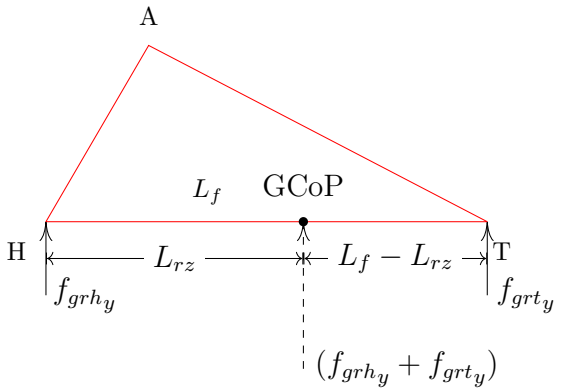

Figure 4.4: Moments of ground contact forces balancing about GCoP of reference foot

for planar biped is achieved by posing the regulation of $x_{cop}(t)$ along certain desired trajectory, $x^d_{cop}(t)$ as a virtual nonholonomic constraint while $x_{rh} < x^d_{cop}(t) < x_{rt}$. The first step for the same is to convert the x^d_{cop} requirement into the desired contact force ratio,

$$\rho^d = \frac{f_{grh_y}}{f_{grt_y}} \tag{4.15}$$

assuming that there are only two ground contact points for the reference foot in FF state as shown in Fig 4.4.

Equating the sum of moments due to f_{grh_y} and f_{grt_y} about the GCoP (or ZMP) to zero, we obtain the expression for ρ^d as,

$$\rho^d = \frac{L_f}{L_{rz}} - 1 \text{ where } L_{rz} = \sqrt{(x^d_{cop} - x_{rh})^2 + (y^d_{cop} - y_{rh})^2} \tag{4.16}$$

L_{rz} is the distance between the GCoP and the reference foot heel along the foot sole and $y^d_{cop} = y_G(x^d_{cop})$ is obtained from (3.5). The second step is to pose the regulation of ρ^d as a virtual nonholonomic constraint of the form,

$$H_{cop}(q)\ddot{q} = B_{cop}(q, \dot{q}),\ H_{cop} \in \mathbb{R}^{1\times n_J}, B_{cop} \in \mathbb{R}^1 \tag{4.17}$$

for incorporating in (3.22). Based on (3.23), the passive underactuated dynamics of the biped during FF state can be written as,

$$D_p\ddot{q} + \mathcal{G}_p = J'_{grh_p}F_{grh} + J'_{grt_p}F_{grt} \tag{4.18}$$

The R.H.S. of (4.18) can be further expanded to get,

$$\begin{aligned} D_p\ddot{q} + \mathcal{G}_p =& J'_{grh_{px}}f_{grh_x} + J'_{grt_{px}}f_{grt_x} \\ &+ J'_{grh_{py}}f_{grh_y} + J'_{grt_{py}}f_{grt_y} \end{aligned} \tag{4.19}$$

where $J'_{grh_p} = \begin{bmatrix} J'_{grh_{px}} & J'_{grh_{py}} \end{bmatrix}$. Since the heel and toe of the reference foot are rigidly connected and and they lie along $\overrightarrow{O_gX_g}$, the effect of f_{grh_x} and f_{grt_x} on the biped joints will be similar which means that $J'_{grt_{px}} = J'_{grh_{px}}$. Hence (4.19) can be simplified to get,

$$\begin{aligned} D_p\ddot{q} + \mathcal{G}_p =& J'_{grh_{px}}(f_{grh_x} + f_{grt_x}) \\ &+ J'_{grh_{py}}f_{grh_y} + J'_{grt_{py}}f_{grt_y} \end{aligned} \tag{4.20}$$

Since ρ^d is independent of the tangential components of ground contact forces, we can project (4.20) to the space orthogonal to the range space of $J'_{grh_{px}}$ without loss of rank of the required constraint. The space orthogonal to the range space of $J'_{grh_{px}}$ is the same as the null space of $(J'_{grh_{px}})'$ and hence the required projection matrix is obtained as [80]

$$P_{z1} = I_3 - J^+_{rx}J_{rx},\ J_{rx} = (J'_{grh_{px}})' \tag{4.21}$$

Thus by premultiplying (4.20) by P_{z1}, the first term on the R.H.S. will vanish to yield,

$$P_{z1}\left[D_p\ddot{q} + \mathcal{G}_p\right] = P_{z1}\left[J'_{grh_{py}}f_{grh_y} + J'_{grt_{py}}f_{grt_y}\right] \tag{4.22}$$

Assuming that the GCoP constraint is active, $f_{grh_y} = \rho^d f_{grt_y}$ and hence (4.22) can be

further simplified to get,

$$P_{z1}\left[D_p\ddot{q}+\mathcal{G}_p\right]=P_{z1}\left[\rho^d J'_{grh_{py}}+J'_{grt_{py}}\right]f_{grt_y} \tag{4.23}$$

$$=J'_z f_{grt_y},\ \forall f_{grt_y}>0 \tag{4.24}$$

$$\text{where } J'_z=P_{z1}\left[\rho^d J'_{grh_{py}}+J'_{grt_{py}}\right] \tag{4.25}$$

Since ρ^d depends only on the force ratio as per (4.15) and independent of the actual value of f_{grt_y}, it is necessary to get rid of the dependency of (4.24) on f_{grt_y} to get the minimal rank algebraic expression for the GCoP constraint. This can be done by projecting both sides of (4.24) to the null space of J_z using the projection matrix, $P_{z2}=I_3-(J_z)^+(J_z)$ which leads to,

$$P_{z2}P_{z1}\left(D_p\ddot{q}+\mathcal{G}_p\right)=0 \tag{4.26}$$

This can be expressed in the standard form of (4.17) by using the substitutions,

$$H_{cop}=P_{z2}P_{z1}D_p, B_{cop}=-P_{z2}P_{z1}\mathcal{G}_p \tag{4.27}$$

Even though H_{cop} and B_{cop} obtained from (4.27) have three rows, it represents only a rank-1 constraint. Hence the same can be reduced to equivalent single row elements as defined in (4.17) using the SVD based regularization approach mentioned in Appendix A. If the generalized acceleration, $\ddot{q}$ satisfies the nonholonomic constraint expressed by (4.26), the desired force ratio ρ^d and hence the desired location of GCoP will be ensured.

4.5.2 Normal contact force limit constraint

The ground contact force is not explicitly controlled in HyDAC during the normal course of operation as the total DoF of the actuated joints is only just sufficient to meet the kinematic motion requirements as will be explained in Section 4.8.5. This can lead to violation of unilateral force constraint on one side and high value of contact force generating large upward acceleration on the other side. HyDAC handles this situation by putting explicit constraints on contact force as and when the violation is detected. Let us represent the sum of normal components of ground contact forces expressed in $\{O_g\}$ frame by f_{gy}. The upper bound of f_{gy} is represented by f_{gy+} and the lower bound of f_{gy} is represented by f_{gy-}. f_{gy+} is assigned a constant value of 4000κ with $\kappa=M_{bp}g/(830)$ to limit the upward acceleration and f_{gy-} is assigned a constant value of 200κ to ensure unilateral ground contact state of reference foot with sufficient margin. The upper force bound on

f_{gy} is normally active just after heel strike and during the subsequent hip rise period. A larger value of f_{gy+} will lead to excess build-up of upward velocity, V_{comy} resulting in subsequent activation of f_{gy-} limit (often associated with the activation of friction cone limit also) for longer duration. On the other hand, a smaller value of f_{gy+} will reduce the rate of hip rise after heel strike especially while climbing over large slopes. Moreover, a smaller value of f_{gy+} will demand excess actuation of heavy links like torso for reducing f_{gy} through inertial forces, thereby necessitating higher actuator torque capacity. The lower force bound becomes normally active when the control algorithm tries to reduce the excess upward velocity of biped-CoM. Thus shaping of f_{gy} bounds plays an important role in the generation feasible gait trajectory with respect to vertical motion.

4.5.2.1 Normal force limit constraint for HR-SW and TR-SW states

The normal contact force, f_{gy} tries to cross the upper bound, f_{gy+} just after heel strike event and tries to cross the lower bound, f_{gy-} prior to foot-off event in every walking gait. Consider the situation when f_{gy} is either greater than f_{gy+} or less than f_{gy-} during any control computation step necessitating to impose the normal force limit constraint, $f_{gy} = f^d_{gy}$ where f^d_{gy} equals either f_{gy+} or f_{gy-} based on the active limit. For single point contact state, only one of the contact forces out of F_{grh} or F_{grt} will be present and hence the passive dynamics given in (4.18) can be simplified to

$$D_p\ddot{q} + \mathcal{G}_p = J'_{gr_p}F_{gr} = J'_{gr_{px}}f_{gr_x} + J'_{gr_{py}}f_{gr_y} \tag{4.28}$$

$$= J'_{gr_{px}}f_{gr_x} + J'_{gr_{py}}f^d_{gy} \tag{4.29}$$

where $J'_{gr_p}F_{gr}$ represents either $J'_{grh_p}F_{grh}$ or $J'_{grt_p}F_{grt}$ depending on the contact state. To get rid of the dependency of (4.29) on f_{gr_x}, both sides of the equation is projected onto the orthogonal space of $J'_{gr_{px}}f_{gr_x}$ using the projection matrix, $P_{Nx} = I_3 - J^+_{gr_{px}}J_{gr_{px}}$ to get,

$$P_{Nx}\left(D_p\ddot{q} + \mathcal{G}_p\right) = P_{Nx}\left(J'_{gr_{px}}f_{gr_x} + J'_{gr_{py}}f^d_{gy}\right) = P_{Nx}J'_{gr_{py}}f^d_{gy} \tag{4.30}$$

$$\text{or } P_{Nx}D_p\ddot{q} = P_{Nx}\left(J'_{gr_{py}}f^d_{gy} - \mathcal{G}_p\right) \tag{4.31}$$

which is in the general form (3.22) of nonholonomic constraint. This is a rank-2 constraint equation having three rows and its minimal row formulation can be obtained based on SVD procedure as discussed early. Out of the rank-2 constraint, one of the ranks is attributed to the normal force limit and the other rank is attributed to the passive rotation constraint

about the active single contact point.

4.5.2.2 Normal force limit constraint for FF-SW state

The derivation of normal force limit constraint for single point contact state can be extended to FF-SW state of biped under the assumption that GCoP constraint is active and the relation (4.15) is holding good. When the normal force limit constraint is active with *FyrFlg*=1, the sum of normal components of ground contact forces has to be constrained to $f_{gy}^{d} = f_{gy+}$ or f_{gy-} depending on the case of upper bound or lower bound. Under this condition, the values of individual components of normal force can be given as,

$$f_{grh_y} = \frac{\rho^d}{1+\rho^d} f_{gy}^{d},\ f_{grt_y} = \frac{1}{1+\rho^d} f_{gy}^{d} \tag{4.32}$$

Combining (4.20) and (4.32), the passive underactuated dynamics of the biped can be written as

$$\begin{aligned} D_p \ddot{q} + \mathcal{G}_p =& J'_{grh_{px}}(f_{grh_x} + f_{grt_x}) \\ &+ \left(\rho^d J'_{grh_{py}} + J'_{grt_{py}}\right) \frac{f_{gy}^{d}}{1+\rho^d} \end{aligned} \tag{4.33}$$

We can get rid of the first term on the R.H.S. by projecting (4.33) to the null space of $(J'_{grh_{px}})'$ which leads to,

$$P_{yr}\left(D_p \ddot{q} + \mathcal{G}_p\right) = P_{yr}\left(\rho^d J'_{grh_{py}} + J'_{grt_{py}}\right) \frac{f_{gy}^{d}}{1+\rho^d} \tag{4.34}$$

$$\text{where, } P_{yr} = I_3 - \left((J'_{grh_{px}})'\right)^{+} (J'_{grh_{px}})' \tag{4.35}$$

Hence the force limit constraint in FF-SW state can be expressed in the standard form of (3.24) as,

$$H_{c_n} = H_{yr} = P_{yr} D_p \tag{4.36}$$

$$B_{c_n} = B_{yr} = -P_{yr}\mathcal{G}_p + P_{yr}\left(\rho^d J'_{grh_{py}} + J'_{grt_{py}}\right) \frac{f_{gy}^{d}}{1+\rho^d} \tag{4.37}$$

4.5.3 Joint torque limit constraint

This is a physical constraint associated with the speed-torque boundary of the torque motors driving the biped joints and the state of the flag, *TdjFlg* is used to activate the corresponding

constraint in HyDAC formulation. Assuming the simplest case of bilateral symmetry for the torque limit with extreme values of $\pm\Gamma_{j+}$ for Γ_{d_j}, the virtual nonholonomic constraint corresponding to the jth joint drive torque limit can be derived from (3.1) as [80],

$$D_j\ddot{q} + \mathcal{G}_j = \Gamma_{j+}\,\mathrm{sgn}(\Gamma_{d_j}^{u}) + J'_{cj}F_c \tag{4.38}$$

where $\mathrm{sgn}(\Gamma_{d_j}^{u})$ is the sign of the unconstrained value of jth joint torque command. Projection of (4.38) to the null space of $(J'_{cj})'$ and converting to the standard nonholonomic form of (3.22) gives,

$$H_{\Gamma j} = P_{\Gamma j}D_j,\ B_{\Gamma j} = P_{\Gamma j}\left(\Gamma_{j+}\,\mathrm{sgn}(\Gamma_{d_j}^{u}) - \mathcal{G}_j\right) \tag{4.39}$$

$$\text{where, } P_{\Gamma j} = 1 - (J'_{cj})'^{+}(J'_{cj})' \tag{4.40}$$

4.5.4 Friction cone constraint

Friction cone has to be incorporated as an active equality constraint in HyDAC if *FgrFlg* =1. Friction cone constraint can be expressed in the general form $H_{cr}\ddot{q} = B_{cr}$ consuming only 1-DoF from the joint acceleration vector space as given in [80]. Separate expressions are derived for single point contact cases like HR or TR states of reference foot and for the FF state of reference foot.

4.5.4.1 Friction cone constraint for HR-SW and TR-SW states

For single point contact state, only one of the contact forces out of F_{grh} or F_{grt} will be present and hence the passive dynamics given in (4.18) can be simplified as in (4.28). Whenever the computed ground contact force during the control syntheis iteration is found to be violating the friction cone bounds, the same is to be kept within the friction cone as stated in (3.10) with a safety margin of 5% by imposing a virtual constraint of ,

$$f_{gr_x} = 0.95\mu_c f_{gr_y}\mathrm{sgn}(f_{gr_x}^{u}) = \psi_{cs}f_{gr_y} \tag{4.41}$$

where $\mathrm{sgn}(f_{gr_x}^{u})$ is the sign of the unconstrained value of f_{gr_x} and $\psi_{cs} = 0.95\mu_c\mathrm{sgn}(f_{gr_x}^{u})$. As HyDAC ensures unilateral force constraint for the normal component of contact force, $f_{gr_y} > 0$ under all walking phases. Substitution of f_{gr_x} in terms of f_{gr_y} in (4.28) gives,

$$D_p\ddot{q} + \mathcal{G}_p = \left(\psi_{cs}J'_{gr_{px}} + J'_{gr_{py}}\right)f_{gr_y} = J'_{frl}f_{gr_y},\ \forall\, f_{gr_y} > 0 \tag{4.42}$$

In order to make the R.H.S. of (4.42) independent of f_{gr_y}, it is necessary to project both sides of the equation to the null space of $J_{fr1} = \left(\psi_{cs} J'_{gr_{px}} + J'_{gr_{py}}\right)'$ using the projection matrix, $P_{fr1} = I_3 - (J_{fr1})^+(J_{fr1})$ which leads to,

$$P_{fr1}\left(D_p \ddot{q} + \mathcal{G}_p\right) = 0 \tag{4.43}$$

This can be expressed in the standard form of (3.24) by using the substitutions,

$$H_{fr1} = P_{fr1} D_p, B_{fr1} = -P_{fr1}\mathcal{G}_p \tag{4.44}$$

The 3-row elements (H_{fr1}, B_{fr1}) can be reduced to its equivalent 1-row elements as in the previous section without affecting its rank.

4.5.4.2 Friction cone constraint for FF-SW state

Assuming that the GCoP constraint is active during the FF-SW state of biped, the underactuated part of system dynamics can be obtained by combining (4.20) and (4.15) which can be written as,

$$\begin{aligned} D_p \ddot{q} + \mathcal{G}_p =& J'_{grh_{px}}(f_{grh_x} + f_{grt_x}) \\ &+ \left(\rho^d J'_{grh_{py}} + J'_{grt_{py}}\right) f_{grt_y} \end{aligned} \tag{4.45}$$

As mentioned earlier, when the friction cone constraint is active, we have to ensure that

$$\begin{aligned} f_{grh_x} + f_{grt_x} &= 0.95\mu_c(\rho^d + 1) f_{grt_y} \mathrm{sgn}(f^u_{grh_x} + f^u_{grt_x}) \\ &= \psi_{cf} f_{grt_y} \end{aligned} \tag{4.46}$$

Combining (4.45) and (4.46),

$$\begin{aligned} D_p \ddot{q} + \mathcal{G}_p &= \left(\psi_{cf} J'_{grh_{px}} + \rho^d J'_{grh_{py}} + J'_{grt_{py}}\right) f_{grt_y} \\ &= J'_{fr2} f_{grt_y} \end{aligned} \tag{4.47}$$

Following the steps of the previous section, the friction cone constraint can be expressed in the standard form of (3.22) as,

$$H_{fr2} = P_{fr2} D_p,\ B_{fr2} = -P_{fr2}\mathcal{G}_p \tag{4.48}$$

$$\text{where } P_{fr2} = I_3 - (J_{fr2})^+(J_{fr2}) \tag{4.49}$$

4.6 Forward velocity control by Direct Regulation of GCoP

For a floating body, multilink robot like biped, the best choice of the representative point for controlling the forward velocity is the CoM. Representing the inertial frame coordinates of biped-CoM by (x_{com}, y_{com}), the motion dynamics of the biped along $\overrightarrow{O_0X_0}$ can be written based on the first row of (3.1) as,

$$D_1\ddot{q} + \mathcal{G}_1 = f_{cx} = f_{rhx} + f_{rtx} = M_{bp}\ddot{x}_{com} \tag{4.50}$$

which can be formulated as a virtual nonholonomic constraint of the form (3.22) with $H_{c_n} = D_1$ and $B_{c_n} = M_{bp}\ddot{x}^d_{com} - \mathcal{G}_1$ where $\ddot{x}^d_{com}$ is designed to meet the required regulation of forward velocity, $\dot{x}_{com} = V_{comx}$ with respect to a specific value of V_{fc}. But the explicit control of f_{cx} as per the above virtual constraint will dynamically interfere with other motion control primitives which are essential for the regulation of postural configuration states. Hence it is necessary to device a less interfering approach for V_{comx} regulation which can coexist with the posture regulation primitives. This is the motivation behind the proposed approach for V_{comx} control by direct regulation of GCoP. The GCoP regulation scheme will not constrain the ground contact force explicitly, rather only modulates its CoP location in the ground plane to utilize the gravity moment about GCoP to achieve the required velocity regulation. GCoP is also referred to as ZMP in the literature as long as the former remains within the foot support polygon. The direct regulation of ZMP[4] has been reported in the literature for bipedal walking control to avoid unexpected rotation of the support foot [31]. However, to the best of authors' knowledge, it is the first time that the same has been proposed for the regulation of forward velocity .

The proposed forward velocity control algorithm (FVCA) makes use of an inverted pendulum model of planar biped with its total mass, M_{bp} concentrated at the biped-CoM location, (x_{com}, y_{com}). M_{bp} is assumed to be supported by a massless link pivoted at the GCoP of the biped as shown in Fig 4.5. The pendulum length, l_c and pendulum orientation, θ_c are calculated online from the measured values of biped joint angles, q and GCoP location, (x_{cop}, y_{cop}) using the equations,

$$l_c^2 = (x_{cop} - x_{com})^2 + (y_{cop} - y_{com})^2 \tag{4.51}$$

$$tan\theta_c = \frac{x_{cop} - x_{com}}{y_{com} - y_{cop}} \tag{4.52}$$

[4]However, the direct ZMP regulation is embedded within an orbit synthesized a priori in the cited literature.

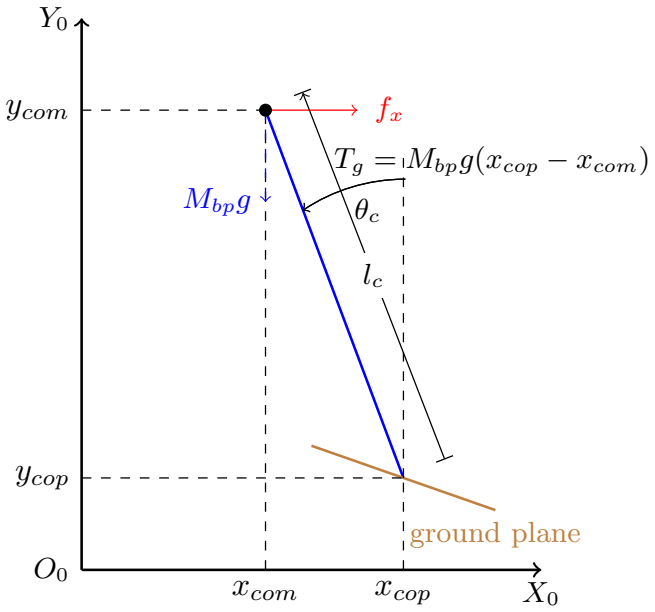

Figure 4.5: Inverted pendulum model of planar biped

We make an assumption that the force acting on the biped-CoM which generates the control torque about the GCoP is only due to $M_{bp}g$ acting vertically downward as shown in Fig 4.5. This is true as long as there is no external force acting on biped other than ground reaction force and gravity force. In order to steer the inverted pendulum mass M_{bp} along the forward direction, $\overrightarrow{O_0X_0}$ with an acceleration, $\ddot{x}^d_{com}$, we have to exert a forward force of $f_x = M_{bp}\ddot{x}^d_{com}$ on it as shown in Fig 4.5. This is equivalent to applying a control torque of $T_c = -l_c cos\theta_c f_x$ about the pivot point, GCoP. The control torque due to the gravitation force about GCoP is given by, $T_g = M_{bp}g(x_{cop} - x_{com})$. Equating T_c and T_g, we get the following expression for the desired value of x_{cop}.

$$x^d_{cop} = x_{com} - \frac{l_c}{g} cos\theta_c \ddot{x}^d_{com} \tag{4.53}$$

There are two parts for FVC algorithm. The first part is to derive the required value of $\ddot{x}^d_{com}$ online. If x_{com} has to track a desired trajectory, x^d_{com} with an induced second order type trajectory attractor dynamics [57], the desired forward acceleration can be obtained as

$$\ddot{x}^d_{com} = \omega_v^2 \left(x^d_{com} - x_{com} \right) + 2\zeta_v \omega_v (\dot{x}^d_{com} - \dot{x}_{com}) \tag{4.54}$$

where ω_v is the bandwidth and ζ_v is the damping factor for the trajectory attractor. However, to realize a stable dynamic walking algorithm extending down to even a stable stance

condition for $V_{fc} = 0$ requires a hybrid state based definition for $\ddot{x}^{d}_{com}$. For $V_{fc} = 0$, we should ensure that the biped gets stabilized to the mid stance posture which demands stabilization of the equivalent inverted pendulum in position mode about some equilibrium point, say $x_{rc} = (x_{rh} + x_{rt})/2$. This leads to,

$$\ddot{x}^{d1}_{com} = \omega_{\nu}^{2}\left(x_{rc} - x_{com}\right) - 2\zeta_{\nu}\omega_{\nu}\dot{x}_{com} \tag{4.55}$$

On the other hand, for $V_{fc} > 0$, the forward velocity regulation demands a forward acceleration requirement of,

$$\ddot{x}^{d2}_{com} = K_{\nu}(\dot{x}^{d}_{com} - \dot{x}_{com}) = K_{\nu}(V_{fc} - \dot{x}_{com}) \tag{4.56}$$

During pre-mid stance zone of each walking gait, the dominant of the above two requirements should decide the required forward acceleration. Hence for the case with $V_{fc} > 0$, $\ddot{x}^{d}_{com} = \max\left(\ddot{x}^{d1}_{com}, \ddot{x}^{d2}_{com}\right)$ for $x_{com} < x_{rc}$ and $\ddot{x}^{d}_{com} = \ddot{x}^{d2}$ for $x_{com} \geqslant x_{rc}$, whereas for the case with $V_{fc} = 0$, $\ddot{x}^{d}_{com} = \ddot{x}^{d1}$. Finally, the desired value, x^{d}_{cop} for the direct regulation of GCoP is obtained by substituting the value of $\ddot{x}^{d}_{com}$ in (4.53). It should be noted that the GCoP control will be effective only if $x_{rh} < x^{d}_{cop} < x_{rt}$ during the current walking step, as HyDAC uses only the reference foot contact forces for the required control. Till that instant, the biped has to rotate like a passive inverted pendulum about the ground contact point. Based on simulation based optimization, the values of $(\omega_{\nu}, \zeta_{\nu})$ are selected as $(\omega_{p}, 0.8)$ and value of K_{ν} as $3\omega_{p}$. If the biped is climbing up or down along a slope or stairs, FVC algorithm has to regulate only the forward velocity, V_{comx} along the horizontal direction as per the command, V_{fc}. The postural orientation control primitives will ensure the required upward motion, V_{comy} along $\overrightarrow{O_0Y_0}$ so as to maintain the adequate ground clearance and to ensure proper touch down.

The second part of FVC algorithm is to regulate the actual position of x_{cop} along x^{d}_{cop} without any a priori path planning while $x_{rh} < x^{d}_{cop} < x_{rt}$ as mentioned in Section 4.5.1.

4.7 Postural configuration state for Bipedal dynamic walk

The postural configuration of the biped is independent of its actual location and hence the same can be represented by a reduced number of coordinates excluding the position coordinates of its base. As will be explained later, four important variables to be controlled during bipedal walking are V_{comx}, forward offset of biped-CoM with respect to stance foot, forward offset of swing foot with respect to biped-CoM and orientation of upper-body in

the inertial frame. In posture control point of view, it would be better if these variables do directly reflect in the state vector of biped. Hence let us define a minimal dimensional vector called, the *Postural Configuration State*, $\mathbf{x}_{Pc} \in \mathcal{C} \subset \mathbb{R}^{n_P}$ with n_P=12, to represent the essential postural features of biped during locomotion and is given by,

$$\mathbf{x}_{Pc_{t\in[t_k,t_{k+1})}} := \begin{bmatrix} \theta_{solr} & \theta_{kner} & \theta_{tor} & \theta_{knet} & \theta_{solt} & \theta_{rhc} & \theta_{cth} & \boldsymbol{\theta}'_{ubd} \end{bmatrix}' \tag{4.57}$$

$$\text{where } \theta_{rhc} := \frac{x_{com} - x_{th}(t_k^-)}{h_{com}} \tag{4.58}$$

$$\theta_{cth} := \frac{x_{th} - x_{com}}{h_{com}} \tag{4.59}$$

$$\boldsymbol{\theta}_{ubd} = [q_7 \;\; q_{11} \;\; q_{12} \;\; q_{13} \;\; q_{14}]' \tag{4.60}$$

where $\mathcal{C}$ is a simply-connected, open subset of $[-\pi, \pi)^{n_P}$ known as the *Postural Configuration Space* associated with locomotion related postural dynamics, θ_{solr} denotes the angle between the reference foot sole and ground measured about reference toe, $\theta_{kner} := q_5$, denotes the reference knee joint angle, θ_{tor} denotes the inertial orientation of torso measured with respect to vertical axis, $\overrightarrow{O_0Y_0}$, $\theta_{knet} := q_9$, denotes the transit knee joint angle, θ_{solt} denotes the angle between the transit foot sole and ground measured about transit toe, (x_{th}, y_{th}) denote the coordinates of transit foot heel, (x_{com}, y_{com}) denote the coordinates of the biped-CoM, and h_{com} denotes the height of biped-CoM in nominal stance state of biped on level ground. All translational variables of $\mathbf{x}_{Pc}$ are expressed with respect to inertial frame, $\{O_0\}$. The half open interval, $[t_k, t_{k+1})$ represents the time interval corresponding to the k^{th} walking step with t_k denoting the time of k^{th} heel impact on ground. Accordingly, $x_{th}(t_k^-)$ represents the x-coordinate of k^{th} heel strike location on ground. The forward offset of biped-CoM with respect to stance foot heel is represented by, θ_{rhc} and the forward offset of swing foot heel with respect to biped-CoM is represented by θ_{cth}, both in normalized form. The relative orientation of upper body links, namely head and upper limbs, with respect to torso is represented by $\boldsymbol{\theta}_{ubd}$. Even though the upper body links are free to execute independent tasks during locomotion, it is required to keep them under autonomous regulator type control without any external task command to ensure that the postural dynamics of the biped to remain as an autonomous system for the analysis of periodic stability.

Let us define a switching function, $\xi : \mathbb{R}^{n_P} \to \mathbb{R}$ as,

$$\xi(\mathbf{x}_{Pc}) = \frac{y_{th}(\mathbf{x}_{Pc}) - y_G(x_{th}(\mathbf{x}_{Pc}))}{h_{hip}} \tag{4.61}$$

where h_{hip} denotes the height of biped hip joint in nominal stance state of biped on level ground with straight knee. Let us define the switching set, $\mathcal{S}$ as[5]

$$\begin{aligned}\mathcal{S} := \big\{ & [\mathbf{x}'_{Pc} \ \dot{\mathbf{x}}'_{Pc}]' \in T\mathcal{C} \mid \Sigma\pi_{m(1:2)} \geqslant 1, \Sigma\mathbf{x}_{Pc(6:7)} > 0, \\ & \xi(\mathbf{x}_{Pc}) = 0 \ \& \ \dot{\xi}(\mathbf{x}_{Pc}) < 0 \big\} \end{aligned} \tag{4.62}$$

where $T\mathcal{C} := \left\{ [\mathbf{x}'_{Pc} \ \dot{\mathbf{x}}'_{Pc}]', \mathbf{x}_{Pc} \in \mathcal{C}, \dot{\mathbf{x}}_{Pc} \in \mathbb{R}^{n_P} \right\}$ is the state space associated with postural dynamics of bipedal locomotion and $\mathbf{x}_P := [\mathbf{x}'_{Pc} \ \dot{\mathbf{x}}'_{Pc}]' \in T\mathcal{C}$ is the postural state. As per the new definition given in (4.62), the switching set $\mathcal{S}$ admits only the heel strike event with[6] $x_{th} > x_{rt}$ and excludes static double support phase with $\dot{\xi}(\mathbf{x}_{Pc}) = 0$.

Fig 4.6 shows how the elements of $\mathbf{x}_{Pc}$ along with the terrain slope, σ_G uniquely determine the postural configuration of the biped for a given position of reference foot heel, $x_{rh}(t_k) = x_{th}(t_k^-)$ at the starting instant, t_k of k^{th} bipedal gait. For easy representation, the entire upper body is represented by a single thick line in Fig 4.6 with its CoM location in $\{O_6\}$ determined by θ_{ubd}. It should be noted that $x_{rh}(t) \, \forall \, t \in [t_k, t_{k+1})$ will remain same as $x_{rh}(t_k)$ whenever the reference heel is in contact with the ground. Similarly $x_{rt}(t) = x_{rh}(t_k) + L_f \cos\sigma_G \, \forall \, t \in [t_k, t_{k+1})$ whenever the reference toe is in contact with the ground. In other words, $x_{th}(t_k^-)$ along with $\theta_{solr} = \mathbf{x}_{Pc1}$ will uniquely determine the position of the reference foot ankle joint, $O_4 \, \forall \, t \in [t_k, t_{k+1})$. O_4O_6 represents a virtual link from the reference foot ankle joint to the biped hip joint and its length, $\rho_{hr}(t)$ is determined by the value of $\mathbf{x}_{Pc2}(t)$. Similarly, O_6O_{10} represents a virtual link from the biped hip joint to transit foot ankle joint and its length, $\rho_{ht}(t)$ is determined by the value of $\mathbf{x}_{Pc4}(t)$. Thus the values of $\mathbf{x}_{Pc1}(t)$ and $\mathbf{x}_{Pc5}(t)$ along with σ_G determine the inertial orientations of reference and transit foot links respectively and the value of $\mathbf{x}_{Pc3}(t)$ along with $\theta_{ubd}(t)$ determine the inertial orientation of the upper body links. The biped-CoM, O_c is constrained to move along the vertical line passing through A, having an offset determined by the value of $\mathbf{x}_{Pc6}(t)$. Similarly, the value of $\mathbf{x}_{Pc7}(t)$ constrains the locus of transit heel along the vertical line passing through B which inturn constrains the locus of transit ankle joint, O_{10} along the vertical line passing through C. The postural configuration of the biped during the period, $t \in [t_k, t_{k+1})$ is uniquely determined by rotating the hip joint about O_4 as shown in Fig 4.6 along the circular arc while keeping the horizontal position and orientation of transit foot until the biped-CoM falls on the vertical line passing through A. The elements of $\mathbf{x}_{Pc}$ are directly linked to various motion control primitives

[5]The MATLAB conventions are followed here to represent rows and column of vectors and matrices. For example, $\mathbf{y} = \mathbf{x}_{(i:j,k:l)}$ means that $\mathbf{y}$ is formed by i^{th} to j^{th} rows and k^{th} to l^{th} columns of $\mathbf{x}$.

[6]Since $x_{rh} = x_{th}(t_k^-) \, \forall t \in [t_k, t_{k+1}^-)$, $\Sigma\mathbf{x}_{Pc(6:7)} > 0$ implies $x_{th} > x_{rh}$.

of TLC as will be discussed and hence during the actual controlled motion, the effect of closed loop inverse kinematics control [81] embedded within the TLC will steer the biped postural configuration automatically to the unique posture as determined above. During

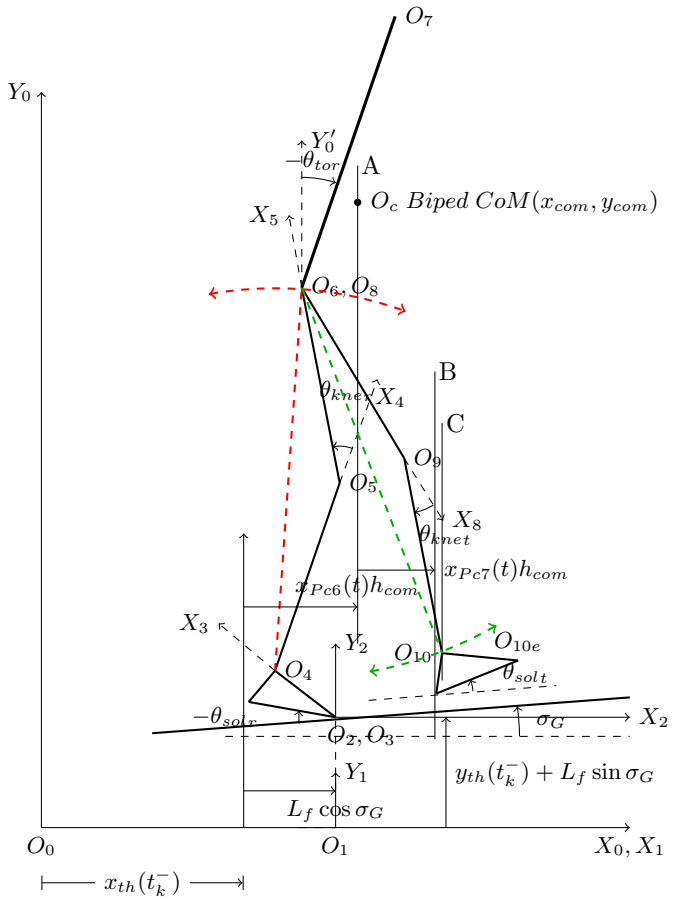

Figure 4.6: Postural configuration representation of biped by $\mathbf{x}_{\mathrm{Pc}}$ during the touch down phase of k$^{\text{th}}$ walking step of uniform terrain walking with transit heel impact

pre-touchdown phase with *FwdTDFlg*=0, the transit knee joint angle, $\mathbf{x}_{\mathrm{Pc}4}$ is not explicitly controlled, rather controlled implicitly to meet the goals of transit foot ground clearance, $\mathtt{h}_{\mathtt{hip}}\xi(\mathbf{x}_{\mathrm{Pc}})$.

4.8 Orbital stability and Control requirements

Since the dynamic bipedal walking over uniform terrain is a recurrent process, mere joint space stability is neither sufficient nor necessary for ensuring the sustained repetitive walking. In this context, the actual requirement is to ensure that the postural state trajectories

converge to a periodically repetitive trajectory or orbit as they evolve consistent with the environmental constraints. Hence, it is essential to extend the basic stability concepts associated with equilibrium points to stability of equilibrium orbits.

4.8.1 Basic stability definitions for nonlinear dynamical systems

Following are the basic definitions and theorems required for arriving at a viable definition of gait orbital stability for realistic bipedal walk. We follow, in general, the notations and definitions used in the text books of Haddad et al. [82] and Khalil [83] in this context.

4.8.1.1 Lyapunov Stability definitions associated with an equilibrium point

Let us consider an n-dimensional autonomous nonlinear dynamical system represented by the ordinary differential equation,

$$\dot{\mathbf{x}}(t) = \mathbf{f}(\mathbf{x}(t)),\ \mathbf{x}(t_0) = \mathbf{x}_0,\ t \in [t_0,\ \infty) \tag{4.63}$$

where $\mathbf{x} \in \mathcal{D} \subseteq \mathbb{R}^n$, $\mathcal{D}$ being an open subset of $\mathbb{R}^n$ and $\mathbf{f} : \mathcal{D} \to \mathbb{R}^n$ is Lipschitz continuous vector field on $\mathcal{D}$. Then there exists a unique solution or trajectory $\mathbf{x}(t)$ for every initial condition, $\mathbf{x}_0$ at $t = t_0$ and is denoted by the flow, $s_t(t_0, \mathbf{x}_0) = s(t, t_0, \mathbf{x}_0)$ with $s(t_0, t_0, \mathbf{x}_0) = \mathbf{x}_0$. Thus the flow, $s_t(t_0, \mathbf{x}_0)$ assigns a trajectory, $\mathbf{x}(t)$ to every initial value $\mathbf{x}_0$. Being an autonomous system, the solution $s_t(t_0, \mathbf{x}_0)$ depends only on $(t - t_0)$ instead of t. The following are the basic stability definitions in the sense of Lyapunov associated with the equilibrium , $\mathbf{x}(t) = \mathbf{x}_e$ of the nonlinear dynamical system given by (4.63) on the assumption that $\mathbf{f}(\mathbf{x}_e) = \mathbf{0}$.

Definition 4.1. ***Stability in the sense of Lyapunov for continuous time dynamical system*** *[82]*

i) The equilibrium solution to (4.63) is Lyapunov stable if, for every $\epsilon > 0$, there exists $\delta = \delta(\epsilon) > 0$ such that if $\| \boldsymbol{x}(t_0) - \boldsymbol{x}_e \| < \delta$, then $\| \boldsymbol{x}(t) - \boldsymbol{x}_e \| < \epsilon$, for all $t \geqslant t_0$.

ii) The equilibrium solution to (4.63) is ultimately bounded with bound, ϵ if there exists $\gamma > 0$ such that, for every $\delta \in (0, \gamma)$, there exists $T = T(\delta, \epsilon) > 0$ such that $\| \boldsymbol{x}(t_0) - \boldsymbol{x}_e \| < \delta$ implies $\| \boldsymbol{x}(t) - \boldsymbol{x}_e \| < \epsilon$, for all $t \geqslant t_0 + T$.

iii) The equilibrium solution to (4.63) is (locally) asymptotically stable if it is Lyapunov stable and there exists, $\delta > 0$ such that if $\| \boldsymbol{x}(t_0) - \boldsymbol{x}_e) \| < \delta$, then $\lim_{t \to \infty} \| \boldsymbol{x}(t) - \boldsymbol{x}_e \| = 0$.

iv) The equilibrium solution to (4.63) is (locally) exponentially stable if there exists positive constants α, β, *and* δ *such that if* $\| \boldsymbol{x}(t_0) - \boldsymbol{x}_e \| < \delta$, *then* $\| \boldsymbol{x}(t) - \boldsymbol{x}_e \| \leqslant \alpha \| \boldsymbol{x}(t_0) - \boldsymbol{x}_e \| e^{-\beta(t-t_0)}$, *for all* $t \geqslant t_0$.

v) The equilibrium solution to (4.63) is unstable if it is neither Lyapunov stable nor ultimately bounded.

We are also interested in the Lyapunov stability definitions associated with the discrete dynamic version of (4.63). Consider the n-dimensional autonomous nonlinear discrete dynamical system given by,

$$\mathbf{z}(k+1) = \mathbf{f}(\mathbf{z}(k)),\ \mathbf{z}(0) = \mathbf{z}_0,\ k \in \bar{\mathbb{Z}}_+ \tag{4.64}$$

where $\mathbf{z}(k) \in \mathcal{D} \subseteq \mathbb{R}^n$, $\mathcal{D}$ being an open subset of $\mathbb{R}^n$ and $\mathbf{f} : \mathcal{D} \to \mathbb{R}^n$ is continuous vector field on $\mathcal{D}$. Then there exists a unique solution or trajectory $\mathbf{z}(k)$ for every initial condition, $\mathbf{z}_0 \in \mathcal{D}$ which coincides with $t = t_0$ and is denoted by the flow, $s_k(\mathbf{z}_0) = s(k, \mathbf{z}_0)$. Thus the flow, $s_k(\mathbf{z}_0)$ assigns a trajectory, $\mathbf{z}(k)$ to every initial value $\mathbf{z}_0$. The equilibrium solution to (4.64) is given by $\mathbf{z}(k) = \mathbf{z}_e$ so that $\mathbf{f}(\mathbf{z}_e) = \mathbf{z}_e$. The following are various stability definitions associated with the equilibrium point, $\mathbf{z}_e$ of (4.64).

Definition 4.2. ***Stability in the sense of Lyapunov for discrete time dynamical system*** *[82]*

i) The equilibrium solution to (4.64) is Lyapunov stable if, for every $\epsilon > 0$, *there exists* $\delta = \delta(\epsilon) > 0$ *such that if* $\| z_0 - z_e \| < \delta$, *then* $\| z(k) - z_e \| < \epsilon$, *for all* $k \in \bar{\mathbb{Z}}_+$.

ii) The equilibrium solution to (4.64) is ultimately bounded with bound, ϵ *if there exists* $\gamma > 0$ *such that, for every* $\delta \in (0, \gamma)$, *there exists* $K = K(\delta, \epsilon) > 0$ *such that* $\| z_0 - z_e \| < \delta$ *implies* $\| z(k) - z_e \| < \epsilon$, *for all* $k \geqslant K$.

iii) The equilibrium solution to (4.64) is (locally) asymptotically stable if it is Lyapunov stable and there exists, $\delta > 0$ *such that if* $\| z_0 - z_e \| < \delta$, *then* $\lim_{k\to\infty} \| z(k) - z_e \| = 0$.

iv) The equilibrium solution to (4.64) is (locally) geometrically stable if there exists positive constants $\alpha, \beta > 1$, *and* δ *such that if* $\| z_0 - z_e \| < \delta$, *then* $\| z(k) - z_e \| \leqslant \alpha \| z_0 - z_e \| \beta^{-k}$, *for all* $k \in \bar{\mathbb{Z}}_+$.

v) The equilibrium solution to (4.64) is unstable if it is neither Lyapunov stable nor ultimately bounded.

4.8.1.2 Invariant sets and Lyapunov stability

Definition 4.3. ***Positively invariant set*** *[82]*

A set $\mathcal{M} \subset \mathcal{D} \subseteq \mathbb{R}^n$ is a positively invariant set with respect to the nonlinear dynamical system represented by (4.63) if $s_t(t_0, \mathcal{M}) \subseteq \mathcal{M}$ for all $t \geqslant t_0$, where $s_t(t_0, \mathcal{M}) := \{s_t(t_0, \boldsymbol{x}) : \boldsymbol{x} \in \mathcal{M}\}$.

The definition of Lyapunov stability for invariant sets of an ODE is similar to the definition for an equilibrium point.

Definition 4.4. ***Lyapunov stability of closed invariant set*** *[82]*

Let $\mathcal{M} \subseteq \mathcal{D}$ be a closed invariant set for (4.63) and let $\mathcal{N}_\epsilon := \{\boldsymbol{x} \in \mathcal{D} | \, dist(\boldsymbol{x}, \mathcal{M}) < \epsilon\}$ be an ϵ-neighbourhood of $\mathcal{M}$ with $dist(\boldsymbol{x}, \mathcal{M}) = \inf_{\boldsymbol{y} \in \mathcal{M}} \parallel \boldsymbol{x} - \boldsymbol{y} \parallel$. The closed invariant set $\mathcal{M}$ is stable if, for every $\epsilon > 0$ there exists a $\delta > 0$ such that if $\boldsymbol{x}(t_0) \in \mathcal{N}_\delta$, it follows that $\boldsymbol{x}(t) \in \mathcal{N}_\epsilon$ for all time, t. The closed invariant set $\mathcal{M}$ is asymptotically stable if there exists a $\delta > 0$, such that if $\boldsymbol{x}(t_0) \in \mathcal{N}_\delta$, it follows that $\lim_{t \to \infty} dist(\boldsymbol{x}, \mathcal{M}) = 0$.

4.8.1.3 Periodic orbits and Lyapunov stability

Definition 4.5. ***Periodic solution and Periodic orbits*** *[82]*

A solution $s(t, t_0, \boldsymbol{x}_0)$ of (4.63) is periodic if there exists a finite time $T > 0$ such that $s(t+T, t_0, \boldsymbol{x}_0) = s(t, t_0, \boldsymbol{x}_0)$ for all $t \geqslant t_0$. The minimal T for which the solution $s(t, t_0, \boldsymbol{x}_0)$ of (4.63) is periodic is called the period. A set $\mathcal{O} \subset \mathcal{D}$ is a periodic orbit of (4.63) if $\mathcal{O} = \{\boldsymbol{x} \in \mathcal{D} : \boldsymbol{x} = s(t, t_0, \boldsymbol{x}_0), t \in [t_0 \, \infty)\}$ for some periodic solution $s(t, t_0, \boldsymbol{x}_0)$ of (4.63).

Definition 4.6. ***Lyapunov stability of periodic orbit*** *[82]*

A periodic orbit $\mathcal{O}$ of (4.63) is Lyapunov stable if, for every $\epsilon > 0$, there exists $\delta = \delta(\epsilon) > 0$ such that if $dist(\boldsymbol{x}_0, \mathcal{O}) < \delta$, then $dist(s(t, t_0, \boldsymbol{x}_0), \mathcal{O}) < \epsilon$, for all $t \geqslant t_0$. A periodic orbit $\mathcal{O}$ of (4.63) is asymptotically stable if it is Lyapunov stable and there exists $\delta > 0$ such that if $dist(\boldsymbol{x}_0, \mathcal{O}) < \delta$, then $dist(s(t, t_0, \boldsymbol{x}_0), \mathcal{O}) \to 0$ as $t \to \infty$.

A schematic representation of various terms involved in the above definition are given in Fig 4.7 for a three dimensional domain $\mathcal{D}$. Note that $\mathcal{O}$ is a compact invariant set and hence the definitions of Lyapunov stability given in Definition 4.1 and Definition 4.6 are similar.

4.8.1.4 Periodic stability criterion based on Poincaré return map

The Lyapunov type asymptotic stability concept of periodic orbit attaches an attractive property for the orbit at each and every point of $\mathcal{O}$. However, this point-wise attraction

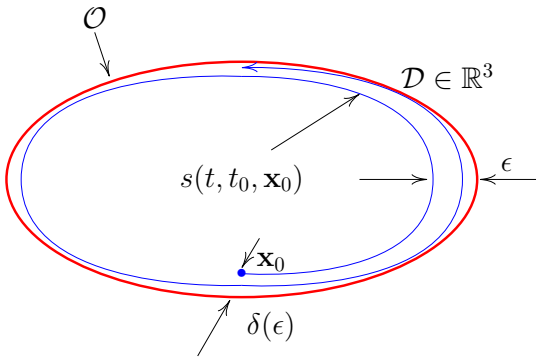

Figure 4.7: Periodic stability of orbits in Lyapunov sense

requirement of periodic orbit will call for a stiff path tracking type controller whenever there is a demand to improve the stability margin of the orbit. Stiff path tracking controllers have practical problems like non-compliant interaction with environment and requirement of a priori information of feasible periodic orbits. This situation can be overcome if we make use of Poincaré stability theory for periodic orbits. The simplification comes from the fact that Poincaré has visualized the aggregate effect of orbital divergence or convergence integrated over one full cycle as equivalently reflected in the stability properties of orbital intersection points with any transverse hyperplane of dimension $(n-1)$. However, prior to introducing the Poincaré stability, it is necessary to provide formal definitions of various associated terms as given below [82, 84].

Let us assume that $s(t, t_0, \mathbf{p}) : t \geqslant t_0$ generates a periodic orbit $\mathcal{O}$ passing through certain point, $\mathbf{p} \in \mathcal{D}$ for $\dot{\mathbf{x}} = \mathbf{f}(\mathbf{x})$ with period, $T > 0$ such that,

$$\mathcal{O} := \{\mathbf{x} \in \mathcal{D} : \mathbf{x} = s(t, t_0, \mathbf{p}), t_0 \leqslant t \leqslant t_0 + T\} \tag{4.65}$$

Let us further assume that there exists a continuous differentiable function, $\xi : \mathcal{D} \to \mathbb{R}$ such that the $(n-1)$-dimensional hyperplane defined by $\mathcal{H} := \{\mathbf{x} \in \mathcal{D}, \xi(\mathbf{x}) = 0\}$ contains the point $\mathbf{x} = \mathbf{p}$ and $\xi'(\mathbf{p}) \neq 0$, and with the additional property that $\xi'(\mathbf{p})\mathbf{f}(\mathbf{p}) \neq 0$[7]. This will ensure that $\mathcal{H}$ is not tangent to $\mathcal{O}$ at $\mathbf{x} = \mathbf{p}$ and the periodic trajectory of (4.63) crosses $\mathcal{H}$ with a finite velocity. Let us further define a subset, $\mathcal{S} \subset \mathcal{H}$, called the *Switching set*[8]

[7] $\xi'(\mathbf{p})$ denotes the Fréchet derivative of ξ at $\mathbf{x} = \mathbf{p}$.

[8] The term switching set is meaningful only with respect to hybrid dynamical systems where real switching takes place between different continuous system domains.

containing the point **p** by,

$$\mathcal{S} := \{\mathbf{x} \in \mathcal{H} : \xi'(\mathbf{x}) \neq \mathbf{0}, \xi'(\mathbf{x})\mathbf{f}(\mathbf{x}) \neq 0\} \tag{4.66}$$

so that no trajectories of (4.63) crossing at $\mathbf{x} \in \mathcal{S}$ is tangent to $\mathcal{H}$. Let us define a subset, $\mathcal{S}_P \subset \mathcal{S} \subset \mathcal{H}$, called the *Proper switching set* containing the point, **p** which has the additional property that all trajectories starting at $\mathbf{x} \in \mathcal{S}_P, t = t_0$ intersects $\mathcal{S}$ within a finite time, $\tau(\mathbf{x}) > 0$. $\mathcal{S}_P$ can be precisely defined as,

$$\begin{aligned}\mathcal{S}_P :=& \{\mathbf{x} \in \mathcal{S}_P \subset \mathcal{S} : \text{there exists } 0 < \hat{\tau} < \infty \text{ such that } s(t_0 + \hat{\tau}, t_0, \mathbf{x}) \in \mathcal{S} \\ & \text{and } s(t, t_0, \mathbf{x}) \notin \mathcal{S}, t_0 < t < \hat{\tau}\}\end{aligned} \tag{4.67}$$

The intersecting time, $\tau : \mathcal{S}_P \to \mathbb{R}_+$ can be defined as the function,

$$\tau(\mathbf{x}) := \{0 < \hat{\tau} < \infty : \mathbf{x} \in \mathcal{S}_P, s(t_0 + \hat{\tau}, t_0, \mathbf{x}) \in \mathcal{S} \text{ and } s(t, t_0, \mathbf{x}) \notin \mathcal{S}, t_0 < t < t_0 + \hat{\tau}\} \tag{4.68}$$

A value of $\tau(\mathbf{x}) = \infty$ means the solution $s(t, t_0, \mathbf{x})$ will either deviate away from $\mathcal{S}$ or stop on the path, both resulting in no intersection with $\mathcal{S}$. Let us once again define a subset, $\mathcal{S}_{SP} \subset \mathcal{S}_P \subset \mathcal{S} \subset \mathcal{H}$, called the *Strictly proper switching set* containing the point **p** which has the additional property that all trajectories of (4.63) starting at $\mathbf{x} \in \mathcal{S}_{SP}, t = t_0$ are guaranteed to intersect the same subset $\mathcal{S}_{SP}$ at $t = t_0 + \tau(\mathbf{x})$ and no trajectory starting from an $\mathbf{x} \notin \mathcal{S}_{SP}$ at $t = t_0$ does not intersect $\mathcal{S}_{SP}$ for $t > t_0$.

$$\begin{aligned}\text{i.e. } \mathcal{S}_{SP} := \{\mathbf{x} \in \mathcal{S}_P : s(t_0 + \tau(\mathbf{x}), t_0, \mathbf{x}) \in \mathcal{S}_{SP} \text{ iff } \mathbf{x} \in \mathcal{S}_{SP} \text{ at } t = t_0 \\ \text{and } s(t, t_0, \mathbf{x}) \notin \mathcal{S}, t_0 < t < t_0 + \tau(\mathbf{x})\}\end{aligned} \tag{4.69}$$

Thus $\mathcal{S}_{SP}$ is the largest positively invariant subset of $\mathcal{S}_P$. A similar one in meaning, but a different type of definition for strictly proper switching set is given in [84]. From stability point of view, any flow $s(t, t_0, \mathbf{x})$ starting from an $\mathbf{x} \in \mathcal{N}_\epsilon(\mathbf{y}), \mathbf{y} \in \partial\mathcal{S}_{SP}, \mathbf{x} \notin \bar{\mathcal{S}}_{SP}$ will move away from $\partial\mathcal{S}_{SP}$ at least for $\epsilon \to 0$ when $t = t_0 + \tau(\mathbf{x})$. On the other hand, any flow $s(t, t_0, \mathbf{x})$ starting from an $\mathbf{x} \in \mathcal{N}_\epsilon(\mathbf{y}), \mathbf{y} \in \partial\mathcal{S}_{SP}, \mathbf{x} \in \bar{\mathcal{S}}_{SP}$ will remain in $\bar{\mathcal{S}}_{SP}$ as $\epsilon \to 0$ when $t = t_0 + \tau(\mathbf{x})$. Hence there should be a boundary layer of thickness $\epsilon > 0$ for $\mathcal{S}_{SP}$ defined as $\mathcal{B}_\epsilon := \mathcal{N}_\epsilon(\partial\mathcal{S}_{SP}) \cap \bar{\mathcal{S}}_{SP}$ which is either positively invariant or inward projective under the map, $s(t_0 + \tau(\mathcal{B}_\epsilon), t_0, \mathcal{B}_\epsilon)$.

Definition 4.7. ***Strictly proper trajectory and set of all strictly proper trajectories***

A strictly proper trajectory, $\psi_{SP}(t_0, \boldsymbol{x})$ for dynamical system (4.63) is defined as

$$\psi_{SP}(t_0, \boldsymbol{x}) = \{s(t, t_0, \boldsymbol{x}) : \boldsymbol{x} \in \mathcal{S}_{SP} \text{ at } t = t_0, t_0 \leqslant t \leqslant t_0 + \tau(\boldsymbol{x})\} \tag{4.70}$$

The set of all strictly proper trajectories is defined as $\boldsymbol{\Psi}_{SP}(t_0) := \{\psi_{SP}(t_0, \boldsymbol{x}) : \boldsymbol{x} \in \mathcal{S}_{SP}\}$

The pictorial representation of various switching sets are given in Fig 4.8. It can be

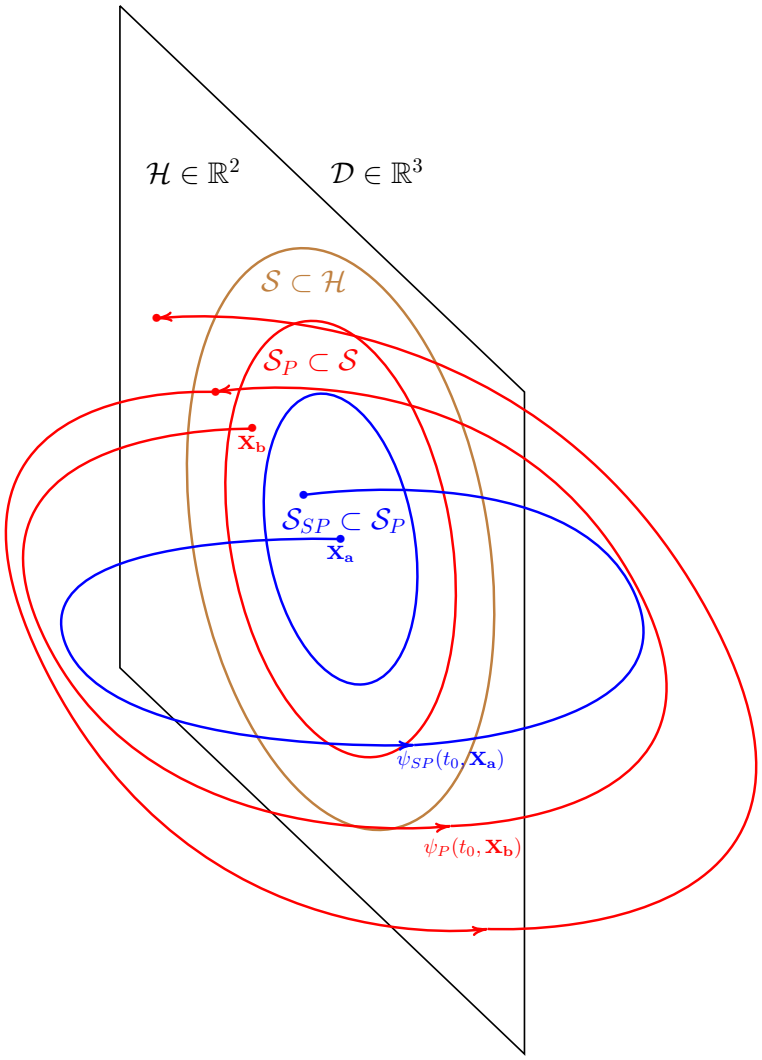

Figure 4.8: Visualization of various switching sets and associated trajectories

observed that $\psi_{SP}(t_0, \mathbf{x}_a)$ starting at $\mathbf{x}_a \in \mathcal{S}_{SP}$ continues to intersect $\mathcal{S}_{SP}$ on every forth-

coming cycle whereas $\psi_P(t_0, \mathbf{x}_b)$ starting at $\mathbf{x}_b \in \mathcal{S}_P$ intersects $\mathcal{S}$ in the next cycle, which can be inside or outside $\mathcal{S}_P$. If the intersecting point is outside $\mathcal{S}_P$, it may not even intersect either $\mathcal{S}$ or $\mathcal{H}$ in the second cycle terminating the cyclic nature of the solution trajectory, $s(t, t_0, \mathbf{x})$. Hence to ensure the sustained cyclic nature (need not be periodic) of certain solution trajectory, $s(t, t_0, \mathbf{x})$ for the autonomous dynamical system (4.63), it is necessary that the trajectory belongs to $\mathbf{\Psi}_{SP}(t_0)$. Next, we can define Poincaré return map, $\mathcal{P} : \mathcal{S}_{SP} \to \mathcal{S}_P$ by,

$$\mathcal{P}(\mathbf{x}) := s(t_0 + \tau(\mathbf{x}), t_0, \mathbf{x}), \mathbf{x} \in \mathcal{S}_{SP} \text{ at } t = t_0 \tag{4.71}$$

The equivalent representation of Poincaré return map in discrete time domain can be written as,

$$\mathbf{z}(k+1) = \mathcal{P}(\mathbf{z}(k)); \mathbf{z}(k) \in \mathcal{S}_{SP}, k \in \bar{\mathbb{Z}}_+ \tag{4.72}$$

where $\bar{\mathbb{Z}}_+$ is the set of all nonnegative integers. Clearly, $\mathbf{z}(k) = \mathbf{p}$ is a fixed point of (4.72) so that $\mathbf{p} = \mathcal{P}(\mathbf{p})$. Further, the definitions provided in (4.69) and (4.72) ensure that $\mathcal{S}_{SP}$ is a positively invariant set of the Poincaré return map as $s_k(\mathcal{S}_{SP}) \subseteq \mathcal{S}_{SP}$ for all $k \in \bar{\mathbb{Z}}_+$. The pictorial representation of Poincaré map for a 3-dimensional domain is shown in Fig 4.9. Linearizing (4.72) about the fixed point, $\mathbf{z}(k) = \mathbf{p}$, we obtain,

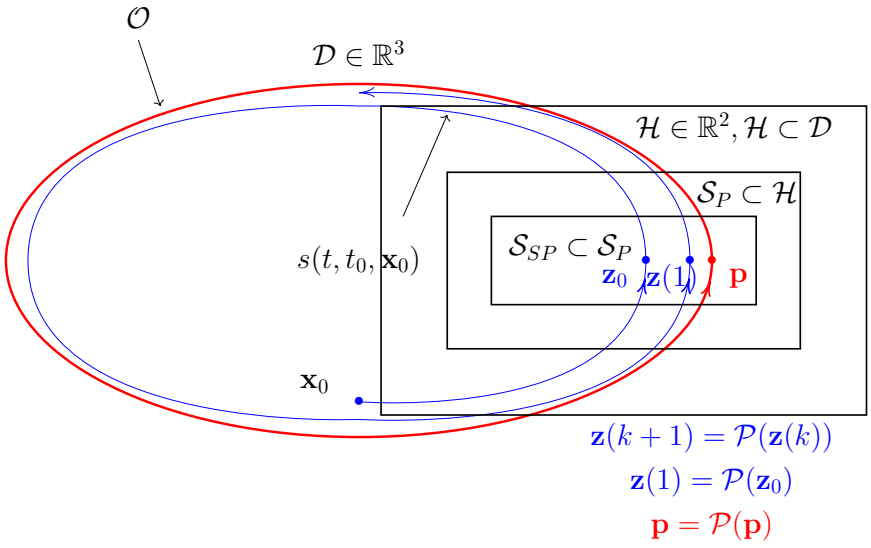

Figure 4.9: Poincaré map for $\mathcal{D} \in \mathbb{R}^3$

$$\delta\mathbf{z}(k+1) = \mathcal{P}'(\mathbf{p})\delta\mathbf{z}(k) \tag{4.73}$$

Since $\mathbf{z}(k) \in \mathcal{S}_{SP}$, its perturbation with respect to $\mathbf{p} \in \mathcal{S}_{SP}$ lies completely in the (n-1)-dimensional hyperplane $\mathcal{H}$. Let us define a new $(n-1)$-dimensional coordinate system, $\bar{\Sigma}_{\mathcal{H}}$ to represent any point belonging to $\mathcal{H}$ by a coordinate vector, $\bar{\mathbf{z}} \in \mathbb{R}^{n-1}$ based on a set of $(n-1)$ basis vectors completely belonging to the hyperplane $\mathcal{H}$ of codimension-1. Then we can represent the Poincaré map in $\bar{\Sigma}_{\mathcal{H}}$ as $\bar{\mathcal{P}}(\bar{\mathbf{p}})$ and the corresponding linearized Poincaré map as $\bar{\mathcal{P}}'(\bar{\mathbf{p}})$ having $(n-1)$ eigenvalues so that

$$\delta\bar{\mathbf{z}}(k+1) = \bar{\mathcal{P}}'(\bar{\mathbf{p}})\delta\bar{\mathbf{z}}(k) \tag{4.74}$$

where $\delta\bar{\mathbf{z}}(k+1)$ and $\bar{\mathbf{p}}$ are representations of $\delta\mathbf{z}(k+1)$ and $\mathbf{p}$ respectively in $\bar{\Sigma}_{\mathcal{H}}$. If the spectral radius $\rho(\bar{\mathcal{P}}'(\bar{\mathbf{p}})) < 1$, then the fixed point $\mathbf{z} = \mathbf{p}$ of the nonlinear discrete dynamical system (4.72) is asymptotically stable[9]. This is Lyapunov's indirect method for nonlinear discrete time system dealing with only the local stability at the fixed point, $\mathbf{p}$.

However, to ensure the stability of Poincaré return map over a larger domain of attraction, $\mathcal{S}_{SP}^{C} \subseteq \mathring{\mathcal{S}}_{SP}$[10], we have to make use of Lyapunov's direct method for discrete time systems based on Definition 4.2 and are given below with respect to the equilibrium point, $\mathbf{z}_e = \mathbf{p}$.

4.8.1.5 Stability of Poincaré return map using Lyapunov function

Definition 4.8. *Let $\mathcal{S}_{SP}^{C} \subseteq \mathring{\mathcal{S}}_{SP}$ be the compact positively invariant set of maximum size for the discrete nonlinear Poincaré return map represented in (4.72) with the fixed point, $\boldsymbol{p} \in \mathcal{S}_{SP}^{C}$. Let there exists a continuous function $V : \mathcal{D} \to \mathbb{R}$ such that*

$$V(\boldsymbol{p}) = 0, \tag{4.75}$$

$$V(z) > 0, z \in \mathcal{S}_{SP}^{C}, z \neq \boldsymbol{p} \tag{4.76}$$

i) The equilibrium solution, $z(k) = \boldsymbol{p}$ to (4.72) is Lyapunov stable if

$$V(\mathcal{P}(z)) - V(z) \leqslant 0, z \in \mathcal{S}_{SP}^{C} \tag{4.77}$$

ii) The equilibrium solution, $z(k) = \boldsymbol{p}$ to (4.72) ultimately bounded with bound, ϵ if there exists $\gamma > 0$ such that, for every $\delta \in (0, \gamma)$, there exists $K = K(\delta, \epsilon) > 0$ such that $\| z_0 - \boldsymbol{p} \| < \delta$ implies $V(z(k)) < \epsilon$, $k \geqslant K$.

[9] $\mathcal{P}'$ represents the Freché t derivative of $\mathcal{P}$.

[10] $\mathring{\mathcal{S}}_{SP}$ represents the interior of $\mathcal{S}_{SP}$.

iii) The equilibrium solution, $z(k) = \boldsymbol{p}$ to (4.72) is asymptotically stable if

$$V(\mathcal{P}(z)) - V(z) < 0,\, z \in \mathcal{S}_{SP}^{C},\, z \neq \boldsymbol{p} \tag{4.78}$$

Then $z(k) \to \boldsymbol{p}$ as $k \to \infty$.

iv) The equilibrium solution, $z(k) = \boldsymbol{p}$ to (4.72) is geometrically stable if there exists positive constants $\alpha, \beta > 1$ such that

$$V(\mathcal{P}^{k}(z_0)) \leqslant \alpha V(z_0)\beta^{-k}, k \in \bar{\mathbb{Z}}_{+} \tag{4.79}$$

Then $z(k) \to \boldsymbol{p}$ as $k \to \infty$ with a minimum rate of geometric convergence quantified by the common ratio of $1/\beta$.

v) The equilibrium solution to (4.72) is unstable if it is neither Lyapunov stable nor ultimately bounded.

For cases (ii) to (iv) of the above definition, $\mathcal{S}_{SP}^{C}$ is called the domain of attraction. One of the feasible candidate for $V(.)$ is $V(\mathbf{z}(k)) = \| \mathbf{z}(k) - \mathbf{p} \|_2^2$ which ensures that $V(\mathbf{p}) = 0$ and $V(\mathbf{z}) > 0, \mathbf{z} \in \mathcal{S}_{SP}^{C}, \mathbf{z} \neq \mathbf{p}$. We can also incorporate a positive definite real symmetric matrix, $P \in \mathbb{R}^{n}$ to define $V(.)$ as,

$$V(\mathbf{z}) = (\mathbf{z} - \mathbf{p})^{T} P (\mathbf{z} - \mathbf{p}) \tag{4.80}$$

which can ensure almost similar influence by all the elements of $\mathbf{z}$ on $V(\mathbf{z})$ during any time window of the transient response. The above definition provides a computationally feasible procedure to estimate the stability margin as well as domain of attraction for bipedal locomotion. The geometric convergence stated in (4.79) can be expressed in recursive form to provide a more meaningful interpretation as follows. Rewriting (4.79) for $k - 1$,

$$V(\mathcal{P}^{k-1}(\mathbf{z}_0)) \leqslant \alpha V(\mathbf{z}_0)\beta^{-(k-1)}, k \in \bar{\mathbb{Z}}_{+} \tag{4.81}$$

By combining (4.79) and (4.81), a more conservative statement can be written as,

$$V(\mathcal{P}^{k}(\mathbf{z}_0)) \leqslant \rho\, V(\mathcal{P}^{k-1}(\mathbf{z}_0)), k \in \bar{\mathbb{Z}}_{+}, \rho = 1/\beta < 1 \tag{4.82}$$

By using the Euclidian norm expression for $V(\mathbf{z})$, (4.82) can be written as,

$$\| \mathbf{z}(k) - \mathbf{p} \|_2 \leqslant \sqrt{\rho}\, \| \mathbf{z}(k-1) - \mathbf{p} \|_2, k \in \bar{\mathbb{Z}}_{+}, \rho < 1 \tag{4.83}$$

Thus the geometrical stability of $\mathbf{z}(k)$ in Lyapunov sense with common ratio $1/\beta$ is equivalent to contraction of the distance of $\mathbf{z}(k)$ from the fixed point $\mathbf{p}$ with a contraction factor of $1/\sqrt{\beta}$. Moreover, the comparison of (4.83) with (4.74) reveals that $\min(\sqrt{\rho})$ will coincide with $\sigma_{max}(\bar{\mathcal{P}}(\bar{\mathbf{p}}))$ when $\mathbf{z}(k) \to \mathbf{p}$.

4.8.1.6 Poincaré 's Stability Theorem

Poincaré 's stability theorem provides equivalence between the Lyapunov stabilities of a periodic orbit and its fixed point [82].

Theorem 4.1. *Consider the nonlinear dynamical system (4.63) with the Poincaré return map defined by (4.72). Assume that the point* $\boldsymbol{p} \in \mathcal{D}$ *generates the periodic orbit* $\mathcal{O} := \{\boldsymbol{x} \in \mathcal{D} : \boldsymbol{x} = s(t, t_0, \boldsymbol{p}), t_0 \leqslant t \leqslant t_0 + T\}$*, where* $s(t, t_0, \boldsymbol{p}), t \geqslant t_0$*, is the periodic solution with period* $T \equiv \tau(\boldsymbol{p})$*. Then the following statements hold:*

i) $\boldsymbol{p} \in \mathcal{D}$ *is a Lyapunov stable fixed point of (4.72) if and only if the periodic orbit* $\mathcal{O}$ *generated by* $\boldsymbol{p}$ *is Lyapunov stable.*

ii) $\boldsymbol{p} \in \mathcal{D}$ *is an asymptotically stable fixed point of (4.72) if and only if the periodic orbit* $\mathcal{O}$ *generated by* $\boldsymbol{p}$ *is asymptotically stable.*

Thus the stability properties of the periodic orbit $\mathcal{O}$ are equivalently mapped to the stability properties of the fixed point, $\mathbf{p}$ which facilitates computationally feasible approaches for stability analysis and design.

4.8.2 Periodic orbital stability based on Contraction mapping

Definition 4.6 provides the definition of asymptotic stability of a periodic orbit, $\mathcal{O}$ in Lyapunov sense whereas Theorem 4.1 establish the unique relation between the asymptotic stabilities of a periodic orbit $\mathcal{O}$ and its fixed point, $\mathbf{p}$. Hence to establish the asymptotic stability of the solution of certain periodic dynamical system, it is necessary to first determine the equilibrium orbit and the associated fixed point followed by proving the asymptotic stability of the fixed point in Lyapunov sense. This is the *classical approach* for establishing the stability of periodic systems. There are two practical difficulties associated with the classical approach when applied for control applications such as realistic bipedal walk. Firstly, the online estimation of feasible periodic orbit along with its fixed point is computationally a complex task. Secondly, stabilization of the computed periodic orbit will normally call for stiff path tracking type controllers with all their associated drawbacks as discussed earlier in detail.

The distinguishing feature of contraction mapping theorem, when compared to Lyapunov approach is that the asymptotic stability of the equilibrium point (i.e. the final convergence point or fixed point of a discrete sequence) is stated independent of the same and makes use only of the contraction property of consecutive elements of the sequence or contraction between the corresponding elements of any two independent sequences belonging to a positively invariant compact subset of a linear space. Further, based on Theorem 4.1, the visualization of stability requirement as a contraction property or *induced mutual attraction* between the sequence of Poincaré maps, $\mathbf{z}_1(\mathrm{k}), \mathbf{z}_2(\mathrm{k}), \cdots \in \mathcal{S}^{\mathrm{C}}_{\mathrm{SP}}$ gets directly translated to the requirement of *induced mutual attraction between the corresponding set of trajectories* in an integrated sense over each cycle. Hence the trajectory controller need not have to enforce stiff tracking with respect to any pre-synthesized periodic orbit $\mathcal{O}$, instead it should only induce virtual attraction between the trajectories belonging to certain feasible set [85] which in turn will induce mutual attraction between their Poincaré maps establishing the asymptotic stability of the evolved periodic orbit, $\mathcal{O}$. This is the theoretical basis for the periodic orbital stability concept based on contraction mapping theorem.

4.8.2.1 Contraction mapping theorem

Theorem 4.2. ***Contraction Mapping [83]***

Let $\mathcal{S}^{\mathrm{C}}$ be a closed subset of a Banach space $\mathcal{X}$ and let T be a mapping that maps $\mathcal{S}^{\mathrm{C}}$ into $\mathcal{S}^{\mathrm{C}}$. Suppose that

$$\| \mathsf{T}(\boldsymbol{x}) - \mathsf{T}(\boldsymbol{y}) \| \leqslant \rho_{\mathrm{c}} \| \boldsymbol{x} - \boldsymbol{y} \|, \forall \boldsymbol{x}, \boldsymbol{y} \in \mathcal{S}^{\mathrm{C}}, \, 0 \leqslant \rho_{\mathrm{c}} < 1 \tag{4.84}$$

then

- *there exists a unique vector $\boldsymbol{z}^* \in \mathcal{S}^{\mathrm{C}}$ satisfying $\boldsymbol{z}^* = \mathsf{T}(\boldsymbol{z}^*)$.*
- *$\boldsymbol{z}^*$ can be obtained by the method of successive approximation, starting from any arbitrary initial vector in $\mathcal{S}^{\mathrm{C}}$.*

Further, the sequence $\mathbf{z}(\mathrm{k}+1) = \mathsf{T}(\mathbf{z}(\mathrm{k})), \forall \mathbf{z}(\mathrm{k}) \in \mathcal{S}^{\mathrm{C}}$ is Cauchy [83]. This can be proved as follows. Select an arbitrary $\mathbf{z}(1) \in \mathcal{S}^{\mathrm{C}}$ and define the sequence $\{\mathbf{z}(\mathrm{k})\}$ by the formula $\mathbf{z}(\mathrm{k}+1) = \mathsf{T}(\mathbf{z}(\mathrm{k}))$. Since $\mathcal{S}^{\mathrm{C}}$ is a closed subset of Banach space under the map T, $\mathbf{z}(\mathrm{k}) \in \mathcal{S}^{\mathrm{C}}$ for all $\mathrm{k} \geqslant 1$. Hence,

$$\begin{aligned} \| \mathbf{z}(\mathrm{k}+1) - \mathbf{z}(\mathrm{k}) \| &= \| \mathsf{T}(\mathbf{z}(\mathrm{k})) - \mathsf{T}(\mathbf{z}(\mathrm{k}-1)) \| \leqslant \rho_{\mathrm{c}} \| \mathbf{z}(\mathrm{k}) - \mathbf{z}(\mathrm{k}-1) \| \\ &\leqslant \rho_{\mathrm{c}}^2 \| \mathbf{z}(\mathrm{k}-1) - \mathbf{z}(\mathrm{k}-2) \| \; ... \leqslant \rho_{\mathrm{c}}^{\mathrm{k}-1} \| \mathbf{z}(2) - \mathbf{z}(1) \| \end{aligned} \tag{4.85}$$

Thus the distance between the consecutive elements of the sequence decreases monotonically with a geometric reduction factor of ρ_c. Further,

$$\begin{aligned} \| \mathbf{z}(k+r) - \mathbf{z}(k) \| \leqslant & \| \mathbf{z}(k+r) - \mathbf{z}(k+r-1) \| + \| \mathbf{z}(k+r-1) - \mathbf{z}(k+r-2) \| \\ & + \cdots + \| \mathbf{z}(k+1) - \mathbf{z}(k) \| \qquad (4.86) \\ & \leqslant \left[\rho_c^{k+r-2} + \rho_c^{k+r-3} + \cdots + \rho_c^{k-1} \right] \| \mathbf{z}(2) - \mathbf{z}(1) \| \\ & \leqslant \frac{\rho_c^{k-1}}{1-\rho_c} \| \mathbf{z}(2) - \mathbf{z}(1) \| \qquad (4.87) \end{aligned}$$

As $k \to \infty$, the RHS tends to zero and hence the contracting sequence is proved to be Cauchy. Further as $\mathcal{X}$ is a Banach space, $\mathbf{z}(k) \to \mathbf{z}^* \in \mathcal{X}$ as $k \to \infty$. In other words, the monotonic contraction (or attraction) between corresponding elements of any two different sequences, $T(\mathbf{x}(k))$ and $T(\mathbf{y}(k))$ implies the monotonic contraction between the consecutive elements $\mathbf{z}(k)$ and $\mathbf{z}(k+1)$ of any sequence $T(\mathbf{z}(k))$ which further implies the asymptotic stability of the limit point, $\mathbf{z}^* = \lim_{k\to\infty} \mathbf{z}(k)$ under the map $\mathbf{z}(k+1) = T(\mathbf{z}(k))$, as long as $\mathbf{z}(k), \mathbf{x}(k), \mathbf{y}(k) \in \mathcal{S}^C \subset \mathcal{X}$. This interpretation may be compared with the recursive contraction type interpretation of asymptotic stability in the sense of Lyapunov given by (4.83). Moreover, the contraction based stability concept is useful even if the sequence is not asypmtotically converging, rather only ultimately bounded with a truncated sequence of convergence. In such cases, the relative stability can be assessed from the initial part of converging sequence of $\| \mathbf{z}(k) \|$ prior to its entry into the perturbation band. Hence the method is quite useful for the stability analysis of realistic bipedal walk.

4.8.2.2 Contraction Stability theorem for periodic dynamical systems

Contraction Stability theorem provides a control oriented theorem for periodic orbital stability by combining the asymptotic stability requirement of periodic orbit in Lyapunov sense, Poincaré theorem correlating the asymptotic stabilities of periodic orbit and the corresponding fixed point and contraction mapping theorem for establishing the asymptotic stability of contracting Poincaré return map, while all of these are applied for periodic nonlinear dynamical systems.

Theorem 4.3. ***Contraction Stability theorem***

Consider the controlled autonomous dynamical system described by the nonlinear differential equation,

$$\dot{\boldsymbol{x}}(t) = \boldsymbol{f}(\boldsymbol{x}(t), \boldsymbol{u}), \boldsymbol{u}_{[t_0,t)} = \phi(\boldsymbol{x}) \in \mathcal{U}, \boldsymbol{x}(t_0) = \boldsymbol{x}_0 = z_0, t \in [t_0, \infty) \qquad (4.88)$$

where $\boldsymbol{x} \in \mathcal{D} \subseteq \mathbb{R}^n$, $\mathcal{D}$ *being an open subset of* $\mathbb{R}^n$ *and* $\boldsymbol{f} : \mathcal{D} \to \mathbb{R}^n$ *and* $\phi : \mathcal{D} \to \mathbb{R}^m$ *are Lipschitz continuous vector fields on* $\mathcal{D}$ *and* $\mathcal{U}$ *is the set of feasible controllers*[11]. *Let us denote the controlled flow,* $s^u(t, t_0, z_0, \boldsymbol{u}_{[t_0,t)}) \in \mathbb{R}^n$ *as the solution of the system dynamics at time* $t \in [t_0, \infty)$ *with initial condition,* $z_0 \in \mathcal{S}_{SP}^{Cu}$ *where* $\mathcal{S}_{SP}^{Cu}$ *is defined as a compact subset of the strictly proper switching set of codimension-1 for the controlled system dynamics. Then the strictly proper trajectory segments of the dynamical system defined by*

$$\begin{aligned}\psi_{SP}^{Cu}(t_{i-1}, z(i-1)) := &\big\{ s^u(t, t_{i-1}, z(i-1), \boldsymbol{u}_{[t_{i-1},t)}) : z(i-1) := \boldsymbol{x}(t_{i-1}) \in \mathcal{S}_{SP}^{Cu}, \\ &t_{i-1} \leqslant t \leqslant t_i \big\} \\ &\textit{with } t_i := t_{i-1} + \tau(z(i-1)),\ i \in \mathbb{Z}_+\end{aligned} \tag{4.89}$$

will asymptotically converge to a periodic orbit, $\mathcal{O} \in \mathcal{D} \subseteq \mathbb{R}^n$ *as* $i \to \infty$ *if the controller,* $\boldsymbol{u} \in \mathcal{U}$ *is able to induce mutual attraction between any pair of strictly proper trajectory segments,* $\psi_{SP}^{Cu}(t_{i-1}, z(i-1))$ *starting from different values of* $z_0 \in \mathcal{S}_{SP}^{Cu}$ *at* $t = t_0$ *in the sense that the distance between the trajectory intersections with* $\mathcal{S}_{SP}^{Cu}$ *is a contraction sequence for* $i \in \mathbb{Z}_+$.

Proof:

Starting from $\mathbf{z}_0 = \mathbf{x}_0 = \mathbf{x}(t_0) \in \mathcal{S}_{SP}^{Cu}$ at $k = 0$ and $t = t_0$ and as per the definition of strictly proper set of trajectories given by (4.89) and also based on the definition of Poincaré map given by (4.71)-(4.72), $\psi_{SP}^{Cu}(t_0, \mathbf{x}(t_0)) \cap \mathcal{S}_{SP}^{Cu} = \mathbf{x}(t_1(\mathbf{x}_0)) = \mathbf{z}_1 = \mathcal{P}(\mathbf{z}_0)$. This can be generalized for the $(k+1)^{\text{th}}$ trajectory segment as $\psi_{SP}^{Cu}(t_k, \mathbf{x}(t_k)) \cap \mathcal{S}_{SP}^{Cu} = \mathbf{x}(t_{k+1}) = \mathbf{z}(k+1) = \mathcal{P}(\mathbf{z}(k))$. Since the intersections of any pair of trajectory segments with the switching set are guaranteed to be a contraction sequence, by Contraction mapping theorem, the asymptotic convergence of Poincaré map sequence, $\mathbf{z}(k)$ is also guaranteed. Further, the sequence $\mathbf{z}(k)$ will asymptotically converge to a unique point in $\mathcal{S}_{SP}^{Cu}$ as $k \to \infty$ given by $\mathbf{p} = \lim_{k\to\infty} \mathbf{z}(k)$. The unique relation between the asymptotic stability of an orbit and its fixed point as per Theorem 4.1 directly translates the contraction property of Poincaré return map, $\mathbf{z}(k)$ to its generating trajectory. Thus $\psi_{SP}^{Cu}(t_k, \mathbf{x}(t_k))$ asymptotically converges to the periodic orbit $\mathcal{O}$ associated with the fixed point, $\mathbf{p}$ while the sequence of the associated intersection points, $\mathbf{z}(k)$ with $\mathcal{S}_{SP}^{Cu}$ asymptotically converges towards $\mathbf{p}$. This proves the contraction stability theorem.

Any standard norm can be used for measuring the distance between the trajectory intersections with the switching set, $\mathcal{S}_{SP}^{Cu}$. Since the norm based stability is a stronger criterion

[11] The feasible controllers are functions of $\mathbf{x}$ consistent with all system constraints specified additionally.

compared to the eigenvalue based stability applied to the corresponding linearized Poncaré map, the former will be conservative, however with the added benefit of extra robustness margin.

4.8.2.3 Perturbations in contraction mapping and ultimate bounded stability

The effect of perturbations in contraction mapping, $\mathrm{T}(.)$ can be easily depicted by Fig 4.10 when applied to a scalar sequence, $z(\mathrm{k})$. In ideal situation, the fixed point is represented

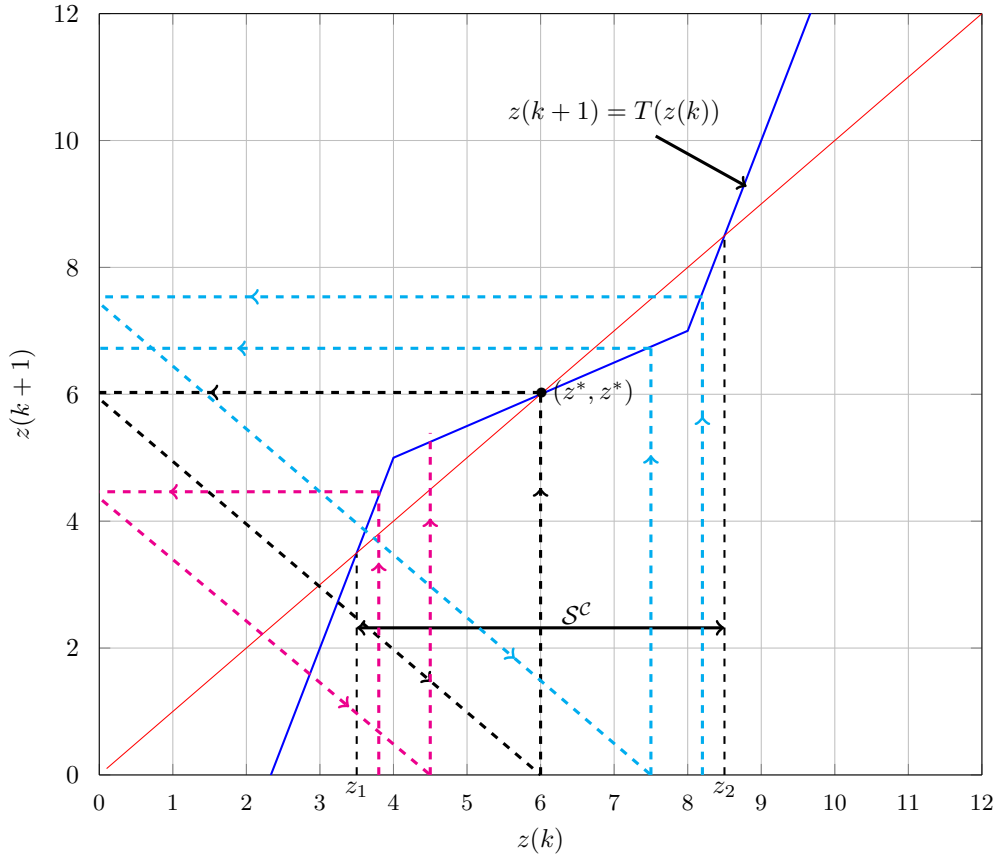

Figure 4.10: Graphical representation of contraction map for scalar sequence, $z(\mathrm{k}+1) = \mathrm{T}(z(\mathrm{k}))$ with domain of attraction, $\mathcal{S}^{\mathrm{C}}$ and fixed point, z^*.

by z^*, the point of intersection between the curve, $z(\mathrm{k}+1) = \mathrm{T}(z(\mathrm{k}))$ and the unity slope straight line passing through the origin. The domain of attraction, $\mathcal{S}^{\mathrm{C}}$ is represented by the interval, $[z_1, z_2]$. There are two-fold effects due to the perturbations in $\mathrm{T}(.)$. The random perturbation of $\mathrm{T}(z)$ will lead to both random changes in its slope, $\frac{\mathrm{dT}(z)}{\mathrm{dz}}$ as well

as the point of intersection, z^*. Let us first assume that the fixed point remains same as z^*, but the slope changes from cycle to cycle, as in realistic bipedal walk, represented by $\rho_c(z(k), t_k) = |\frac{dT(z)}{dz}|$ at $z = z(k), \& \, t = t_k$. Then mapping relation of (4.84) becomes,

$$\| T_{k+1}(z(k+1)) - T_k(z(k)) \| \leqslant \bar{\rho}_c(k) \| z(k+1) - z(k) \|, \forall z(k), z(k+1) \in \mathcal{S}^C$$
$$0 \leqslant \bar{\rho}_c(k) \leqslant \max(\rho_c(z(k), t_k), \rho_c(z(k+1), t_{k+1}) < 1 \tag{4.90}$$

As per contraction mapping theorem, $\lim_{k\to\infty} z(k) = z^*$ and hence the fixed point and the converged periodic orbit remain the same as in unperturbed case. Thus the perturbation in the slope, ρ_{ck} of return map affects only the convergence rate to the fixed point. However, the second part of random perturbation, $\delta z^*(k)$ in the fixed point will affect the contraction mapping when $\|z(k+1) - z(k)\|$ converges to a value comparable to $|\delta z^*(k)|$. Thus the net effect of perturbation in $T(.)$ is to produce a band of convergence points, z^* after an initial period of convergence provided the upper bound of slope, $\bar{\rho}_c(k)$ remains less than unity. As per the definition given in Definition 4.2(ii), such a behaviour belongs to the class of ultimately bounded type stability. The final converged domain of discrete intersection points, $\mathbf{z}^*(k)$ is represented by $\mathcal{C}_S$, the *Convergence set* with respect to the generic system dynamics represented in (4.88) and can be defined as the positively invariant set of minimum size so that $\mathcal{P}(\mathbf{z}_P(k)) \in \mathcal{C}_S$ if $\mathbf{z}_P(k) \in \mathcal{C}_S \subseteq \mathcal{S}^C_{SP}$ under random perturbations in system dynamics. Let us designate the mapping function which results in a sequence which converges monotonically to the bounded convergence set, $\mathcal{C}_S$ by *truncated contraction mapping*. From a periodic stability perspective, the relative stability of systems exhibiting truncated contraction and uniform contraction are similar during the initial portions if the contraction factors, $\rho_c(z)$ are of similar values during the initial contraction zone.

4.8.2.4 Extension for impulsive dynamical systems

The mathematical model of planar bipedal gait developed in Chapter 3 belongs to the class of impulsive dynamical system which is a subclass of general hybrid dynamical system. Hence it is necessary to extend the stability results developed so far to impulsive dynamical systems also. It has been shown by the team of W. M. Haddad [86, 87, 88] that the Lyapunov-Poincaré stability concepts can be directly extended to a class of recurrent impulsive dynamical systems characterized by strong left-continuous properties with intermittent state dependent impulsive dynamics. We make use of their results in the subsequent

formulation to extend the contraction stability theorem for impulsive bipedal gait dynamics.

In general, the dynamics of an impulsive dynamical system can be represented as,

$$\dot{\mathbf{x}}(t) = \mathbf{f}_c\left(\mathbf{x}(t)\right); \mathbf{x}(t_0) = \mathbf{x}_0; \mathbf{x}(t) \notin \mathcal{S}_i, i \in [1, N_I] \tag{4.91}$$

$$\mathbf{x}(t^+) = \Delta_i\left(\mathbf{x}(t)\right); \mathbf{x}(t) \in \mathcal{S}_i; \tag{4.92}$$

where $\mathcal{S}_i \subset \mathcal{D} \subseteq \mathbb{R}^n, i \in [1, N_I]$ are the switching hyperplanes of co-dimension 1 and which lie transverse to the solution trajectory $s(t, t_0, \mathbf{x}_0)$ on the i^{th} impulsive impact event of every cycle. There are basically three parts for an impulsive dynamical system; namely, a continuous-time differential equation as given by (4.91), which governs the motion of the dynamical system between impulsive or resetting events; a difference equation as given by (4.92), which governs the way the system states are instantaneously changed when a resetting event occurs; and a criterion for determining when the states of the system are to be reset as given by the switching set, $\mathcal{S}_i$. In continuous dynamical systems, the switching set, $\mathcal{S}_{SP}$ required for defining Poincaré map can be selected at any point, $\mathbf{x} \in \mathcal{O}$ as a transverse plane to the orbit, $\mathcal{O}$. However in impulsive dynamical systems, $\mathcal{S}_{SP}$ is to be defined at the point of the orbit where the physical impact or resetting occurs. If there are more than one instance of impulsive impact during each cycle as formulated above, the most distinguishing impact point is to be selected to define Poincaré section like transit heel impact event in the case of uniform terrain bipedal walk or transit toe impact event in the case of staircase walk. The generalization of Poincaré stability theorem starts with the definition of strong left continuous systems in place of the continuous time dynamical system represented by (4.63). The major results presented in [86, 87, 88] in this context are stated below without proofs and detailed explanations.

Definition 4.9. *The finitely or infinitely countable set,* $\mathcal{T}_{Sx0} := \{\tau_i(\boldsymbol{x}_0); i \in \mathcal{N}$ *with* $\tau_0(\boldsymbol{x}_0) := t_0$ *and* $\tau_1(\boldsymbol{x}_0) < \tau_2(\boldsymbol{x}_0) <, ...; \boldsymbol{x}_0 \in \mathcal{D} \subseteq \mathbb{R}^n\}$ *is defined as the resetting or switching times where there will be discontinuous transition for the trajectory,* $s(t, t_0, \boldsymbol{x}_0)$. $\mathcal{T}_{x0} := \{t \in [t_0, \infty); s(t, t_0, \boldsymbol{x}_0) = s(t^+, t_0, \boldsymbol{x}_0), \boldsymbol{x}_0 \in \mathcal{D} \subseteq \mathcal{R}^n\}$ *is a dense subset of the semiinfinite interval,* $[t_0, \infty)$ *such that* $[t_0, \infty) \setminus \mathcal{T}_{x0} \equiv \mathcal{T}_{Sx0}$.

In other words, the system trajectory evolves as per (4.91) while $t \in \mathcal{T}_{x0}$ and will have discrete transition as per (4.92) while $t \in \mathcal{T}_{Sx0}$.

Assumption 4.1. *[88] For every* $i \in \mathcal{N}$, $\tau_i(.)$ *is continuous and for every* $\boldsymbol{x}_0 \in \mathcal{D}$, *there exists* $\epsilon(\boldsymbol{x}_0) > 0$ *such that* $\tau_{i+1}(\boldsymbol{x}_0) - \tau_i(\boldsymbol{x}_0) \geqslant \epsilon(\boldsymbol{x}_0), i \in \mathcal{N}$.

Definition 4.10. ***Left continuous dynamical system*** *[88]*

A left-continuous dynamical system on $\mathcal{D}$ *is the triple* $(\mathcal{D}, [t_0, \infty), s)$ *where* $s : [t_0, \infty) \times \mathcal{D} \to \mathcal{D}$ *is such that the following axioms hold:*

i) (Left-continuity): $s(t, t_0, \boldsymbol{x}_0)$ *is left-continuous in t, i.e.* $\lim_{\tau \nearrow t^-} s(\tau, t_0, \boldsymbol{x}_0) = s(t, t_0, \boldsymbol{x}_0)$ *for all* $\boldsymbol{x}_0 \in \mathcal{D}$ *and* $t \in (t_0, \infty)$.

ii) (Consistency): $s(t_0, t_0, \boldsymbol{x}_0) = \boldsymbol{x}_0$ *for all* $\boldsymbol{x}_0 \in \mathcal{D}$.

iii) (Semi-group property): $s(t_2, t_1, s(t_1, t_0, \boldsymbol{x}_0)) = s(t_2, t_0, \boldsymbol{x}_0)$ *for all* $\boldsymbol{x}_0 \in \mathcal{D}$ *and* $t_1 \in [t_0, \infty), t_2 \in [t_1, \infty)$.

iv) (Quasi-continuous dependence): For every $\boldsymbol{x}_0 \in \mathcal{D}$, *there exists* $\mathcal{T}_{x0} \subseteq [t_0, \infty)$ *and corresponding* $\mathcal{T}_{Sx0}$ *and for every* $\epsilon > 0$ *and* $t \in \mathcal{T}_{x0}$, *there exists* $\delta(\epsilon, \boldsymbol{x}_0, t) > 0$ *such that if* $\| \boldsymbol{x}_0 - \boldsymbol{y} \| < \delta(\epsilon, \boldsymbol{x}_0, t), \boldsymbol{y} \in \mathcal{D}$, *then* $\| s(t, t_0, \boldsymbol{x}_0) - s(t, t_0, \boldsymbol{y}) \| < \epsilon$.

It is easy to show that bipedal dynamic walking satisfies the above requirements. Assuming, 't' as the instant of transit heel impact on ground during any walking step, the requirement of left continuity is satisfied. On the contrary, bipedal dynamic walking is not right continuous on impact events since $\lim_{\tau \searrow t^+} s(\tau, t_0, \mathbf{x}_0) \neq s(t, t_0, \mathbf{x}_0)$ due to the impact reset map given by (3.46). The quasi-continuous dependence of solutions as stated above is equivalent to Lyapunov stability of impulsive dynamical systems as defined in [88]. This demands continuity of flow $s(t, t_0, \mathbf{x}_0)$ with respect to the initial condition $\mathbf{x}_0$ even across impulsive dynamics events. The new velocity impact map, proposed in the thesis given by (3.37) meets this requirement as long as the elements of $\Delta^{iv}(q)$ are continuous with respect to the bipedal joint variable, q.

Definition 4.11. ***Jointly continuous system*** *[88].*

The trajectory of a left continuous system $(\mathcal{D}, [t_0, \infty), s)$ *is jointly continuous between resetting events if for every* $\epsilon > 0$ *and* $k \in \mathcal{N}$, *there exists* $\delta = \delta(\epsilon, k) > 0$ *such that if* $|t - t'| + \| \boldsymbol{x}_0 - \boldsymbol{y} \| < \delta$, *then* $\| s(t, t_0, \boldsymbol{x}_0) - s(t', t_0, \boldsymbol{y}) \| < \epsilon$, *where* $\boldsymbol{x}_0, \boldsymbol{y} \in \mathcal{D}, t \in (\tau_k(\boldsymbol{x}_0), \tau_{k+1}(\boldsymbol{x}_0)]$, *and* $t' \in (\tau_k(\boldsymbol{y}), \tau_{k+1}(\boldsymbol{y})]$.

The joint continuity property with respect to both t and $\mathbf{x}$ is to be comapred with the quasi-continuous dependence with respect to $\mathbf{x}_0$ alone as given in Definition 4.10(iv). For the autonomous system given in (4.91)-(4.92), the flow $s(t, t_0, \mathbf{x}_0)$ depends only on $\mathbf{x}_0$ and $(t - t_0)$. In the case of two independent trajectories starting from $\mathbf{x}_0$ and $\mathbf{y}$ at the same time t_0, the trajectory perturbations at two different times, t and t' hence depends on the perturbation variables, $(t - t')$ and $\mathbf{x}_0 - \mathbf{y}$. Thus the joint continuity as per Definition 4.11

defines the continuity of $s(t, t_0, \mathbf{x}_0)$ with respect to the combination of independent variables $(t - t_0)$ and $\mathbf{x}_0$.

Definition 4.12. ***Strong left continuous system*** *[88]*

The dynamical system $(\mathcal{D}, [t_0, \infty), s)$ *satisfying axioms i) to iii) of Definition 4.10 and Assumption 4.1 is called strong left-continuous system if its trajectory* $s(t, t_0, \boldsymbol{x}_0), t \geqslant t_0$ *is jointly continuous between the resetting events.*

Definition 4.13. ***Periodic solution and Periodic orbits for left continuous dynamical systems*** *[82]*

The solution $s(t, t_0, \boldsymbol{x}_0)$ *of a left continuous dynamical system is periodic if there exists a finite time* $T > 0$ *such that* $s(t + T, t_0, \boldsymbol{x}_0) = s(t, t_0, \boldsymbol{x}_0)$ *for all* $t \geqslant t_0$*. The minimal* T *for which the solution* $s(t, t_0, \boldsymbol{x}_0)$ *is periodic is called the period. A set* $\mathcal{O} \subset \mathcal{D}$ *is a periodic orbit of left continuous dynamical system if,* $\mathcal{O} = \{\boldsymbol{x} \in \mathcal{D} : \boldsymbol{x} = s(t, t_0, \boldsymbol{x}_0), t_0 \leqslant t \leqslant t_0 + T\}$ *for some periodic solution* $s(t, t_0, \boldsymbol{x}_0)$ *of the system.*

If there are N_I impact events during each periodic cycle, for every $\mathbf{x}_0 \in \mathcal{O}$, we get the periodic relation, $\tau_{i+N_I}(\mathbf{x}_0) = \tau_i(\mathbf{x}_0) + T, i \in \bar{\mathbb{Z}}_+$ and $t_{k+1}(\mathbf{x}_0) = t_k(\mathbf{x}_0) + T; k \in \bar{\mathbb{Z}}_+$ with $\tau_0(\mathbf{x}_0) = t_0(\mathbf{x}_0) = t_0$. For planar bipedal walk $N_I = 2$, corresponding to the events of transit heel ground impact and subsequent toe impact.

4.8.2.5 Poincaré return map for impulsive dynamical systems

The next requirement for the extension of Poincaré return map for impulsive dynamical systems is the modifications for various switching sets like $\mathcal{S}, \mathcal{S}_P, \mathcal{S}_{SP}$ and $\mathcal{S}_{SP}^C$. As mentioned earlier, the switching hyperplane, $\mathcal{H}$ has to be selected as the transverse plane of codimension-1 at the point, $\mathbf{x} \in \mathcal{O}$ when the most important impact event of the cycle occurs like transit heel strike on ground for a bipedal walk on uniform terrain. Let us denote this point as $\mathbf{x} = \mathbf{p}$, the fixed point of the orbit, $\mathcal{O}$ and let the transverse hyperplane containing $\mathbf{x} = \mathbf{p}$ be represented by $\mathcal{H}_I$. The definitions of $\mathcal{S}, \mathcal{S}_P, \mathcal{S}_{SP}$ and $\mathcal{S}_{SP}^C$ remain the same as previous with $\mathcal{S}_{SP}^C \subseteq \mathcal{S}_{SP} \subset \mathcal{S}_P \subset \mathcal{S} \subset \mathcal{H}_I$. Next, we can define Poincaré return map, $\mathcal{P} : \mathcal{S}_{SP} \to \mathcal{S}_P$ by,

$$\mathcal{P}(\mathbf{x}) := s(\tau_{N_I}(\mathbf{x}), t_0, \mathbf{x}),\ \mathbf{x} \in \mathcal{S}_{SP} \text{ at } t = t_0 \tag{4.93}$$

Since $\mathbf{p} \in \mathcal{O} \cap \mathcal{S}_{SP}$, $s(\tau_{N_I}(\mathbf{p}), t_0, \mathbf{p}) = \mathbf{p}$ and hence $\mathcal{P}(\mathbf{p}) = \mathbf{p}$. Further, $\mathcal{P}(.)$ is a well defined function as $\tau_{N_I}(.)$ is continuous as per Assumption 4.1. The equivalent representation of Poincaré return map in discrete time domain for the impulsive dynamical system can be written as,

$$\mathbf{z}(k + 1) = \mathcal{P}(\mathbf{z}(k)); \mathbf{z}(k) \in \mathcal{S}_{SP}, k \in \bar{\mathbb{Z}}_+ \tag{4.94}$$

Clearly, $\mathbf{z}(\mathtt{k}) = \mathbf{p}$ is a fixed point of (4.94) so that $\mathbf{p} = \mathcal{P}(\mathbf{p})$.

The Lyapunov stability definitions of the periodic orbit $\mathcal{O}$ for strong left continuous dynamical system having impulsive dynamics remain the same as that given in Definition 4.6. Similarly the equivalence between Lyapunov stabilities of periodic orbit and its fixed point as stated by Poincaré 's theorem (Theorem 4.1) also holds good for the strong left continuous dynamical system as proved in [88, 86]. As a consequence, the Contraction stability theorem stated in Theorem 4.3 holds good for strong left continuous type periodic impulsive dynamical systems as well.

4.8.2.6 Application of Contraction stability theorem to planar bipedal dynamic walking

The postural dynamics of planar biped during dynamic walking can be represented as a nonlinear autonomous system with state vector, $\mathbf{x}_{\mathtt{P}} = [\mathbf{x}'_{\mathtt{Pc}}\ \dot{\mathbf{x}}'_{\mathtt{Pc}}]' \in T\mathcal{C} \subset \mathbb{R}^{2\mathtt{n}_{\mathtt{P}}}; \mathtt{n}_{\mathtt{P}} = 12$ as explained in Section 4.7

Definition 4.14. ***H_{es}*** *is defined as the set of feasible sequence of $\mathbb{H}^{\mathtt{i}}_{\mathtt{es}}, \mathtt{i} \in [1, \mathtt{n}_{\mathtt{es}}]$ to realize the specified pattern of dynamic walking gait for the planar biped, where $\mathtt{n}_{\mathtt{es}}$ is the total number of hybrid dynamical phases in a single walking gait.*

The definitions of transverse hyperplanes intersecting with periodic solutions of continuous system dynamics given in Section 4.8.1.4 are to be redefined for bipedal postural dynamics introduced in Section 4.7 to accommodate for the additional effect of impact dynamics and hybrid state driven control. The modified definitions are given below.

Definition 4.15. ***Controlled switching sets for planar bipedal dynamic walk over uniform terrain***

The controlled switching set, $\mathcal{S}^{\mathtt{u}}$ for a planar bipedal dynamic walk over uniform terrain is a nonempty, $(2\mathtt{n}_{\mathtt{P}}-1)$ dimensional subset of $T\mathcal{C} \subset \mathbb{R}^{2\mathtt{n}_{\mathtt{P}}}$ and there exists a differentiable function $\xi(\boldsymbol{x}_{\mathtt{Pc}}) : \mathcal{C} \to \mathbb{R}$ such that [80]

$$\mathcal{S}^{\mathtt{u}} := \big\{\boldsymbol{x}_{\mathtt{P}} \in T\mathcal{C} \subset \mathbb{R}^{2\mathtt{n}_{\mathtt{P}}} : \Sigma\pi_{\mathtt{m}(1:2)} \geqslant 1, \Sigma\boldsymbol{x}_{\mathtt{Pc}(6:7)} > 0, \xi(\boldsymbol{x}_{\mathtt{Pc}}) = 0, \dot{\xi}(\boldsymbol{x}_{\mathtt{Pc}}) < 0, \quad (4.95)$$

$$\overline{\Delta^{\mathtt{i}}(\mathcal{S}^{\mathtt{u}})} \cap \mathcal{S}^{\mathtt{u}} = \emptyset \textit{ for any }, \boldsymbol{u} \in \mathcal{U}\big\}. \quad (4.96)$$

$\mathcal{S}^{\mathtt{u}}$ admits only the heel strike event with[12] $\mathtt{x}_{\mathtt{th}} > \mathtt{x}_{\mathtt{rt}}$ and excludes static double support phase with $\dot{\xi}(\mathbf{x}_{\mathtt{Pc}}) = 0$. The additional requirement of $\overline{\Delta^{\mathtt{i}}(\mathcal{S}^{\mathtt{u}})} \cap \mathcal{S}^{\mathtt{u}} = \emptyset$ insists that the

[12] Since $\mathtt{x}_{\mathtt{rh}} = \mathtt{x}_{\mathtt{th}}(\mathtt{t}_{\mathtt{k}}^{-})\ \forall \mathtt{t} \in [\mathtt{t}_{\mathtt{k}}, \mathtt{t}_{\mathtt{k}+1}^{-})$, $\Sigma\mathbf{x}_{\mathtt{Pc}(6:7)} > 0$ implies $\mathtt{x}_{\mathtt{th}} > \mathtt{x}_{\mathtt{rh}}$.

discrete velocity change due to transit foot ground impact should take away the postural state velocity away from $\mathcal{S}^u$, for any control action, u belonging to the set of feasible controllers, $\mathcal{U}$. The *proper controlled switching set*, $\mathcal{S}^u_P \subset \mathcal{S}^u$ has the additional property that all trajectories starting at $\mathbf{x}_{P0} \in \mathcal{S}^u_P$ intersects $\mathcal{S}^u$ within a finite time, $\tau(\mathbf{x}_{P0}) > 0$. The physical requirement of $\mathcal{S}^u_P$ is that the biped should neither stop nor fall backwards for any trajectory starting at $\mathbf{x}_{P0} \in \mathcal{S}^u_P$.

Definition 4.16. ***Proper set of task level controllers***

The proper set of task level controllers, $\mathcal{U}_P := \{u^i; i \in [1, n_{es}]\} \subset \mathbb{R}^{n_P}$ *is defined as the set of all task level controller sequences* $u^i; i \in [1, n_{es}]$ *designed for the specified* $\boldsymbol{H}_{es}$ *spanning over* $t \in [t_0, t_0 + \tau(\boldsymbol{x}_{P0}))$ *which can drive the biped postural state,* $\boldsymbol{x}_P := [\boldsymbol{x}'_{Pc}\, \dot{\boldsymbol{x}}'_{Pc}]' \in T\mathcal{C}$ *starting from* $\boldsymbol{x}_P = \boldsymbol{x}_{P0} \in \mathcal{S}^u_P$ *at* $t = t_0$ *to reach* $\mathcal{S}^u$ *within finite time interval* $\tau(\boldsymbol{x}_{P0})$ *without violating any of the system constraints*[13] *relevant during various* $\mathbb{H}^i_{es} \in \boldsymbol{H}_{es}$ *of the gait.*

Physically, $u^i \in \mathcal{U}_p$ for bipedal dynamics corresponds to the joint torque command vector, $\Gamma_{d\,(3:14)}$ which are synthesized to be consistent with the system constraints[14]. Under the action of proper set of controllers, the postural dynamics of the planar biped during the k^{th} gait of dynamic walking can be written as follows:

$$\mathbf{x}_P(t_k^+) = \Delta_h(\mathbf{x}_{Pc}(t_k)); \mathbf{x}_P(t_k) \in \mathcal{S}^u_{SP}, t_0 = 0; k \in \bar{\mathbb{Z}}_+, \mathbf{x}_P(t_k) \in T\mathcal{C} \subset \mathbb{R}^{2n_P} \tag{4.97}$$

$$\begin{aligned} \dot{\mathbf{x}}_P(t) &= \mathbf{f}_{Pc}(\mathbf{x}_P(t), u^i); u^i \equiv \phi^i(\mathbf{x}_P) \in \mathcal{U}_P, \mathbb{H}_{es} \equiv \mathbb{H}^i_{es}, i \in [1, n_t] \\ &\qquad \text{for } t_k^+ \leqslant t \leqslant t_{tk} \text{ such that } \mathbf{x}_P(t_{tk}) \in \mathcal{S}^u_t \end{aligned} \tag{4.98}$$

$$\mathbf{x}_P(t_{tk}^+) = \Delta^i_{rt}(\mathbf{x}_{Pc}(t_{tk})); \tag{4.99}$$

$$\begin{aligned} \dot{\mathbf{x}}_P(t) &= \mathbf{f}_{Pc}(\mathbf{x}_P(t), u^j); u^j \equiv \phi^j(\mathbf{x}_P) \in \mathcal{U}_P, \mathbb{H}_{es} \equiv \mathbb{H}^j_{es}, j \in [n_t + 1, n_{es}] \\ &\qquad \text{for } t_{tk}^+ \leqslant t \leqslant t_{k+1} \end{aligned} \tag{4.100}$$

where Δ_h refers to the transit heel impact reset map taking care of both velocity impact map as well as index resetting, Δ^i_{rt} represents the reference toe impact map following the heel strike of the same foot, $\mathcal{S}^u_t$ represents the $(2n_P - 1)$ dimensional transverse switching plane on every reference toe impact on ground, $\mathbf{f}_{Pc}(.,.)$ represents the continuous time postural state dynamics of the planar biped in between consecutive impact events, $u^i, i \in [1,\, n_t]$ represents the postural state based feedback control during the $\mathbb{H}^i_{es}$ states between the heel

[13] System constraints include lower/upper bounds on normal component of ground contact force, friction cone constraints, joint torque limits, joint kinematic limits etc.

[14] Consistency with passive dynamic constraint on reference toe keeps $\Gamma_{d3} = 0$

impact and toe impact events and $u^j, j \in [n_t+1,\ n_{es}]$ represents the postural state based feedback control during the $\mathbb{H}^j_{es}$ states between the reference toe impact and subsequent transit heel impact events. The feedback control function, $\phi^i : T\mathcal{C} \to \mathbb{R}^{n_P}$ is a continuous mapping representing the feedback control action from the postural state vector to joint torque command vector. The change in the value of the index, i is associated with change in at least one of the components of ϕ^i associated with the change in the hybrid event state, $\mathbb{H}^i_{es}$.

Definition 4.17. ***Controlled flow of postural dynamics***

Controlled flow of postural dynamics, $s^u(t, t_0, \boldsymbol{x}_{P0}, u_{[t_0,t)}) \in \mathbb{R}^{2n_P}$ *is defined as the solution of the planar bipedal postural dynamics given by (4.97-4.100) at time* $t \in \mathbb{R}$ *with initial condition,* $\boldsymbol{x}_P = \boldsymbol{x}_{P0} \in \mathcal{S}^u_P$ *at* $t = t_0$ *and control* $u_{[t_0,t)} \in \mathcal{U}_P$.

For planar bipedal dynamics with two state dependent velocity impact maps, one index resetting map and driven by state dependent closed loop feedback regulators for actuated joints with remaining joints as passive, the controlled flow of postural dynamics, $s^u(t, t_0, \mathbf{x}_{P0}, u_{[t_0,t)})$ belongs to the class of strong left continuous dynamical systems as defined in Definition 4.12. In line with (4.69), let us define a subset, $\mathcal{S}^u_{SP} \subset \mathcal{S}^u_P$, called the *strictly proper controlled switching set* which has the additional property that all the controlled flow of postural dynamics starting at $\mathbf{x}_P = \mathbf{x}_{P0} \in \mathcal{S}^u_{SP}, t = t_0$ are guaranteed to intersect the same subset $\mathcal{S}^u_{SP}$ at $t = t_0 + \tau(\mathbf{x}_{P0})$ and no trajectory starting from an $\mathbf{x}_{P0} \notin \mathcal{S}^u_{SP}$ does not intersect $\mathcal{S}^u_{SP}$ at $t > t_0$.

$$\begin{aligned}\mathcal{S}^u_{SP} :=\{&\mathbf{x}_P \in \mathcal{S}^u_P : s^u\left(t_0 + \tau(\mathbf{x}_P), t_0, \mathbf{x}_P, u_{[t_0,t_0+\tau(\mathbf{x}_P))}\right) \in \mathcal{S}^u_{SP} \text{ iff } \mathbf{x}_P \in \mathcal{S}^u_{SP} \\ &\text{and } s^u(t, t_0, \mathbf{x}_P, u_{[t_0,t)}) \notin \mathcal{S}^u, t_0 < t < t_0 + \tau(\mathbf{x}_P)\}\end{aligned} \tag{4.101}$$

In other words, there exists a $u_{[t_0,t)} \in \mathcal{U}_P$ such that $s^u\left(t_0 + \tau(\mathcal{S}^u_{SP}), t_0, \mathcal{S}^u_{SP}, u_{[t_0+\tau(\mathcal{S}^u_{SP}))}\right) = \mathcal{S}^u_{SP}$ and hence $\mathcal{S}^u_{SP}$ can be considered as the positively invariant set of maximum size for the postural dynamics of planar bipedal dynamic walk over uniform terrain under the control action, $\mathcal{U}_P$. The physical requirement of $\mathcal{S}^u_{SP}$ is that the biped should neither stop nor fall backwards for any trajectory starting at $\mathcal{S}^u_{SP}$ and in addition the biped should repeat the same properties for all subsequent gait cycles, which means the biped should neither fall forward also. Finally, let us represent the largest compact subset of $\mathcal{S}^u_{SP}$ by $\mathcal{S}^{Cu}_{SP}$.

Definition 4.18. ***Strictly proper controlled trajectory and set of all strictly proper controlled trajectories for planar bipedal dynamic walk***

A strictly proper controlled trajectory, $\psi^{Cu}_{SP}(t_0, \boldsymbol{x}_P)$ *for a planar bipedal dynamic walk*

represented by (4.97-4.100) over uniform terrain is defined as

$$\psi_{SP}^{Cu}(t_0, \boldsymbol{x}_P) := \{s^u(t, t_0, \boldsymbol{x}_P, u_{[t_0,t)}) : \boldsymbol{x}_P \in \mathcal{S}_{SP}^{Cu} \text{ at } t = t_0, t_0 \leqslant t \leqslant t_0 + \tau(\boldsymbol{x}_P)\} \quad (4.102)$$

The set of all strictly proper controlled trajectories is defined as $\boldsymbol{\Psi}_{SP}^{Cu}(t_0) := \{\psi_{SP}^{Cu}(t_0, \boldsymbol{x}_P) : \boldsymbol{x}_P \in \mathcal{S}_{SP}^{Cu}\}$

4.8.2.7 Contraction stability theorem for planar bipedal walk

The planar bipedal dynamics stated in (4.97) to (4.100) belongs to the class of strong left continuous type impulsive dynamical system as justified in Section 4.8.2.4 and hence the contraction mapping theorem is applicable for bipedal dynamic walk also. However, for the sake of completion and precision, let us restate the contraction stability theorem in this context.

Theorem 4.4. ***Contraction Stability theorem for planar bipedal walk***

Consider the autonomous controlled dynamical system of planar bipedal walking described by the hybrid dynamics given in (4.97) to (4.100). Let us denote the controlled flow, $s^u(t, t_0, \boldsymbol{x}_{P0}, u_{[t_0,t)}) \in \mathbb{R}^{2n_P}$ *as the solution of the system dynamics at time* $t \in [t_0, \infty)$ *with initial condition,* $\boldsymbol{x}_{P0} = z_{P0} \in \mathcal{S}_{SP}^{Cu}$ *where* $\mathcal{S}_{SP}^{Cu}$ *is defined as the largest compact subset of the strictly proper switching set,* $\mathcal{S}_{SP}^{u}$ *of codimension-1 for the controlled system dynamics. Then the strictly proper trajectory segments of the dynamical system defined by*

$$\psi_{SP}^{Cu}(t_{i-1}, z_P(i-1)) := \big\{s^u(t, t_{i-1}, z_P(i-1), u_{[t_{i-1},t)}) : z_P(i-1) := \boldsymbol{x}_P(t_{i-1}) \in \mathcal{S}_{SP}^{Cu}, \\ t_{i-1} \leqslant t \leqslant t_i\big\} \text{with } t_i := t_{i-1} + \tau(z_P(i-1)),\ i \in \mathbb{Z}_+ \quad (4.103)$$

will asymptotically converge to a periodic orbit, $\mathcal{O}_P^u \in \mathcal{D}_P \subseteq \mathbb{R}^{2n_P}$ *as* $i \to \infty$ *if the controller,* $u \in \mathcal{U}_P$ *is able to induce mutual attraction between any pair of strictly proper trajectory segments,* $\psi_{SP}^{Cu}(t_{i-1}, z_P(i-1))$ *starting from different values of* $z_{P0} \in \mathcal{S}_{SP}^{Cu}$ *at* $t = t_0$ *in the sense that the distance between their intersections with* $\mathcal{S}_{SP}^{Cu}$ *is a contraction sequence for* $i \in \mathbb{Z}_+$.

Proof: The contraction stability theorem stated originally for non-impulsive dynamical systems are applicable to strong left continuous type impulsive dynamical system as justified in Section 4.8.2.5. Since the bipedal dynamics also belongs to the same class, as explained along with the statements of Definition 4.10 and Definition 4.11, contraction stability theorem is applicable to them also.

4.8.3 Multi-phase goal seeking approach for periodic stability regulation

The contraction stability theorem provides a constructive approach for the design of bipedal walking controller, $u_{[t_k\, t_{k+1}]} \in \mathcal{U}_P$ to ensure periodic stability. The requirement on the proper set of task level controllers, $\mathcal{U}_P$ can be summarized as follows:

i) $\mathcal{U}_P$ should be constraint consistent.

ii) All trajectories belonging to $\mathbf{\Psi}_{SP}^{Cu}$ starting from any point $\mathbf{x}_P \in \mathcal{S}_{SP}^{C}$ should be steered to reach $\mathcal{S}_{SP}^{C}$ itself after a finite time interval $\tau(\mathbf{x}_P)$.

iii) $\mathcal{U}_P$ should ensure incremental convergence between any two trajectories, $\psi_{SP}^{Cu}(t_0, \mathbf{x}_{P1})$ and $\psi_{SP}^{Cu}(t_0, \mathbf{x}_{P2})$ as they intersect $\mathcal{S}_{SP}^{C}$ every time.

If $\mathcal{U}_P$ satisfies all the above three requirements, any trajectory $\psi_{SP}^{Cu}(t_0, \mathbf{x}_P), \mathbf{x}_P \in \mathcal{S}_{SP}^{C}$ will asymptotically converge to the unique periodic orbit $\mathcal{O}_P^u$. Unlike other approaches like HZD or ZMP based controllers, contraction stability based control does not demand any a priori information regarding the final converged periodic orbit, $\mathcal{O}_P^u$. Rather, the periodic orbit evolves autonomously under the action of $\mathcal{U}_P$ while the biped walks over the terrain. Besides simplicity of control, the evolved orbit, $\mathcal{O}_P^u$ will be robust with respect to terrain as well as with external disturbance by virtue of its autonomous generation.

One possible method to ensure convergence between any two trajectories belonging to $\mathbf{\Psi}_{SP}^{Cu}$ is to attract them towards a common goal. However a single stationary goal like the desired fixed point, $\mathbf{p}$ of periodic orbit, will only lead to a *stable focus* in the phase plane to which all trajectories will converge. This can be solved by using either moving goal along another suitable orbit or by using switched multiple subgoals distributed around the desired postural orbit, $\mathcal{O}_P^u$. The former is not a viable scheme as it also demands the determination of another periodic orbit for goal sweeping. However, the latter scheme can be easily implemented by attaching a subgoal for each hybrid dynamic phase, $\mathbb{H}_{es}^{i}$ and placing it ahead of the switching plane for the respective $\mathbb{H}_{es}^{i}$ as shown in Fig 4.11 [80].

Fig 4.11 schematically illustrates the switched multi-phase goal seeking concept for a typical six-phase non-impulsive switched dynamical system. Let us represent the initial state of $\mathbf{x}_P$ by $\mathbf{x}_{P0}$, and the set of intermediate subgoals by, $\{\mathbf{x}_P^1, \mathbf{x}_P^2, ..., \mathbf{x}_P^6\}$ with each, $\mathbf{x}_P^i \in \mathbb{H}_{es}^{i} \cap \mathbb{H}_{es}^{i+1}$. Each hybrid event phase, $\mathbb{H}_{es}^{i}$ is equipped with a specific set of behaviour primitives forming the subtask, $u^i \in \mathcal{U}_P$ to drive the trajectory of $\mathbf{x}_P$ starting from an admissible set, $\mathcal{A}^i \subset \mathbb{H}_{es}^{i}$ towards the respective subgoal point, $\mathbf{x}_P^i \in \mathbb{H}_{es}^{i} \cap \mathbb{H}_{es}^{i+1}$ shown

by bullets in Fig 4.11. However, prior to reaching the subgoal point $\mathbf{x}_{\mathrm{P}}^{\mathrm{i}}$, the $\mathbf{x}_{\mathrm{P}}$ trajectory will enter into the admissible domain, $\mathcal{A}^{\mathrm{i}+1}$ of the next hybrid phase, $\mathbb{H}_{\mathrm{es}}^{\mathrm{i}+1}$ crossing the switching set, $\mathcal{S}_{\mathrm{u}}^{\mathrm{i}+1}$. As the trajectory of $\mathbf{x}_{\mathrm{P}}$ crosses $\mathcal{S}_{\mathrm{u}}^{\mathrm{i}+1}$, the control law as well as the subgoal get switched to $\mathrm{u}^{\mathrm{i}+1}$ and $\mathbf{x}_{\mathrm{P}}^{\mathrm{i}+1}$ respectively. In another words, u^{i} ensures that the state trajectories, $\mathbf{x}_{\mathrm{P}}$ starting from $\mathcal{A}^{\mathrm{i}}$ definitely cross $\mathcal{S}_{\mathrm{u}}^{\mathrm{i}+1}$ during its traversal towards $\mathbf{x}_{\mathrm{P}}^{\mathrm{i}}$. The parameters of the task level control law, u^{i} as well as the associated subgoal values are decided autonomously by the supervisory level controller, SLC designed a priori for meeting orbital stability of the recurrent hybrid dynamical system. As $\mathbf{x}_{\mathrm{P}}^{\mathrm{i}}$ belongs to both $\mathbb{H}_{\mathrm{es}}^{\mathrm{i}}$ and $\mathbb{H}_{\mathrm{es}}^{\mathrm{i}+1}$, the closed loop control u^{i} indirectly ensures the admissibility of $\mathbf{x}_{\mathrm{P}}$ trajectories with respect to $\mathbb{H}_{\mathrm{es}}^{\mathrm{i}+1}$ in a robust manner as long as the existence of sub task level control, $\mathrm{u}^{\mathrm{i}} \in \mathcal{U}_{\mathrm{P}}$ is guaranteed during every $\mathbb{H}_{\mathrm{es}}^{\mathrm{i}} \in \mathbf{H}_{\mathrm{es}}$.

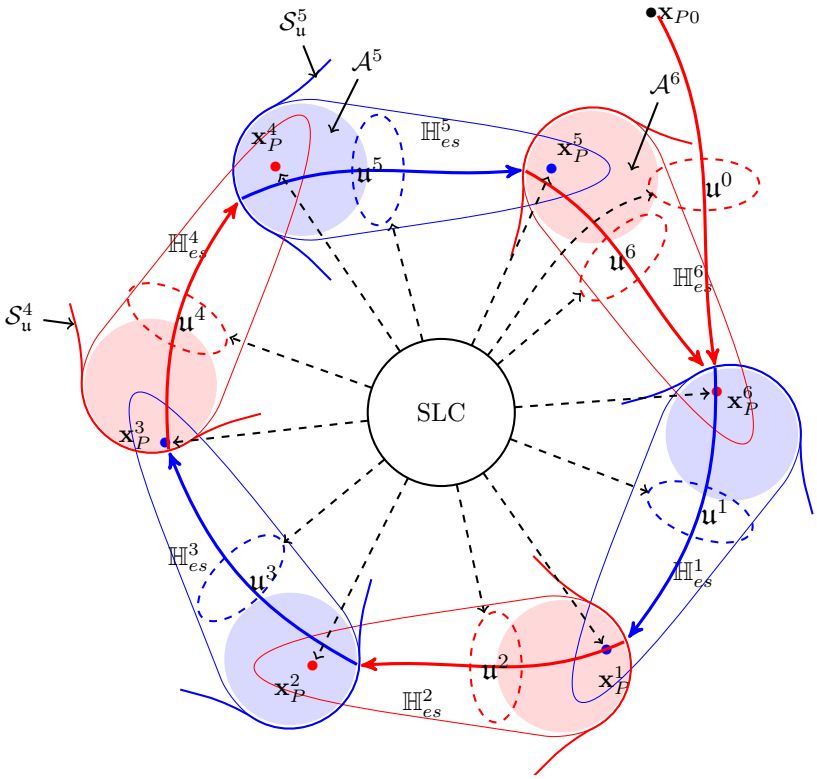

Figure 4.11: Visualization of multi-phase goal seeking concept for periodic stability regulation of a typical six-phase hybrid dynamical system

There is a strong connection between the targeted value of fixed point, $\mathbf{p} \in \mathcal{S}_{\mathrm{SP}}^{\mathrm{Cu}}$ and the existence of corresponding $\mathcal{U}_{\mathrm{P}}$ for underactuated dynamical systems. For example, in planar bipedal walking, the most critical element of $\mathbf{p}$ is λ_{h}, the desired value of θ_{cth}

as given in (4.59). The active regulation of forward velocity, V_{comx} is executed through direct regulation of GCoP of biped during the FF state of reference foot. However, the controllable range of GCoP is limited to the span of foot sole, and hence the same get easily saturated with an improper value of previous landing offset, λ_h. A larger value of λ_h results in GCoP saturation at x_{rh} and smaller value of λ_h results in GCoP saturation at x_{rt}. The former case leads to backward fall of biped and the latter case leads to eventual forward fall. Hence an improper selection of λ_h will reduce the size of the domain of attraction, $\mathcal{S}_{SP}^{Cu}$. On the other hand, an optimal selection of λ_h results in minimum control requirement for GCoP regulation and hence on ankle torque, resulting in better energetic efficiency of walking. Likewise a small value of $\mathbf{x}_{P2}$ component in $\mathbf{p} \in \mathcal{S}_{SP}^{Cu}$ results in near-straight knee walking with reduced knee torque and better efficiency. A proper value of forward lean, $\mathbf{x}_{P3}$ as a function of terrain slope and forward velocity in $\mathbf{p}$ is important for increasing the size of domain of attraction as in human locomotion. Thus for the best performance in terms of efficiency and robustness, there is an optimal impact posture which should be the effective target value for the fixed point[15], $\mathbf{p} \in \mathcal{S}_{SP}^{Cu}$ of the periodic orbit of dynamic gait.

In addition to inducing virtual attraction between perturbed trajectories during each cycle, the multi-phase goal seeking control can satisfy the second requirement of $\mathcal{U}_P$ by proper selection of subgoal values for each $\mathbb{H}_{es}^{i}$. The concept of realizing asymptotically stable periodic orbit with multi-phase goal seeking approach can be demonstrated by a 4-dimensional 4-phase hybrid dynamical system having four quadrant switching as shown in Fig 4.12. $\mathbf{y}_{Pc} = [y_{Pc1}\, y_{Pc2}]' \in \mathbb{R}^2$ represents the postural configuration vector and $\mathbf{y}_P = [y_{Pc1}\, y_{Pc2}\, \dot{y}_{Pc1}\, \dot{y}_{Pc2}]'$ represents the postural state. The four switching hyperplanes $\mathcal{S}_u^i, i \in [1,4]$ separates the four hybrid dynamic states (or phases) $\mathbb{H}_{es}^{i}, i \in [1,4]$ of the switched hybrid dynamical system and can be defined as,

$$\mathcal{S}_u^i := \{\mathbf{y}_P \in \mathbb{R}^4 : y_{Pc1} = \sqrt{y_{Pc1}^2 + y_{Pc2}^2}\sin\theta_i, y_{Pc2} = \sqrt{y_{Pc1}^2 + y_{Pc2}^2}\cos\theta_i, \\ \dot{y}_{Pc2} < \dot{y}_{Pc1}\tan\theta_i, \theta_i = (1.5+i)\pi/2\} \tag{4.104}$$

The relation $\dot{y}_{Pc2} < \dot{y}_{Pc1}\tan\theta_i$ in (4.104) ensures that the switching of hybrid state occurs only if the trajectory of $[y_{Pc1}\ y_{Pc2}]'$ intersects the radial lines at angle θ_i in CCW direction. The regulator subgoal for each $\mathbb{H}_{es}^{i}$ is given by

$$y_P^i = [y_{Pc1}^i\ y_{Pc2}^i\ 0\ 0]' \tag{4.105}$$

[15]The actual target for the impact posture should be sufficiently ahead of the effective target as the control loop never gets enough time to settle to the actual target during the dynamic orbital motion.

such that each y_P^i is located at an offset of $\theta_g^i = \pi/6$ rad ahead of the respective switching plane, $\mathcal{S}_u^i$ and at a radial distance of $Rg^i = 5$ when projected onto the postural configuration plane as shown in Fig. 4.12. The dynamics of each postural configuration variable,

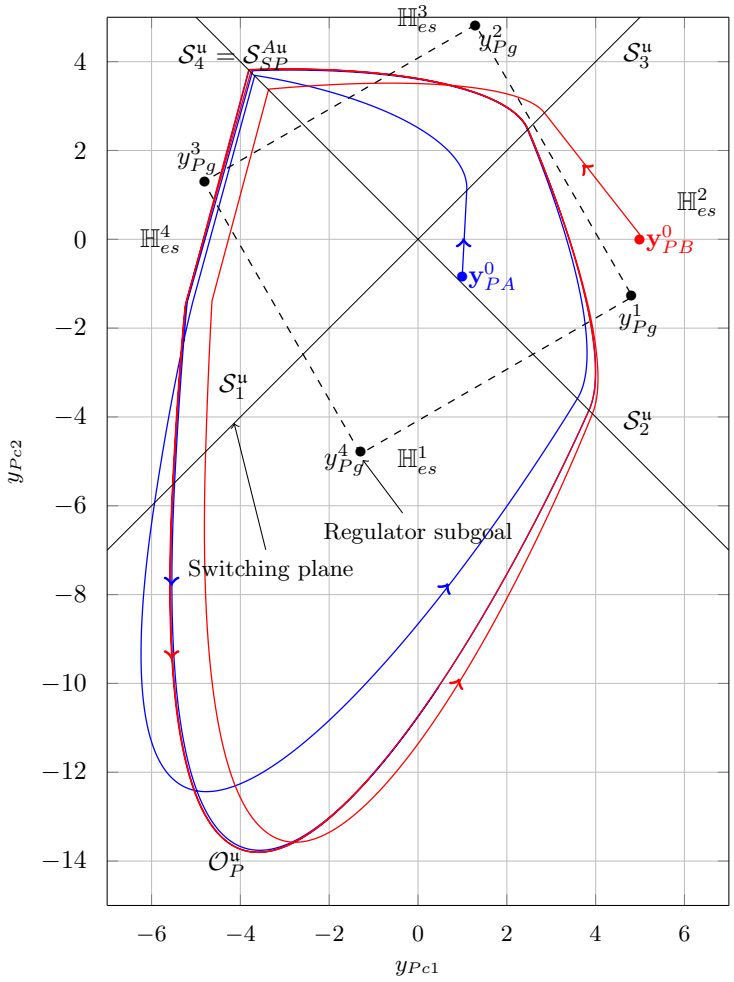

Figure 4.12: Evolution of periodic orbit $\mathcal{O}_P^u$ under multiphase goal seeking control when projected on the postural configuration plane of $y_{Pc1}-y_{Pc2}$

$y_{Pcj}; j = 1, 2$ is controlled as a second order regulator with parameters $(\omega_{Pj}^i, \zeta_{Pj}^i)$ with the subgoal value of y_{Pcj}^i. The controlled hybrid system dynamics in each $\mathbb{H}_{es}^i$ can be

expressed in state space form as,

$$\begin{bmatrix} \dot{y}_{Pc1} \\ \dot{y}_{Pc2} \\ \ddot{y}_{Pc1} \\ \ddot{y}_{Pc2} \end{bmatrix} = \begin{bmatrix} 0 & 0 & 1 & 0 \\ 0 & 0 & 0 & 1 \\ -{\omega^i_{P1}}^2 & 0 & -2\zeta^i_{P1}\omega^i_{P1} & 0 \\ 0 & -{\omega^i_{P2}}^2 & 0 & -2\zeta^i_{P2}\omega^i_{P2} \end{bmatrix} \begin{bmatrix} y_{Pc1} \\ y_{Pc2} \\ \dot{y}_{Pc1} \\ \dot{y}_{Pc2} \end{bmatrix} + \begin{bmatrix} 0 & 0 \\ 0 & 0 \\ {\omega^i_{P1}}^2 & 0 \\ 0 & {\omega^i_{P2}}^2 \end{bmatrix} \begin{bmatrix} y^i_{Pc1} \\ y^i_{Pc2} \end{bmatrix} \tag{4.106}$$

In addition to control switching, $\mathcal{S}^4_u$ is assigned the special role of strictly proper switching set, $\mathcal{S}^{Cu}_{SP}$ by associating discrete transition maps for velocity and position variables of $\mathbf{y}_P$ as in bipedal dynamic walk on transit heel strike. The velocity impact map used in the example is given by $y^+_P = \Delta^I y_P$ where

$$\Delta^I = \begin{bmatrix} 1 & 0 & 0 & 0 \\ 0 & 1 & 0 & 0 \\ 0 & 0 & 1+\delta_{11} & \delta_{12} \\ 0 & 0 & \delta_{21} & 1+\delta_{22} \end{bmatrix} \tag{4.107}$$

A numerical value of 0.75 is assumed for all δ_{ij}. The above velocity impact map includes perturbation due to cross coupling between the postural velocity terms in addition to self perturbation. A phenomenon somewhat equivalent to index reset map during leg exchange in bipedal walk is generated in the example by rotating both postural configuration vector and postural velocity vector by an angle of $\Theta = \pi/3$ rad. in CCW direction, represented by $y^+_P = \Delta^R y^-_P$ where

$$\Delta^R = \begin{bmatrix} \cos\Theta & -\sin\Theta & 0 & 0 \\ \sin\Theta & \cos\Theta & 0 & 0 \\ 0 & 0 & \cos\Theta & -\sin\Theta \\ 0 & 0 & \sin\Theta & \cos\Theta \end{bmatrix} \tag{4.108}$$

Thus the overall discrete transition for $\mathbf{y}_P$ as it crosses $\mathcal{S}^{Cu}_{SP}$ in the transverse direction is given by $y^+_P = \Delta^R \Delta^I y^-_P$.

The numerical values of regulator frequency parameters are $\omega^i_{Pj} = 2\pi$ rad/s for all $i = 1,2,3,4$ and $j = 1,2$. The regulator damping factors are $\zeta^1_{Pj} = 0.9, \zeta^2_{Pj} = 0.9, \zeta^3_{Pj} = -0.1$ and $\zeta^4_{Pj} = -0.9$ for $j = 1,2$. The regulator dynamics in $\mathbb{H}^3_{es}$ and $\mathbb{H}^4_{es}$ are made deliberatively unstable to represent the unstable passive rotation phase of planar bipedal dynamic walk during pre-impact and post-impact zones with ZMP at the edges of the stance foot. The evolutionary paths of two different trajectories of y_P starting from two different

points $y^0_{PA} = [1 \ -0.75 \ 0 \ 0]'$ and $y^0_{PB} = [5 \ 0.1 \ 0 \ 0]'$ when projected on the postural configuration plane of (y_{Pc1}, y_{Pc2}) are shown in Fig 4.12 and the corresponding velocity variable trajectories are given in Fig 4.13 .

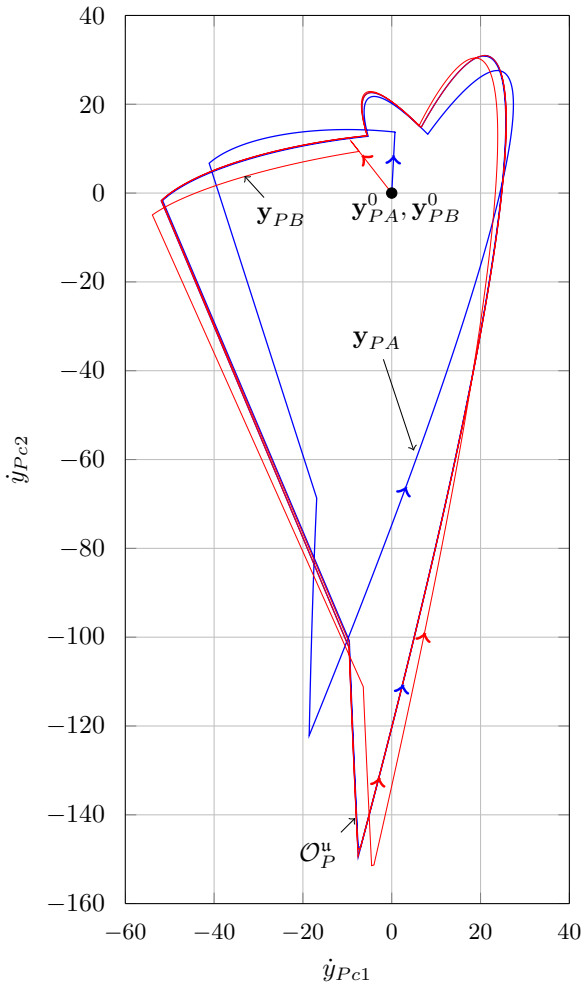

Figure 4.13: Evolution of periodic orbit $\mathcal{O}^u_P$ under multiphase goal seeking control when projected on the postural velocity plane of $\dot{y}_{Pc1} - \dot{y}_{Pc2}$

Both of the trajectories start with zero velocity and move toward the common subgoal y^2_{Pg} under stable regulator dynamics of $(\omega^2_{Pj}, \zeta^2_{Pj}); j = 1, 2$ respectively for the variables $(y_{Pc1}, \dot{y}_{Pc1})$ and $(y_{Pc2}, \dot{y}_{Pc2})$ until they cross $\mathcal{S}^3_u$. The distance between the trajectories is measured by the Euclidian norm given by

$$\delta^i_{AB} = \| \ y^i_{PA} - y^i_{PB} \ \|_2 \tag{4.109}$$

when they cross switching plane, $\mathcal{S}_u^i$ and the variation of δ_{AB}^i with cumulative switching event number starting from 0 is shown in Fig 4.14. When the trajectories cross $\mathcal{S}_u^3$, the

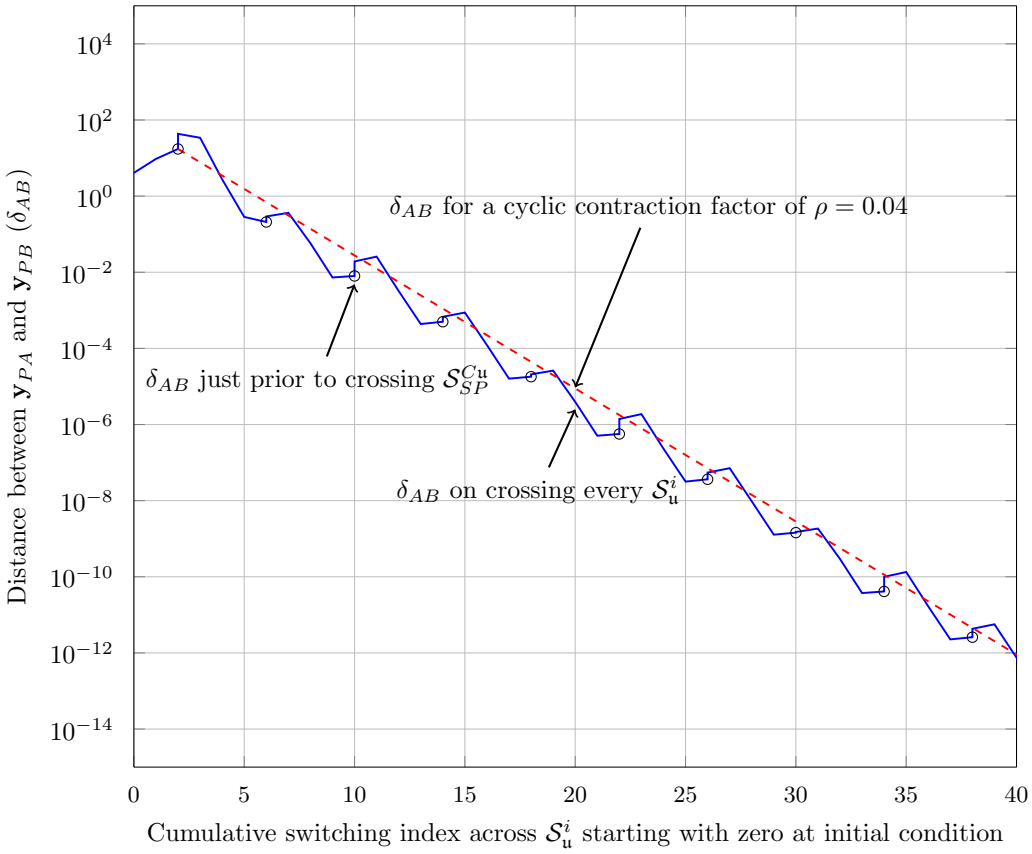

Figure 4.14: Convergence profile of δ_{AB} with cumulative switching index

regulation subgoal and controller get switched to y_{Pg}^3 and $(\omega_{Pj}^3, \zeta_{Pj}^3)$ respectively. As the trajectories cross $\mathcal{S}_u^4$ or $\mathcal{S}_{SP}^{Cu}$, they undergo discrete transformation given by $y_P^+ = \Delta^R \Delta^I y_P^-$. The velocity impact map, $\Delta^I y_P^-$ results in sudden divergence in δ_{AB}^i as seen from Fig 4.14 at the encircled locations. There will not be any trajectory divergence associated with Δ^R transformation since both the trajectories undergo pure rotational transformation without any relative scattering similar to the index swapping phenomenon in bipedal gait. This is evident from Fig 4.12 and Fig 4.13. The position trajectories in Fig 4.12 undergo discrete CCW rotation by Φ rad about the origin on crossing $\mathcal{S}_{SP}^{Cu}$ whereas the velocity trajectories in Fig 4.13 have extra transformation due to velocity impact map in addition to the discrete CCW rotation by Φ rad. The transformed trajectories are thereafter steered by the unstable regulator controller $(\omega_{Pj}^4, \zeta_{Pj}^4)$ towards the goal y_{Pg}^4. It can be seen from Fig 4.14 that after a few cycles of transient periods, δ_{AB}^i increases during the pre-impact and post impact

zones due to the unstable regulator dynamics indicating incremental trajectory divergence. However, the subsequent two phases, i.e.$\mathbb{H}^1_{es}$ and $\mathbb{H}^2_{es}$ result in decrement in the value of δ^i_{AB} due to the convergence effect of stable regulator dynamics. The hybrid system parameters are selected in such a way that the trajectories undergo net relative convergence over each cycle and as a result δ^4_{AB}, estimated prior to impact, geometrically converges to zero with a contraction factor $\rho_c = 0.04$ over each cycle. This demonstrates that how a multiphase goal seeking controller with net convergence over a cycle can generate a contraction mapping with respect to intersection point on $\mathcal{S}^{Cu}_{SP}$ leading to an asymptotically stable periodic orbit for an impulsive type hybrid dynamic recurrent system as per contraction stability theorem. Fig 4.15 shows the initial few cycles of the time domain plots of each configuration state and its derivative for the trajectory starting from $\mathbf{y}^0_{PB}$. It can be seen that the waveforms almost settle to the periodic trajectory within the first 3 cycles itself. We have used 4^{th} order Runge-Kutta numerical integration with a computation interval of $T_s = 0.001$ s for generating the above results. The contraction properties are not affected till $T_s = 0.005$ s. For $T_s = 0.01$ s, the contraction property is lost due to the non-convergence of numerical integration.

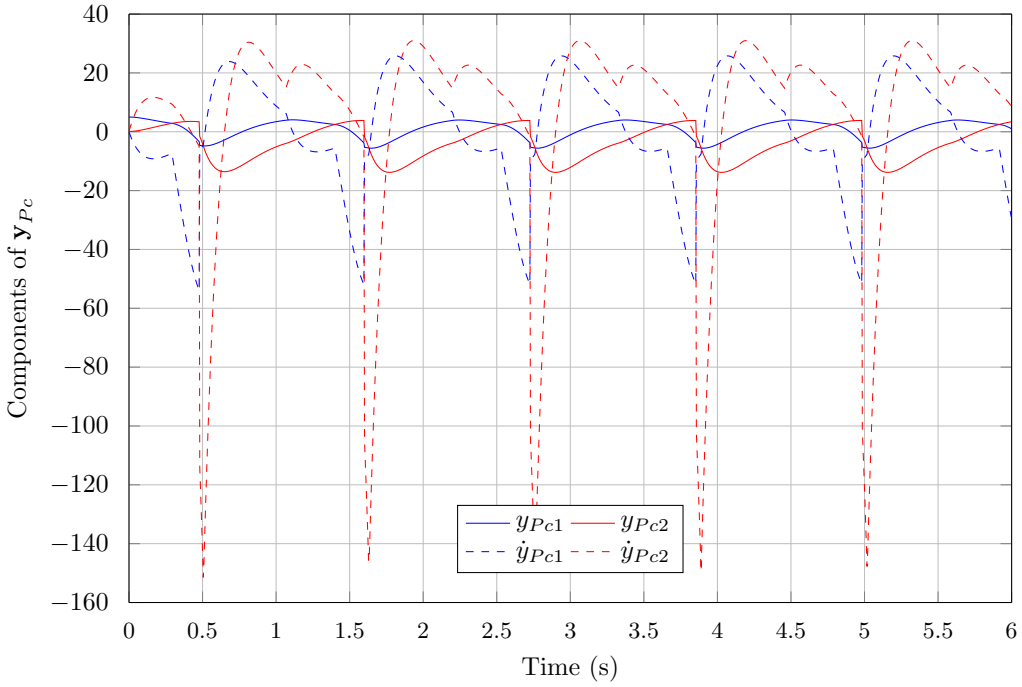

Figure 4.15: Converging profile of system state trajectories

In the case of planar biped, postural configuration state, $\mathbf{x}_{Pc}$ has a dimension of 12 and there are a total of 11 actuated joints including 2 ankle actuators, 2 knee actuators, 1

torso actuator and 1 actuator for transit thigh joint. During TR-SW and HR-SW phases, the reference ankle actuator torque is used for controlling $\mathbf{x}_{Pc1} = \theta_{solr}$. During these phases $\mathbf{x}_{Pc6}$, the relative horizontal position of biped-CoM with respect to ground, remains unactuated and hence evolves under passive unstable dynamics as happened for $\mathbb{H}^3_{es}$ and $\mathbb{H}^4_{es}$ in the above numerical example. However during FF-SW phase, $\mathbf{x}_{Pc1}$ is held at zero value by the holonomic ground contact constraint and reference ankle actuator torque becomes free for regulating $\mathbf{x}_{Pc6}$ with stable dynamics as happened during $\mathbb{H}^1_{es}$ and $\mathbb{H}^2_{es}$ of the example. Thus the stable regulation of $\mathbf{x}_{Pc6}$ or $\dot{\mathbf{x}}_{Pc6}$ by direct regulation of GCoP implemented through the reference ankle actuator during FF-SW phase can generate converging orbit for the postural state $\mathbf{x}_P$ even though the biped is underactuated in other phases, as demonstrated in the numerical example provided λ_h ensures the existence of finite size $\mathcal{S}^{Cu}_{SP}$.

The previous example has considered the case where both the postural configuration states are becoming unstable (or unactuated unstable passive dynamics) during some portion of cycle. In the case of bipedal walking, all the postural configuration states except $\mathbf{x}_{Pc6}$ are always controllable as long as $u^i \in \mathcal{U}_P$. Since they are always regulated towards multiphase subgoals under stable regulator dynamics, it is much easy to ensure contraction for their components in the trajectory intersection points with $\mathcal{S}^{Cu}_{SP}$. However, it should be noted that the intersection points can diverge leading to unstable trajectory even with all controllable stable postural states under certain switching sequence with inadequate dwell time [89]. On the other hand there is no need of ensuring arbitrarily small closeness to the regulation subgoals in each $\mathbb{H}^i_{es}$ for ensuring periodic contraction. Hence the requirements for contraction stability with respect to control bandwidth is much benign compared to stiff trajectory tracking type walking controllers.

4.8.4 Practical considerations for non-periodic orbits and Event periodic stability

The two-level control architecture based on multi-phase switched regulator is shown to provide an elegant scheme for realizing periodically stable orbits for impulsive hybrid dynamical systems. Moreover, Theorem 4.1 along with Definition 4.7 provides a computationally feasible method for quantifying the stability measure in terms of contraction factor, ρ_c as well as the domain of attraction, $\mathcal{S}^C_{SP}$ for periodic orbits. However, in practical situations such as outdoor bipedal walking, the perturbations in impact dynamics will limit the contraction between any two perturbed trajectories to certain tolerance band resulting in

truncated contraction with the impact postures getting settled within an invariant set called convergence set, $\mathcal{C}_S$ as defined earlier. The effect of perturbed impact dynamics can be illustrated by introducing random perturbation in Δ^I of the previous numerical example. The values of δ_{ij} in (4.107) are multiplied by $1 + r(k)$ where $r(k) \in [-\delta_\epsilon, \delta_\epsilon]$ is a random number having uniform distribution generated by 'rand' command of MATLAB with 'k' as the impact event index. Fig 4.16 shows various cases of random perturbation in δ_{ij} compared with the nominal case with no perturbation (i.e.$\delta_\epsilon = 0$) as already plotted in Fig 4.14. When trajectories starting at $\mathbf{y}^0_{PA}$ and $\mathbf{y}^0_{PB}$ are subjected to independent random perturbations for impact dynamics, the trajectories do not converge beyond certain limit depending on the value of δ_ϵ. For $\delta_\epsilon = 0.01$, the contraction pattern follows as per the nominal case for two cycles whereas for $\delta_\epsilon = 0.1$, the contraction pattern follows the nominal case for only one cycle. However, if both the trajectories are subjected to a common sequence of random perturbation, it has negligible effect on contraction pattern as shown for the case with $\delta_\epsilon = 0.01$. This is a true merit of contraction stability theorem, since stability is not affected by common perturbation even though it induce persistent perturbation on every trajectory[16]. However the effect of perturbation in impact dynamics on the actual trajectories of system states is quite insignificant as shown in Fig 4.17. Here the trajectories of y_{Pc1} and $\dot{y}_{Pc1}$ starting from $\mathbf{y}^0_{PB}$ for nominal case as well as with perturbed impact dynamics having $\delta_\epsilon = 0.1$ are compared.

Even on perfectly level terrain with fixed impact dynamics, the bounded randomness associated with digital control algorithms will cause similar truncated contraction behaviour. In other words, we cannot achieve ideal periodic orbits for realistic bipedal walk due to bounded randomness of terrain as well as of control algorithm and it is essential to look for a better stability notion in place of the ideal notion of periodic stability [19]. In this context, we would like to propose *Event periodic stability* as an appropriate stability notion for bipedal locomotion. It is generic enough to accommodate non-periodic dynamic walking gaits over uneven terrain or over obstacles or during turning, starting, and stopping; but it is stringent enough to exclude locomotion gaits with missing hybrid events[17]. Event periodic stability can be characterized by two parameters,namely the *Contraction factor* for truncated contraction series, ρ_C [18] and the radius, $\mathcal{R}_C$ of the convergence set, $\mathcal{C}_S$, which can be called in short as *Radius of convergence*[19]. The numerical value of $\mathcal{R}_C$ can be estimated as,

[16]This situation is equivalent to no fixed point where Poincaré stability concept is not applicable.

[17] A hybrid event is defined as the instant at which the postural state trajectories, $\mathbf{x}_P$ reach the admissible domain, $\mathcal{A}^i$ for a specific hybrid state, $\mathbb{H}^i_{es}$.

[18]The contraction factor for uniform contraction series is represented by ρ_c.

[19]$\mathcal{R}_C$ for truncated contraction mapping is the same as the parameter, ϵ for ultimate bounded type stability

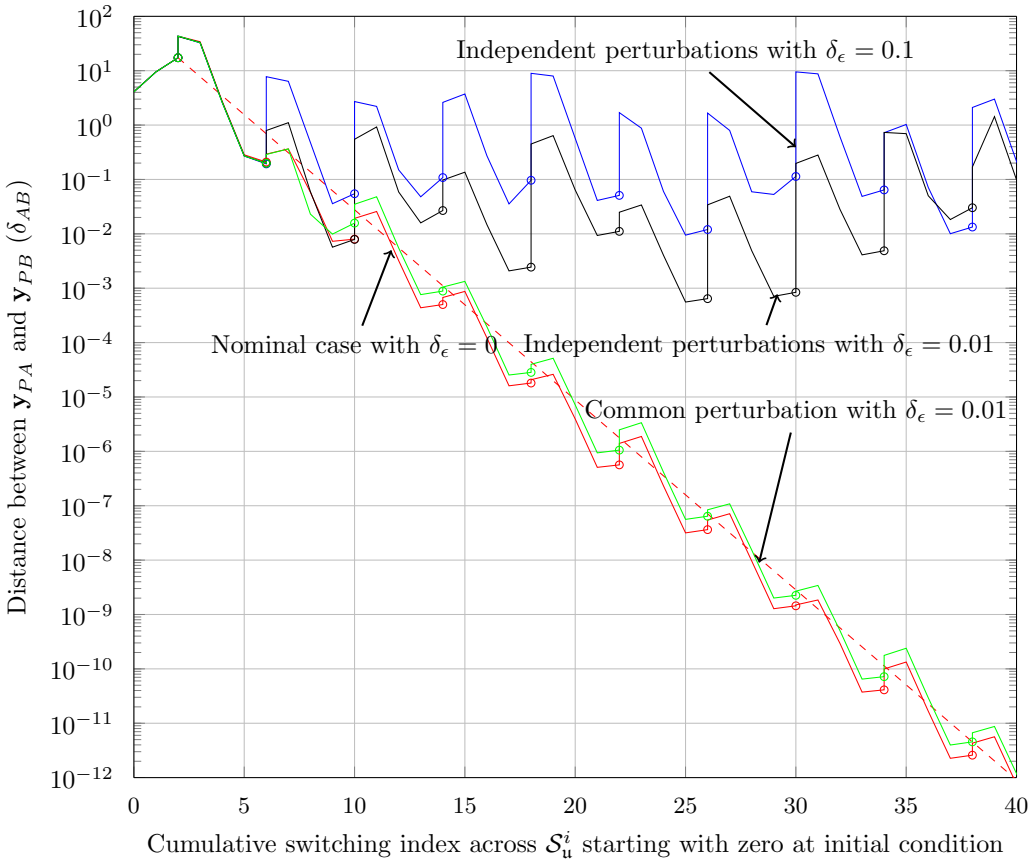

Figure 4.16: Effect of random perturbation in impact dynamics on δ_{AB} profile.

$$\mathcal{R}_C = \sup_{\mathbf{z}_{Pj},\mathbf{z}_{Pi}\in\mathcal{C}_s,k\geqslant K} \| \mathbf{z}_{Pj}(k) - \mathbf{z}_{Pi}(k) \|_2 / 2 \tag{4.110}$$

where i, j refer to different perturbed trajectories and $\mathbf{z}_{Pj}(k)$ refers to the impact posture state while the j^{th} trajectory of postural state intersect $\mathcal{S}_{SP}^{Cu}$ on k^{th} impact event. K refers to the value of k at which the contraction sequence enters into $\mathcal{C}_S$. The contraction factor, ρ_C is a function of the $\mathbf{z}_P$ and can be written as $\rho_C(\mathbf{z}_P)$. For uniform contraction mapping, $\rho_C(\mathbf{z}_P(k)) = \rho_c(\mathbf{z}_P(k)) < 1 \,\forall\, k \in \bar{\mathbb{Z}}_+$, resulting in monotonic asymptotic convergence. However, it is possible to have different types of contraction patterns for truncated contraction mapping depending on the local value of $\rho_C(\mathbf{z}_P(k))$ for $k < K$ provided the aggregate effect of $\rho_C(\mathbf{z}_P(k))$ over multiple adjacent values of k leads to contraction. The numerical value of $\rho_C(\mathbf{z}_P(k))$ as well its effective value over r consecutive samples can be estimated

specified in Definition 4.2(ii)

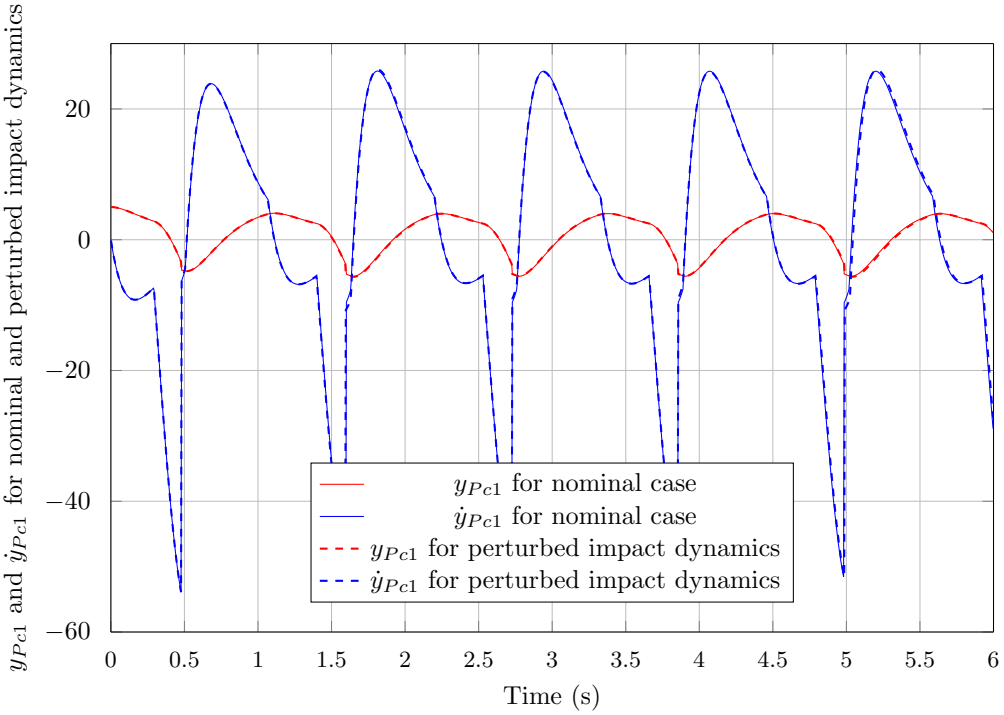

Figure 4.17: Effect of random perturbation in impact dynamics on system state trajectories.

as follows from the contraction profile of δ_{ij} prior to its entry into $\mathcal{C}_S$.

$$\rho_C(\mathbf{z}_P(k)) = \rho_C(k) = \frac{\delta_{ij}(k+1)}{\delta_{ij}(k)} \tag{4.111}$$

$$\bar{\rho}_C(k,r) = \left(\frac{\delta_{ij}(k+r)}{\delta_{ij}(k)}\right)^{(1/r)} \tag{4.112}$$

$$\text{where } \delta_{ij}(k) = \| \mathbf{z}_{Pj}(k) - \mathbf{z}_{Pi}(k) \|_2 \tag{4.113}$$

4.8.5 Selection of impact posture goal and adequacy of control-DoF

For uniform terrain walk, the impact posture goal (IPG), $\mathbf{x}_P^o = [\mathbf{x}_{Pc}^{o\prime}\ \dot{\mathbf{x}}_{Pc}^{o\prime}]'$ for the planar biped corresponding to the $\mathbf{x}_{Pc}$ defined in (4.57)-(4.60) can be selected as,

$$\mathbf{x}_{Pc}^o = \Big[0\ \ \theta_{kner}^o\ \ \theta_{dna}\ \ \theta_{knet}^o\ \ \theta_{solt}^o \int_{t_k^-}^{t_{k+1}^-} \dot{\theta}_{rhc}\, dt - \theta_{cth}(t_k^-)\ \ \lambda_h\ \ \theta^{o\prime}{}_{ubd}\Big]' \tag{4.114}$$

$$\dot{\mathbf{x}}_{Pc}^o = \Big[0\ \ 0\ \ 0\ \ 0\ \ 0\ \ \frac{V_{fc}}{h_{com}}\ \ 0\ \ \mathbf{0}_{1\times 5}\Big]' \tag{4.115}$$

where, λ_h is the desired value of normalized forward landing offset, θ_{cth} on heel impact, θ_{dna} is the target value for θ_{tor} and ${\theta^o}_{ubd}$ is the desired value for θ_{ubd}. The criteria for selecting the individual elements of $\mathbf{x}^o_{Pc}$ are given in Section 5.2

The adequacy of the control-DoF for driving $\mathbf{x}_P$ towards IPG can be proved as follows. Excluding the upper body joints, there are 9 DoF for the planar biped as per the configuration structure shown in Fig 4.6. Excluding the first 3 passive DoF which are consumed by the rank-3 constraint due to ground contact state[20], there are only 9-3=6 actuated DoF available for locomotion control. Let us partition $\mathbf{x}_{Pc(1:7)}$ into two parts, viz. $\mathbf{x}^A_{Pc} := [\mathbf{x}'_{Pc(1:5)}\, \mathbf{x}_{Pc7}]'$ and $\mathbf{x}^U_{Pc} := \mathbf{x}_{Pc6}$. $\mathbf{x}^A_{Pc}$ corresponds to the fully actuated part of $\mathbf{x}_{Pc(1:7)}$ whereas $\mathbf{x}^U_{Pc}$ is the underactuated part. $\mathbf{x}^A_P$ represents a set of 6 second order dynamical systems with a total number of 12 states, viz. $\mathbf{x}^A_P = (\mathbf{x}^A_{Pc}, \dot{\mathbf{x}}^A_{Pc})$ which can be controlled by well damped second order regulators actuated by the available 6 DoF control and their trajectories can be steered to the respective goals given in (4.114) and (4.115) provided there is sufficient dwell time[21] in the respective $\mathbb{H}^i_{es}$. Unlike other postural state elements, there are two differences for $\mathbf{x}^U_P$. As per its name, $\mathbf{x}^U_P$ is actuatable only during some portion of the gait as explained in Section 4.6. During HR-SW or TR-SW contact states, the biped-CoM rotates like an inverted pendulum with respect to the ground contact point under the force of gravity. By proper design of the forward landing offset, λ_h, the extra forward velocity build-up during the touch down phase is nearly compensated by the heel impact effect and the subsequent upward passive rotation of inverted pendulum during the next gait. In between the upward and downward passive rotation phases of each gait, there is a zone with $x_{rh} < x_{cop} < x_{rt}$ during the FF-SW state while $\mathbf{x}^U_P$ can be controlled by direct regulation of GCoP. The second difference for $\mathbf{x}^U_P$ is in the primary part for control. For all other postural state variables, the control objective is to regulate the position part, $\mathbf{x}^A_{Pcj}$ towards the respective goal, $\mathbf{x}^{Ao}_{Pcj}$ using well damped second order type closed loop regulators. In the absence of control switching, $\dot{\mathbf{x}}^A_{Pcj} \to 0$ as $t \to 0$. However for $\mathbf{x}^U_P$, the requirement is to regulate the derivative part, $\dot{\mathbf{x}}^U_{Pc}$ towards its goal, V_{fc}/h_{com} as per $\mathcal{CFR}3$. Regulation of $\dot{\mathbf{x}}^U_{Pc}$ will not permit regulation of $\mathbf{x}^U_{Pc}$ to any constant goal, rather the same leads to ramp type variation of $\mathbf{x}^U_{Pc}$. Hence, a floating ramp type goal is defined for

[20] Single point contact state like HR-SW or TR-SW has rank-2 holonomic constraint and rank-1 nonholonomic constraint due to passive rotation whereas FF-SW contact state has rank-3 holonomic type contact constraint.

[21] As the forward speed increases, the gait period and dwell time in each $\mathbb{H}^i_{es}$ decreases resulting in loss of gait stability beyond certain speed.

$\mathbf{x}^{U}_{Pc}$, given by

$$\mathbf{x}^{Uo}_{Pc} = \int_{t_k^-}^{t_{k+1}^-} \dot{\theta}_{rhc}\, dt - \theta_{cth}(t_k^-) \tag{4.116}$$

This goal is always guaranteed[22] to be satisfied since it is the outcome of integration of $\dot{\mathbf{x}}^{U}_{Pc}$ over the k^{th} gait period. The online GCoP regulation for controlling $\mathbf{x}^{U}_{P}$ is posed as a virtual nonholonomic constraint as discussed in Section 4.6 which will increase the rank of constraint from the earlier value of 3 to 4. However, during the FF-SW state, there is no need to regulate $(\mathbf{x}_{Pc1}, \dot{\mathbf{x}}_{Pc1})$, thereby reducing the control-DoF requirement for $\mathbf{x}^{A}_{P}$ from 6 to 5. Thus the total 6 actuated DoF of lower body cater to the locomotion related state regulation as either *rank-6 task* or *(rank-1 virtual constraint + rank-5 task)* provided the IPG and the task regulator dynamics are properly coordinated so as not to activate any further constraints. However, beyond certain values of V_{fc} and σ_G, it will become difficult to keep the force constraints in passive state leading to the loss of control-DoF.

4.9 Formulation of HyDAC as a Constrained Optimization problem

HyDAC is an autonomous control scheme for dynamic walking where the control laws and their goals are autonomously decided based on the hybrid event state of biped. The hybrid event states, $\mathbb{H}_{es}$ are defined in terms of the associated discrete-event states, $\mathbb{D}_{es}$ specified by π_m and the relevant continuous system-event states flags, C_{SF}. A total of nine C_{SF} are defined for HyDAC, which together with π_m define the binary vector, π_h representing the hybrid event state vector of planar biped for dynamic walking over uniform terrain. HyDAC is designed as a two-level hierarchical control scheme in order to meet 10 basic control functional requirements stated as $\mathcal{CFR}1$ to $\mathcal{CFR}10$ in Section. 4.2. The block schematic representation of HyDAC control algorithm is shown in Fig 4.2.

The detection of current $\mathbb{H}_{es}$ and activation of appropriate task level control (TLC) along with their performance parameters and goals is the job of supervisory level control (SLC). The inner level control, TLC is basically a set of dynamically coordinated motion behaviours associated with different branches of biped tailor-made to mimic human locomotion behaviours to the feasible extent. Each motion behaviour primitive is represented in differential form of (4.4)-(4.5) with an induced stable attractor dynamics and is referred

[22]From (4.58), $h_{com}\theta_{rhc}(t_{k+1}^-) = x_{com}(t_{k+1}^-) - x_{com}(t_k^-) - (x_{th}(t_k^-) - x_{com}(t_k^-)) = \int_{t_k^-}^{t_{k+1}^-} \dot{x}_{com}\, dt - h_{com}\theta_{cth}(t_k^-)$. Hence $\theta^{o}_{rhc} = \theta_{rhc}(t_{k+1}^-) = \int_{t_k^-}^{t_{k+1}^-} \dot{\theta}_{rhc} dt - \theta_{cth}(t_k^-)$ as given in (4.115).

to as the corresponding motion control primitive. HyDAC control synthesis is posed as a quadratic optimization problem in terms $\ddot{q}_d$ of with linear equality constraints as follows:

$$\text{Minimize} \quad \psi_o(\ddot{q}_d) = \left\| H_t \ddot{q}_d - B_t(q, \dot{q}) \right\|_2^2 \text{ over all } \ddot{q}_d \in \mathbb{R}^{n_J \times 1} \qquad (4.117)$$
$$\text{with } H_t \in \mathbb{R}^{n_t \times n_J},\ B_t \in \mathbb{R}^{n_t \times 1}$$

subject to constraints,

$$H_c \ddot{q}_d = B_c(q, \dot{q}),\ H_c \in \mathbb{R}^{n_C \times n_J}, B_c \in \mathbb{R}^{n_C \times 1} \qquad (4.118)$$

where[23] (H_t, B_t) represents the entire set of active motion control primitives to be executed by the biped during locomotion which includes locomotion specific primitives, (H_{t_l}, B_{t_l}) and upper body primitives, (H_{t_u}, B_{t_u}), those are active during the current hybrid event state or more precisely,

$$H_t = [H'_{t_l}\ \ H'_{t_u}]', \quad B_t = [B'_{t_l}\ \ B'_{t_u}]' \qquad (4.119)$$

with locomotion and upper body primitives expressed by,

$$H_{t_l} \ddot{q}_d = B_{t_l}(q, \dot{q}),\ H_{t_l} \in \mathbb{R}^{n_l \times n_J}, B_{t_l} \in \mathbb{R}^{n_l \times 1} \qquad (4.120)$$
$$H_{t_u} \ddot{q}_d = B_{t_u}(q, \dot{q}),\ H_{t_u} \in \mathbb{R}^{n_u \times n_J}, B_{t_u} \in \mathbb{R}^{n_u \times 1} \qquad (4.121)$$

The individual elements of the active system constraints, (H_c, B_c) can be given as,

$$H_c = [H'_{c_n}\ H'_{c_h}]', \quad B_c = [B'_{c_n}\ B'_{c_h}]' \qquad (4.122)$$

where (H_{c_n}, B_{c_n}) represents nonholonomic type dynamic constraints of the form (3.22) derived in Section 3.3.2 and Section 4.5 corresponding to passive joint dynamics as well as virtual constraints like contact force limits, friction cone, torque limits and GCoP regulation etc. and (H_{c_h}, B_{c_h}) represents the holonomic type contact constraints expressed by (3.15). The optimal solution for (4.117), subject to the system constraints, $H_c \ddot{q}_d = B_c$ can be obtained following the four step iterative algorithm described in the two-part flowchart shown in Fig 4.18 - Fig 4.19. The constrained optimal solution for the joint acceleration vector is obtained as

$$\ddot{q}_d^* = H_c^+ B_c + \bar{H}_t^+ (B_t - H_t H_c^+ B_c) \qquad (4.123)$$

where[24] $\bar{H}_t = H_t P_c$, $P_c = I_{n_J} - H_c^+ H_c$ and $()^+$ represents the Moore-Penrose generalized

[23] We have not included joint torques and contact force in the objective function for optimization due to inadequate control DoF.

[24] If $\bar{H}_t$ is ill-conditioned, the constrained residual primitive, $(\bar{H}_t, B_t - H t H_c^+ B_c)$ is to be regularized using

inverse [61]. The passive dynamic constraint of the biped expressed by (3.29) provides the least norm solution for the ground contact force, F_g^* for a given $\ddot{q}_d^*$ under the assumed contact state with Jacobian, J_g and can be written as,

$$F_g^* = J_{gp}'^{+} \left[D_p \ddot{q}_d^* + \mathcal{G}_p \right] \tag{4.124}$$

Finally, the inverse dynamic solution for the joint torque command [60] required to realize the desired joint acceleration vector $\ddot{q}_d^*$ for a given robot dynamic state $(q, \dot{q})$ in the presence of the computed ground contact force, F_g^* can be derived from (3.20) as,

$$\Gamma_d(q, \dot{q}, \ddot{q}_d^*, F_g^*) = D(q)\ddot{q}_d^* + \mathcal{G}(q, \dot{q}) - J_g'(q)F_g^* \tag{4.125}$$

which gives the explicit analytic expression for joint torque command based on HyDAC algorithm. The computational aspects of inverse dynamics control for robotic manipulators are given in [56, 90].

The entire steps explained above have to be repeated for a maximum number of four passes to convert all the active inequality constraints to equality constraints to form a part of (H_{c_n}, B_{c_n}). In pass-1, we assume that all the ground contact force constraints as well as the joint torque limits are passive and hence they are not included in (H_{c_n}, B_{c_n}). The computed force, F_g^* and joint torque, Γ_d are verified against the respective bounds and if none are found to be active at the end of pass-1, there will not be any pass-2. If any one of the inequality constraints is found to be crossing its respective bound, pass-2 is executed by augmenting (H_{c_n}, B_{c_n}) with the corresponding equality constraint. This process is repeated for a maximum number of three times to incorporate all the force and joint torque constraints that get activated when introduced in a sequential manner. Due to the limited control DoF, there is provision to include only one joint torque limit, Γ_{j+} in HyDAC for planar biped and accordingly there can be a maximum number of four passes for HyDAC.

4.10 Chapter Summary

The formulation of HyDAC was the major topic of discussion of this chapter. Initially, the two-level hierarchical structure of HyDAC with its supervisory (SLC) and task level controls (TLC) were justified in comparison with the locomotor system architecture in vertebrates and based on the control functional requirements for dynamic walking. A set

the SVD based truncation scheme mentioned in the Appendix A.

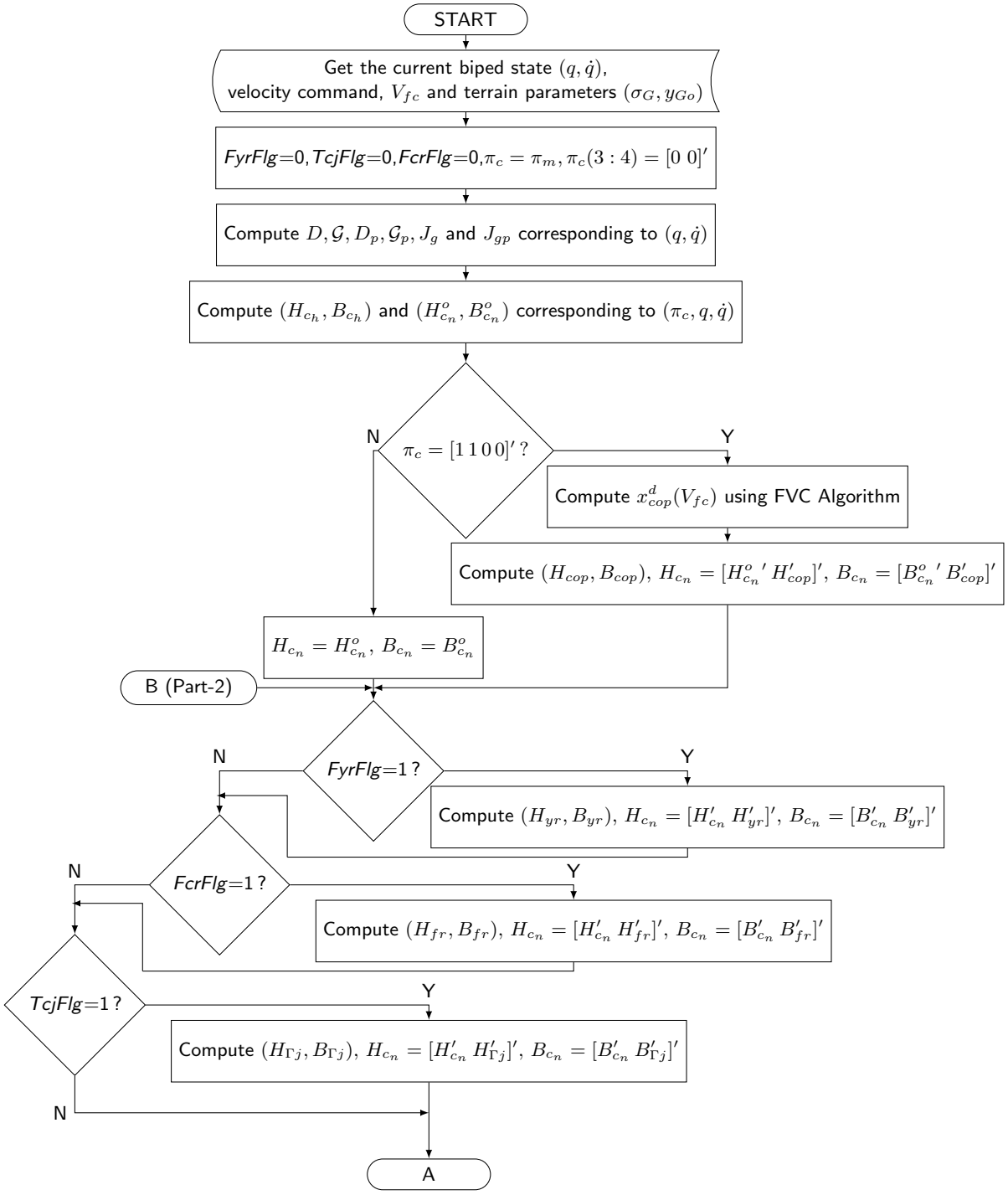

Figure 4.18: HyDAC Flowchart (Part-1)

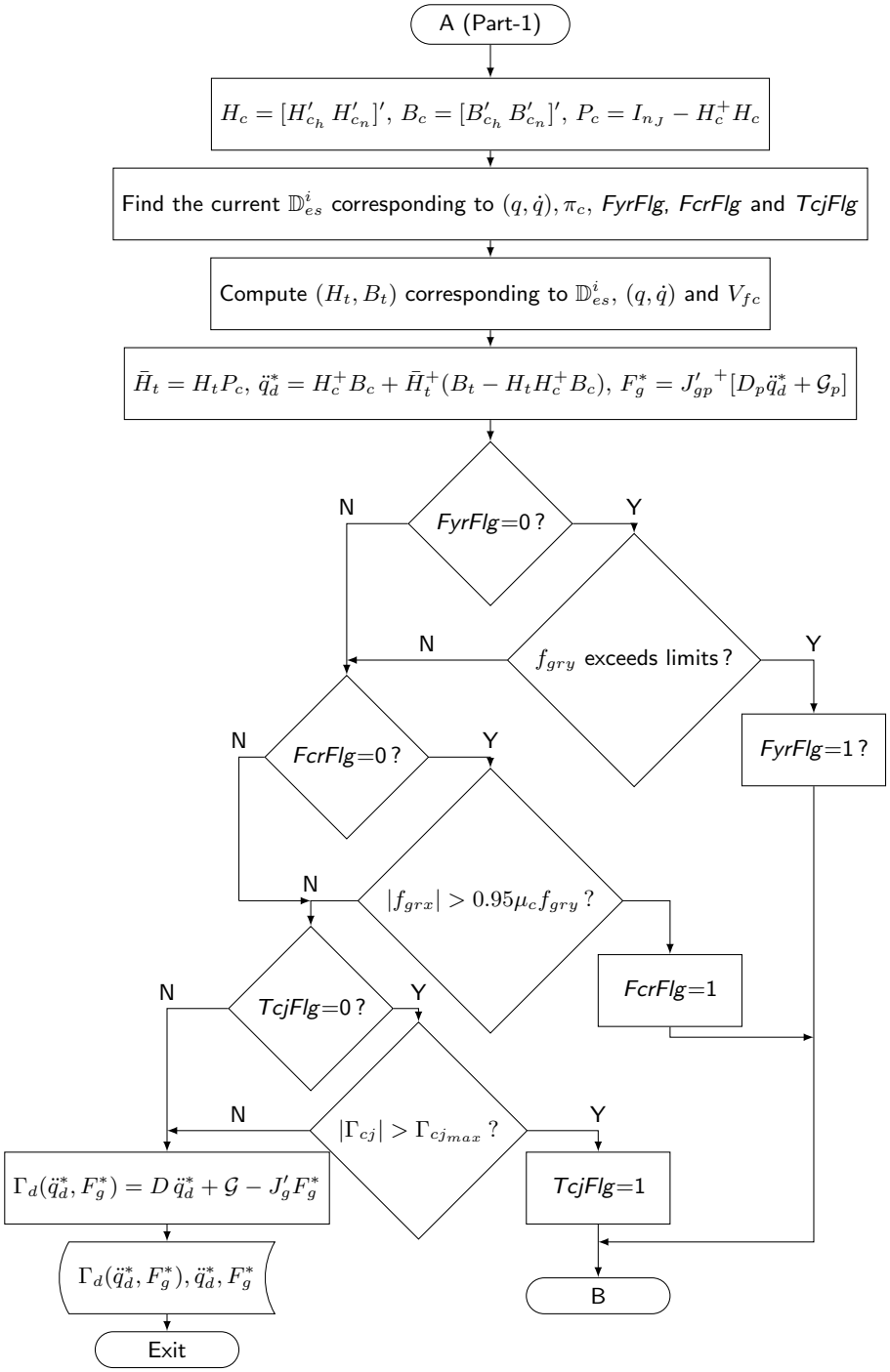

Figure 4.19: HyDAC Flowchart (Part-2).

of virtual nonholonomic constraints were defined in a unified differential form to ensure the bounds on contact force components and joint torques. A notable contribution of the chapter is the development of a novel forward velocity regulation algorithm based on online regulation of GCoP.

The major portion of the chapter was devoted to the development of a control oriented stability criterion for bipedal walking by integrating the stability concepts of Lyapunov and Poincaré with contraction mapping theorem and the same was named as contraction stability theorem. Statement of contraction stability theorem provides a constructive design approach for bipedal walking controller to ensure periodic stability. The advantage comes from the fact that the periodic stability according to contraction stability theorem is purely based on contraction of the distance between perturbed admissible trajectories on every ground impact event. On the other hand, the classical approach is to ensure the contraction of the distance between the perturbed impact postures and the final converged impact posture called fixed point. In other words, contraction based stability follows a differential mode approach for establishing orbital stability, whereas the classical stability based on Lyapunov and Poincaré theorems follows a common mode approach, with the final fixed point as the common goal for asymptotic stability for all the trajectories belonging to the admissible set. Hence an inherently stable periodic system on uniform terrain which appears to be aperiodic on uneven terrain due to perturbations in impact dynamics, cannot be analysed by classical method due to the absence of fixed point. However, the contraction stability theorem provides two normalized stability parameters called, contraction factor, ρ_C and radius of convergence, $\mathcal{R}_C$ under such situations to compare the orbital stability performance across various bipeds and across different terrains.

Another important contribution was the formulation of multi-phase goal seeking philosophy of HyDAC in postural state space which induces virtual attraction between the strictly proper set of trajectories as well steers them towards the impact posture goal guided through multi-phase subgoals. This control framework provides a transparent and constructive control synthesis procedure to realize asymptotically stable bipedal gait. The procedure applies well for uneven terrain also resulting in event periodic stability (EPS) instead of periodic stability, with stability properties quantified by ρ_C and $\mathcal{R}_C$. The task level control of HyDAC was then formulated as a quadratic optimization problem with linear equality constraints which is known to have explicit analytic solution for online implementation.

Chapter 5

HyDAC for Bipedal Dynamic walk over Uniform terrain

5.1 Introduction

The animal world around us exhibits a wide variety of legged locomotion patterns over the land. The bio-mechanical walking gait of an animal is the outcome of the kinematic configuration and mass-inertia properties of its body segments, limb configuration, speed-force characteristics of actuating group of muscles and its foot architecture [91]. Having selected the bipedal configuration for the robot similar to an adult sized human being, it is quite natural to select the walking style also resembling with human walking gait. The efficiency of human walk is partially attributed to the use of the inherent passive dynamics for forward locomotion [92]. To achieve better walking efficiency, bipedal robots also should make use of motion trajectories evolving out of its passive dynamics to the maximum feasible extent. However, the biped joint trajectories thus achieved will be different from human gait due to the differences in terms of joint DoF, mass-inertia properties, and actuation-sensor system characteristics. Nevertheless, depending on the gross-level similarity with respect to the above parameters, similarity in terms of the *walking dynamics*[1] can be achieved to a reasonable extent which is referred to as *human-like walking* in the context of the thesis. The passive forward rolling phases before and after heel strike and near straight-knee configuration of stance leg are the essential features to utilize the benefit of passive dynamics of planar biped [93]. Hence the motion control primitives of HyDAC are designed with this objective in mind while serving other requirements leading to periodic stability for joint trajectories along with leg exchange on every heel strike. As mentioned in Sec. 4.4.1.1,

[1]However, there can be differences in joint orbits due to the difference in system parameter values.

HyDAC makes use induced behaviour concept instead of imposed behaviour, so that the actual joint trajectories evolve out of the interaction of control law with the passive dynamics of the biped subject to various active constraints. Thus human-likeness in HyDAC is only in terms of the dynamical formulation of behaviour primitives and not in terms of the actual joint trajectories.

The following section gives the detailed formulation of all behavioural primitives for dynamic walking over uniform terrain. The primitives for each hybrid event state are selected on an intuitive basis to realize human-like planar walking gait and the parameter values are optimized based on intensive simulation trials carried out by substituting the task level controls in (4.119). The versatility of HyDAC is then illustrated based on a variety of simulation experiments conducted on the 12-link planar biped walking over uniform terrain.

5.2 Behaviour Primitives for Bipedal Dynamic walk

We have adopted a tailor-made procedure for the design of behaviour primitives to drive each of the elements of postural configuration state, $\mathbf{x}_{Pc}$ through various hybrid event phases of the gait. To ensure that $\mathbf{x}_P$ is reachable towards the impact posture goal, $\mathbf{x}_P^o \in \mathcal{S}_{SP}^{Cu}$ during the k^{th} gait, there are two essential requirements for HyDAC. One is the aggregate controllability[2] of V_{comx} by the modulation of GCoP and the other is the availability of 6-DoF actuated control for torso and leg joints, in an aggregate sense, without getting additionally constrained by any ground contact force bounds as described in Section 4.8.5. These requirements lead to certain *desirable* conditions to be satisfied by HyDAC for ensuring event periodically stable gait [41]. They are defined as *Control Design Requirements* ($\mathcal{CDR}$) for a planar bipedal dynamic walk[3] and are listed below.

(i) $\mathcal{CDR}1$: The postural orientation of biped given by $\mathbf{x}_{Pc}$ should be closely regulated to an impact posture goal on every heel strike.

(ii) $\mathcal{CDR}2$: The reference foot should be kept in the flat-foot state (FF) for maximum possible duration in each gait for regulating V_{comx}.

(iii) $\mathcal{CDR}3$: The torso link of the biped should be regulated along the optimal inertial orientation to get the best utilization of gravity moment arm, $(x_{com} - x_{cop})$ for regulating V_{comx}.

[2] Aggregate controllability refers to the state when the average value of V_{comx} over each gait is controllable.

[3] $\mathcal{CDR}$'s are the same as $\mathcal{PSR}$'s given in [41].

(iv) $\mathcal{CDR}4$: The impact posture goal, $\mathbf{x}_P^o$ should be selected in such a manner that the lower limb control actions subsequent to the heel strike should be compatible with V_{comx} regulation by generating ground contact forces which remain well within the unilateral and friction cone bounds without any need for explicitly enforcing the same.

(v) $\mathcal{CDR}5$: For a kinematically driven control algorithm like HyDAC, the motions of reference and transit legs represented by the trajectories of $x_{Pc2}, x_{Pc4}, x_{Pc5}$ and x_{Pc7} should be dynamically coordinated mutually as well as with the passive dynamics of the biped, while regulating towards $\mathbf{x}_P^o$, in such a way that the resulting ground contact forces are well within the unilateral and friction cone bounds without any need for explicitly enforcing the same.

The above design requirements for HyDAC, should be treated only as heuristic requirements for gait stability. The general form of behaviour primitives for bipedal dynamic walk is given by (4.4)-(4.5) and all of these can be expressed as a function of $\mathbf{x}_P$. They are grouped into four categories depending on the joints responsible for primitive execution; namely, torso orientation control primitive, reference leg control primitives, transit leg control primitives, and upper body control primitive. The proposed set of motion control primitives and the associated activation logic need not necessarily be unique nor optimal, however they demonstrate the feasibility of the approach to design for a stable locomotion. The motion control primitives are characterized by parameters like, undamped natural frequency (ω_n), damping factor (ζ), intermediate saturation limits, regulation targets etc. The numerical values of all these parameters are finalized based on extensive simulation studies using the full state model of 12-link planar biped mentioned in Section 3.2 to achieve the best possible dynamic coordination among various elements of $\mathbf{x}_{Pc}$ so as to ensure event-periodic stability of the gait. The philosophy behind the design of each locomotion behaviour primitive and the criterion for the design of its regulation goal and controller parameters are detailed in the following sections. In general, all behaviour primitives used in HyDAC are expressed as second order type kinematic closed loop regulators with bandwidths of the order of 2 to 6 times of $\omega_p = \sqrt{g/h_{com}}$. The diagrammatic representation of motion control primitives active during different phases of bipedal dynamic walking gait are shown in Fig 5.1.

5.2.1 Torso Orientation Control (TOC) Primitive

It has been reported that in natural human walk, the spin angular momentum in the sagittal plane is regulated very close to zero and is directly related to the energetic efficiency of

human walk [21]. Biomechanical experiments reveals that the dimensionless spin angular momentum normalized with respect to $M_{bp} h_{com} V_{comx}$ remains less than 0.02 throughout the gait cycle and maximum whole body angular excursions about the CoM are regulated within 1 deg for sagittal plane, 0.2 deg for coronal plane and 2 deg for transverse plane. Being a floating base manipulator, it is desirable for the biped to have an inertially fixed reference axis along which the massive upper body (torso) is to be aligned during dynamic walking. This reference inertial axis is named as *Dynamic Neutral Axis* [41] and its orientation with respect to the inertial vertical axis, $\overrightarrow{O_0Y_0}$ in CCW direction is designated as θ_{dna}. The objective of torso orientation control primitive is to regulate the inertial orientation of torso link along the dynamic neutral axis so that $\theta_{tor} = \theta_{dna}$. The value of θ_{dna} is normally selected to give the maximum stability at nominal stance posture. However it is varied to an optimal forward lean posture for higher forward speed and for steeper positive ground slopes. The torso orientation control is active during the entire biped walking phase including free floating phase if it exists.

Let us first define the hip Jacobian, J_{hip} which provides the spatial velocity[4] of the biped torso link at the hip joint with respect to the inertial frame, $\{O_0\}$ according to,

$$\begin{bmatrix} \dot{\theta}_{tor} & \dot{x}_{hip} & \dot{y}_{hip} \end{bmatrix}' = \begin{bmatrix} \omega_{tor} & V_{hipx} & V_{hipy} \end{bmatrix}' = J_{hip}\dot{q} \tag{5.1}$$

The TOCP primitive can be realized as a kinematic closed loop regulator with relevant characteristic vectors,

$$H(q) = \begin{bmatrix} 1 & 0 & 0 \end{bmatrix} J_{hip} \tag{5.2}$$

$$B(q,\dot{q}) = \omega_b^2\ \theta_{tor}^e - 2\zeta\omega_b\dot{\theta}_{tor} - \begin{bmatrix} 1 & 0 & 0 \end{bmatrix} \dot{J}_{hip}\dot{q} \tag{5.3}$$

where $\theta_{tor}^e = (\theta_{dna} - \theta_{tor})$ and $\theta_{tor} = \Sigma q_{(3:6)} - \pi/2$ is the orientation of torso link measured in CCW direction with respect to local vertical parallel to $\overrightarrow{O_0Y_0}$ axis and passing through the hip joint, O_6 and $(\omega_b, \zeta) = (6\omega_p, 0.7)$. In a dynamic situation when either ground slope or forward velocity command is changing, the maximum rate of increase of θ_{dna} is limited to 25 deg/s and the maximum rate of decrease of θ_{dna} is limited to -50 deg/s to avoid fast torso rotation leading to large inertial disturbance.

The numerical value of θ_{dna} is very important with respect to locomotion efficiency

[4]Spatial velocity for generic 3D motion space is defined as the column array obtained by vertically stacking 3D angular velocity and 3D translational velocity [56]. However we consider the part of spatial velocity relevant to sagittal plane only which has 1D rotational part about z-axis and 2D translational part along x,y directions.

and postural stability of biped. The importance of torso orientation regulation for balancing legged robots had been emphasized by Reibert [1]. For climbing up along a ramp, it is preferable to have the dynamic neutral axis leaning forward as it will keep the CoM of biped ahead of GCoP. Similar is the case when the biped has to move with large forward velocity even on level ground. During simple standing posture, θ_{dna} is to be selected in such a way that the ground projection of CoM falls at the middle of foot support polygon for a 3D biped or at the middle of foot support line segment for planar biped; i.e. $x_{com} = (x_{rt} + x_{rh})/2$. Intelligent manipulation of θ_{dna} can provide additional transient stability for the biped to recover from falls caused by disturbances. The TOCP primitive is pivotal for the stability of dynamic walk. The empirical formula for θ_{dna} is arrived at based on simulation trials and is given by

$$\theta_{dna} = \max\left(\left(-0.5\sigma_G - \pi\min(V_{fc}, 1)/18\right), 0\right) \tag{5.4}$$

TOCP is activated by SLC to meet $\mathcal{CDR}3$.

5.2.2 Reference Leg Control Primitives

The reference leg control primitives are responsible for controlling the reference leg joint angles, q_2 to q_5 and the details of various task primitives involved are given below.

5.2.2.1 Heel Roll Reset Control (HRRC) primitive

This task primitive is activated by SLC to steer the reference foot from HR state to FF state during the hybrid event state defined by:

$$\mathbb{H}_{es} : \left(\pi_c = [1\ 0\ 0\ 0]\right)\ \&\ \left(\text{rank}(H_{c_n}) \leqslant 2\right) \tag{5.5}$$

HRRC is executed by a PD type regulator control pulling down the reference foot toe to its ground projection. The objective of HRRC primitive is to bring the reference foot to FF state so that FVC algorithm can be activated at the earliest for regulating the forward velocity. The primitive can be expressed in terms of the generalized coordinate variables

as in (4.4) with[5]

$$H(q) = [0\ 1\ 0\ \cdots 0] \in \mathbb{R}^{1\times n_J} \tag{5.6}$$

$$B(q,\dot{q}) = \omega_b^2(y_R - q_2) - 2\zeta\,\omega_b\dot{q}_2 \tag{5.7}$$

where y_R is the target vertical position for pulling down the toe of reference foot and can be derived from (3.5) as

$$y_R = y_{Go}(x_{rt}) + x_{rt}\tan\sigma_G(x_{rt}) + \epsilon_{tr} \tag{5.8}$$

Here, ϵ_{tr} is an additional offset and is assigned a value of -0.05 m to avoid the sluggish response while the toe approaches the ground surface. A control bandwidth of $\omega_b = 5\omega_p$ and damping factor of, $\zeta = 1.5$ are assigned to HRRC for nominal situations. However a faster dynamics with $\omega_b = 7\omega_p$ and damping factor of, $\zeta = 1.0$ are assigned for the cases described by the logical condition given below.

$$\big(V_{fc} \geqslant 1.0 \text{ and } \sigma_G \geqslant \pi/12\big) \text{ or } \big(V_{fc} \geqslant 1.25 \text{ and } \sigma_G \geqslant \pi/18\big) \text{ or } \big(V_{fc} \geqslant 1.75 \text{ and } \sigma_G \geqslant 0\big) \tag{5.9}$$

When $\text{rank}(H_{c_n}) \geqslant 2$, this primitive is pushed down to lower priority category by SLC and hence not activated.

5.2.2.2 Reference Knee Joint Control (RKJC) primitive

RKJC primitive is activated by SLC during the hybrid event phase,

$$\mathbb{H}_{es} : \big(\Sigma\pi_{c\,(1:2)} \geqslant 1\big) \tag{5.10}$$

to execute the control functions of $\mathcal{CFR}7, \mathcal{CDR}1, \mathcal{CDR}4$ and $\mathcal{CDR}5$. This primitive is responsible to provide braking and forward thrusting during bipedal locomotion in an implicit manner. As the biped stays in FF state during most part of the locomotion, RKJC is instrumental for controlling y_{com} and y_{hip}. Hence setting of regulation targets and bandwidths for RKJC control loop during different hybrid event phases of gait is crucial for realizing optimal gait orbit. Another important function of RKJC primitive is to avoid the singular configuration of reference knee with $q_5 = 0$. RKJC has two modes of operation, namely *rising-mode* and *drooping-mode*. Rising-mode is the normal mode of operation of RKJC

[5] $B(q,\dot{q})$ can be expressed independent of q_2 since q_2 is a unique function of $\mathbf{x}_{pc1}$ for a given contact state of reference foot and for given foot-link parameters.

which begins with the heel impact of transit foot on ground which will subsequently be designated as reference foot. During this mode, the reference knee joint will behave like a virtual torsional spring with its neutral orientation along $q_5 = \theta^o_{kner}$. The algorithm for finding the value of θ_{kner}^o for the rising mode is given in Algorithm 5.1. The value of θ^o_{kner} lies normally in the range of 10-20 deg, so that the hip joint of biped is raised almost to the maximum level. Subsequent to this, for down-slope and step-down terrains, it is required to lower the hip vertical position during the touch down phase so that the transit foot can land on the ground surface which lies below the current stance foot level, without much extension of transit knee. The required hip drooping is achieved by flexing the reference knee joint, q_5 towards a reference orientation of $\theta^o_{kner} = 50\pi/180$ rad. This is sufficiently large enough to accommodate the drooping requirement for any acceptable down-slopes.

Algorithm 5.1: Computation of θ^o_{kner} as a function of σ_G and V_{fc}

Data: x_{rh}, x_{rt}, x_{tt}, and V_{fc}
$\sigma_{Gr} = \sigma_G((x_{rh} + x_{rt})/2)$ ▷ Ground slope at the mid point of reference foot
$\bar{\sigma}_G = (\sigma_{Gr} + \sigma_G(x_{tt}))/2$ ▷ Average ground slope with respect to reference and transit feet
$\theta^o_{kner} \leftarrow \pi/18$
if $\bar{\sigma}_G \leqslant -\pi/36$ **then**
  $\theta^o_{kner} \leftarrow \theta^o_{kner} - (\bar{\sigma}_G + \pi/36)/3$
  if $V_{fc} \geqslant 1$ **then**
    $\theta^o_{kner} \leftarrow \theta^o_{kner} + (V_{fc} - 1)\pi/27$ ▷ θ^o_{kner} for slope-down terrain
  end
else if $\bar{\sigma}_G \geqslant \pi/36$ **then**
  $\theta^o_{kner} \leftarrow \theta^o_{kner} + (\bar{\sigma}_G - \pi/36)$
  if $V_{fc} \geqslant 1$ **then**
    $\theta^o_{kner} \leftarrow \theta^o_{kner} + (V_{fc} - 1)\pi/9$ ▷ θ^o_{kner} for slope-up terrain
  end
else if $|\bar{\sigma}_G| < \pi/36$ ***and*** $V_{fc} > 1$ **then**
  $\theta^o_{kner} \leftarrow \theta^o_{kner} + (V_{fc} - 1)\pi/18$
end

The expressions for the task primitive vectors corresponding to the PD type control laws for both of the above modes can be written as

$$H(q) = \begin{bmatrix} 0\,0\,0\,0\,1\,0\,\cdots 0 \end{bmatrix} \in \mathbb{R}^{1\times n_J} \tag{5.11}$$

$$B(q, \dot{q}) = \omega_b^2 q_{ke} - 2\zeta\,\omega_b \dot{q}(5) \tag{5.12}$$

with $q_{ke} = \theta^o_{kner} - q_5$, $\omega_b = 5\omega_p$ and $\zeta = 1$. In addition, the slew rate of the regulation loop is indirectly limited by way of limiting the absolute value of feedback position error,

q_{ke} to an upper bound, q_{ke+} given by ,

$$q_{ke+} = \max(0.1, V_{fc})\,\pi/9 \text{ for rising-mode} \tag{5.13}$$

$$= \max(0.1, V_{fc})1.6\,\pi/9 \text{ for drooping-mode} \tag{5.14}$$

A minimum value is ensured for q_{ke+} by the term, 0.1 in the R.H.S. of above equations to ensure a minimum value for slew rate, especially when $V_{fc} = 0$ during stance or stopping phases.

5.2.2.3 Reference leg Floating State Control (RFSC) primitive

In case the biped lifts off from ground for short duration as a result of some abnormal event, the joint accelerations of the reference leg are to be driven to zero value as a safe mode operation. The task primitive vectors for RFSC can be given as

$$H(q) = \begin{bmatrix} \mathbf{I}_5 & \mathbf{0}_{5\times 9} \end{bmatrix}, \; B(q, \dot{q}) = \mathbf{0}_{5\times 1} \tag{5.15}$$

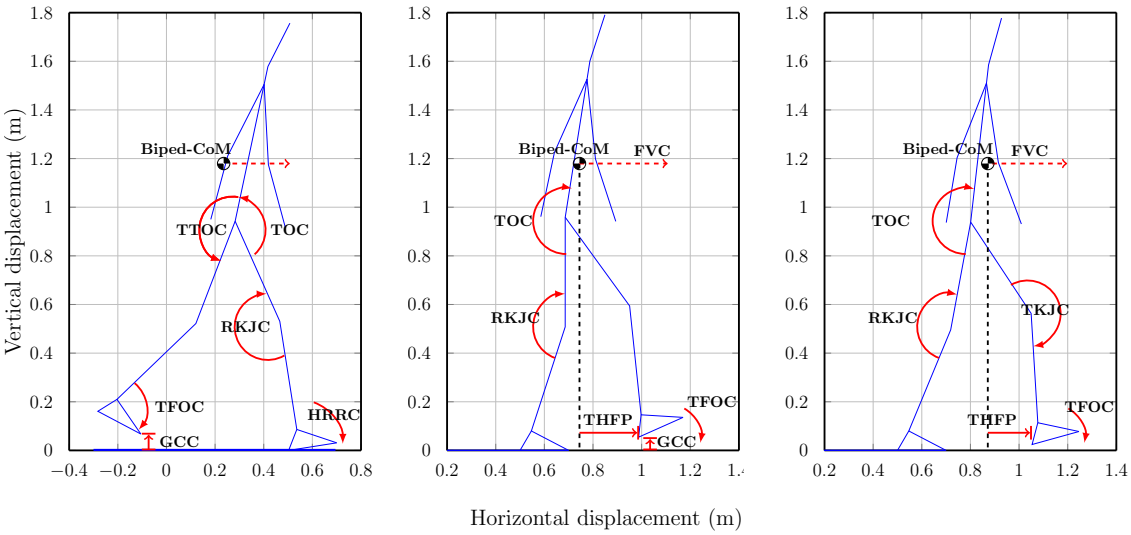

(a) Pre-midswing (b) Post-midswing Pre-touchdown (c) Touchdown

Figure 5.1: Motion control primitives for different phases of planar dynamic walking

5.2.3 Transit Leg Control Primitives

The transit leg control primitives are responsible for the guidance and control of the transit foot from the lift-off event from ground to the subsequent touch down event. The details of various task primitives to be activated during this period are given below.

5.2.3.1 Ground Clearance Control (GCC) primitive

The GCC primitive is activated by SLC during the hybrid event state defined by ,

$$\mathbb{H}_{es} : \Big(\Sigma\pi_{c\,(1:2)} > 0\Big)\ \&\ \Big(\Sigma\pi_{c\,(3:4)} = 0\Big)\ \&\ \Big(FwdTDFlg = 0\Big)\ \&\ \Big(TrnKneExt = 0\Big) \quad (5.16)$$

The objective of ground clearance control primitive is to ensure adequate clearance between transit foot sole and ground surface to avoid scuffing prior to the controlled heel strike as per $\mathcal{CFR}2$. In addition, GCC is responsible for the lift-off action of the rear foot from ground subsequent to the heel strike event of front foot.

Here also, we use regulator type task primitive to ensure the desired ground clearance. Some authors use repulsive type task primitives [58] for similar purposes. The disadvantage of repulsive task primitive is that the transit leg can have redundant DoF, whenever the foot goes outside the ground clearance zone which may lead to undesired vertical motion unless properly controlled. Besides this, the transit foot sole should be as close as possible to the ground for emergency touch down at any time which is not possible if the foot is simply kept outside the ground clearance zone. For the current planar bipedal model, the foot sole is represented by a line segment joining heel and toe and we assume that if both of these corner points are kept outside the ground clearance zone, all points of the foot sole satisfy the ground clearance requirement. Hence the ground clearance primitive is specified only in terms of the bottom-most corner points of the transit foot. Let the symbol '$\mathtt{tb}$' represent the bottom-most point of the transit foot out of '$\mathtt{th}$' or '$\mathtt{tt}$' and let the corresponding Jacobian be represented as J_{tb} which corresponds to either J_{th} or J_{tt}. The Jacobian for '$\mathtt{tb}$' resolved along inclined ground coordinate frame, $\{O_g\}$ is defined as,

$$J_{gb} = R_g(\sigma_G)\ J_{tb},\ \dot{J}_{gb} = R_g(\sigma_G)\ \dot{J}_{tb} \quad (5.17)$$

Using the expression for ground profile given by (3.5) , the y-coordinate of a point on ground with $x_g = x_{tb}$, expressed in $\{O_0\}$ can be written as

$$y_g(x_{tb}) = y_{G0}(x_{tb}) + x_{tb} \tan\sigma_G(x_{tb}) \quad (5.18)$$

The elements of regulator type task expression for ground clearance control primitive are given by,

$$H(q) = \begin{bmatrix} \mathbf{0}_{1\times 7} & J_{gb\,(2,8:10)} & \mathbf{0}_{1\times 4} \end{bmatrix} \tag{5.19}$$

$$\begin{aligned} B(q,\dot{q}) = {} & \omega_b^2 \left(\rho_{gc} - \rho_{cl}\cos\sigma_G(x_{tb})\right) \\ & - \left(2\zeta\omega_{gc} J_{gb\,(2,:)} + \dot{J}_{gb\,(2,:)}\right)\dot{q} \end{aligned} \tag{5.20}$$

where ρ_{gc} is the desired ground clearance between transit foot sole bottom point and ground, $\rho_{cl} = (y_{tb} - y_g(x_{tb}))$, $\omega_b = 6\omega_p$ and $\zeta = 1$. If $V_{fc} < 1$, the value of ω_b can be reduced to $5\omega_p$. ρ_{cl} represents the current value of ground clearance between transit foot bottom and ground along the vertical direction, $\overrightarrow{O_0Y_0}$ and $\rho_{cl}\cos\sigma_G(x_{tb})$ gives the ground clearance normal to ground along $\overrightarrow{O_gY_g}$. The nominal value of ground clearance is taken as, $\rho_{gc}^o = 0.04$. To the above nominal profile, we have to provide an additional offset as a function of forward velocity as given below for avoiding scuffing and premature heel strike.

$$\delta\rho_{gc} = 0.5\left(\max(V_{fc}, V_{comx}) - 1\right)\rho_{gc}^o \text{ if } \max(V_{fc}, V_{comx}) > 1 \tag{5.21}$$

Thus the general expression for the required ground clearance profile is given by,

$$\rho_{gc} = \rho_{gc}^o + \delta\rho_{gc} \tag{5.22}$$

The ground clearance error, $\left(\rho_{gc} - \rho_{cl}\cos\sigma_G(x_{tb})\right)$ is limited to a maximum value of 0.01 m to limit the slew rate of control loop. Even though the desired ground clearance is expressed as a step function, the actual trajectory of transit foot will be a smooth profile, shaped according to the transient behaviour of GCC primitive during the swing period of transit foot. Once $FwdTDFlg = 1$, the ground clearance primitive is called off and the transit foot heel is guided to the desired touchdown location.

5.2.3.2 Transit Thigh Orientation Control (TTOC) primitive

The TTOC primitive is activated by SLC during the hybrid event state defined by,

$$\mathbb{H}_{es} : \left(\Sigma\pi_{c\,(1:2)} > 0\right) \,\&\, \left(\Sigma\pi_{c\,(3:4)} = 0\right) \,\&\, \left(MidSwgFlg = 0\right) \tag{5.23}$$

to fulfil the requirement of $\mathcal{CDR}5$ with respect to the postural state, $\mathbf{x}_{Pc\,7}$. The forward motion of transit leg in swing phase is divided into three segments. The first segment is up to mid-swing when the mid-point of the transit foot crosses the mid-point of reference foot

in forward direction at the first time during each walking step; i.e. when $(x_{th} + x_{tt})/2 = (x_{rh} + x_{rt})/2$. The second segment is from mid-swing to the starting instant of forward touchdown phase of transit foot. The third segment is the remaining period of swing phase till the transit foot strikes on the ground.

In human walk, the forward motion of transit leg is initiated by CCW rotation of transit leg thigh about hip joint in the sagittal plane with a joint torque suitable for the particular ground slope and forward locomotion velocity. This is achieved in HyDAC during the pre-midswing phase by giving a step command to transit leg thigh joint so as to orient it along an angle of q_T^o measured in CCW direction from the local vertical passing through the hip joint and pointing downward. The thigh reference angle, q_T^o is an important parameter controlling the step length of dynamic walk and hence the gait stability. The empirical expression for q_T^o arrived at for different speeds and ground slopes based on simulation studies can be given as,

$$q_T^o = \max\Big(1, \min(1.5, V_{fc})\Big)\ \pi/9 + \delta q_T^o \tag{5.24}$$

where δq_T^o is an additional offset to be added as a function of σ_G and V_{fc}. For $\sigma_G \geqslant 0$, $\delta q_T^o = 0.25\sigma_G V_{fc}$ and for $\sigma_G < 0$, $\delta q_T^o = 0.375\sigma_G$. However for steeper slopes with $\sigma_G < -\pi/12$, $\delta q_T^o = 0.5\sigma_G$. Further, for large velocity commands with $V_{fc} > 1.75$ m/s, the value of δq_T^o is reduced by $\pi/36$ to reduce the forward landing offset. Finally, the value of q_T^o is limited to an upper bound of $35\pi/180$. The forward step command for transit thigh provides a larger forward push on thigh at the beginning with its reaction acting backward on biped hip effectively transferring part of the torso's kinetic energy to forward swing leg. The expression for task primitive vectors can be written as,

$$H(q) = \Big[\mathbf{0}_{1\times 7}\ 1\ \mathbf{0}_{1\times 6}\Big] \tag{5.25}$$

$$B(q, \dot{q}) = \omega_b^2 q_{Te} - 2\zeta\omega_b \Big[0\ 0\ 1\ 1\ 1\ 1\ 0\ 1\ \mathbf{0}_{1\times 6}\Big]\ \dot{q} \tag{5.26}$$

$$q_{Te} = q_T^o - q_{TI} \tag{5.27}$$

where, $\zeta_T = 0.8$, and q_{TI} is the inertial orientation of the transit thigh given by $q_{TI} = \Sigma q_{(3:6)} + q_8 - 3\pi/2$. The absolute value of q_{Te} is limited to a maximum value of $25\,\pi/180$ to limit the slew rate of control loop. For defining the desired control bandwidth for transit leg forward motion, we make use of an intermediate frequency, denoted by ω_{pL} defined as

$$\omega_{pL} := 4\omega_p.\max\big(0.5, \min(V_{fc}, 1)\big) \tag{5.28}$$

In nominal situations, the control bandwidth for TTOC is assigned as, $\omega_b = 0.75\omega_{pL}$. However, if $|\sigma_G| \geqslant 5\pi/180$ or $V_{fc} > 1.25$, then $\omega_b = \omega_{pL}$. If $V_{fc} > 1.75$, then $\omega_b = 1.25\omega_{pL}$.

5.2.3.3 Transit Heel Forward Positioning (THFP) primitive

The THFP primitive is activated by SLC during the hybrid event state defined by ,

$$\mathbb{H}_{es} : \Big(\Sigma\pi_{c\,(1:2)} > 0\Big)\ \&\ \Big(\Sigma\pi_{c\,(3:4)} = 0\Big)\ \&\ \Big(\mathit{MidSwgFlg} = 1\Big) \tag{5.29}$$

to fulfil the requirement of $\mathcal{CDR}5$ with respect to the postural state, $\mathbf{x}_{Pc7}$ and it drives the transit heel to the desired landing location, (x^o_{Lh}, y^o_{Lh}) on ground expressed in the inertial frame, $\{O_0\}$. Prior to touch down phase of transit foot, the desired landing location is specified only in terms of x^o_{Lh} for all types of terrain as GCC primitive is active to ensure ground clearance. We would like to define a new term, the effective landing slope, σ_{GL} as the slope measured between the current estimated landing site, (x^o_{Lh}, y^o_{Lh}) for transit foot and the ground projection of the current location of reference toe, $(x_{rt}, y_g(x_{rt}))$ in the presence of step and slope discontinuities on ground profile. It is given by,

$$\sigma_{GL} = \tan^{-1}\frac{y^o_{Lh} - y_g(x_{rt})}{x^o_{Lh} - x_{rt}} \tag{5.30}$$

If $\sigma_{GL} \leqslant 5\,\pi/180$, the vertical motion of transit foot is rendered as passive during the touchdown phase and hence the specification for THFP primitive continues as in pre-touchdown phase. However, if $\sigma_{GL} > 5\,\pi/180$, the transit foot is to be steered along the effective upward slope, σ_{GL} towards (x^o_{Lh}, y^o_{Lh}) to prevent the transit foot hitting the ground prior to reaching the desired horizontal location, x^o_{Lh}. Prior to touchdown phase, $B(q, \dot{q})$ for the control primitive of THFP can be written as,

$$B(q, \dot{q}) = \omega_b^2\, x_{Le} - \dot{J}_{th\,(1,:)}\dot{q} + 2\zeta\omega_b.\nu_{Le} \tag{5.31}$$

$$x_{Le} = x^o_{Lh} - x_{th} \tag{5.32}$$

$$\nu_{Le} = V_{comx} - J_{th\,(1,:)}\,\dot{q} \tag{5.33}$$

where $\omega_b = 5\omega_p$ and $\zeta = 1$. The absolute value of landing position error, x_{Le} is limited to $x_{Le+} = 0.1$ m and the absolute value of landing velocity error, ν_{Le} is limited to $\nu_{Le+} = 0.05\,\omega_b$ m/s prior to its substitution in (5.31). The position error and velocity error limits are selected in such a way that $\omega_b^2\, x_{Le+} = 2\zeta\omega_b\,\nu_{Le+}$. The expression for the task

primitive Jacobian, $H(q)$ prior to touchdown phase is given by,

$$H(q) = \begin{bmatrix} \mathbf{0}_{1\times 7} & J_{th\,(1,8:9)} & \mathbf{0}_{1\times 5} \end{bmatrix} \tag{5.34}$$

The expressions for $B(q,\dot{q})$ and $H(q)$ are valid during touchdown phase also if $\sigma_{GL} \leqslant 5\pi/180$. However, if $\sigma_{GL} > 5\pi/180$, we have to make use of the equivalent Jacobian, J_{eth} instead of J_{th} in (5.34) to drive the transit foot heel along the effective landing slope of ground. The values of J_{eth} and $\dot{J}_{eth}$ can be derived using the effective landing slope, σ_{GL} as $J_{eth} = R_{gL} J_{th}$ and $\dot{J}_{eth} = R_{gL}\dot{J}_{th}$ where $R_{gL} = R_g(\sigma_{GL})$. For $\sigma_{GL} > 5\pi/180$, the expressions for the relevant characteristic vectors, $H(q)$ and $B(q,\dot{q})$ are modified as,

$$H(q) = \begin{bmatrix} \mathbf{0}_{1\times 7} & J_{eth\,(1,8:9)} & \mathbf{0}_{1\times 5} \end{bmatrix} \tag{5.35}$$

$$B(q,\dot{q}) = \omega_b^2\, x_{Le} - \dot{J}_{eth\,(1,:)}\dot{q} + 2\zeta\omega_b . v_{Le} \tag{5.36}$$

$$x_{Le} = R_g(\sigma_{GL})_{(1,:)} \begin{bmatrix} x^o_{Lh} - x_{th} \\ y^o_{Lh} - y_{th} \end{bmatrix} \tag{5.37}$$

$$v_{Le} = R_g(\sigma_{GL})_{(1,:)} V_{com} - J_{eth\,(1,:)}\,\dot{q} \tag{5.38}$$

where $\omega_b = 0.5\omega_{pL}$. The landing position error and landing velocity error given by (5.37) and (5.38) are estimated along the effective landing slope, σ_{GL} and are also limited to x_{Le+} and v_{Le+} respectively as done for the other cases. If *TrnKneExt*=1, the transit knee joint, q_9 will not be available for this primitive and hence $H(q)_9$ in (5.34) and (5.35) are to be made zero. Further, both the limits x_{Le+} and v_{Le+} are doubled for $|\sigma_G| > 5\pi/180$ to improve the transient response for higher terrain slopes.

5.2.3.4 Expression for Landing location

The optimal selection of transit heel landing location, x^o_{Lh} is very important with respect to stability and efficiency of dynamic walk. The distance between two consecutive heel landing locations is called step length and is equal to half of stride length. The basic requirement of touchdown location is that it should be ahead of x_{com} by an offset just sufficient to impart the minimum braking to suppress the excess forward velocity built up during the passive forward rolling phase prior to heel strike. If the braking force is excess, the biped will get unduly retarded reducing the efficiency of walk or even stop or fall backward in the next cycle itself. If the braking force is less, the forward velocity will increase gradually over the subsequent cycles leading to eventual forward fall. Hence, x^o_{Lh} is to be fixed to avoid the more sensitive backward falling situation in a control perspective.

Pratt et.al have used the concept of 1-step capture point to estimate the landing location of transit foot by approximating the biped dynamics by a 3D linear inverted pendulum [18]. This is based on the concept of foot capturability where the stability of bipedal walk is perceived with respect to preventing fall by means of stopping the biped. N-step capturability is defined as the ability of a system to come to a stop without falling by taking N or fewer steps, given its dynamics and actuation limits [51]. The concept of capture point is transverse to the concept of periodic stability of passive dynamic walker, i.e. the impact should sustain the forward velocity with repeatable performance. Further, for the sake of analytical tractability, capture point calculation does not consider the vertical dynamics of pendulum, which is a crucial element in controlling the periodic stability of dynamic walk [10]. Similarly the dynamics of swing leg and impact dynamics are also not considered in the derivation of foot capture point. A similar work, named foot placement estimator (FPE), is reported in [94] to derive the foot placement location to stabilize planar bipedal walk by way of stopping the same. FPE uses 2D inverted pendulum model with two massless legs with fixed length and having biped mass and centroidal MI concentrated at a point.

HyDAC does not use either of the above two approaches for the calculation of transit foot placement due to the following reasons. Firstly, the objective of landing site is not to stop walking, but to sustain walking with minimum energy loss during foot impact. Secondly, landing location is not an absolute location on ground (assuming sufficiently even ground) with respect to previous foothold, but it is a relative location with respect to the moving GCoM of biped. Hence the associated behaviour loop has to track a ramp command, which will bound to have finite position error, not only because of type-1 property of the forward path transfer function, but also due to the insufficient dwell time for the controller during the touch down phase. Further, the empirical formula derived based on full model simulation experiments will be more accurate and more versatile to take care of diverse walking situations and transients of the foot placement controller. Hence HyDAC has chosen the route of simulation based optimization to derive the empirical formula for landing location, x^{o}_{Lh} and the pseudo code for the same is given in Algorithm 5.2.

5.2.3.5 Transit Foot Orientation (TFO) primitive

The TFO primitive is activated by SLC during the hybrid event state defined by the logical condition, $\Sigma(\pi_{c\,(1:2)}) > 0$ and $\Sigma(\pi_{c\,(3:4)}) = 0$ to fulfil the requirement of $\mathcal{CDR}1$ with respect to the postural state, $\mathbf{x}_{Pc5}$. The nominal orientation of transit foot sole with respect to ground surface is kept at θ_{solt}=10 π/180 rad so that transit foot will strike the ground with its heel. The orientation reference for the transit ankle joint for TFO primitive can be

Algorithm 5.2: Computation of forward landing offset, λ_h and landing location, x^o_{Lh}

Data: $\sigma_G(\max(x_{th}, x_{rt}))$, x_{rt}, x_{com}, V_{fc}, h_{com}, and N_{stp}
if $x_{th} < x_{hip}$ **then**
  $\lambda_h \leftarrow 0.053\min(1, V_{fc})$, $x^o_{Lh} \leftarrow \max(x_{rt}, x_{com}) + \lambda_h h_{com}$
else
  $\lambda_h \leftarrow 0.053\ \big(1 + \min(0, (-180\,\sigma_G/\pi + 7.5)/10\big)\ \min(1.5, V_{fc})$
  if $\sigma_G \leqslant -\pi/18$ **then**
    $\lambda_h \leftarrow 0.053\ \big(1 + (-180\,\sigma_G/\pi - 10)/15\big)\ \min(1.5, V_{fc})$
  end
  if $V_{fc} > 1.5$ **then**
    $\lambda_h \leftarrow \lambda_h - 0.159\,(V_{fc} - 1.5)$ ▷ To reduce braking force for large velocity
  end
  if $N_{stp} = 1$ **then**
    $\lambda_h \leftarrow 0.053\,\min(1, V_{fc})$ ▷ To provide larger initial forward thrust for $V_{fc} > 1$
  end
  $x^o_{Lh} \leftarrow x_{com} + \lambda_h h_{com}$
end

given as

$$q^o_{10} = \pi + \sigma_G - \gamma - q_{sh} + \theta_{solt} \tag{5.39}$$

where $q_{sh} = \Sigma q_{(3:9)} - q_7 - \pi$ is the inertial orientation of transit tibia (shank) link. However for larger velocities and for steeper slopes, θ_{solt} is kept as zero to ensure faster toe strike after heel strike and such situations can be represented by the logical condition,

$$(V_{fc} \geqslant 1.0 \text{ and } \sigma_G \geqslant \pi/12) \text{ or } (V_{fc} \geqslant 1.25 \text{ and } \sigma_G \geqslant \pi/18) \text{ or } (V_{fc} \geqslant 1.75 \text{ and } \sigma_G \geqslant 0) \tag{5.40}$$

The characteristic vectors for TFO primitive can be written as,

$$H(q) = \Big[\mathbf{0}_{1\times 7}\ \Big|1\ 1\ 1\ \Big|\mathbf{0}_{1\times 4}\Big] \tag{5.41}$$

$$B(q, \dot{q}) = \omega_b^2\ \Big(q^o_{10} - q_{10}\Big) - 2\zeta\omega_b \dot{q}_{10} \tag{5.42}$$

with $\zeta = 0.7$ and $\omega_b = 5\omega_p$. The maximum value of the absolute position error, $|q^o_{10} - q_{10}|$ is limited to $12\,\pi/180$ to limit the slew rate of control loop. If *TrnKneExt*=1, the transit knee joint, q_9 will not be available for this primitive and hence $H(q)_9$ in (5.41) is to be made zero.

5.2.3.6 Transit Knee Joint Control (TKJC) primitive

The TKJC primitive is activated by SLC during the hybrid event state defined by

$$\mathbb{H}_{es} : \Big(\Sigma\pi_{c\,(1:2)} > 0\Big) \,\&\, \Big(\Sigma\pi_{c\,(3:4)} = 0\Big) \,\&\, \Big(FwdTDFlg = 1\Big) \tag{5.43}$$

to fulfil the requirement of $\mathcal{CDR}1$ and $\mathcal{CDR}5$ with respect to the postural state, $\mathbf{x}_{Pc\,4}$ as well as the requirement of $\mathcal{CFR}7$. The transit knee joint angle at the time of heel touchdown is an important parameter which affects the gait stability. An excess bent knee during heel strike is not suitable for regulating the height of y_{com} in the subsequent stance phase and a straight knee during heel strike leads to excess velocity reduction as well as kinematic singular state. The TKJC primitive execution is carried out with two different objectives during the post midswing phase. If *TrnKneExt*=1, the TKJC is executed to bring the transit knee out of straight knee zone by a closed loop regulator control with a target value of $\theta^{o}_{knet} = -15\pi/180$. The expressions for the characteristic vectors can be written as,

$$H(q) = \begin{bmatrix} \mathbf{0}_{1\times 8} & 1 & \mathbf{0}_{1\times 5} \end{bmatrix} \tag{5.44}$$

$$B(q,\dot{q}) = \omega_b^2(\theta^{o}_{knet} - q_9) - 2\zeta\omega_b\dot{q}_9 \tag{5.45}$$

with $\omega_b = 6\omega_p$ and $\zeta = 0.9$. If *TrnKneExt*=0 and *FwdTDFlg*=1, the value of θ^{o}_{knet} is programmed as a function of V_{fc} and σ_G as given in Algorithm 5.3.

Algorithm 5.3: Computation of θ^{o}_{knet} as a function of σ_G and V_{fc}

Data: σ_G and V_{fc}
$\theta^{o}_{knet} \leftarrow \pi/6 - 1.5\sigma_G$
if $V_{fc} > 1$ **then**
  if $\sigma_G \geqslant \pi/36$ **then**
    $\theta^{o}_{knet} \leftarrow \theta^{o}_{knet} - (V_{fc} - 1)\pi/12$ ▷ $\theta^{o}_{knet}(V_{fc})$ for slope-up terrain
  else if $\sigma_G < -\pi/36$ **then**
    $\theta^{o}_{knet} \leftarrow \theta^{o}_{knet} + (V_{fc} - 1)\pi/18$ ▷ $\theta^{o}_{knet}(V_{fc})$ for slope-down terrain
  end
end
if $\theta^{o}_{knet} \leqslant -\pi/3$ **then**
  $\theta^{o}_{knet} \leftarrow -\pi/3$ ▷ Limiting the value of θ^{o}_{knet}
else if $\theta^{o}_{knet} \geqslant -\pi/18$ **then**
  $\theta^{o}_{knet} \leftarrow -\pi/18$
end

5.2.3.7 Transit leg Floating State Control (TFSC) primitive

During the free floating state of biped characterized by $\mathbb{H}_{es} : \Sigma\pi_{c\,(:)} = 0$, it is recommended to keep the acceleration of all the joints of transit leg as zero. This corresponds to the primitive description,

$$H(q) = \begin{bmatrix} \mathbf{0}_{3\times7} & I_3 & \mathbf{0}_{3\times4} \end{bmatrix}, \; B(q,\dot{q}) = \mathbf{0}_{3\times1} \tag{5.46}$$

5.2.4 Upper Body Control Primitives

The joints of upper body consisting of the joints of both the upper limbs and neck, can be assigned any useful task as long as they can be executed without disturbing the position and orientation of torso while the biped is in forward motion. The additional contact forces if any between the upper body parts and the environment should also be within the tolerable limits. If no specific tasks are allotted to the upper arm joints, the same can be left passive by equating the respective joint torques as zero. At present, we have assigned only simple kinematic tasks to keep the joint angles, θ_{ubd} along certain nominal orientations, θ^{o}_{ubd} .

5.2.4.1 Upper Limb Orientation Control (ULOC) primitive

This primitive regulates the deflections of shoulder and elbow joints of both the upper arms to the assigned values. The ULOC primitive can be described by the characteristic vectors,

$$H(q) = [\mathbf{0}_{4\times10} \quad I_4] \tag{5.47}$$

$$B(q,\dot{q}) = \omega_b^2(q_u^o - q_u) - 2\zeta\omega_b\dot{q}_u \in \mathbb{R}^{4\times1} \tag{5.48}$$

where $q_u = q_{(11:14)} \in \mathbb{R}^{4\times1}$ and q_u^o representing the reference angles for q_u given by $q_u^o = \theta^o_{ubd(2:5)} = [180 \quad 15 \quad 180 \quad 15]'\pi/180$, $\omega_b = \omega_p/2$ and $\zeta = 1$. ULOC has an additional responsibility of acting like virtual spring if the elbow joints approach towards the fully extended, singular orientations. As the elbow joints approach the singular orientation, the C_{SF} flags, *RgtElbExt* or *LftElbExt* takes value of 1 and ULC is executed with modified values of $\omega_b = 3\omega_p$ and $\zeta = 0.7$ for the corresponding joint elements to drive the respective elbow joints out of singular state at a faster rate.

5.2.4.2 Neck Joint Control (NJC) primitive

This primitive regulates the orientation of head with respect to torso link. The desired deflection of neck joint with respect to torso link is taken as $q_7^o = \theta^o_{ubd(1)} - 5\pi/180$. The

NJC primitive is described by the characteristic vectors,

$$H(q) = [\mathbf{0}_{1\times 6} \quad 1 \quad \mathbf{0}_{1\times 7}] \tag{5.49}$$

$$B(q, \dot{q}) = \omega_b^2 \left(q_7^o - q_7\right) - 2\zeta\omega_b \dot{q}_7 \tag{5.50}$$

5.2.5 Behavior modifications for handling walking transients

It is necessary to modify some of the locomotion behaviour parameters for ensuring stable walking under transient situations of dynamic walking. The objective of this section is only to demonstrate only few of transient situations such as starting, stopping, and walking down over single step. However, the concept can be easily extended for handling other walking transients as well. The step-up transient situation is not considered here as the same is considered under the extension of HyDAC for nonuniform random staircase.

5.2.5.1 Acceleration phase

The biped derives the forward thrust for starting phase by manipulation of the GCoP with respect to the current location of GCoM as discussed in Section 4.6, provided the current foothold of stance foot support the same. During staring phase with initial forward velocity as zero, it is important to provide larger forward thrust for larger values of V_{fc}. Hence the forward landing offset, λ_h is kept as a constant irrespective of the velocity command, if $V_{fc} > 1$ as given in Algorithm 5.2. Another parameter to be controlled during the first two steps is q_T^o, the target orientation for transit thigh in TTOC primitive. As the transit foot is starting from rest during $N_{stp} = 1$, and since the pre-midswing phase is relatively short, a higher value of $q_T^o = \pi/6 \max\left(1, \min(1.5, V_{fc})\right)$ is used for $N_{stp} \leqslant 2$. A third parameter to be controlled is effective V_{fc} itself, if the requirement is greater than 1. It is recommended to increase V_{fc} in steps of 0.5 m/s once in every 2 steps for the excess part of V_{fc} over 1 m/s.

5.2.5.2 Deceleration phase

Like the acceleration phase, if the velocity is to be decreased, the same is recommended to be done in steps of 0.25 m/s in every consecutive step until the required command level is arrived at. If the purpose is to stop the forward motion, a stop flag named *StpFlg* is set if $V_{comx} > 0.2$ m/s on heel strike. If *StpFlg*=1, the forward landing offset, λ_h is increased by an extra angle of $0.5L_f/h_{com}$ rad.

5.2.5.3 Walking down over single step

During uneven terrain locomotion, the biped may have to jump down over a step without any trajectory pre-planning. As in the human walk, four precautions are taken to avoid a forward fall and to limit the forward velocity. One is to set the RKJC primitive to drooping mode as in down-slope terrain, but with a larger target angle of $\theta^{o}_{kner} = 70\pi/180$ rad and another is to ensure transit foot ground strike with its toe in the first step on jump down by keeping θ_{solt}=-10 π/180 rad in TFO primitive. Another set of precautions is to increase λ_h by an extra angle of $0.5L_f/h_{com}$ rad and increase q^{o}_{7} by $\pi/18$ rad in the subsequent two steps including step down to retard down the excess forward velocity accumulated during step down. A terrain discontinuity is considered as a step down only if the additional slope due to the same is more than $\pi/18$ rad when measured over the span of $[x_{rt}\ x_{tt}]$.

5.3 Simulation Results

The stability and agility of the proposed control scheme are demonstrated based on simulation experiments conducted using the mathematical model of 12-link planar biped (Fig 3.1) with parameters values given in Table 3.1. The planar biped has a total mass of 84.5 kg and a total height 1.83 m in nominal stance condition having joint angle values given as in Table 5.1[6] and has similar size and mass distribution of an adult-sized human being projected onto sagittal plane [95]. The numerical values of other two important parameters are, $h_{hip} = 0.9807$ m and $h_{com} = 1.1314$ m. The torque limits of torso joint actuator is set at $\pm$600 N-m in the control algorithm itself as a nonholonomic constraint. The joint torque limits for lower limb actuators, namely for thigh, knee and ankle are implemented as explicit saturation limits of $\pm$600 N-m, $\pm$500 N-m and $\pm$400 N-m just after the computation of Γ_d prior to passing over to the integration routine for system dynamics simulation.

Table 5.1: Initial values of generalized position variables, q of planar biped in rad

q_3	q_4	q_5	q_6	q_7	q_8	q_9	q_{10}	q_{11}, q_{13}	q_{12}, q_{14}
$\pi + \sigma_G - \gamma$	$-0.55\pi - \sigma_G + \gamma$	0.1π	$-0.05\pi - \sigma_G$	0	$1.067\pi + \sigma_G$	-π/6	$0.6\pi + \sigma_G - \gamma$	π	0.067π

The numerical simulation program for HyDAC algorithm along with planar bipedal dynamics is coded in MATLAB using fourth order Runge-Kutta (RK4) numerical integration algorithm with a control computation interval of 0.002 s. The rates of various Jacobians,

[6]The initial values of q_1 and q_2 are taken as zeros.

$J(q)$ are derived by making use of a bank of low pass filters with their feedback error signal providing $\dot{J}(q)$. Simulation runs are taken by giving different forward velocity commands, V_{fc} to the biped having an initial stationary stance posture on single foot with sufficient forward inclination. Minor modifications are given to the regulation targets of motion control primitives and SLC as mentioned in Section 5.2.5.1 during the first walking step so that the biped operates in forward touchdown phase under gravity pull to initiate forward locomotion. Subsequently, the autonomous control of HyDAC accelerates the biped in forward direction and regulates the forward velocity with event periodic stability for the dynamic walking gait.

5.3.1 Simulation results with nominal parameters

Simulation experiments are conducted for different values of V_{fc} ranging from 0.1 m/s to 2 m/s and for ground slopes, σ_G ranging from -20 deg to 20 deg including even step-down discontinuity up to 0.3 m. The observations of various simulation runs are given below.

The stick diagram given in Fig 5.2(a)-(c) shows how the bipedal links are rotating and advancing during a typical walking step over ground profile with different slopes of σ_G=20 deg, 0 deg and -20 deg for V_{fc}= 1 m/s. The forward lean of torso increases with forward velocity as well as with positive ground slope to ensure sufficient forward thrust through FVC algorithm. The video links corresponding to the simulation results given below are provided in Table B.1. The ground contact force acting on the reference foot heel and toe corresponding to these walking profiles are shown in Fig 5.3. The profiles of V_{com_x} and V_{com_y} are also included in the same plot. The upper bound of the perpendicular component of heel contact force is kept at f_{cy+}= 4 kN on each heel strike. During upslope walking, the forward thrust provided by the positive value of f_{grh_x} is used to raise V_{com_x} towards the commanded value of V_{fc} =1 m/s as shown in Fig 5.3(a) whereas during downslope walking, the braking force provided by the negative value of f_{grh_x} or f_{grt_x} are used to regulate V_{com_x} as shown in Fig 5.3(c). During level ground locomotion, both positive and negative values of tangential force are used to closely regulate the V_{com_x}.

The contact force profiles for V_{fc}=0.5 m/s and 1.5 m/s on level terrain walking for a typical gait are shown in Fig 5.4. Theses plots can be compared along with the contact force profiles for the case with V_{fc}= 1 m/s, σ_G=0 given in Fig 5.3(b). It can be seen that the normal component of the ground contact force, $(f_{grh_y} + f_{grt_y})$ is within the bounds of 4000 N and 200 N. The forward velocity, V_{com_x} is also well regulated to the respective commanded values. The forward velocity profiles while biped is commanded with different values of

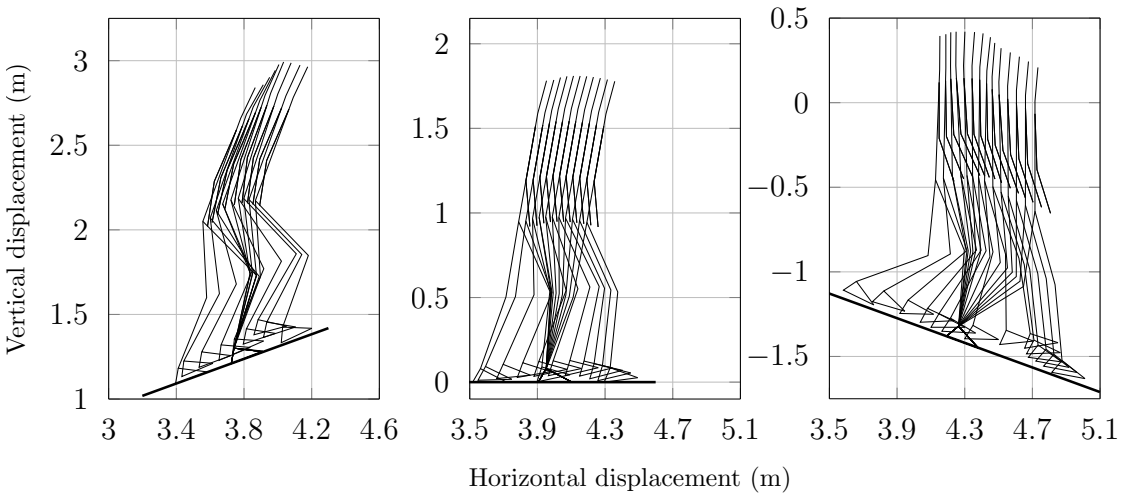

(a) $\sigma_G = 20^o$ (b) $\sigma_G = 0^o$ (c) $\sigma_G = -20^o$

Figure 5.2: Stick diagram for single step with V_{fc}=1 m/s and with different ground slopes (Data sampled @ 0.04 s)

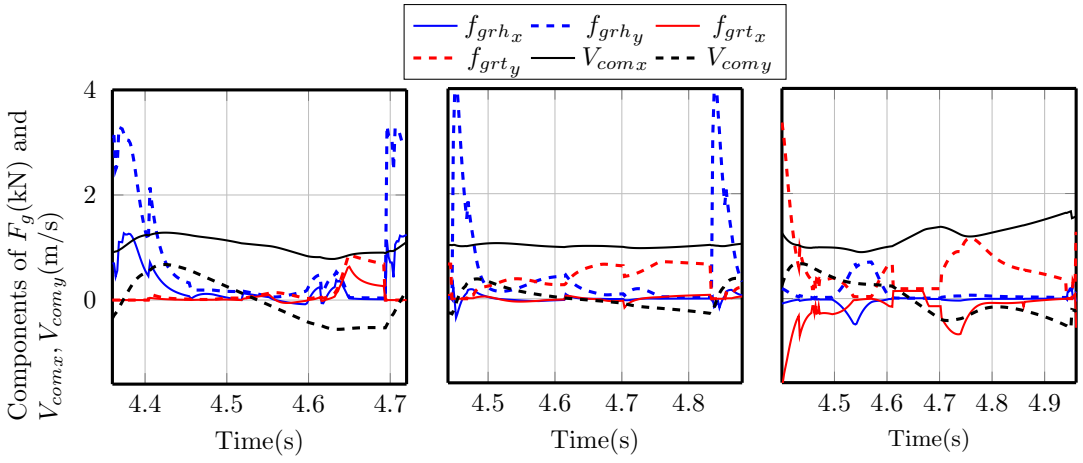

(a) $\sigma_G = 20^o$ (b) $\sigma_G = 0^o$ (c) $\sigma_G = -20^o$

Figure 5.3: Components of ground contact forces acting on reference foot and components of biped-CoM velocity corresponding to walking steps shown in Fig 5.2

$V_{fc} \in [0.1\ 2]$ m/s on level ground are shown in Fig 5.5. The velocity increases during each passive forward rotation phase of a gait followed by decrease after each heel strike event

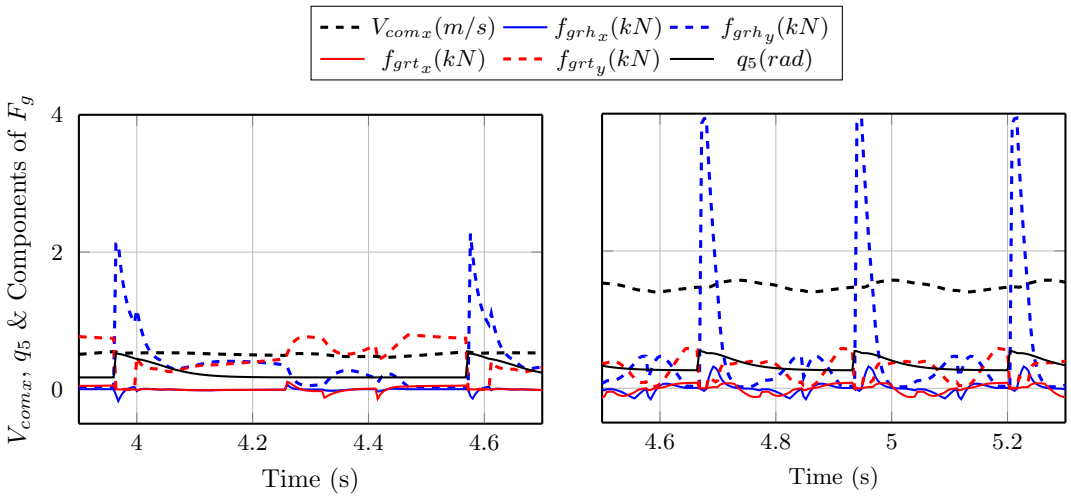

(a) for $V_{fc} = 0.5m/s$ (b) for $V_{fc} = 1.5m/s$

Figure 5.4: Components of reference foot contact force and Forward velocity of biped-CoM on level ground

and restores back to the commanded value due to the action of FVC algorithm. The plot demonstrates periodic behaviour of planar bipedal gait in all the cases except for V_{fc}=2 m/s where the gait becomes almost biperiodic. This is due to the poor stability margin at larger velocity commands which will be explicitly brought out in Fig 5.16. The forward velocity pattern for upslope and downslope terrains with different velocity commands are shown in Fig 5.6 for the biped which started its motion at t = 0 s. The periodicity of the gait pattern is quite good even though the tracking error increases for $|\sigma_G| > 10$ deg. The biped can even walk with little inferior periodicity when commanded with V_{fc}=1.5 m/s over a terrain having slopes $+/-10$ deg. Fig 5.7 shows the excellent periodicity of joint angle profiles during level ground walking for V_{fc}= 0.5 m/s. The joint torque profiles during level ground walking with V_{fc}= 1 m/s are shown in Fig 5.8. The torso joint torque, Γ_{d6} takes the maximum value and transit ankle joint torque, Γ_{d10} takes the minimum value. The joint torque commands remain within the respective bounds as mentioned.

5.3.2 Results for perturbation cases

We consider here four cases for robustness evaluation, namely robustness with respect to terrain parameter perturbation, payload mass perturbation, external limiting of torque commands, and finally with respect to external force disturbance.

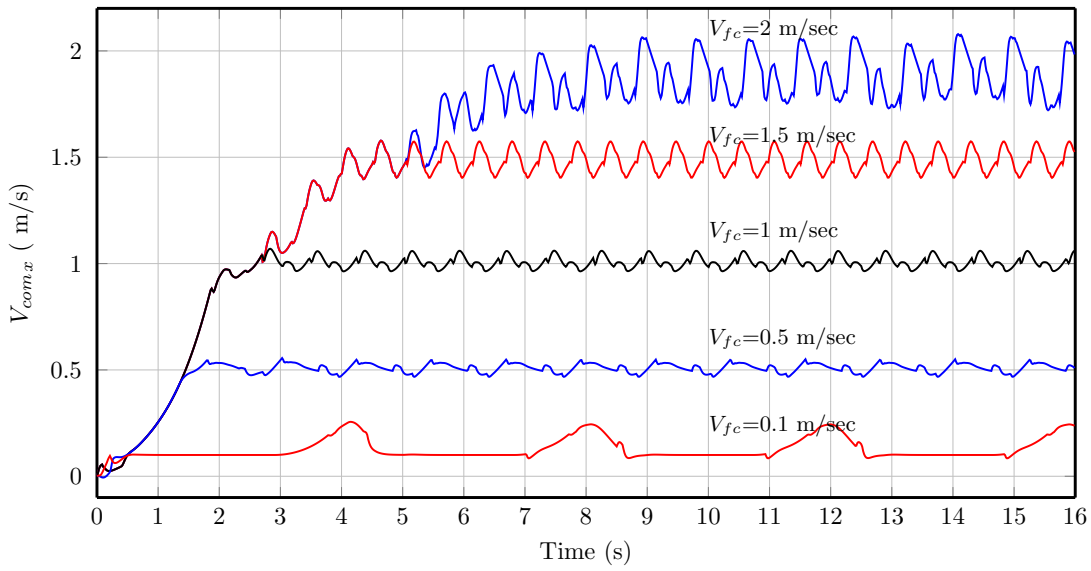

Figure 5.5: Forward velocity of biped-CoM for different velocity commands (V_{fc}) on level ground

5.3.2.1 Robustness with respect to terrain-parameter perturbation

The robustness of HyDAC with respect to unexpected variations in terrain parameters, y_{Go} and σ_G [7] is demonstrated in Fig 5.9-Fig 5.11 while the biped is commanded to walk with $V_{fc} = 1\ m/s$ along a terrain having a down step of 0.3 m and slope variations of ± 20 deg.

The forward velocity and torso orientation are regulated quickly to the expected steady state value overcoming the sudden disturbance due to both step and slope discontinuities of ground. The simulation result demonstrate the agility of HyDAC to autonomously adapt to terrain conditions without any a priori gait planning and prove the potential of HyDAC for generic uneven terrain locomotion. The plots of x_{tc} and x_{com} shown in Fig 5.11 demonstrate the robust performance of the coordinated motion of transit foot with respect to the moving CoM location of biped in the presence of terrain perturbation. There is further scope for improving the velocity regulation by optimizing the forward landing offset parameter, λ_h with respect to the terrain-parameters, y_{Go} and σ_G.

[7] Unexpected in the sense that data of y_{Go} and σ_G are known only for the next immediate foot step

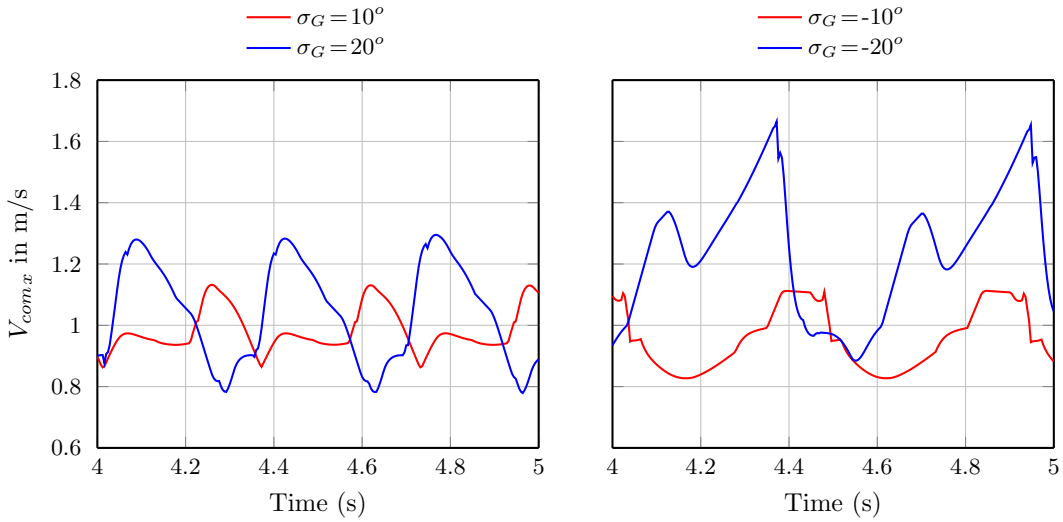

Figure 5.6: Forward velocity of biped-CoM on inclined terrain with different slopes for V_{fc}=1 m/s

5.3.2.2 Robustness with respect to payload mass variation

The objective of second case of perturbation study is to demonstrate the robustness of basic HyDAC law shown in Fig 4.2 like definition C_{SF} flags and $\mathbb{H}^{i}_{es}$ transition conditions, and TLC parameters such as ω_b, ζ and slew rate limits e.t.c. with respect to link mass perturbation. The other functional blocks of HyDAC like, biped-CoM related computation, various nonholonomic constraint models, and inverse dynamics control, all make use of the perturbed actual value of link mass. Normally, once the biped has been physically realized, there is little chance for variation of its link dimensions and mass-inertia values. However, the control algorithm should be robust against parameter variation caused by additional mass of payload, sensors or instrumentation attached to biped depending on its mission. The most common case is the mass perturbation caused by additional payload attached to biped torso.

The set of behaviour primitives represented by (H_t, B_t) as per (4.119) is designed purely on the basis of biped kinematics and are independent of link masses even though, the final control solution, $\ddot{q}^*_d$ given by (4.123) depends on link mass parameters through the terms, H_{c_n}, and B_{c_n}. According to (4.123), the condition for the existence of solution, $\ddot{q}_d$ for realizing (H_t, B_t) is that $\bar{H}_t$ has a minimum rank equal to the number of rows of B_t. As explained in Section 4.8.5, this condition will be satisfied as long as the virtual contact

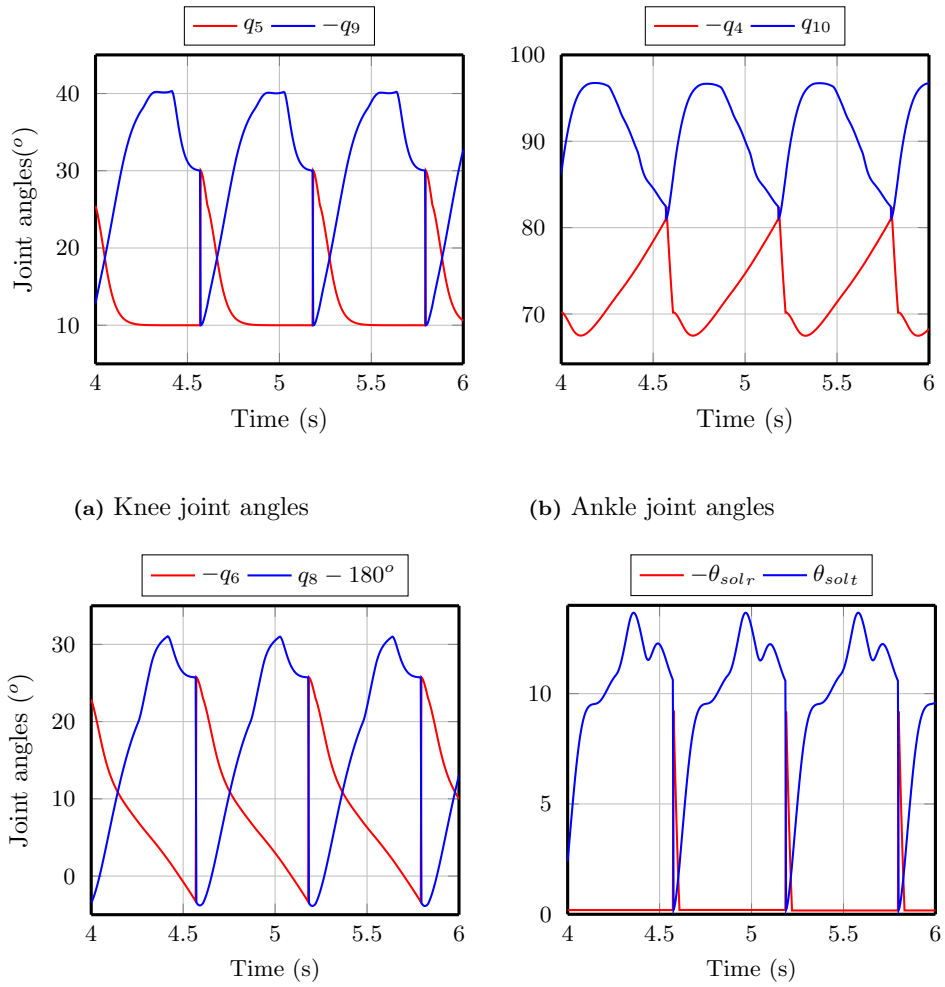

(a) Knee joint angles

(b) Ankle joint angles

(c) Hip joint angles

(d) Foot sole angles

Figure 5.7: Various joint angle profiles of biped while walking with V_{fc}=0.5 m/s over level ground with σ_G=0

force constraints are passive. By proper design of supervisory level control, the virtual contact force constraints can be kept in passive state for a wide range of link mass variation, thereby enabling $\ddot{q}_d$ to dynamically compensate for the mass perturbation effects entering through mass dependent terms of (4.123), provided the task control loops of (H_t, B_t) are fast enough to compensate for the unstable modes of bipedal passive dynamics.[8] Thus the motion control primitives of HyDAC are inherently robust against link mass variation.

[8]The unstable inverted pendulum dynamics of biped is modelled as passive dynamics in (H_{c_n}, B_{c_n}).

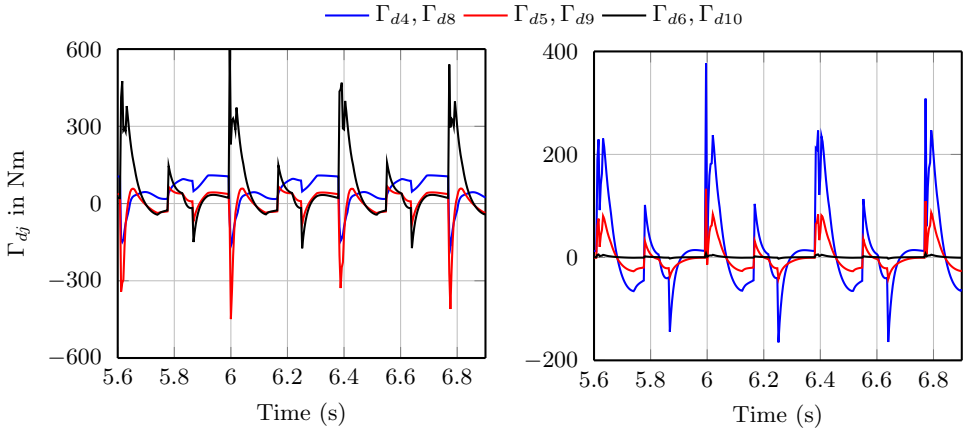

(a) Γ_{dj} for Reference leg and Torso (b) Γ_{dj} for Transit leg

Figure 5.8: Joint torque commands, Γ_{dj} during level ground walk with V_{fc}=1 m/s.

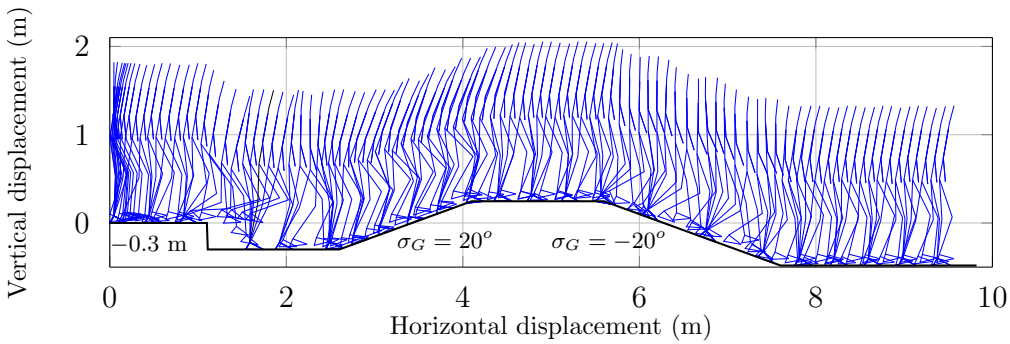

Figure 5.9: Stick diagram sampled @ 0.1 s while biped is commanded with $Vfc = 1\ m/s$ over terrain with step transition of -0.3 m and and slope discontinuity of ± 20 deg

The other parts of HyDAC, namely the nonholonomic constraints (H_{c_n}, B_{c_n}) and the final inverse dynamics control are expressed in terms of mass parameters and hence they are adaptive with respect to known variations of link mass as well as payload mass. The effect of payload mass variation on dynamic walk is studied by increasing the torso mass to the maximum extent possible for different combinations of V_{fc} and σ_G without destabilizing the biped. It is further assumed that the torso-CoM location does not change.[9] The

[9]In practical situation, the additional payload mass can be estimated from the ground contact force

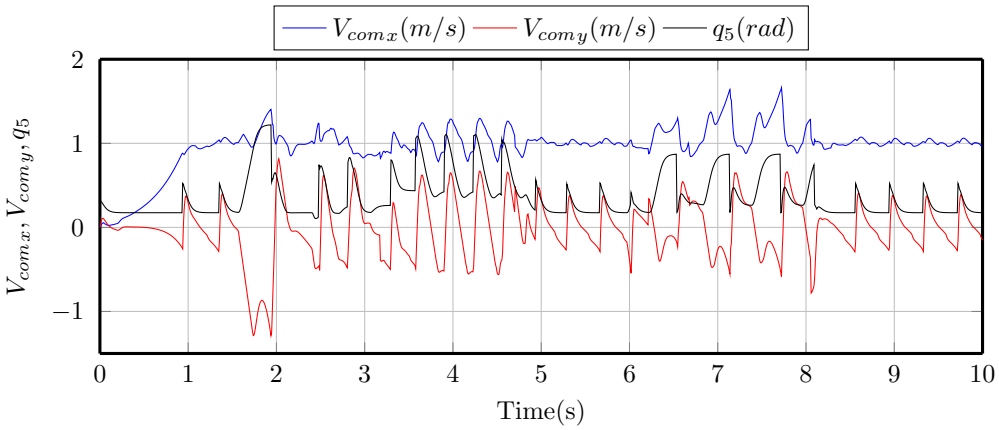

Figure 5.10: Horizontal and vertical components of V_{com} and reference knee joint angle corresponding to the locomotion pattern shown in Fig 5.9

comparison of normal ground contact force, $f_{gry} = f_{grh_y} + f_{grt_y}$ and forward velocity, V_{comx} between the nominal and perturbed cases for $V_{fc} = 1\,m/s, \sigma_G = 0$ is shown in Fig 5.12. Here the torso mass is increased by 300% (i.e by an extra mass of 122 kg for a biped of total nominal mass of 84 kg!) with no shift in torso CoM location. The effect of torso mass increase is to slightly delay the velocity rise and to increase the normal ground reaction force by an equivalent amount corresponding to 122 kg. Even though there is no noticeable change in velocity pattern, the stability of the gait is affected as will be shown in Section 5.3.3. The limits of torso mass perturbation for other walking conditions are given in Table 5.2.

Table 5.2: Upper limit of torso mass increase

V_{fc}	σ_G	Torso Mass increase	Increase in Biped mass
2 m/s	0	50%	24%
1 m/s	0	300%	144 %
1 m/s	-10 deg	200%	96%
1 m/s	10 deg	250%	120%
1 m/s	-20 deg	150%	72%
0.5 m/s	0	450%	217%

measurements in static condition and biped-CoM location can be re-estimated online using efficient algorithms [96].

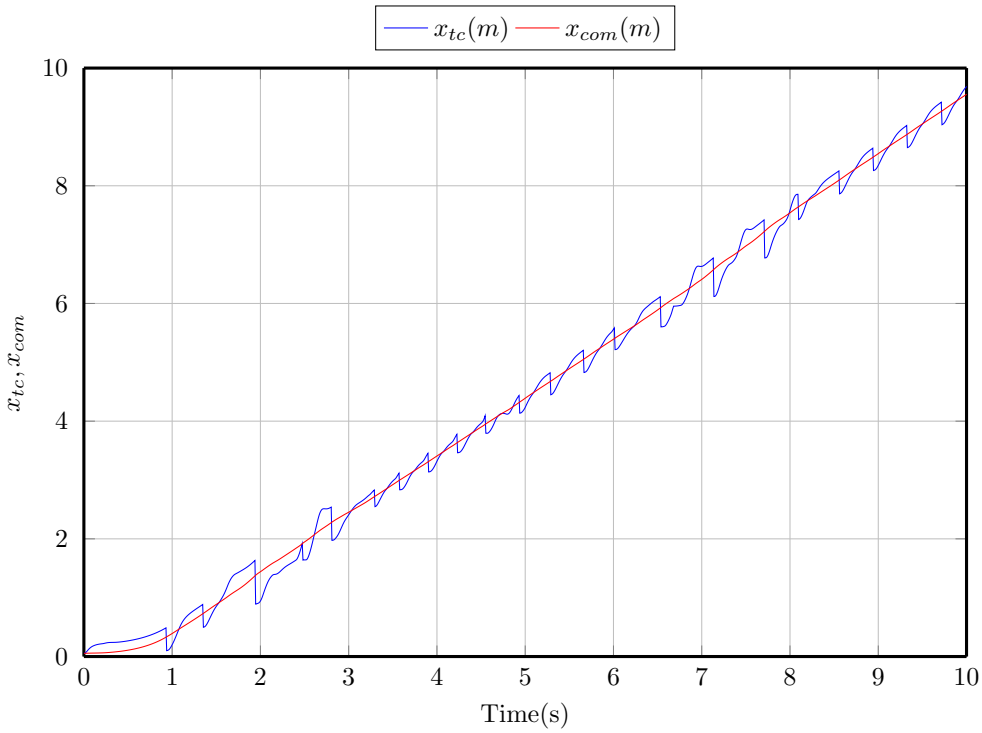

Figure 5.11: Horizontal displacements of biped-CoM and centre of transit foot sole corresponding to the locomotion pattern shown in Fig 5.9

5.3.2.3 Robustness with respect to external torque limit

The HyDAC control law is derived based on the assumption that the actuator attached to each joint realizes the same value of torque as the commanded one, Γ_{dj}. However, being a high power hardware element with its own finite bandwidth and parameter dispersion over the course of operation, there can be difference between the realized joint torque, Γ_{j} and Γ_{dj}. One method is to incorporate the actuator speed-torque limits as nonholonomic constraint in the control algorithm itself as explained in Section 4.5.3. However, constraining the control torque in this fashion will be done only for one or two prominent actuators since such constraints will eat away the available control DoF. Hence it is important to verify the effect of torque limiting external to the control algorithm. As mentioned earlier, all the simulation results presented so far have been taken with external torque limits on lower limb actuators. However to demonstrate the robustness of HyDAC with respect to external torque limiting, additional simulation results are generated as shown in Fig 5.13 for walking

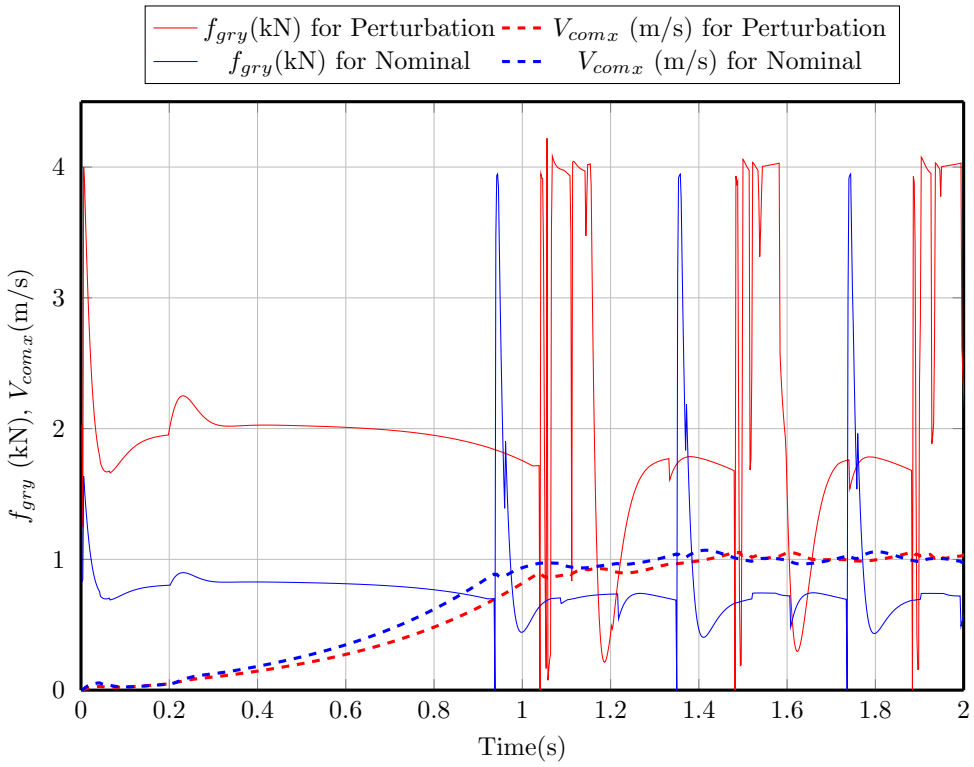

Figure 5.12: Effect of torso mass increase by 300% on bipedal gait with $V_{fc} = 1\,m/s$ and $\sigma_G = 0$

on level terrain with $V_{fc} = 1\,m/s$. Prior to t=3 s, only Γ_{d6} is limited to $\pm$ 600 N-m as a virtual constraint inside the HyDAC routine with no limiting applied to other joint torques. Beyond t=3 s, both the knee joint toques, Γ_5 and Γ_9 are limited to $\pm$200 N-m and thigh joint torque, Γ_8 is limited to $\pm$600 N-m to maintain equivalence with Γ_{d6} , and both the ankle joint torques, Γ_4 and Γ_{10} are limited to $\pm$100 N-m, all executed external to the HyDAC routine. It can be observed from the plot that there is no visible change in the forward velocity and walking pattern of the biped beyond t=3 s due to the external limiting of joint torques. This robustness is attributed to the closed loop structure of TLC which is able to correct for the disparity between the commanded torque by HyDAC controller and realized torque by joint drives during the subsequent control samples.

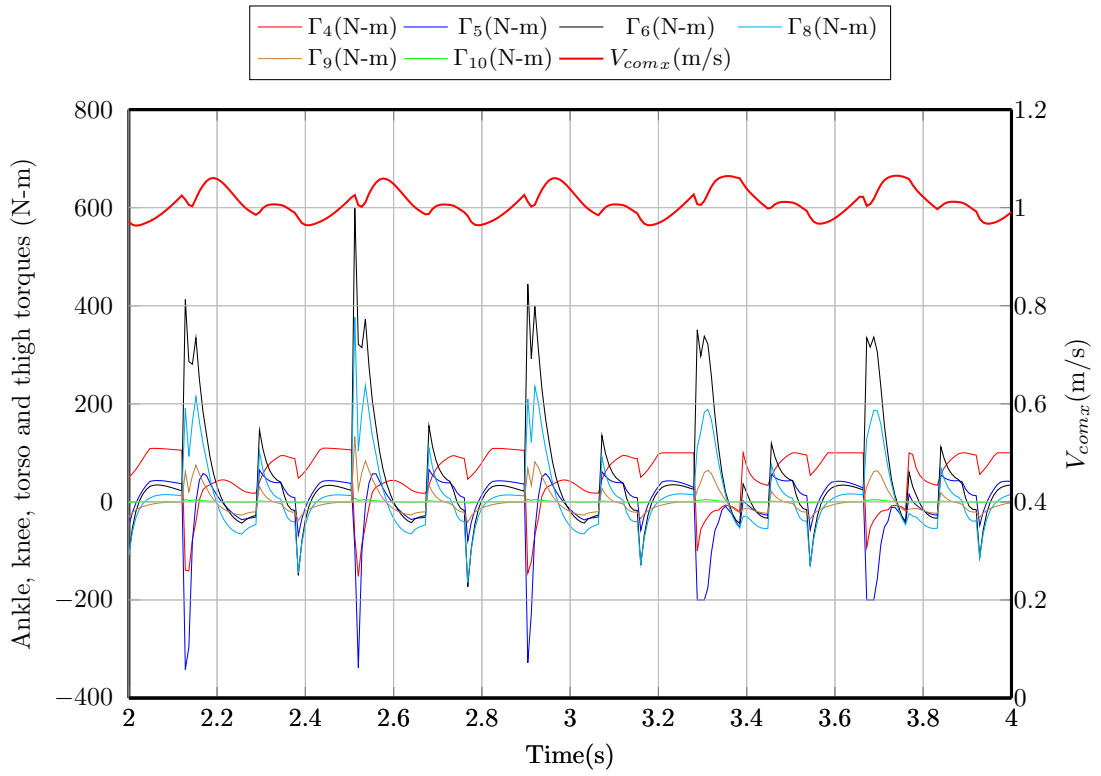

Figure 5.13: Effect of external torque limit on bipedal gait with $V_{fc} = 1\ m/s$ and $\sigma_G = 0$

5.3.2.4 Robustness against external push disturbance

The robustness study with respect to external disturbance is conducted by applying an external disturbance force of 100 N on the neck joint of biped along the forward direction, $-\overrightarrow{O_7Y_7}$ at t=1.6 s for a duration of 0.5 s while the biped is walking over level terrain with $V_{fc} = 1\ m/s$. The disturbance induced transients in the forward velocity and trajectories of x_{com} and x_{cop} are given in Fig 5.14. The forward velocity goes on increasing till the end of forward push and captures back to the regulated state within 1.1 s after the removal of disturbance. It can be observed that the GCoP remains saturated at the support foot toe for four steps to brake out the extra forward velocity build up, thus validating the performance of FVC algorithm. The application of external push force is indicated by an extra line appearing at the neck joint of biped in the attached video. The result truly demonstrates the reflex stability performance of HyDAC against sudden unexpected external disturbance. Similar simulation experiments have been conducted by applying disturbance at hip joint and transit knee joints as well. The stability margins of the perturbed

trajectories are analysed and the results are discussed in the next section.

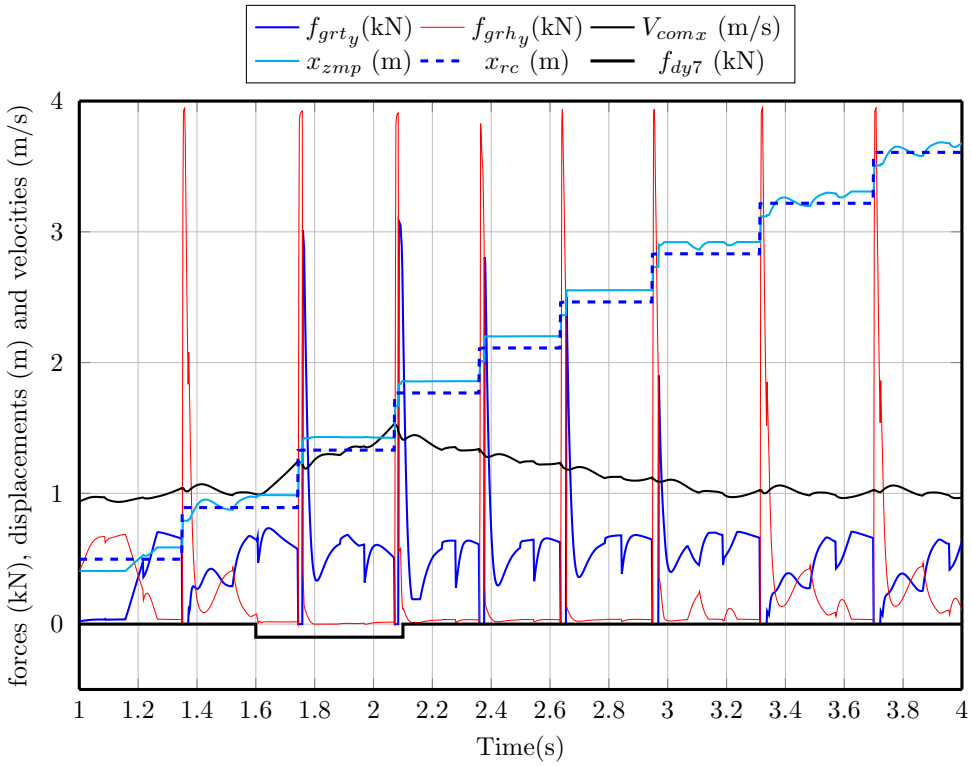

Figure 5.14: Effect of external forward push disturbance of 100 N on neck joint at t=1.6 s for a duration of 0.5 s during level terrain walk with $V_{fc} = 1\,m/s$ and $\sigma_G = 0$

5.3.3 Stability analysis

The robustness of HyDAC under various realistic perturbations have been established in the previous sections using simulation studies. Even though the results illustrate stable dynamic walk for different velocity commands and for different terrain slopes under wide range of perturbing conditions, it will be more meaningful if the explicit stability margins are brought out based on certain standard norms. The contraction factor of contraction stability concept proposed in Section 4.8.4 can be successfully applied to the simulation results to assess the stability margins in different conditions as shown below.

To assess the contraction stability margins for any trajectory of the bipedal walk, it is required to generate a perturbed trajectory close to the original one. Different techniques like perturbing the initial orientations of biped joints, initial perturbation in velocity com-

mand, application of external disturbance force on certain biped joints during the initial phase etc. can be used for generating the perturbed trajectory. We have used the last option, with $f_{dy7} = 1$ N applied along $-\overrightarrow{O_7Y_7}$ direction providing a forward push on the neck joint for a duration of 0.5 s starting at $t = t_0 + 1.6$ s. The distance between the trajectories, δ_{AB} is measured using (4.109). The contraction sequence for planar bipedal walk with $V_{fc} = 1$ m/s over uniform terrain having different slopes, σ_G are generated from the simulation results and plotted in Fig 5.15. The cases with $\sigma_G = 0$ and $\sigma_G = 10$ deg exhibit stable performance with an initial contraction factor of ρ_C =0.25 for $\delta_{AB} > 10^{-3}$ followed by ρ_C =0.68 < 1 during asymptotic contraction . However, the contraction pattern has two alternating local slopes, with one slope even exceeding unity for $\sigma_G = 0$. In fact, the steeper second slope only makes the average slope negative ensuring the asymptotically stable performance. The cause for this is associated with the near biperiodic nature of the gait which is not visible from V_{comx}, but evident from the joint torque plot of Fig 5.13. As discussed in Section 4.8.5, one of the postural configuration state, x_{Pc6} is underactuated and the same is controlled indirectly by its rate, $\dot{x}_{Pc6}$. Hence even if there is sufficient dwell time for perfectly controlling $\dot{x}_{Pc6}$ towards its goal V_{fc}, any initial offset of x_{Pc6} during the current gait will remain till the next impact event, thus affecting the impact velocity map, $\Delta^i(q)$. Thus the underactuated configuration state, $\dot{x}_{Pc6}$ will introduce partially uncontrolled perturbation in impact map which can lead to aperiodic behaviour of the orbits as demonstrated in Section 4.8.4. Moreover, a smaller value of $x_{Pc6}(t_k)$ will result, in general, a larger value for V_{comx} during the initial phase of the following step leading to a larger value of $x_{Pc6}(t_{k+1})$. By the same argument, $x_{Pc6}(t_{k+2})$ will be smaller than $x_{Pc6}(t_{k+1})$ leading to near biperiodic type gait. The extent of orbital dispersion due to a biperiodic orbit can be obtained by plotting the self contraction norm, $\delta^k_{AB} = \| \mathbf{x}_P(t_k) - \mathbf{x}_P(t_{k-1}) \|_2$. Due to the biperiodicity, the perturbed trajectory for the case with $\sigma_G = 10$ deg in Fig 5.15 has become out of phase with the nominal one and hence we had to redefine the contraction norm as $\delta^k_{AB} = \| \mathbf{x}_{PA}(t_k) - \mathbf{x}_{PB}(t_{k-1}) \|_2$ which is indicated in the plot-legend by $\delta k = 1$. Only problem with this offset, $\delta k = 1$ is that δ^k_{AB} will start from a large initial value due to large initial difference between the alternate samples of perturbed trajectories. The bipedal gaits with $V_{fc} = 1$ m/s and $\sigma_G = \pm 20$ deg do not have asymptotic contraction as expected, but they are event periodically stable (EPS) with a radius of convergence, $\mathcal{R}_C$=0.325. They are truly the two boundary performance cases with respect to terrain slope for V_{fc}=1 for the current controller parameter values of HyDAC. The bipedal gait for $\sigma_G = 10$ deg has better stability with smaller value of $\mathcal{R}_C$=0.025 even though it is not asymptotically contracting.

The stability of bipedal gaits on level terrain for different forward velocities and also

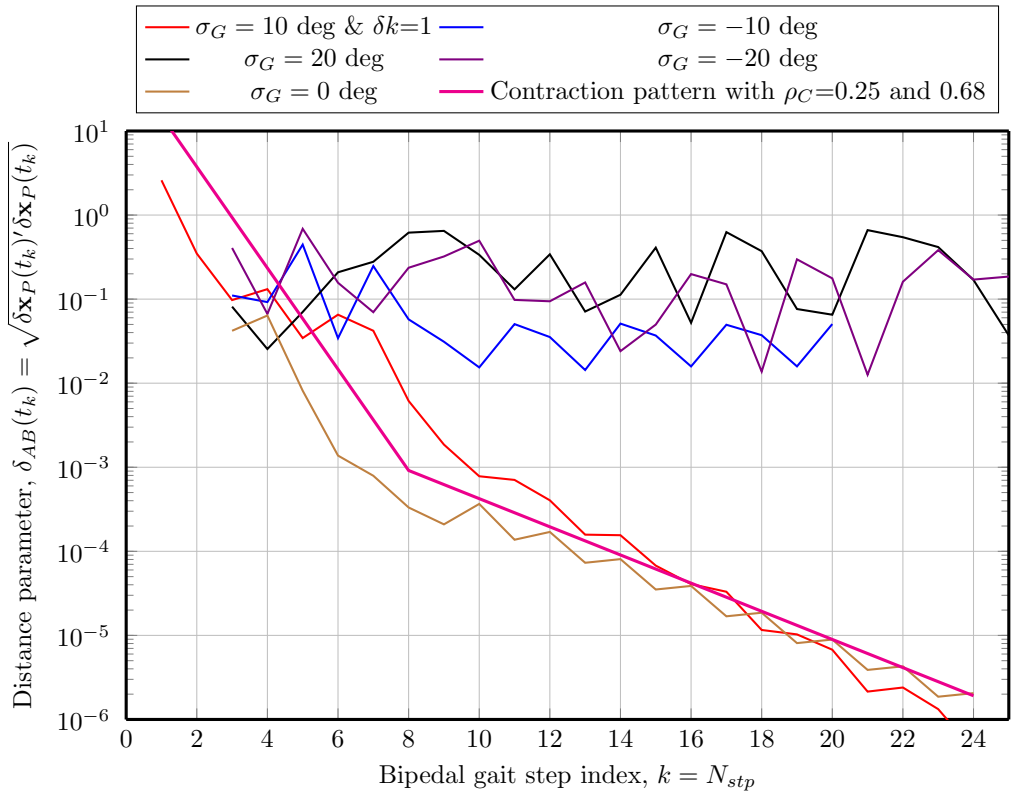

Figure 5.15: Contraction sequence for planar bipedal walk with V_{fc}=1 m/s over uniform terrain with different slopes, σ_G

for some perturbation cases are shown in Fig 5.16. A combined contraction pattern for ρ_C=0.25 during the initial phase followed by ρ_C=0.68 is used as a common reference for comparing across Fig 5.15 - Fig 5.17. The best stability performance is for the gait corresponding to $V_{fc} = 1.5\,m/s$ and σ_G=0 deg having the asymptotic contraction with $\rho_C = 0.35$. It can be seen that the contraction pattern is uniform without any biperiodic behaviour for the orbit, leading to a larger contraction rate compared to that for $V_{fc} = 1$ m/s. This can be a special case for the present controller parameters where regulation of $\dot{x}_{Pc6}$ provides accurate regulation of x_{Pc6} as well. The case for $V_{fc} = 1\,m/s$, F_{dy7}=-100 N corresponds to a disturbed trajectory generated by an external disturbance force of $|F_{dy7}|$ =100 N in the forward direction, $-\overrightarrow{O_7Y_7}$ on the neck joint, O_7 at t = t_0+1.6 s for a duration of 0.5 s. The additional small perturbation for the trajectory with respect to the previous one is generated by applying F_{dy7} =-101 N instead of -100 N. Due to the out of phase behaviour between the two biperiodic trajectories, we had to use an offset of $\delta k = 1$ as indicated

which results in large initial value for $\delta_{AB}(t_k)$ as seen from the plot. However, the initial contraction pattern for $\delta_{AB} > 10^{-3}$ and subsequent asymptotic contraction pattern remain almost similar to the nominal case. Thus the contraction property as well as the final orbit remain the same for a larger domain of attraction, $\mathcal{S}_{SP}^{Cu}$. The gaits for $V_{fc} = 2$ m/s and for the extreme perturbed case with torso mass increased by 300% along with $V_{fc} = 1$ m/s do not possess the asymptotic contraction as can be seen from the plot as they correspond to performance limit cases. However, the gaits possess EPS with $\mathcal{R}_C$=0.5. The cases with lower velocity commands, $V_{fc} = 0.5$ m/s and 0.25 m/s are also not showing asymptotic contraction due to the underactuated postural state x_{Pc6}, but with sufficiently small value of $\mathcal{R}_C = 0.5 \times 10^{-2}$ and 0.5×10^{-4} respectively. Hence the orbits can be taken as periodic in all practical respects. The contraction behaviour for level terrain walk with $V_{fc} = 1$ m/s

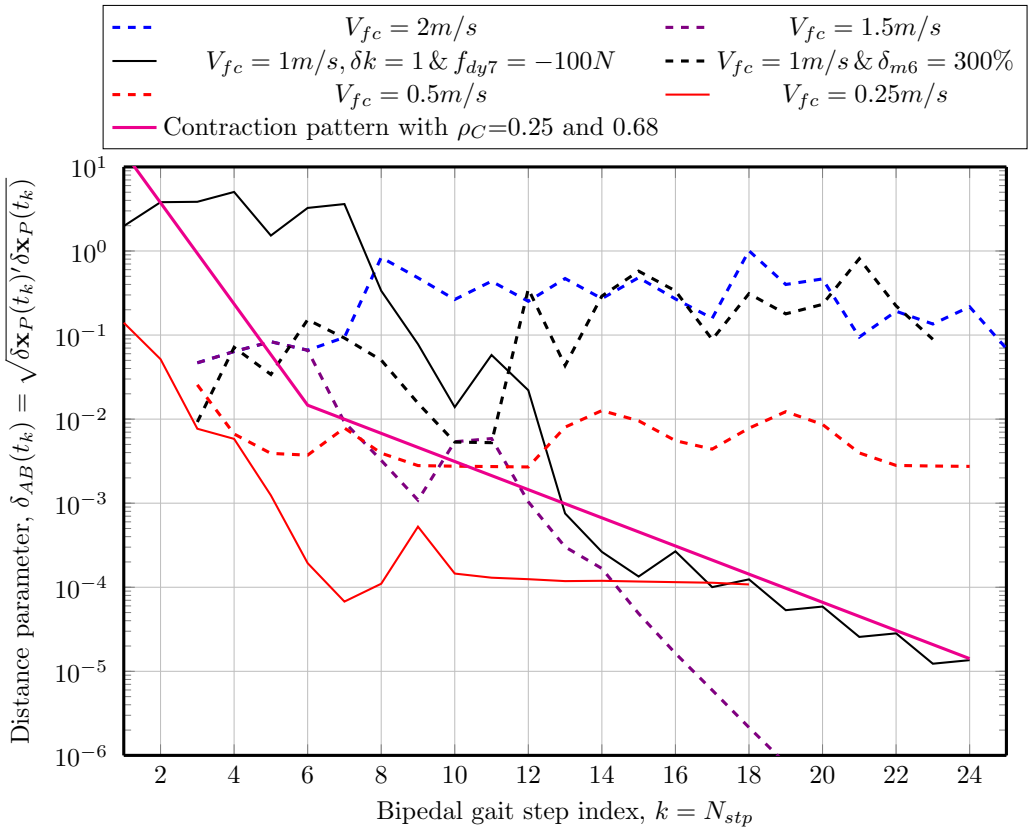

Figure 5.16: Contraction sequence for planar bipedal walk over level terrain with different velocities, external disturbance and link mass perturbation

for large initial perturbation between the trajectories A and B are plotted in Fig 5.17. The general observation is that the initial few values of $\delta_{AB}(t_k)$ are large due to large devia-

tion between the trajectories and they quickly die down with an initial contraction factor of $\rho_C = 0.25$ until $\delta_{AB}(t_k) < 10^{-3}$. Thereafter all the trajectories converge with an asymptotic contraction rate of $\rho_C = 0.68$. This once gain proves the robustness of the gait with large perturbation due to either external disturbance or due to dispersion in initial joint angle.

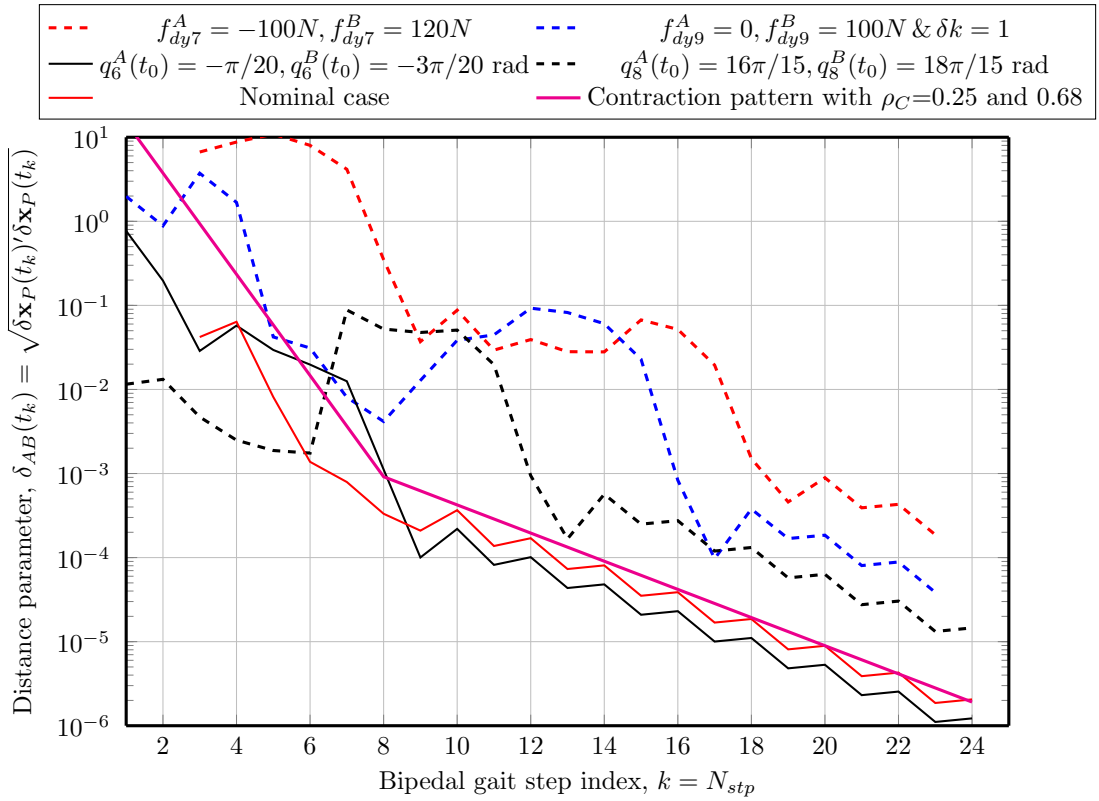

Figure 5.17: Contraction sequence for planar bipedal walk over level terrain with $V_{fc} =$ 1 m/s, under large relative perturbation cases

5.4 Chapter Summary

The behaviour primitives required for planar bipedal locomotion over uniform terrain were developed in this chapter. The set of behaviour primitives was grouped into four categories and the analytic formulation of each behaviour was provided. This was followed by detailed simulation study using full order dynamic model of 12-link planar biped, implemented in MATLAB. The agility of HyDAC for uniform terrain walk was established by driving the

biped for a velocity command range of 0.1 m/s to 2 m/s over level terrain and driving over a slope range of ± 20 deg for velocities up to 1 m/s. The robustness of HyDAC against unexpected terrain uncertainties and against significant payload mass increase were studied in detail. The reflex stability behaviour of HyDAC was demonstrated by the disturbance rejection response to external forward push. The contraction stability margins for different walking experiments were also derived. The video links are provided for each simulation experiments and they demonstrate the versatility of HyDAC for bipedal waking control. The *kinematically-driven dynamically-constrained architecture* of HyDAC built-up over a well coordinated framework of kinematic type behaviour feedback loops with embedded forward velocity regulation provides the high robustness for bipedal walk against perturbation elements like payload mass variation[10], external disturbance, joint torque limits etc. as demonstrated through simulation.

[10]It is assumed that the value of payload mass and its CoM location are known to the control algorithm for using in nonholonomic virtual constraints as well as in the final inverse dynamics control computation.

Chapter 6

Stair-HyDAC for Bipedal Dynamic walk over Non-uniform Stairs

6.1 Introduction

This chapter deals with the extension of HyDAC developed for planar bipedal locomotion to dynamic walking situation over randomly sloped ascending and descending stairs with non-uniform tread depth and riser height. HyDAC law is modified in both task level and supervisory level to meet these demands. Dynamic walking over non-uniform stairs requires to control the swing foot placement at predetermined feasible foothold on each toe-impact event in addition to forward velocity regulation.

To the best of author's knowledge, successful bipedal locomotion control over updown stairs employing actuated ankle has been reported in the literature only by using ZMP control approach [97]. However many such control algorithms have realized only slow walking in practice. In [97], the authors have demonstrated ZMP based dynamic stair-walking on HUBO humanoid which takes 2 s per step. They use a controller structure which employs a feedforward control based on a priori generated walking pattern along with a closed loop balance control. When compared with uniform terrain walking, the larger relative velocity of swing leg with respect to the biped-CoM during stair-walk induces higher inertial disturbance. The resulting larger uncertainty in ZMP trajectory will impose practical limitations for this approach when applied for higher speeds as well as for larger stair dimensions. Moreover, the dependability on pre-planned ZMP trajectory makes this approach not suitable for locomotion over non-uniform stairs. HZD based control also has been extended for staircase bipedal locomotion. However, there are two practical difficulties when the same is to be applied to locomotion over non-uniform stairs. The primary issue is related to the convergence of the optimal solver to a feasible gait for stair-walking and the second

is related to the robustness of control algorithm with respect to the unaccounted stairway dispersions. These issues are addressed by the team of A.D.Ames [98, 34, 99, 100]. Their approach is based on the argument that the human locomotion behaviours can be expressed in terms of three basic algebraic type kinematic functions called, extended canonical human functions (ECHF) corresponding to walking on flat ground, upstairs and down stairs and in terms of four transition modes corresponding to the transition between the above motion patterns [98, 34]. However building task level control (TLC) based on motion control primitives of differential dynamic form is much superior compared to building over pure algebraic type motion control primitives, as explained in Section 4.4.1.

The rest of the chapter starts with the mathematical representation of generic uneven terrain having non-uniform stair type profile. This is followed by definition of modified postural configuration state for stair-walk to take care of the change in ground impact point on transit foot. Then the modifications required in SLC and TLC of HyDAC are described. Finally, the stability margins and robustness of the modified HyDAC for non-uniform stair-walk are demonstrated based on multiple simulation studies conducted using the mathematical model.

6.2 Representation of Non-uniform stairs

The scope of current work on non-uniform terrain locomotion is limited to terrain represented by flights of stairs connected by uniform terrain. The stairs can have random values for tread depth, tread slope and riser height subject to the condition stated in Assumption 6.1. The terrain surface is assumed to be rigid with a dry friction coefficient of $\mu_c = 0.8$ for the purpose of simulation.

Assumption 6.1. *The terrain is assumed to have flat foothold locations within the reachable span of every bipedal foot step.*

Assumption 6.2. *$\mathcal{CFR}$-S1: The control algorithm is assumed to have the capability to place the transit foot on the specified foothold without touching on the convex projections of stairs between the adjacent steps.*

The statements of Remark 3.1 are applicable in the context of Assumption 6.1 for staircase locomotion.

The formulation of HyDAC given in Chapter 5 for uniform terrain dynamic walk is able to take care of moderate ground discontinuities in terms of σ_G and vertical offset y_{Go} if their values are below certain levels or if there is sufficient separation between

consecutive discontinuities. However, if such ground discontinuities repeat prior to the settling of transients emanating from the previous one, the HyDAC algorithm designed for uniform terrain conditions will fail to provide sustained walking. Under such situations, the terrain will be treated as non-uniform and a different strategy has to be adopted for control [80].

The portion of the terrain where there exists at least two sufficiently close discontinuities in terms of either y_{Go} or σ_G or both is treated as a flight of stairs and is represented as a series of line segments as shown in Fig 6.1. There are N_i segments for the i^{th} flight of

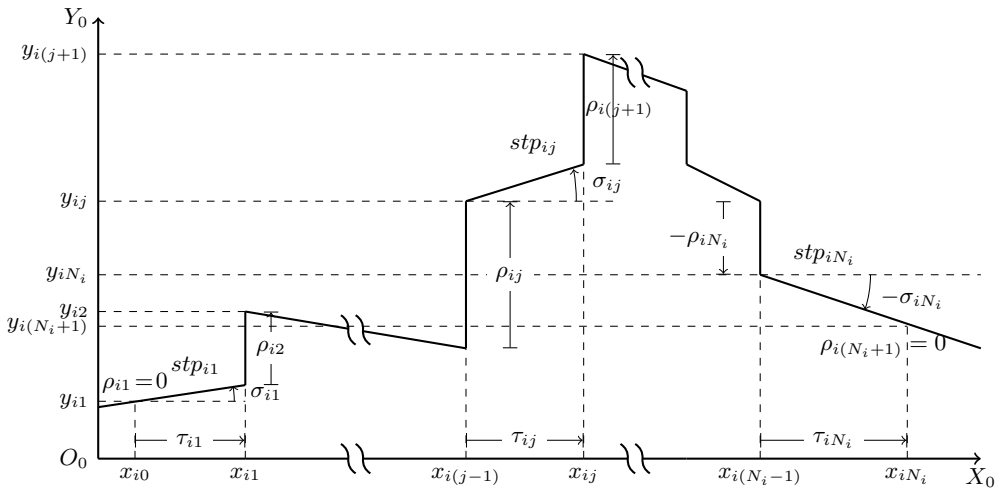

Figure 6.1: Representation of i^{th} flight of stairs

stairs shown in Fig 6.1 with the first segment denoted by stp_{i1} and the last segment denoted by stp_{iN_i}. It is assumed that each step-tread has a minimum depth of $1.5L_f$ so that it can comfortably provide footholds during dynamic walking. There are three parameters for each step, stp_{ij} of stairs, namely tread depth (τ_{ij}), riser height (ρ_{ij}) and tread slope (σ_{ij}) with 'i' representing the stair-flight index and 'j' representing the step index. The (x, y) coordinates of all the points considered in this chapter are represented with respect to the inertial frame, $\{O_0X_0Y_0Z_0\}$ and slopes are measured as CCW rotation with respect to $\overrightarrow{O_0X_0}$ axis. The j^{th} step of i^{th} flight of stairs starts at the point $(x_{i(j-1)}, y_{ij})$ and extends up to $x = x_{ij}$ with a slope of σ_{ij}. Based on Fig 6.1, the relation between the stair-parameters can

be derived as,

$$\tau_{ij} = x_{ij} - x_{i(j-1)} \quad \forall j \in [1, N_i] \tag{6.1}$$

$$\rho_{ij} = y_{ij} - \left(y_{i(j-1)} + \tau_{i(j-1)} \tan \sigma_{i(j-1)}\right) \quad \forall j \in [2, N_{i+1}] \tag{6.2}$$

$$y_G(x_t) = y_{ij} + (x_t - x_{i(j-1)}) \tan \sigma_{ij} \tag{6.3}$$
$$\forall\, x_{i(j-1)} \leqslant x_t \leqslant x_{ij} \text{ and } \forall j \in [1, N_i]$$

The coordinate assignment to various biped joints while standing on j^{th} step of i^{th} stair-flight, represented by stp_{ij}, is shown in Fig 6.2 following the scheme given in Fig. 3.1. For $x_{(i-1)N_{i-1}} \leqslant x_t < x_{i0}$ and $x_{iN_i} \leqslant x_t < x_{(i+1)0}$, the terrain is treated as a part of uniform terrain, where the locomotion is controlled by normal HyDAC. For the sake of easy reference, we would like to name the HyDAC proposed for dynamic walking over non-uniform stairs as, "Stair-HyDAC" to distinguish it from "Normal-HyDAC" developed for dynamic walking over uniform terrain. Stair-HyDAC is designed to take care of different types of staircase patterns with the assumption of vertical rise between steps. Let us classify stp_{ij} as an *ascending step* denoted by, $\mathcal{A}_{ij}$ if $\rho_{i(j+1)} > 0.1L_f$[1]. Similarly, stp_{ij} is classified as a *descending step* or *level step* denoted by symbols, $\mathcal{D}_{ij}$ or $\mathcal{L}_{ij}$ respectively if $\rho_{i(j+1)} < -0.1L_f$ or $|\rho_{i(j+1)}| \leqslant 0.1L_f$. Assuming that the biped is standing on stp_{ij} with its reference foot, the rules for fixing the desired landing location, (x^o_{Lt}, y^o_{Lt}) for transit foot toe for different cases of staircase patterns are given below:

$$\text{Rule-1: } \{\mathcal{A}_{ij}\mathcal{A}_{i(j+1)},\ \mathcal{A}_{ij}\mathcal{L}_{i(j+1)},\ \mathcal{L}_{ij}\mathcal{A}_{i(j+1)},\ \mathcal{A}_{i(j-1)}\mathcal{L}_{ij}\}$$
$$\implies x^o_{Lt} = x_{ij} + 1.25L_f \tag{6.4}$$

$$\text{Rule-2: } \{\mathcal{D}_{ij}\mathcal{D}_{i(j+1)},\ \mathcal{D}_{ij}\mathcal{L}_{i(j+1)},\ \mathcal{L}_{ij}\mathcal{D}_{i(j+1)},\ \mathcal{D}_{i(j-1)}\mathcal{L}_{ij}\}$$
$$\implies x^o_{Lt} = x_{i(j+1)} - 0.25\max(L_f, |\rho_{i(j+1)}|) \tag{6.5}$$

$$\text{Rule-3: } \{\mathcal{A}_{ij}\mathcal{D}_{i(j+1)},\ \mathcal{D}_{ij}\mathcal{A}_{i(j+1)},\ \mathcal{L}_{ij}\mathcal{L}_{i(j+1)},\ \mathcal{L}_{i(j-1)}\mathcal{L}_{ij}\}$$
$$\implies x^o_{Lt} = x_{ij} + 0.5\tau_{i(j+1)} + 0.5L_f \tag{6.6}$$

The first three terms on the R.H.S. of the above rules are to be considered only for $1 \leqslant j \leqslant N_i - 1$ and the fourth term is applicable only for $j = N_i$. The corresponding desired

[1]Terrain perturbation within $|0.1L_f|$ can be taken care by Normal-HyDAC.

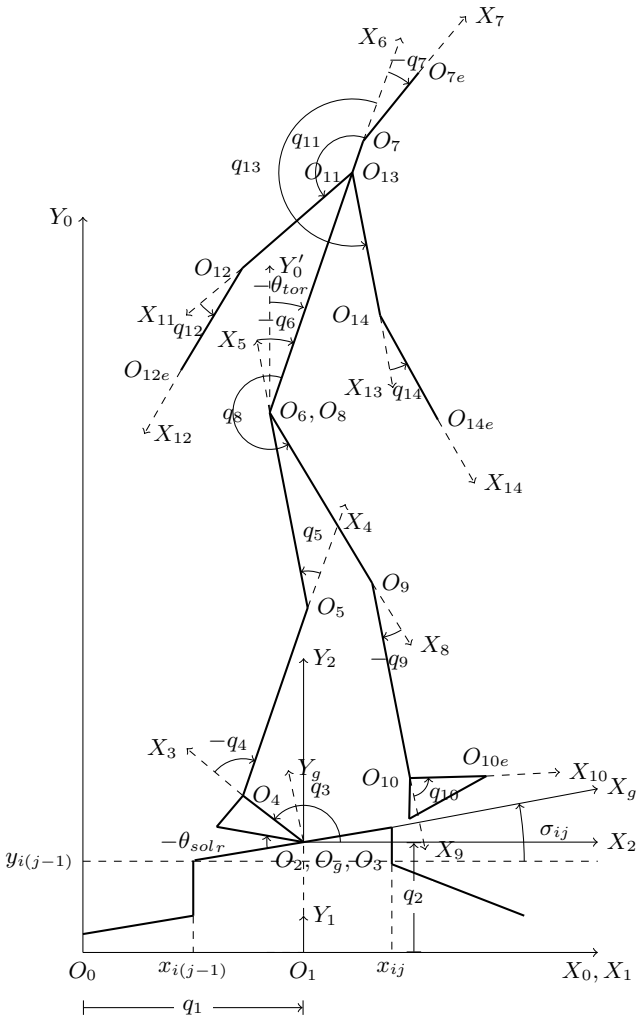

Figure 6.2: Planar biped walking over $\mathtt{stp}_{\mathtt{ij}}$ and its joint coordinate assignment

contact location, $(\mathtt{x}^{\mathtt{o}}_{\mathtt{Lh}}, \mathtt{y}^{\mathtt{o}}_{\mathtt{Lh}})$ for transit foot heel can be given as,

$$\mathtt{x}^{\mathtt{o}}_{\mathtt{Lh}} = \mathtt{x}^{\mathtt{o}}_{\mathtt{Lt}} - \mathtt{L_f} \cos \sigma_{\mathtt{i(j+1)}} \tag{6.7}$$

$$\mathtt{y}^{\mathtt{o}}_{\mathtt{Lh}} = \mathtt{y}_{\mathtt{i(j+1)}} + (\mathtt{x}^{\mathtt{o}}_{\mathtt{Lh}} - \mathtt{x}_{\mathtt{ij}}) \tan \sigma_{\mathtt{i(j+1)}} \tag{6.8}$$

Rule-1 ensures a rear offset of $0.25\mathtt{L_f}$ between $\mathtt{x}^{\mathtt{o}}_{\mathtt{Lh}}$ and rear step boundary and Rule-2 ensures a front offset of $0.25\max(\mathtt{L_f}, |\rho_{\mathtt{i(j+1)}}|)$ between $\mathtt{x}^{\mathtt{o}}_{\mathtt{Lt}}$ and front step boundary. Rule-3 ensures that the target for impact foot centre, $\mathtt{x}^{\mathtt{o}}_{\mathtt{Lc}}$ coincides with the centre of $\mathtt{stp}_{\mathtt{i(j+1)}}$. The

control transition from Normal-HyDAC to Stair-HyDAC takes place on transit foot ground impact if $x_{tt}^{-} > x_{i0}$ and the reverse transition takes place if $x_{tt}^{-} > x_{iN_i}$. In uniform terrain locomotion, the required ground clearance for the transit foot is ensured by a dedicated position regulation loop based on the sensed data of ground profile beneath the transit foot sole. However, in the presence of sudden vertical ground discontinuities as in stairs, such an approach will lead to sudden transients for dynamic walking limiting the forward velocity. The right approach is to drive the transit foot over a smooth envelope over the staircase region between the lift-off and landing positions of the transit foot for the current walking step. There are different choices for shaping such ground envelopes. The present work makes use of a 3-segment linear ground envelope as it ensures minimum slope for the envelope and also due to its analytical simplicity. The expression for the linear envelope segments for different patterns of stairs and the terminal points for each such segment are derived below.

6.2.1 Envelope for ascending stairs

While the biped is climbing over the i^{th} flight of stairs having continuous ascending steps with its reference foot supported on stp_{ij}; $j > 1$, riser heights for the current step and subsequent step will be positive with $\rho_{ij} > 0$ and $\rho_{i(j+1)} > 0$ as shown in Fig 6.3. However, on the first step of ascending stairs with, $j = 1$, the value of ρ_{ij} will be zero as defined in Fig 6.1. Let us consider the case with $j > 1$.

In dynamic human walk over stairs, each walking step is terminated by a toe strike event on ground since it provides better forward velocity control compared to heel strike which will be explained later in Section 6.3.1. This is achieved by keeping transit foot sole orientation, θ_{solt} negative towards the end of its swing motion. As a result, in ascending stair-walking, the point on the transit foot sole having the maximum proximity to staircase boundaries will be its toe tip. Hence the ground envelope is to be defined with respect to the swing path of transit foot toe. Let us represent the coordinates of transit toe at the lift-off instant by $A_1(x_{ge_0}, y_{ge_0})$ which is a point on $stp_{i(j-1)}$ and the desired location for toe strike by $B_3(x_{Lt}^{o}, y_{Lt}^{o})$, a point on $stp_{i(j+1)}$. If there exists a single line segment between these points, the same can be taken as the ground envelope. However in normal stairs, this direct path will be intersecting with the intermediate staircase corners as shown in Fig 6.3. Instead of finding all such protrusion points at a time, we follow a sequential method of finding one after another starting from the transit foot lift-off position. The first protrusion point, P_1 is obtained by finding the location, (x_{gp_1}, y_{gp_1}) on the stairs which maximises

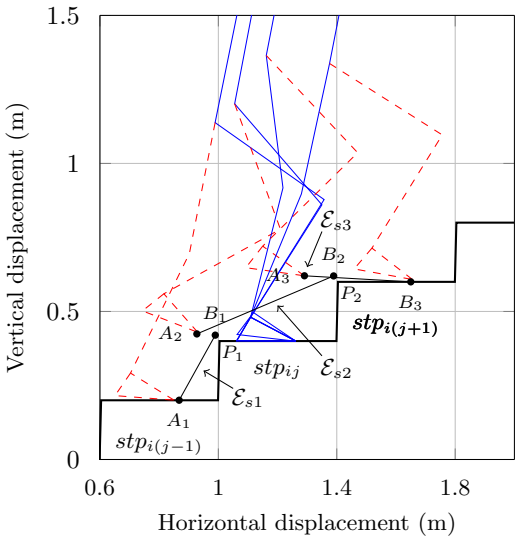

Figure 6.3: Linear envelope segments for ascending stairs

the slope, σ_{p_1} given by

$$\sigma_{p_1}(x_{tt}) = \frac{y_G(x_{tt}) - (y_{ge_0} + \epsilon)}{(x_{tt} - x_{ge_0})} \tag{6.9}$$

over the entire span of transit toe swing, $x_{ge_0} \leqslant x_{tt} \leqslant x^o_{Lt}$. A small positive real number, $\epsilon = 0.05L_f$ is added to y_{ge_0} to avoid misleading values of σ_{p_1} for x_{tt} values on $stp_{i(j-1)}$ if y_{ge_0} is slightly below the stair-step level due to numerical computational inaccuracy. If there are multiple points, take the point with minimum value of x_{tt} as the protrusion point. The terminal point, B_1 of the first segment of ground envelope is selected at an offset of $(-\delta x_o, \delta y_o)$ with respect to the protrusion point, P_1 which is given by,

$$(x_{g_1}, y_{g_1}) = \left(x_{gp_1} - \delta x_o,\ y_{gp_1} + \delta y_o\right) \tag{6.10}$$

A reasonable value for the offsets are $\delta x_o = \max(0.05L_f, 0.035\tau_{ij})$ and δy_o= $\max\left(0.1L_f, 0.07\max(|\rho_{ij}|, |\rho_{i(j+1)}|)\right)$ to ensure adequate turn-around clearance at the staircase corners. Thus the first segment ($\mathcal{E}_{s1}$) of the staircase envelope is represented by the line segment between $A_1(x_{ge_0}, y_{ge_0})$ and $B_1(x_{g_1}, y_{g_1})$ and is having a slope of,

$$\sigma_{ge_1} = \tan^{-1} \frac{y_{g_1} - y_{ge_0}}{x_{g_1} - x_{ge_0}} \tag{6.11}$$

$\mathcal{E}_{s1}$ will serve as the effective ground profile for the motion of transit foot until $y_{tt} > y_{g_1}$. The ground clearance primitive will ensure the specified clearance between transit toe and $\mathcal{E}_{s1}$. Let us represent the position of transit toe at the terminal condition of $\mathcal{E}_{s1}$-zone by $A_2(x_{ge_1}, y_{ge_1})$. The procedure is repeated for the next segment of ground envelope. The second protrusion point, P_2 is obtained by finding the location, (x_{gp_2}, y_{gp_2}) on the stairs which maximises the slope, σ_{p_2} given by

$$\sigma_{p_2}(x_{tt}) = \frac{y_G(x_{tt}) - y_{ge_1}}{(x_{tt} - x_{ge_1})} \tag{6.12}$$

over the remaining span of transit toe swing, $x_{ge_1} \leqslant x_{tt} \leqslant x^o_{Lt}$. If there are multiple points, take the point with minimum value of x_{tt} as the protrusion point. The terminal point, B_2 of the second segment of ground envelope is selected at an offset of $(-\delta x_o, \delta y_o)$ with respect to the protrusion point, P_2 and is given by,

$$(x_{g_2}, y_{g_2}) = \Big(x_{gp_2} - \delta x_o,\ y_{gp_2} + \delta y_o\Big) \tag{6.13}$$

Thus the second segment ($\mathcal{E}_{s2}$) of the staircase envelope is represented by the line segment between $A_2(x_{ge_1}, y_{ge_1})$ and $B_2(x_{g_2}, y_{g_2})$ and is having a slope of,

$$\sigma_{ge_2} = \tan^{-1} \frac{y_{g_2} - y_{ge_1}}{x_{g_2} - x_{ge_1}} \tag{6.14}$$

$\mathcal{E}_{s2}$ will serve as the effective ground profile for the motion of transit foot until $y_{tt} > y_{g_2}$. Let us represent the position of transit toe at the terminal condition of $\mathcal{E}_{s2}$-zone by $A_3(x_{ge_2}, y_{ge_2})$. The third segment of ground envelope, $\mathcal{E}_{s3}$ is obtained directly by joining the point, $A_3(x_{ge_2}, y_{ge_2})$ and the specified landing location, $B_3(x^o_{Lt}, y^o_{Lt})$.

In the case of the first step of ascending stairs with the reference foot supported on stp_{i1}, there will be only two segments for the ground envelope equivalent to $\mathcal{E}_{s1}$ and $\mathcal{E}_{s3}$ of the normal case, as there exists only one protrusion point.

6.2.2 Envelope for descending stairs

While the biped is walking down over the i^{th} flight of stairs having continuous descending steps with its reference foot supported on stp_{ij}; $j > 1$, riser heights for both of the current and subsequent steps will be negative with $\rho_{ij} < 0$ and $\rho_{i(j+1)} \leqslant 0$ as shown in Fig 6.4. However, on the first step of descending stairs with, $j = 1$, the value of ρ_{ij} will be zero as defined in Fig 6.1. Let us consider the case with $j > 1$.

In descending stair-walking, the point on the transit foot sole having the minimum ground clearance with staircase boundaries is not its toe tip as in ascending stairs. While the transit foot is drooping down, the transit foot heel will have the minimum ground clearance except towards landing instant with toe strike. Hence the ground envelope for descending stairs is defined with respect to the swing path of transit foot heel. Let us represent the coordinates of transit foot heel at the lift-off instant by $A_1(x_{ge_0}, y_{ge_0})$ which is on or above over $stp_{i(j-1)}$ as shown in Fig 6.4. The x-coordinate of transit heel when the transit toe

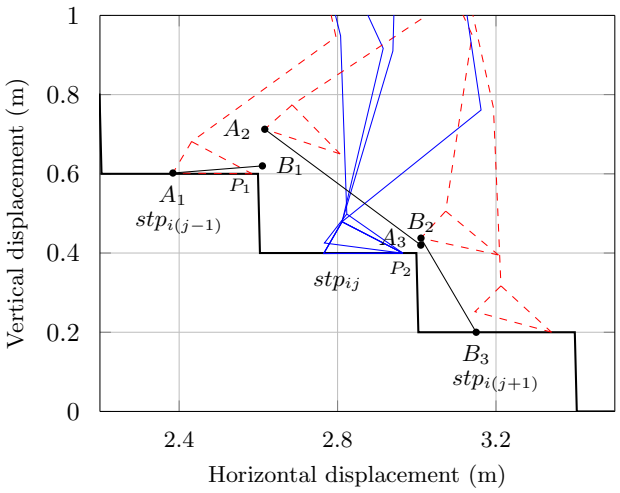

Figure 6.4: Linear envelope segments for descending stairs

strikes at x^o_{Lt} can be derived as $x^o_{Lh} = x^o_{Lt} - L_f \cos(\sigma_{i(j+1)} + \theta_{solt})$. As in ascending case, the first protrusion point, P_1 is obtained by finding the location, (x_{gp_1}, y_{gp_1}) on the stairs which maximises the slope, σ_{p_1} given by

$$\sigma_{p_1}(x_{th}) = \frac{y_G(x_{th}) - (y_{ge_0} + \epsilon)}{(x_{th} - x_{ge_0})} \tag{6.15}$$

over the entire span of transit heel swing, $x_{ge_0} \leqslant x_{th} \leqslant x^o_{Lh}$. If there are multiple points, select the point with minimum value of x_{th} as the protrusion point. The terminal point, B_1 of the first segment of ground envelope is selected at an offset of $(\delta x_o, \delta y_o)$ with respect

to the protrusion point, P_1 and is given by,

$$(x_{g_1}, y_{g_1}) = \Big(x_{gp_1}+\delta x_o,\, y_{gp_1}+\delta y_o\Big) \tag{6.16}$$

Thus the first segment ($\mathcal{E}_{s1}$) of the staircase envelope is represented by the line segment between $A_1(x_{ge_0}, y_{ge_0})$ and $B_1(x_{g_1}, y_{g_1})$ and is having a slope of,

$$\sigma_{ge_1} = \tan^{-1}\frac{y_{g_1} - y_{ge_0}}{x_{g_1} - x_{ge_0}} \tag{6.17}$$

$\mathcal{E}_{s1}$ will serve as the effective ground profile for the motion of transit foot until $y_{tt} > y_{g_1}$ if $\sigma_{ge_1} > 0$ or until $x_{th} > x_{g_1}$ if $\sigma_{ge_1} \leqslant 0$. Let us represent the position of transit heel at the terminal condition of $\mathcal{E}_{s1}$-zone by $A_2(x_{ge_1}, y_{ge_1})$. The procedure is repeated for the next segment of ground envelope. The second protrusion point, P_2 is obtained by finding the location, (x_{gp_2}, y_{gp_2}) on the stairs which maximises the slope, σ_{p_2} given by

$$\sigma_{p_2}(x_{th}) = \frac{y_G(x_{th}) - y_{ge_1}}{(x_{th} - x_{ge_1})} \tag{6.18}$$

over the remaining span of transit heel swing, $x_{ge_1} \leqslant x_{th} \leqslant x^o_{Lh}$. If there are multiple points, take the point with minimum value of x_{th} as the protrusion point. The terminal point, B_2 of the second segment of ground envelope is selected at an offset of $(\delta x_o, \delta y_o)$ with respect to the protrusion point, P_2 and is given by,

$$(x_{g_2}, y_{g_2}) = \Big(x_{gp_2}+\delta x_o,\, y_{gp_2}+\delta y_o\Big) \tag{6.19}$$

Thus the second segment ($\mathcal{E}_{s2}$) of the staircase envelope is represented by the line segment between $A_2(x_{ge_1}, y_{ge_1})$ and $B_2(x_{g_2}, y_{g_2})$ and is having a slope of,

$$\sigma_{ge_2} = \tan^{-1}\frac{y_{g_2} - y_{ge_1}}{x_{g_2} - x_{ge_1}} \tag{6.20}$$

$\mathcal{E}_{s2}$ will serve as the effective ground profile for the motion of transit foot until $x_{th} > x_{g_2}$. Let us represent the position of transit heel at the terminal condition of $\mathcal{E}_{s2}$-zone by $A_3(x_{ge_2}, y_{ge_2})$. The third segment of ground envelope, $\mathcal{E}_{s3}$ is obtained directly by joining the points, $A_3(x_{ge_2}, y_{ge_2})$ and $B_3(x^o_{Lh}, y^o_{Lh})$.

In the case of the first step of descending stairs with the reference foot supported on stp_{i1}, there will be only two segments for the ground envelope equivalent to $\mathcal{E}_{s1}$ and $\mathcal{E}_{s3}$ of the normal case.

6.2.3 Envelope for ascending to descending transition

This is the case when $\rho_{ij} > 0$ and $\rho_{i(j+1)} \leqslant 0$ while the reference foot is supported on stp_{ij} as shown in Fig 6.5.

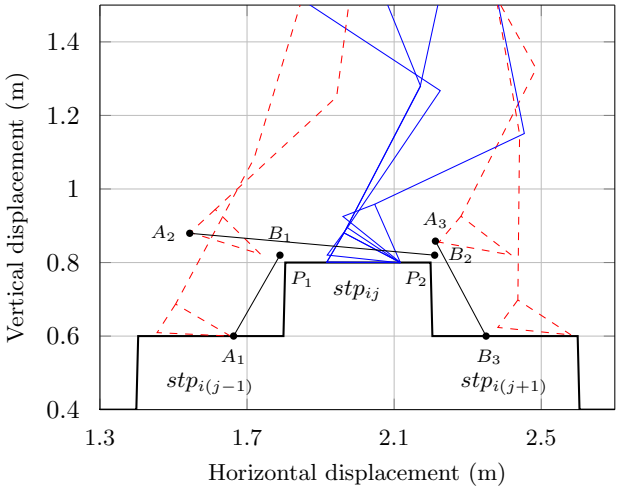

Figure 6.5: Linear envelope segments for ascending to descending transition

Let us consider the case with $\rho_{i(j+1)} < 0$. The first segment of the staircase envelope, $\mathcal{E}_{s1}$ will have a positive slope followed by $\mathcal{E}_{s2}$ and $\mathcal{E}_{s3}$ with negative slopes. Hence the transit toe will have the minimum ground clearance during $\mathcal{E}_{s1}$-zone whereas transit heel will have minimum ground clearance during $\mathcal{E}_{s3}$-zone. During the first part of $\mathcal{E}_{s2}$-zone, transit toe will be closer to stair-step surface and afterwards transit heel will be closer. Hence for the first segment, we follow the ascending staircase approach and for the other two, the descending staircase approach is followed. The first protrusion point, P_1 is obtained by finding the location, (x_{gp_1}, y_{gp_1}) on the stairs which maximises the slope, σ_{p_1} given by

$$\sigma_{p_1}(x_{tt}) = \frac{y_G(x_{tt}) - (y_{ge_0} + \epsilon)}{(x_{tt} - x_{ge_0})} \tag{6.21}$$

over the entire span of transit toe swing, $x_{ge_0} \leqslant x_{tt} \leqslant x^o_{Lt}$. The terminal point, B_1 of the first segment of ground envelope is selected at an offset of $(-\delta x_o, \delta y_o)$ with respect to the protrusion point, P_1 which is given by,

$$(x_{g_1}, y_{g_1}) = \Big(x_{gp_1} - \delta x_o,\ y_{gp_1} + \delta y_o\Big) \tag{6.22}$$

Thus the first segment ($\mathcal{E}_{s1}$) of the staircase envelope during ascending to descending transition is represented by the line segment between $A_1(x_{ge_0}, y_{ge_0})$ and $B_1(x_{g_1}, y_{g_1})$ and is having a slope of,

$$\sigma_{ge_1} = \tan^{-1} \frac{y_{g_1} - y_{ge_0}}{x_{g_1} - x_{ge_0}} \tag{6.23}$$

$\mathcal{E}_{s1}$ will serve as the effective ground profile for the motion of transit foot until $y_{tt} > y_{g_1}$. Let us represent the position of transit heel at the terminal condition of $\mathcal{E}_{s1}$-zone by $A_2(x_{ge_1}, y_{ge_1})$. The second protrusion point, P_2 is obtained by finding the location, (x_{gp_2}, y_{gp_2}) on the stairs which maximises the slope, σ_{p_2} given by

$$\sigma_{p_2}(x_{th}) = \frac{y_G(x_{th}) - y_{ge_1}}{(x_{th} - x_{ge_1})} \tag{6.24}$$

over the remaining span of transit heel swing, $x_{ge_1} \leqslant x_{th} \leqslant x^o_{Lh}$. If there are multiple points, take the point with minimum value of x_{th} as the protrusion point. The terminal point, B_2 of the second segment of ground envelope is selected at an offset of $(\delta x_o, \delta y_o)$ with respect to the protrusion point, P_2 which is given by,

$$(x_{g_2}, y_{g_2}) = \Big(x_{gp_2} + \delta x_o,\ y_{gp_2} + \delta y_o\Big) \tag{6.25}$$

Thus the second segment ($\mathcal{E}_{s2}$) of the staircase envelope is represented by the line segment between $A_2(x_{ge_1}, y_{ge_1})$ and $B_2(x_{g_2}, y_{g_2})$ and is having a slope of,

$$\sigma_{ge_2} = \tan^{-1} \frac{y_{g_2} - y_{ge_1}}{x_{g_2} - x_{ge_1}} \tag{6.26}$$

$\mathcal{E}_{s2}$ will serve as the effective ground profile for the motion of transit foot until $x_{th} > x_{g_2}$. Let us represent the position of transit heel at the terminal condition of $\mathcal{E}_{s2}$-zone by $A_3(x_{ge_2}, y_{ge_2})$. The third segment of ground envelope, $\mathcal{E}_{s3}$ is obtained directly by joining the points, $A_3(x_{ge_2}, y_{ge_2})$ and $B_3(x^o_{Lh}, y^o_{Lh})$.

The second case with $\rho_{i(j+1)} = 0$ corresponds to ascending stairs to uniform terrain transition. In this situation, the landing location $B_3(x^o_{Lh}, y^o_{Lh})$ itself will be the second protrusion point, P_2 and to ensure a finite slope, σ_{ge_3} for the touch down phase, x_{g_2} in (6.19) is limited to the maximum value of $(x^o_{Lh} - 0.1L_f)$. Thus B_2 is represented by the coordinates,

$$(x_{g_2}, y_{g_2}) = \Big(x^o_{Lh} - 0.1L_f,\ y^o_{Lh} + \delta y_o\Big) \tag{6.27}$$

Let us represent the position of transit heel at the terminal condition of $\mathcal{E}_{s2}$-zone by $A_3(x_{ge_2}, y_{ge_2})$. The third segment of ground envelope, $\mathcal{E}_{s3}$ is obtained directly by joining the points, $A_3(x_{ge_2}, y_{ge_2})$ and $B_3(x^o_{Lh}, y^o_{Lh})$.

6.2.4 Envelope for descending to ascending transition

There are three cases under this category when the reference foot is supported on stp_{ij} and $\rho_{ij} < 0$. In Case-1, $\rho_{i(j+1)} \geqslant -\rho_{ij}$ as shown in Fig 6.6 and in Case-2, $0 < \rho_{i(j+1)} < -\rho_{ij}$ and in Case-3, $\rho_{i(j+1)} = 0$. For Case-1 and Case-2, the procedure is same as in ascending case given in Section 6.2.1. However, there will be only one protrusion point, $P_1(x_{gp_1}, y_{gp_1})$ which occurs at the projecting corner of $stp_{i(j+1)}$ for Case-1 and at the projecting corner of $stp_{i(j-1)}$ for Case-2. Hence the landing location, $B_3(x^o_{Lt}, y^o_{Lt})$ itself is treated as the second protrusion point, P_2 and to ensure a finite slope, σ_{ge_3} for the touch down phase, x_{g_2} in (6.13) is limited to the maximum value of $(x^o_{Lt} - 0.1L_f)$. Thus B_2 is represented by the coordinates,

$$(x_{g_2}, y_{g_2}) = \left(x^o_{Lt} - 0.1L_f,\ y^o_{Lt} + \delta y_o\right) \tag{6.28}$$

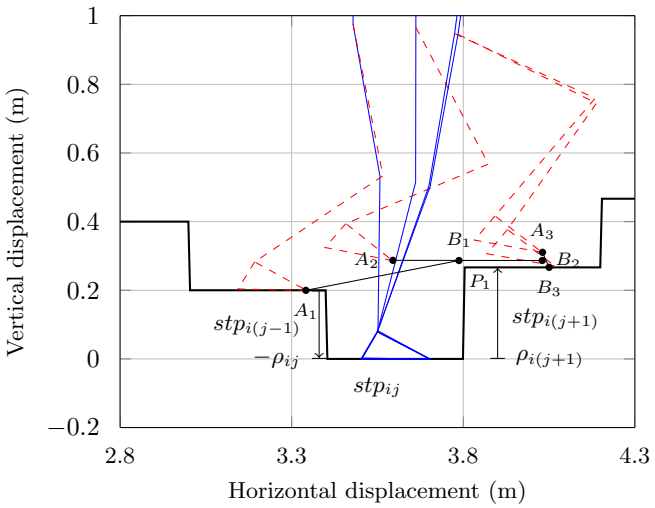

Figure 6.6: Linear envelope segments for descending to ascending transition

Let us represent the position of transit toe at the terminal condition of $\mathcal{E}_{s2}$-zone by $A_3(x_{ge_2}, y_{ge_2})$. The third segment of ground envelope, $\mathcal{E}_{s3}$ is obtained directly by joining

the points, $A_3(x_{ge_2}, y_{ge_2})$ and $B_3(x^o_{Lt}, y^o_{Lt})$. For the worst case, when $-\rho_{ij} \cong \rho_{i(j+1)}$, the protrusion point, P_1 also may get missed due to numerical computational inaccuracy. In such case, the first segment will be cancelled and $\mathcal{E}_{s2}$ will start right from $A_1(x_{ge_0}, y_{ge_0})$ and end at $B_2(x_{g_2}, y_{g_2})$ followed by $\mathcal{E}_{s3}$.

Case-3 with $\rho_{i(j+1)} = 0$ corresponds to descending stairs to uniform terrain transition. The procedure for Case-3 is the same as that for Case-2.

6.3 Modifications for Stair-HyDAC

6.3.1 Postural configuration state for stair-walk

The requirement of a control oriented postural state, $\mathbf{x}_P$ for analysing gait stability of planar biped for uniform terrain locomotion has been discussed in Section 4.7. One major difference between uniform terrain walk and stair-walk is that the walking gait for the latter is terminated by toe strike event of transit foot. This is to provide larger braking moment about biped-CoM with the constrained foothold on landing. The associated pattern of contact state sequence with respect to either of the feet is TR→FF→TR→ SW→TR. To take care of the change in the ground impact point of transit foot associated with stair-walk, we would like to redefine the *Postural Configuration State*, $\mathbf{x}_{Pc} \in \mathcal{C}^s \subset \mathbb{R}^{n_P}$ with n_P=12, to represent the essential postural features of biped during stair-walk and is given by,

$$\mathbf{x}_{Pc_{t\in[t_k,t_{k+1})}} := \left[\theta_{solr}\ \theta_{kner}\ \theta_{tor}\ \theta_{knet}\ \theta_{solt}\ \theta_{rtc}\ \theta_{ctt}\ \boldsymbol{\theta}'_{ubd}\right]' \tag{6.29}$$

$$\text{where } \theta_{rtc} := \frac{x_{com} - x_{tt}(t_k^-)}{h_{com}} \tag{6.30}$$

$$\theta_{ctt} := \frac{x_{tt} - x_{com}}{h_{com}} \tag{6.31}$$

$$\boldsymbol{\theta}_{ubd} = [q_7\ q_{11}\ q_{12}\ q_{13}\ q_{14}]' \tag{6.32}$$

where $\mathcal{C}^s$ is a simply-connected, open subset of $[-\pi, \pi)^{n_P}$ known as the *Postural Configuration Space* for stair-walk oriented postural dynamics. The definition and explanation of many of the symbols appearing in (6.29)-(6.32) remain the same as those given in Section 4.7. The half open interval, $[t_k, t_{k+1})$ represents the time interval corresponding to the k^{th} walking step with t_k denoting the time of k^{th} toe impact on ground. Accordingly, $x_{tt}(t_k^-)$ represents the x-coordinate of k^{th} toe strike location on ground. The forward offset of biped-CoM with respect to stance foot toe is represented by, θ_{rtc} and the forward offset of swing foot toe with respect to biped-CoM is represented by θ_{ctt}, both in normalized

form. The switching function, $\xi : \mathbb{R}^{n_p} \rightarrow \mathbb{R}$ is to be redefined for stair-walk as,

$$\xi(\mathbf{x}_{Pc}) = \frac{y_{tt}(\mathbf{x}_{Pc}) - y_G(x_{tt}(\mathbf{x}_{Pc}))}{h_{hip}} \tag{6.33}$$

and the switching set, $\mathcal{S}$ is redefined as

$$\begin{aligned} \mathcal{S} := \big\{ & [\mathbf{x}'_{Pc}\ \dot{\mathbf{x}}'_{Pc}]' \in T\mathcal{C}^s \mid \Sigma\pi_{m(1:2)} \geqslant 1, \Sigma\mathbf{x}_{Pc(6:7)} > 0, \\ & \xi(\mathbf{x}_{Pc}) = 0 \ \&\ \dot{\xi}(\mathbf{x}_{Pc}) < 0 \big\} \end{aligned} \tag{6.34}$$

where $T\mathcal{C}^s := \left\{ [\mathbf{x}'_{Pc}\ \dot{\mathbf{x}}'_{Pc}]' \mid \mathbf{x}_{Pc} \in \mathcal{C}^s, \dot{\mathbf{x}}_{Pc} \in \mathbb{R}^{n_p} \right\}$ is the state space associated with postural dynamics of bipedal locomotion over staircase and $\mathbf{x}_P := [\mathbf{x}'_{Pc}\ \dot{\mathbf{x}}'_{Pc}]' \in T\mathcal{C}^s$ is the postural state. As per the new definition given in (6.34), the switching set $\mathcal{S}$ admits only the toe strike event with $x_{tt} > x_{rt}$[2] and excludes static double support phase with $\dot{\xi}(\mathbf{x}_{Pc}) = 0$.

Fig 6.7 shows how the elements of $\mathbf{x}_{Pc}$ along with the terrain slope, σ_G uniquely determine the postural configuration of the biped for a given position of reference foot toe, $x_{rt}(t) = x_{tt}(t_k^-)$ for $t \in [t_k, t_{k+1})$. For easy representation, the entire upper body is represented by a single thick line in Fig 6.7 with its CoM location in $\{O_6\}$ determined by θ_{ubd}. O_4O_6 represents a virtual link from the reference foot ankle joint to the biped hip joint and its length, $\rho_{hr}(t)$ is determined by the value of $\mathbf{x}_{Pc2}(t)$. Similarly, O_6O_{10} represents a virtual link from the biped hip joint to transit foot ankle joint and its length, $\rho_{ht}(t)$ is determined by the value of $\mathbf{x}_{Pc4}(t)$. The values of $\mathbf{x}_{Pc1}(t)$ and $\mathbf{x}_{Pc5}(t)$ along with σ_G determine the inertial orientations of reference and transit foot links respectively and the value of $\mathbf{x}_{Pc3}(t)$ along with $\theta_{ubd}(t)$ determine the inertial orientations of the upper body links. The biped-CoM, O_c is constrained to move along the vertical line passing through A, having an offset determined by the value of $\mathbf{x}_{Pc6}(t)$. Similarly, the value of $\mathbf{x}_{Pc7}(t)$ constrains the locus of transit toe along the vertical line passing through B which inturn constrains the locus of transit ankle joint, O_{10} along the vertical line passing through C. The postural configuration of the biped during the period, $t \in [t_k, t_{k+1})$ is uniquely determined by rotating the hip joint about O_4 as shown in Fig 6.7 along the circular arc while keeping the horizontal position and orientation of transit foot until the biped-CoM falls on the vertical line passing through A. During the actual controlled motion, the closed loop inverse kinematics control [81] embedded within the TLC will steer the biped postural configuration automatically to the unique posture as determined above. During pre-touchdown phase with *FwdTDFlg*=0, the transit knee joint angle, $\mathbf{x}_{Pc4}$ is not explicitly controlled,

[2]Since $x_{rt} = x_{tt}(t_k^-)\ \forall t \in [t_k, t_{k+1}^-)$, $\Sigma\mathbf{x}_{Pc(6:7)} > 0$ implies $x_{tt} > x_{rt}$.

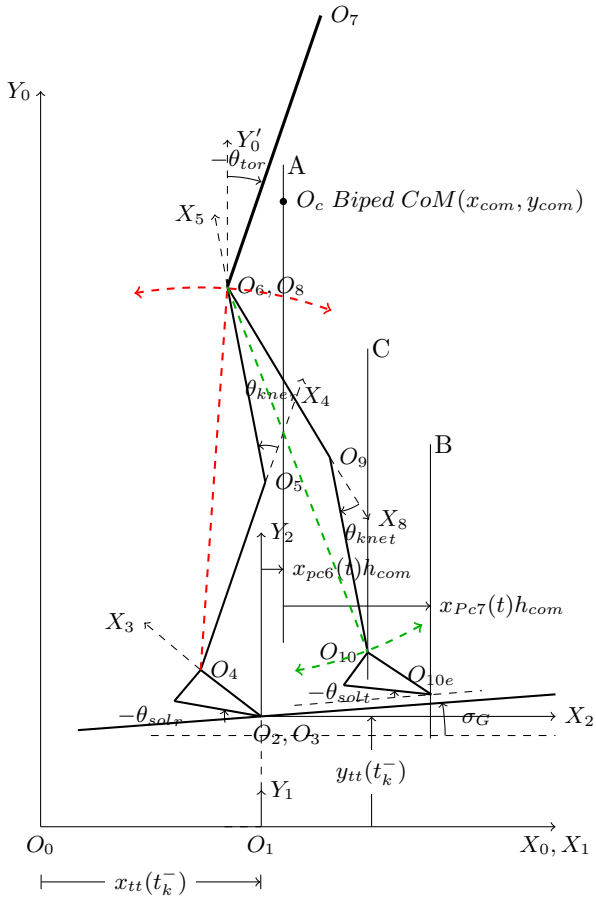

Figure 6.7: Postural configuration representation of biped by $\mathbf{x}_{\mathtt{Pc}}$ during the touch down phase of k$^{\text{th}}$ walking step of uniform terrain walking assuming transit toe impact

rather controlled implicitly to meet the goals of transit foot ground clearance, $\mathtt{h}_{\mathtt{hip}}\xi(\mathbf{x}_{\mathtt{Pc}})$.

6.3.2 Impact posture goal (IPG) for stair-walk

For uniform terrain walk with toe impact[3], the impact posture goal, $\mathbf{x}_P^o = [\mathbf{x}_{Pc}^{o\prime}\ \dot{\mathbf{x}}_{Pc}^{o\prime}]'$ for the planar biped corresponding to the $\mathbf{x}_{Pc}$ defined in (6.29) can be selected as,

$$\mathbf{x}_{Pc}^o = \Big[0\ \ \theta_{kner}^o\ \ \theta_{dna}\ \ \theta_{knet}^o\ \ \theta_{solt}^o \int_{t_k^-}^{t_{k+1}^-} \dot{\theta}_{rtc}\,dt - \theta_{ctt}(t_k^-)\ \ \lambda_t\ \ \theta^{o\prime}_{ubd}\Big]' \tag{6.35}$$

$$\dot{\mathbf{x}}_{Pc}^o = \Big[0\ 0\ 0\ 0\ 0\ \frac{V_{fc}}{h_{com}}\ 0\ \mathbf{0}_{1\times 5}\Big]' \tag{6.36}$$

where, λ_t is the desired value of normalized forward landing offset, θ_{ctt} on toe impact, θ_{dna} is the target value for θ_{tor} and θ_{ubd}^o is the desired value for θ_{ubd}. The criteria for selecting the individual elements of $\mathbf{x}_{Pc}^o$ are given in Section 6.3.5. The adequacy of the control DoF for driving $\mathbf{x}_P$ towards IPG can be proved as per the arguments given in Section 4.8.5.

An important feature of dynamic walk over uniform terrain is that the transit leg trajectory is not tied up with any preassigned point on ground, rather placed relative to the moving GCoM location to ensure a feasible impact posture on every heel strike. However, non-uniform terrain walk has to satisfy an additional control functional requirement stated as $\mathcal{CFR}-S1$ in terms of foot placement location on each transit foot ground impact. Hence it is required to modify both SLC and TLC of original HyDAC formulation to satisfy the foothold constraint with minimal loss of dynamic performance. This additional control requirement is achieved in Stair-HyDAC by driving the reference knee joint variable, $\mathbf{x}_{Pc2}(t)$ along an appropriate trajectory during the touch down phase, instead of driving towards a pre-set constant value of $\mathbf{x}_{Pc2}^o$ as done in Normal-HyDAC. In other words, the passive forward rotation during the touch down phase with almost steady reference knee joint angle is replaced by passive forward rotation along with controlled depression of hip through reference knee joint so as to steer the transit foot towards the specified foothold location.

Let us represent $\mathbf{x}_{Pc}$ excluding $\mathbf{x}_{Pc2}$ by $\bar{\mathbf{x}}_{pc2}$. Fig 6.8 shows how the elements of $\bar{\mathbf{x}}_{pc2}(t)$ along with the desired landing location, (x_{Lt}^o, y_{Lt}^o) and σ_G uniquely determine the postural configuration of biped during the touch down phase of descending stair-walk for a given position of reference toe, $x_{rt}(t) = x_{tt}(t_k^-)$ for $t \in [t_k, t_{k+1})$. For the sake of explanation, let us make a temporary assumption that during the touch down phase of descending stairs, the transit foot heel is steered down perfectly along, $\mathcal{E}_{s3}$ for any forward velocity, V_{comx}

[3]Uniform terrain walk is normally terminated by heel impact event.

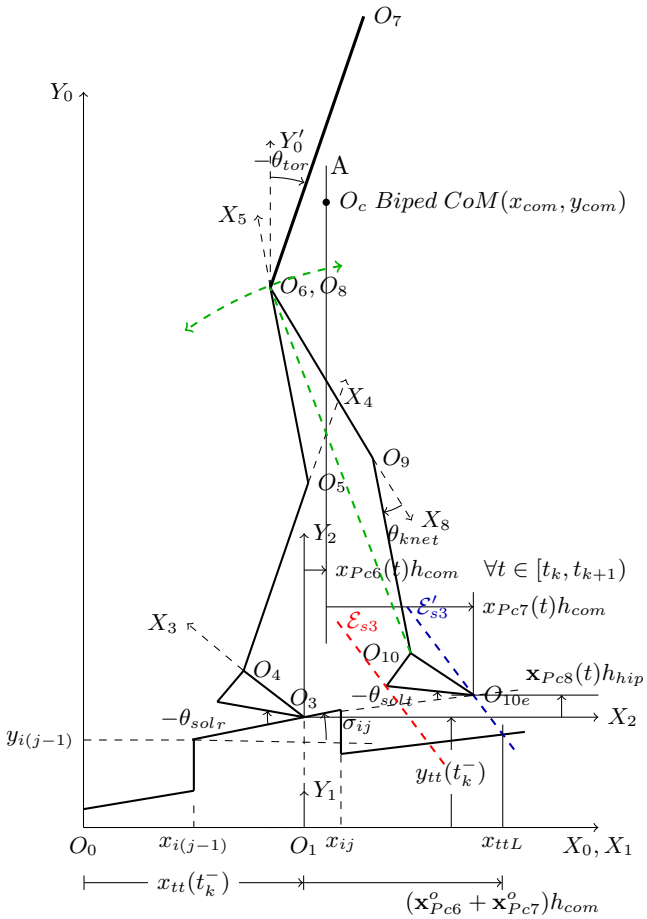

Figure 6.8: Postural configuration representation of biped by $\mathbf{x}_{\mathrm{Pc}}$ during the touch down phase of descending stair-walking

by perfect regulation of $\mathrm{x}_{\mathrm{Pc2}}(\mathrm{t})$ along the appropriate target profile, $\mathrm{x}^{\mathrm{o}}_{\mathrm{Pc2}}(\mathrm{t})$, so that the transit toe will strike the next step on the desired target, $(\mathrm{x}^{\mathrm{o}}_{\mathrm{Lt}}, \mathrm{y}^{\mathrm{o}}_{\mathrm{Lt}})$. Similarly, during the touch down phase of ascending stairs, let us assume that the transit foot toe is steered down perfectly along $\mathcal{E}_{\mathrm{s3}}$ towards $(\mathrm{x}^{\mathrm{o}}_{\mathrm{Lt}}, \mathrm{y}^{\mathrm{o}}_{\mathrm{Lt}})$. It can be observed from Fig 6.8 that $(\mathrm{x}^{\mathrm{o}}_{\mathrm{Lt}}, \mathrm{y}^{\mathrm{o}}_{\mathrm{Lt}})$, σ_{G} and $\mathcal{E}_{\mathrm{s3}}$ along with the configuration state values, $\mathbf{x}_{\mathrm{Pc}(5:7)}(\mathrm{t})$ place the transit foot link in inertial frame, thereby determining the pivot point O_{10} for the virtual transit leg link, $\mathrm{O}_6\mathrm{O}_{10}$ for the current instant. As mentioned, its length, $\rho_{\mathrm{ht}}(\mathrm{t})$ is determined by the value of $\mathbf{x}_{\mathrm{Pc4}}(\mathrm{t})$. Further, the location of reference foot ankle joint, O_4 is determined by the values of $\mathrm{x}_{\mathrm{tt}}(\mathrm{t}_{\mathrm{k}}^-)$ and $\mathbf{x}_{\mathrm{Pc1}}(\mathrm{t})$ for the current instant . Then the hip joint, O_6 is rotated about O_{10} along the arc shown keeping the upper body links along $\mathbf{x}^0_{\mathrm{Pc3}}$ and $\theta^{\mathrm{o}}_{\mathrm{ubd}}$ until

the biped-CoM falls on the vertical line passing through A. Thus, the values of $\bar{\mathbf{x}}_{Pc2}(t)$ along with (x^o_{Lt}, y^o_{Lt}) and σ_G can uniquely determine the postural configuration of biped during the touch down phase of k^{th} walking gait assuming that transit heel is steered down perfectly along $\mathcal{E}_{s3}$. Having determined the unique postural orientation of biped based on $\bar{\mathbf{x}}_{Pc2}(t)$, (x^o_{Lt}, y^o_{Lt}) and σ_G, we can find out the unique value of $\mathbf{x}^o_{Pc2}(t)$ for ensuring the kinematic closure condition as per Fig 6.8. Any deviation of $\mathbf{x}_{Pc2}(t)$ from $\mathbf{x}^o_{Pc2}(t)$ will violate our initial assumption of perfect tracking of transit heel along $\mathcal{E}_{s3}$. Hence, in the general case of imperfect tracking of transit heel along $\mathcal{E}_{s3}$, the values of $\bar{\mathbf{x}}_{Pc2}(t) \oplus \mathbf{x}_{Pc2}(t)$(or $\mathbf{x}_{Pc}(t)$) along with (x^o_{Lt}, y^o_{Lt}) and σ_G uniquely determine the postural configuration of biped during the touch down phase of stair-walk.

The elements for IPG for Stair-HyDAC are given by (6.35) and (6.36) except for the values of $\mathbf{x}^o_{Pc2}$ and $\dot{\mathbf{x}}^o_{pc2}$. The control for $\mathbf{x}_{Pc2}(t)$ is to be executed as a tracking type task control loop with an autonomously generated tracking error expressed as a function of $\bar{\mathbf{x}}_{pc2}, \sigma_G$ and $\mathcal{E}_{s3}$ parameters. Thus, unlike uniform terrain dynamic walk, an additional internal coordination constraint is imposed on IPG to ensure the absolute location of transit foot impact point. The details of coordination control for $\mathbf{x}_{Pc2}$ and transit foot to ensure the desired landing location, (x^o_{Lt}, y^o_{Lt}) are given in Section 6.3.5.3 and Section 6.3.5.5.

6.3.3 Redefinition of *FwdTDFlg*

The Forward Touch Down Flag, *FwdTDFlg* is set as per the conditions given by Algorithm 6.1. *FwdTDFlg* will initiate the touchdown control of transit foot and will be reset

Algorithm 6.1: Flag setting logic for *FwdTDFlg*

Data: *FwdTDFlg*, *MidSwgFlg*, $x_{com}, x_{rt}, x_{tt}, x^o_{Lt}, L_f, \rho_{i(j+1)}, x_{ij}, x_{th}$, index j of stp_{ij},index k of $\mathcal{E}_{sk}$.

```
if ρ_{i(j+1)} > 0 then
    if FwdTDFlg=0 and MidSwgFlg=1 and (x_com > x_rt) and { ( k = 2 and (j = 1 or
    ρ_{i(j+1)} < 0.05L_f) ) or (k = 3 and j > 1)} and (x_tt > (x^o_Lt − L_f/10)) then
        FwdTDFlg ← 1
    end
else
    if FwdTDFlg=0 and MidSwgFlg=1 and (x_com > x_rt) and (x_th > x_ij) then
        FwdTDFlg ← 1
    end
end
```

on transit foot ground strike.

6.3.4 Modifications in the limit of normal contact force

As in Normal-HyDAC, the upper bound of f_{gy} is represented by f_{gy+} and the lower bound of f_{gy} is represented by f_{gy-}. Since the forward velocity, V_{fc} is limited to 0.75 m/s for Stair-HyDAC, the nominal value of f_{gy+} is kept at 1250κ N for an ascending stairs if the tread slope, $\sigma_{ij} > -5\pi/180$ and at 1500κ N if $\sigma_{ij} \leqslant -5\pi/180$ where $\kappa = M_{bp}g/(830)$. The major objective of the reduced value of f_{gy+} is to limit the upward acceleration during ascending stairs. However for descending stairs, a constant value of 4000κ N is assigned for f_{gy+} as in Normal-HyDAC . The value of the lower force bound, f_{gy-} is kept at 200κ N under all situations.

6.3.5 Modifications for motion control primitives

The advantage of HyDAC framework is its easy adaptability to different walking scenarios by suitable modifications in motion control primitives. The general form of motion control primitives belonging to locomotion tasks and upper body tasks are given by (4.120) and (4.121). Stair-HyDAC requires modifications in all locomotion related control primitives represented by (H_l, B_l) except the HRRC primitive. The following subsections give the details of modifications carried out for each of them. The details of various symbols, definitions and expressions, which were already given in Section 5.2 are not repeated here.

6.3.5.1 Torso Orientation Control (TOC) Primitive

The modifications in TOCP are in the expression for θ_{dna}, its limits and rate of change as given below.

$$\theta_{dna} = -\sigma_{Gr}/2 - \pi V_{fc}/18 - 0.1\sigma_{Gd}, \text{ for } \sigma_{Gd} > 0 \tag{6.37}$$
$$\text{where, } \sigma_{Gd} = \tan^{-1}\frac{y^o_{Lc} - y_G(x_{rt})}{x^o_{Lc} - x_{rt}}$$

and $\theta_{dna} = 0$ for $\sigma_{Gd} \leqslant 0$. σ_{Gr} is the slope of ground at $x_{rc} = (x_{rt}+x_{rh})/2$, the centre of reference foot and σ_{Gd} is the effective slope between the current reference toe and landing site for transit foot centre, (x^o_{Lc}, y_{tcL}). The maximum value of θ_{dna} is limited to 0 rad to avoid backward lean. In a dynamic situation when any of the parameters on the RHS of (6.37) changes along the stairs, the rate of change of θ_{dna} is limited to $[-\pi/18,\ \pi/36]$ rad/s to avoid fast torso rotation leading to large inertial disturbance.

6.3.5.2 Toe Roll Reset Control (TRRC) primitive

The TRRC primitive is a new behaviour mode introduced for Stair-HyDAC and is activated by SLC to meet $\mathcal{CDR}2$ during the hybrid event state,

$$\mathbb{H}_{es} : \Big(\pi_c = [0\ 1\ 0\ 0]\Big)\ \&\ \Big(\text{rank}(H_{cp}) \leqslant 2\Big) \tag{6.38}$$

The task vectors for the associated PD regulator are,

$$H(q) = [0\ 0\ 1\ 0\ \cdots 0] \in \mathbb{R}^{1\times n_J} \tag{6.39}$$

$$B(q,\dot{q}) = \omega_b^2\left[q_3^o - q_3\right] - 2\zeta\,\omega_b\dot{q}_3 \tag{6.40}$$

$$\text{with,}\ \ q_3^o = \pi + \sigma_g - \gamma + 0.02/L_f \tag{6.41}$$

The orientation, $q_3 = q_3^o$ corresponds to the FF state of reference foot. A control bandwidth of, $\omega_b = 5\omega_p$ and damping factor of, $\zeta = 1.5$ are assigned to this primitive based on simulation studies. The absolute value of the orientation error, $(q_3^o - q_3)$ is limited to $\pm\pi/60$. The TR-phase does not occur in Normal-HyDAC since each stance phase starts with HR-phase followed by FF phase. Transition from FF to TR-phase is avoided by GCoP constraint.

6.3.5.3 Reference Knee Joint Control (RKJC) primitive

RKJC primitive has two modes of operation, namely rising-mode and drooping-mode. The expressions for the task vectors corresponding to the PD type control law for rising-mode can be given as,

$$H(q) = [0\ 0\ 0\ 0\ 1\ 0\ \cdots 0] \in \mathbb{R}^{1\times n_J} \tag{6.42}$$

$$B(q,\dot{q}) = \omega_b^2 q_{ke} - 2\zeta\,\omega_b\dot{q}_5 \tag{6.43}$$

with $q_{ke} = \theta^o_{kner} - q_5$, $\omega_b = 5\omega_p$ and $\zeta = 1$. In addition, the slew rate of the regulation loop is indirectly set by limiting the absolute value of feedback position error, q_{ke} to the specified values, q_{ke+} based on the current value of q_{ke} as per the following logic[4]: If $-q_{ke} > 70\pi/180, q_{ke+} = \max(1, V_{fc})25\pi/180$, else if $-q_{ke} > 40\pi/180, q_{ke+} = \max(1, V_{fc})15\pi/180$, else, $q_{ke+} = \max(1, V_{fc})10\pi/180$. The slew rate is brought down step by step to keep $\dot{q}_5$ to a sufficiently small value as the knee angle, q_5 approaches the

[4]When the position error of RKJC gets saturated to q_{ke+}, the second order regulator loop dynamics gets reduced to a first order rate loop with an effective rate command of $(\omega_b/2\zeta)q_{ke+}$ rad/s.

full extension to avoid the lift-off tendency of support foot. The value of θ^{o}_{kner} for rising mode is computed using an algorithm similar to Algorithm 5.1 except with the difference that $\bar{\sigma}_G = \sigma_{Gr}$.

The drooping-mode of RKJC is activated during the touch down phase of stair-walk when *FwdTDFlg*=1. As discussed in Section. 6.2.1 and Section. 6.2.2, during the touch down phase of stair-walk, the transit foot toe or heel is steered down along the third ground envelope segment, $\mathcal{E}_{s3}$ by equivalently drooping down the vertical position of hip joint through q_5 control. It is executed by the following task vectors.

$$H(q) = [0\ 0\ 0\ 0\ h_5\ 0\ \cdots 0] \in \mathbb{R}^{1\times n_J} \tag{6.44}$$

$$B(q,\dot{q}) = \omega_b^2 y^e_{tb} - \left(\dot{J}_{hip(3,:)} + 2\zeta\,\omega_b J_{hip(3,:)}\right)\dot{q} \tag{6.45}$$

where J_{hip} is the Jacobian of the hip joint, $\omega_b = 5\omega_p$, $\zeta = 0.9$, and $y^e_{tb} = y_{Ge}(x_{tb}) - y_{tb}$ is the vertical offset between the selected transit foot bottom point (x_{tb}, y_{tb}) and its vertical projection on the ground envelope segment beneath transit foot, by which the vertical position of hip joint is to be lowered for toe touch down. For ascending stairs with $\rho_{i(j+1)} > 0$, 'tb' stands for 'tt' and for descending stairs with $\rho_{i(j+1)} \leqslant 0$, '$tb$' stands for '$th$' based on the explanation given in Sections 6.2.1 and 6.2.2. The expressions for $y_{Ge}(x_{tb})$ under different cases are given by (6.47). An extra downward offset of $\max(\rho_{i(j+1)}/2, -0.02\text{m})$ is added to $y_{Ge}(x_{tb})$ for $\rho_{i(j+1)} < 0$ to reduce the tracking error for vertical drooping motion. The value of the fifth element of $J_{hip(3,5)}$ denoted by h_5 is limited to an upper bound of -0.1 m/rad to avoid CW rotation of reference knee joint[5].

6.3.5.4 Ground Clearance Control (GCC) primitive

The objective of *Ground clearance control primitive* is to ensure adequate clearance between transit foot sole and the active ground envelope segment to avoid collision between transit foot and staircase boundaries prior to the controlled toe strike during the transit foot forward swing. Let the symbol 'tb' represent the corner point of the transit foot out of 'th' or 'tt' having the maximum proximity to the selected ground envelope segment, $\mathcal{E}_{si}$ and let the corresponding Jacobian be represented as J_{tb} which corresponds to either J_{th} or J_{tt}. The Jacobian for 'tb' resolved along $\{O_g\}$ frame attached to the inclined ground envelope, is defined as,

$$J_{gbe} = R_g(\sigma_{ge_i})\ J_{tb},\ \dot{J}_{gbe} = R_g(\sigma_{ge_i})\ \dot{J}_{tb} \tag{6.46}$$

[5]During forward leaning posture of biped with q_5 close to zero, h_5 will become positive resulting in hyper extension of stance knee joint which is to be avoided.

where, R_g represents the 2D rotation matrix defined as per (3.8). The y-coordinate of the ground projection, $y_G(x_{tb})$ used in Normal-HyDAC is replaced by the vertical projection of x_{tb} on $\mathcal{E}_{si}$ under different zones of swing phase and is denoted by $y_{Ge}(x_{tb})$.

$$\begin{aligned} y_{Ge}(x_{tb}) &= y_{ge_0} + (x_{tb} - x_{ge_0}) \tan \sigma_{ge_1} \text{ for } \mathcal{S}_{e1} - \text{ zone} \\ &= y_{ge_1} + (x_{tb} - x_{ge_1}) \tan \sigma_{ge_2} \text{ for } \mathcal{S}_{e2} - \text{ zone} \\ &= y_{ge_2} + (x_{tb} - x_{ge_2}) \tan \sigma_{ge_3} \text{ for } \mathcal{S}_{e3} - \text{ zone} \end{aligned} \tag{6.47}$$

Similar to Normal-HyDAC, the desired ground clearance, ρ_{gc} is taken as a constant value of 0.04 m irrespective of the offset between transit and reference foot. The elements of regulator type task expression are given by,

$$H(q) = \begin{bmatrix} \mathbf{0}_{1\times 7} & J_{gbe(2,8:10)} & \mathbf{0}_{1\times 4} \end{bmatrix} \tag{6.48}$$

$$\begin{aligned} B(q, \dot{q}) &= \omega_b^2 \left(\rho_{gc} - \rho_{cl} \right) \\ &\quad - \left(2\zeta \omega_{gc} J_{gbe(2,:)} + \dot{J}_{gbe(2,:)} \right) \dot{q} \end{aligned} \tag{6.49}$$

where, $\rho_{cl} = \left(y_{tb} - y_{Ge}(x_{tb}) \right) \cos \sigma_{ge_i}$, $\omega_b = 5\omega_p$ and $\zeta = 1$. ρ_{cl} represents the value of ground clearance between transit foot bottom, tb and the active ground envelope, $\mathcal{E}_{si}$, resolved perpendicular to $\mathcal{E}_{si}$ and σ_{ge_i} is the orientation of $\mathcal{E}_{si}$. Once *FwdTDFlg* $= 1$, the ground clearance primitive is called off and the transit foot is guided to the desired touchdown location along $\mathcal{E}_{s3}$ by RKJC primitive as explained in Section. 6.3.5.3.

6.3.5.5 Transit Foot Forward Positioning (TFFP) primitive

The TFFP primitive of Stair-HyDAC replaces both TTOC (Transit Thigh Orientation Control) and THFP (Transit Heel Forward Positioning) primitives in Normal-HyDAC [41] and is active throughout the gait if $V_{fc} > 0$. This has the important function of regulating the position of transit foot centre, x_{tc} relative to biped-CoM position, x_{com}.

The task expressions for TFFP are given by,

$$H(q) = \begin{bmatrix} \mathbf{0}_{1\times 7} & \left(J_{th(1,8)} + J_{tt(1,8)} \right)/2 & \mathbf{0}_{1\times 6} \end{bmatrix} \tag{6.50}$$

$$\begin{aligned} B(q, \dot{q}) &= \omega_b^2 \, x_{tce} - \left[\left(\dot{J}_{th(1,:)} + \dot{J}_{tt(1,:)} \right)/2 \right] \dot{q} \\ &\quad + 2\zeta \omega_b \left[V_{comx} - \left(J_{th(1,:)} + J_{tt(1,:)} \right)/2 \right] \dot{q} \end{aligned} \tag{6.51}$$

where $\zeta = 0.8$, $\omega_b = 5\omega_p$ and x_{tce} is the forward tracking error of the centre of transit foot and is computed based on the normalized forward landing offset, λ_t. The algorithm for the computation of λ_t and x_{tce} is arrived at based on detailed simulation studies using the planar biped model over stairs of different parameter combinations and the same is given in Algorithm 6.2. The expression for $H(q)$ during the $\mathbb{H}_{es}$ with *MidSwgFlg*=1 and

Algorithm 6.2: Computation of forward landing offset, λ_t and tracking error, x_{tce}

Data: $\rho_{i(j+1)}, \rho_{i(j+2)}, h_{com}, x_{rt}, x_{com}, x_{tc}, L_f, V_{fc}$ and *FwdTDFlg*

$\mu_\lambda \leftarrow 1$
if $\rho_{i(j+1)} > L_f/2$ ***and*** $\rho_{i(j+2)} < -L_f/2$ **then**
  if $\tau_{i(j+1)} > 2.25L_f$ **then**
    $\mu_\lambda \leftarrow 2$
  else
    $\mu_\lambda \leftarrow 1.5$
  end
end
if $V_{fc} \leqslant 0.2$ ***and*** $\rho_{i(j+1)} > L_f$ **then**
  $\mu_\lambda \leftarrow 0.5$
end
$\lambda_t \leftarrow 0.088 V_{fc} \mu_\lambda$
if $x_{th} < x_{hip}$ ***and*** *FwdTDFlg=0* **then**
  $x_{tce} \leftarrow \max(x_{rt}, x_{com}) + \lambda_t h_{com} + Lf/2 - x_{tc}$
else
  $x_{tce} \leftarrow x_{com} + \lambda_t h_{com} + Lf/2 - x_{tc}$
end
Return λ_t,x_{tce}

FwdTDFlg=0 is to be modified as given below to provide better coordination with GCC primitive.

$$H(q) = \begin{bmatrix} \mathbf{0}_{1\times 7} & \left(J_{th(1,8:9)} + J_{tt(1,8:9)}\right)/2 & \mathbf{0}_{1\times 5} \end{bmatrix} \tag{6.52}$$

The absolute value of x_{tce} is limited to $0.1\max(0.2, V_{fc})$ m prior to control computation in (6.51) .

6.3.5.6 Transit Foot Orientation (TFO) primitive

During uniform terrain dynamic walking, HyDAC regulates the orientation of transit foot sole to an angle of $\theta_{solt} = 10\,\pi/180$ in CCW direction with respect to ground surface so that transit foot will strike the ground with its heel. However in bipedal walking over stairs, the transit toe impact is preferred over heel impact as discussed earlier and hence the nominal target orientation in TFO primitive is kept at $\theta_{solt} = -5\pi/180$ with respect to step surface. If the step-down height is larger with $\rho_{i(j+1)} < -0.1$m, Stair-HyDAC uses a target orientation of $\theta_{solt} = -15\pi/180$ so that the transit foot can stretch down further to

have an early touch down as in human locomotion. Similarly, if the step-up height is larger with $\rho_{i(j+1)} > 0.1$m, a target orientation of $\theta_{solt} = -10\pi/180$ is used to provide larger braking. However, there are situations in stair-walk which prefer to have transit heel strike instead of toe strike. If $V_{fc} < 0.2$ m/s with $\rho_{i(j+1)} < -L_f$, toe strike will lead to excess braking. Similarly when the biped has reached the final step, stp_{iN_i} of descending stairs with $V_{fc} < 0.2$ m/s, toe strike will lead to excess braking. Another situation is when the biped reach the final step stp_{iN_i} of ascending stairs, irrespective of the velocity command. Under all the above three situations, $\theta_{solt} = 10\pi/180$ is to be used for the TFO primitive.

The orientation reference for the transit ankle joint for TFO primitive is given by,

$$q_{10}^o = \pi + \sigma_{i(j+1)} - \gamma - q_{sh} + \theta_{solt} \tag{6.53}$$

where $q_{sh} = \Sigma q_{(3:6)} + \Sigma q_{(8:9)} - \pi$ is the inertial orientation of transit tibia (shank) link. The task expressions are given by

$$H(q) = \begin{bmatrix} \mathbf{0}_{1\times 9} & 1 & \mathbf{0}_{1\times 4} \end{bmatrix} \tag{6.54}$$

$$B(q, \dot{q}) = \omega_b^2 \left(q_{10}^o - q_{10} \right) - 2\zeta\omega_b \dot{q}_{10} \tag{6.55}$$

where $\omega_b = 5\omega_p$ and $\zeta = 0.7$. The orientation error, $q_{10}^o - q_{10}$ is limited to $\pm 5\pi/180$ to set the slew rate of transit ankle joint.

6.3.5.7 Transit Knee Joint Control (TKJC) primitive

The TKJC primitive execution is carried out with two different objectives during the post midswing phase. If *TrnKneExt*=1, the TKJC is executed to bring the transit knee out of straight knee zone by a closed loop regulator control with a target value of $\theta_{knet}^o = -15\pi/180$. The expressions for the task vectors are given by (5.44)-(5.45) with $\omega_b = 5\omega_p$ and $\zeta = 0.7$. If *TrnKneExt*=0 and *FwdTDFlg*=1, TKJC primitive is used to orient transit knee, q_9 along a desired value of $\theta_{knet}^o = -\pi/6$. The orientation error, $(\theta_{knet}^o - q_9)$ is limited to $\pm 3\pi/180$ to set the slew rate of transit knee joint.

6.4 Simulation studies for Stair-walk

The 12-link planar biped with the parameter values given in Table. 3.1 has been used for the simulation studies. The initial values of the state of biped remain the same as in the previous simulation studies for Normal-HyDAC. More thrust is given to establish validity of Stair-

HyDAC for performance limit cases. The video links corresponding to the simulation runs discussed in this section are given in Table B.2 -Table B.5.

6.4.1 Nominal cases of stair-walk

Compared to uniform terrain locomotion, the dynamic walking over stairs has a larger proportion of under-actuated forward rotation phase and hence there exists an optimal forward velocity for each combination of tread depth and riser height. However, to demonstrate the velocity regulation characteristics of Stair-HyDAC, velocities spanning over 0.1 m/s to 1 m/s are included in the simulation cases with majority of the results taken for V_{fc}=0.5 m/s.. Each Simulation run is carried out for a single flight of stairs and hence for the simplicity of notation, the stair-flight index, 'i' is dropped for the staircase parameters. The stair-tread depth, τ_j is varied from 0.3 m to 0.5 m for the biped with foot span of $L_f = 0.2\,m$. The stair-riser height, ρ_j is varied up to 0.4 m. Every walking simulation starts from rest condition of biped on level terrain. Both ascending to descending (Up-down) as well as descending to ascending (Down-up) staircase combinations are tried. HyDAC makes use of $\mu_c = 0.8$ for coulomb friction model and $\Gamma_{6+} = 600$ N-m for internally limiting the generated torque command for torso joint. The lower limb joint torque commands are externally limited as in uniform terrain walk with the same limits mentioned in Section 5.3.

The stick plots for continuous ascending and descending stair-walk over a staircase having tread depth of $\tau_j = 0.4$ m and riser height of $\rho_j = \pm 0.4$ m for a velocity command of $V_{fc} = 0.5$ m/s are shown in Fig 6.9. The corresponding video links given in Appendix B demonstrate the true picture of the coordinated dynamic behaviour of various link motions. The periodic behaviour of dynamic stair-walk is evident from the trajectories of lower limb joint angles and torso inertial orientation, q_{tor} as shown in Fig 6.10. The value of q_5 reaches almost close to the full extension state with a margin of 10 deg. The pattern of joint torque commands for few joints, namely reference ankle (Γ_4), reference knee (Γ_5), torso (Γ_6), transit thigh (Γ_8), transit knee (Γ_9), and transit ankle (Γ_{10}) are shown in Fig 6.11. It can be observed that joint torques remain within the respective limits. It is possible to further reduce the peak value of joint torque demanded by HyDAC by proper tuning of TLC bandwidths, slew rates as well as by appropriate regularization of primitives prior to algebraic inversion. The forward velocity regulation performance during stair-walk by FVC algorithm is demonstrated in Fig 6.12. The sudden vertical downward transitions in transit foot centre trajectory, x_{tc} is caused by the leg swapping operation on every toe strike event and the repeating positive offset, $x_{tc} - x_{com} \approx \lambda_t h_{com} + L_f/2$ is a good indicator of

gait stability. As every new gait starts at transit toe impact on ground, the GCoP starts at support foot toe, then switches backward to support heel on subsequent CCW rotation of foot sole leading to heel impact, then stays close to heel to provide forward acceleration to CoM, followed by smooth transition towards support toe to provide the necessary velocity regulation as shown by x_{cop}, x_{com} plots of Fig 6.12. The sum of normal contact forces, $(f_{grhy} + f_{grt_y})$ is limited to 4000 N as expected in descending stair-walk.

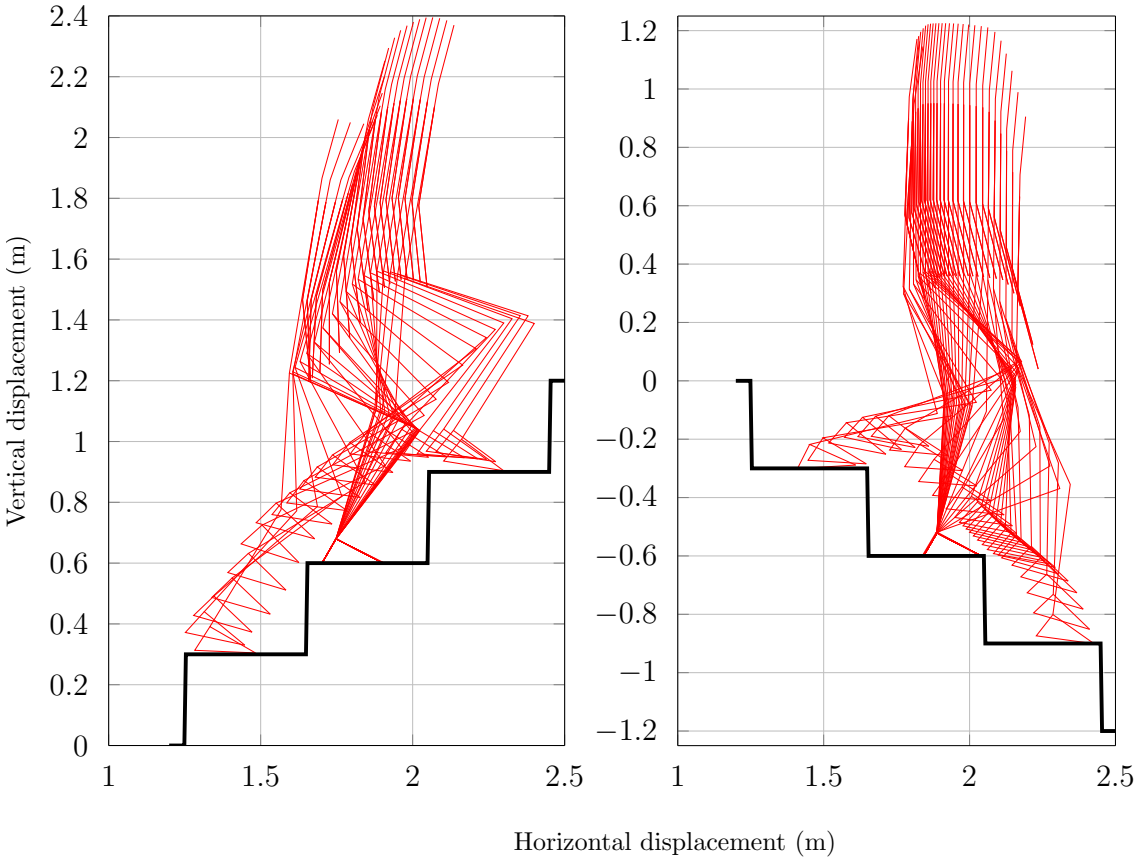

Figure 6.9: Stick plot sampled @40 m.s for dynamic walking over ascending and descending stairs with τ_j=0.4 m and $\rho_j = \pm$ 0.3 m for V_{fc}=0.5 m/s

The ascending stairs with τ_j=0.4 m and ρ_j=0.3 m is taken as a typical staircase for studying the velocity regulation. The forward velocity of biped-CoM measured along $\overrightarrow{O_0X_0}$ are plotted in Fig 6.13 for velocity commands varying from 0.1 m/s to 1 m/s . It can be seen that V_{com_x} is regulated towards V_{fc} until 0.75 m/s. The regulation is not proper

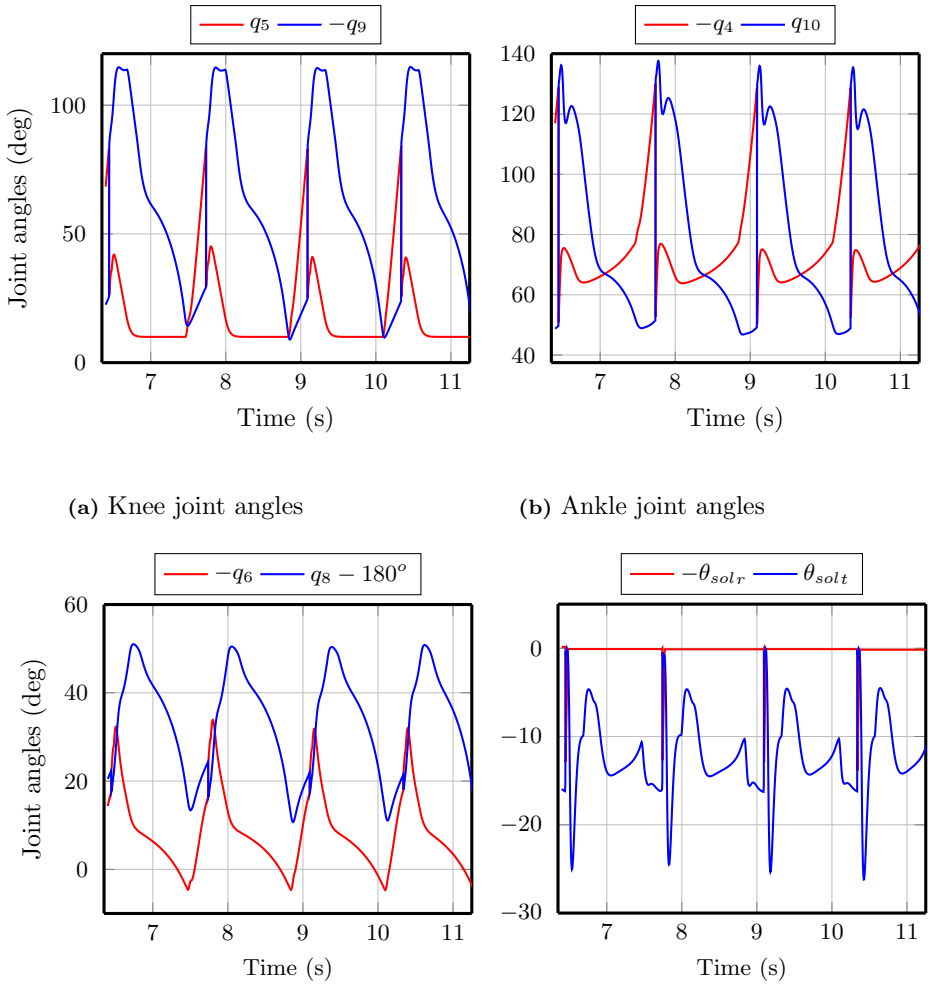

(a) Knee joint angles

(b) Ankle joint angles

(c) Hip joint angles

(d) Foot sole angles

Figure 6.10: Joint angles corresponding to the ascending stair walk shown in Fig 6.9

for V_{fc}=1 m/s even after raising f_{gy+} from 1250 N to 2500 N and Γ_{5+} from 500 N-m to 750 N-m. Hence the upper velocity limit for the current values of Stair-HyDAC controller parameters is found as 0.75 m/s.

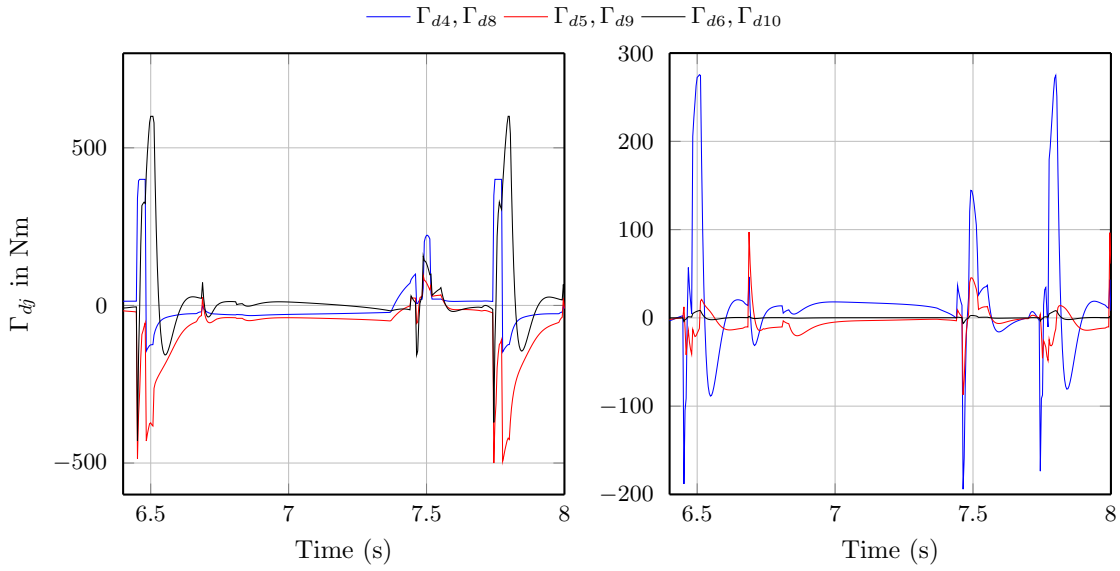

(a) Γ_{dj} for Reference leg and Torso

(b) Γ_{dj} for Transit leg

Figure 6.11: Joint torques corresponding to the ascending stair walk shown in Fig 6.9

6.4.2 Transient response at stair-flight boundaries

The transients at the first and last steps of a flight of stairs for different stair patterns and for different forward velocity commands are shown in Fig 6.14 - Fig 6.18. In order to have smooth velocity transition at stair boundaries, the tread depth, τ_{ij} for $j = 1$ and N_i are kept less than nominal[6] τ_{ij}, in the range of 0.25 m to 0.3 m. Similarly, transit foot orientation is adjusted for the final step for certain stair parameters as discussed in Section 6.3.5.6. to avoid excess braking due to toe strike on ground. The stick plot corresponding to 4-step ascending and descending stair walk with τ_j=0.4 m and $\rho_j = \pm$ 0.3 m for V_{fc}=0.5 m/s are given in Fig 6.14. Important variables like $x_{com}, x_{cop}, x_{tc}, V_{comx}, f_{grhy}$ and f_{grt_y} corresponding to the ascending stair walk are plotted in Fig 6.15 and the same corresponding to the descending stair walk are plotted in Fig 6.16. The stair portion in these plots can be easily identified by f_{grh_y} and f_{grt_y} as their limits are different from the limits of level terrain walk. The ripples in forward velocity for descending stair-walk is relatively more as expected due to the large value of contact force on transit foot ground strike. The GCoP control parameter, $(x_{com} - x_{cop})$ remains almost zero for ascending stair-walk until x_{cop}

[6] τ_{i1} and τ_{iN_i} are part of the uniform terrain before and after the i^{th} flight of stairs as shown in Fig 6.1 and hence they can be assigned any arbitrary values without affecting the actual staircase.

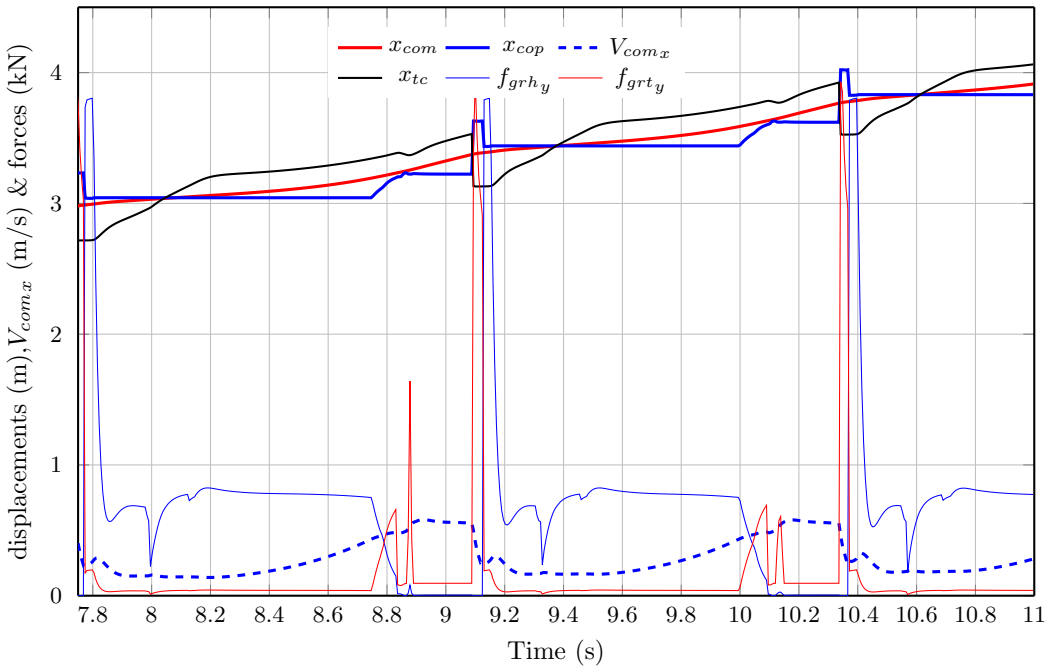

Figure 6.12: $x_{com}, x_{cop}, x_{tc}, V_{comx}, f_{grh_y}$ and f_{grt_y} corresponding to the descending stair walk shown in Fig 6.9

gets limited by x_{rt} whereas the same takes large value for the descending stair-walk until V_{comx} is pushed towards V_{fc}=0.5 m/s. The excellent regulation of $(x_{tc}-x_{com})$ ensures adequate robustness with respect to forward landing offset, λ_t. The video links for different cases of 4-step stair walk with their parameters are given in Table B.2 of Appendix B.

The stick plot during walking over a compound staircase having the pattern, *level* $\rightarrow$ *up* $\rightarrow$ *down* $\rightarrow$ *up*$\rightarrow$ *level* with $\tau_j = 0.5$ m and $\rho_j = \pm 0.3$ m for V_{fc}=0.5 m/s is shown in Fig 6.17. The critical stability controlling offsets, $(x_{cop}-x_{com})$ and $(x_{tc}-x_{com})$ along with the forward velocity are plotted in Fig 6.18. The velocity regulation is not good at various stair pattern transition points as expected. The validity of the linear stair envelop segments formulated in Section 6.2.3- 6.2.4 for ascending to descending and descending to ascending stair transitions are thus demonstrated.

6.4.3 Perturbation cases for stair-walk

We consider here three cases for robustness evaluation, namely robustness with respect to staircase parameter perturbation, payload mass variation, and finally with respect to

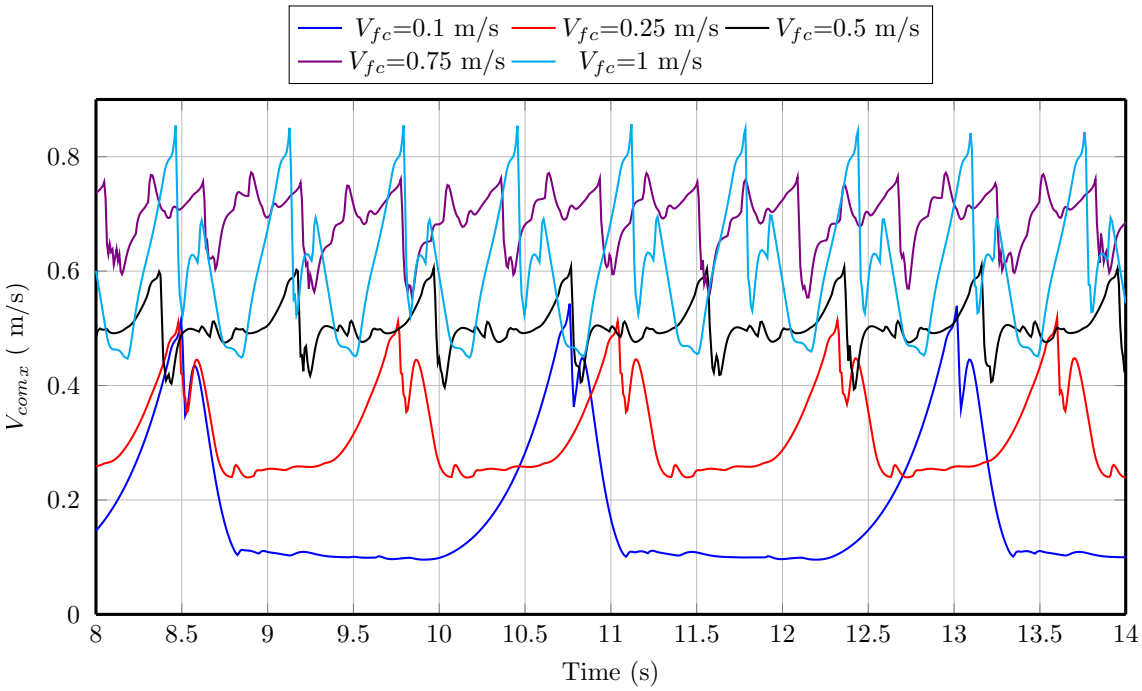

Figure 6.13: Forward velocity of biped-CoM for different velocity commands (V_{fc}) for ascending stair-walk having τ_j=0.4 m and ρ_j=0.3 m.

external force disturbance.

6.4.3.1 Robustness with respect to stair-parameter perturbation

The robustness of Stair-HyDAC with respect to unexpected stair-parameter variations[7] is demonstrated in Fig 6.19. The tread depth, τ_j is varied from 0.3 to 0.5 m during the initial half portion of terrain while keeping a riser height of ρ_j=0.2 m and ρ_j is varied from 0.05 m to 0.4 m in the second half with τ_j=0.35 m. The step-slope, σ_j is perturbed within $\pm$ 15 deg. The simulation results demonstrate the excellent agility of Stair-HyDAC to autonomously adapt to terrain conditions without any a priori gait planning and prove the potential of HyDAC for generic uneven terrain locomotion. The plots of x_{tc} and x_{com} shown in Fig 6.20 demonstrate the robust performance of the coordinated motion of transit foot with respect to the moving CoM of biped in the presence of terrain perturbation. The tangential and normal components of ground contact force acting on the reference foot along with their absolute ratio, i.e. $|(f_{grh_x} + f_{grt_x})/(f_{grh_y} + f_{grt_y})|$ are plotted in Fig 6.21. The normal

[7]Unexpected in the sense that τ_j, ρ_j and σ_j are known only when the support foot reaches stp_{j-1}.

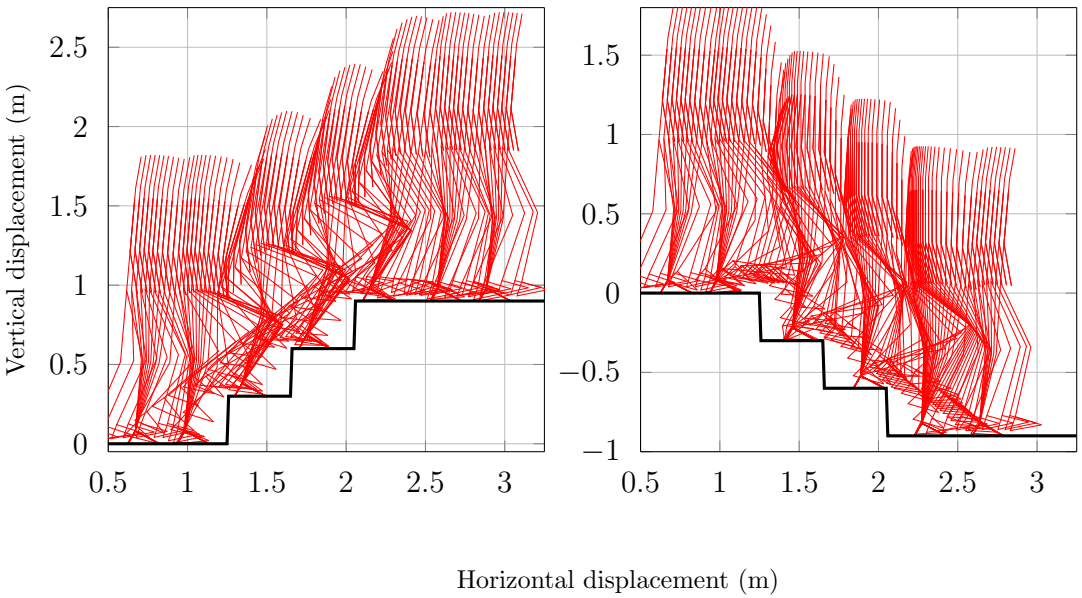

Figure 6.14: Stick plot sampled @40 m.s for dynamic walking over ascending and descending stairs with τ_j=0.4 m and $\rho_j = \pm$ 0.3 m for V_{fc}=0.5 m/s

force, $(f_{grhy} + f_{grty})$ is limited to 1250 N during ascending portion and to 2500 N[8] during the descending portion of stair by the force limit constraint of HyDAC whereas the contact force ratio is limited within $\pm 0.95\mu_c$ by the friction cone constraint. There is further scope for improving the velocity regulation by optimizing the forward landing offset parameter, λ_t with respect to the stair-parameters, τ_j, ρ_j and σ_j.

6.4.3.2 Robustness with respect to payload mass perturbation

As in uniform terrain walk, the robustness of Stair-HyDAC to torso mass variation is studied for the dynamic walk over ascending stairs having τ_j=0.4 m and ρ_j=0.3 m for V_{fc}=0.5 m/s. The torso mass is multiplied by 2.5, equivalent to adding an extra mass of 60 kg to a biped of total nominal mass of 84 kg without shifting the location of torso-CoM. However, to take care of the extra load, the upper force limit of f_{gy+} is increased from the nominal value of 1250 N to 2500 N, and the torque limit of reference knee joint is increased from 500 N-m to 750 N-m. The comparison between nominal and mass-perturbed systems during ascending stair walk is shown in Fig 6.22. It can be seen that the velocity regulation

[8] A smaller value of 2500 N is used for f_{gy+} instead of the normal value of 4000 N for descending stairs to avoid backward fall for small forward velocity under larger value of ρ_j.

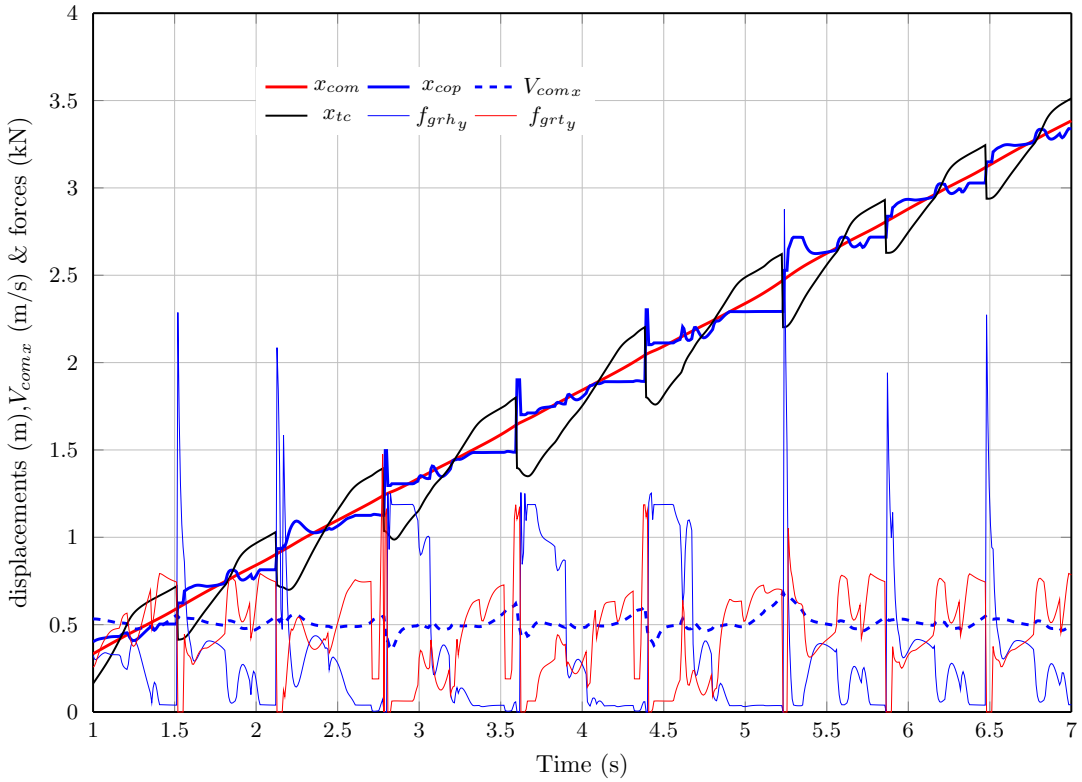

Figure 6.15: $x_{com}, x_{cop}, x_{tc}, V_{comx}, f_{grh_y}$ and f_{grt_y} corresponding to the ascending stair walk shown in Fig 6.14

is not affected due to payload mass increase by utilizing the enhanced stance-knee joint torque resulting in larger value of ground contact force. Thus the Stair-HyDAC is also insensitive to payload mass variation as in Normal-HyDAC.

6.4.3.3 Robustness with respect to external push disturbance

The robustness study with respect to external disturbance is conducted by applying an external disturbance force of 100 N on the neck joint of biped along the forward direction, $-\overrightarrow{O_7Y_7}$ at t=5.4 s for a duration of 0.5 s while the biped is ascending over uniform stairs having parameters, τ_j =0.4 m, ρ_j =0.3 m for V_{fc} =0.5 m/s. The disturbance induced transients in the forward velocity, V_{comx} and in the tangential and normal components of contact forces are given in Fig 6.23. The forward velocity goes on increasing till the end

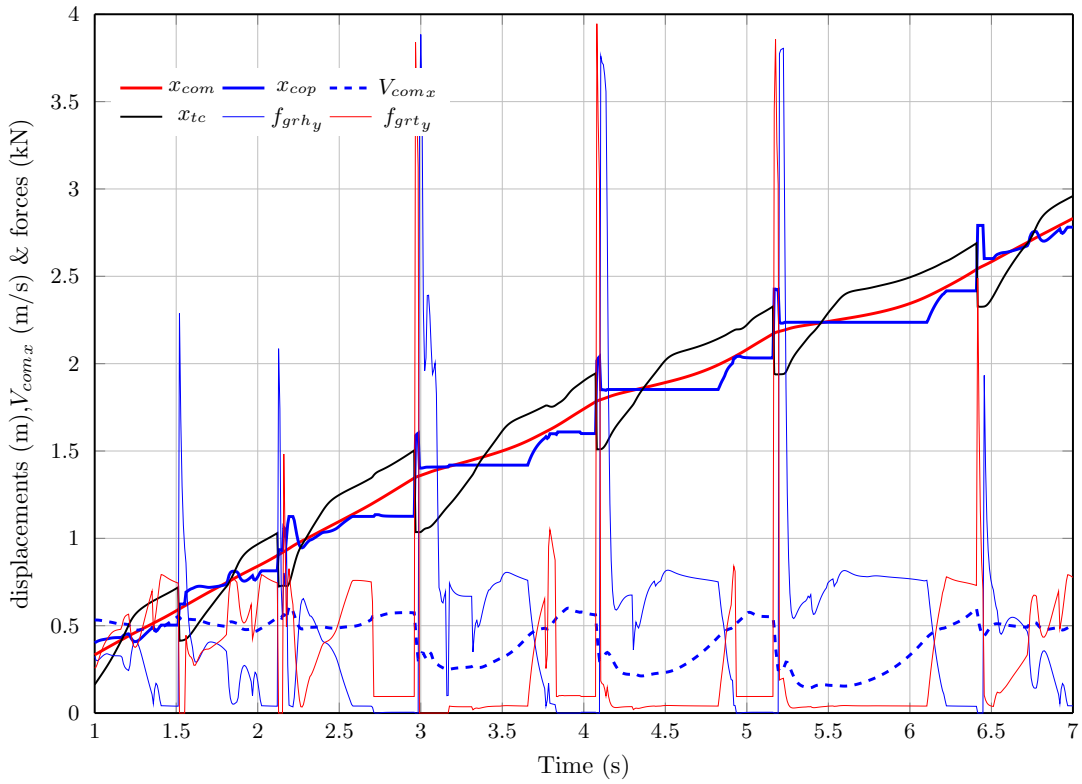

Figure 6.16: $\mathtt{x_{com}}, \mathtt{x_{cop}}, \mathtt{x_{tc}}, \mathtt{V_{comx}}, \mathtt{f_{grh_y}}$ and $\mathtt{f_{grt_y}}$ corresponding to the descending stair walk shown in Fig 6.14

of forward push and captures back to the regulated profile within 0.5 s after the removal of disturbance. It can be observed that the $\mathtt{x_{cop}}$ quickly moves towards the support foot toe on the application of $\mathtt{f_{dy_7}}$ and remains at support foot toe end for the next step also to brake out the extra forward velocity build up, thus validating the performance of FVC algorithm. The application of external push force is indicated by an extra line appearing at the neck joint of biped in the corresponding video. The result truly demonstrates the reflex stability performance of Stair-HyDAC against sudden unplanned external disturbance.

6.4.4 Stability analysis

The quantitative stability margins expressed in terms of contraction factor, ρ_C and radius of convergence, $\mathcal{R}_C$ in the sense of contraction stability are obtained for uniform stair walk also as estimated in the case of uniform walk in Chapter 4. The nominal trajectory for uni-

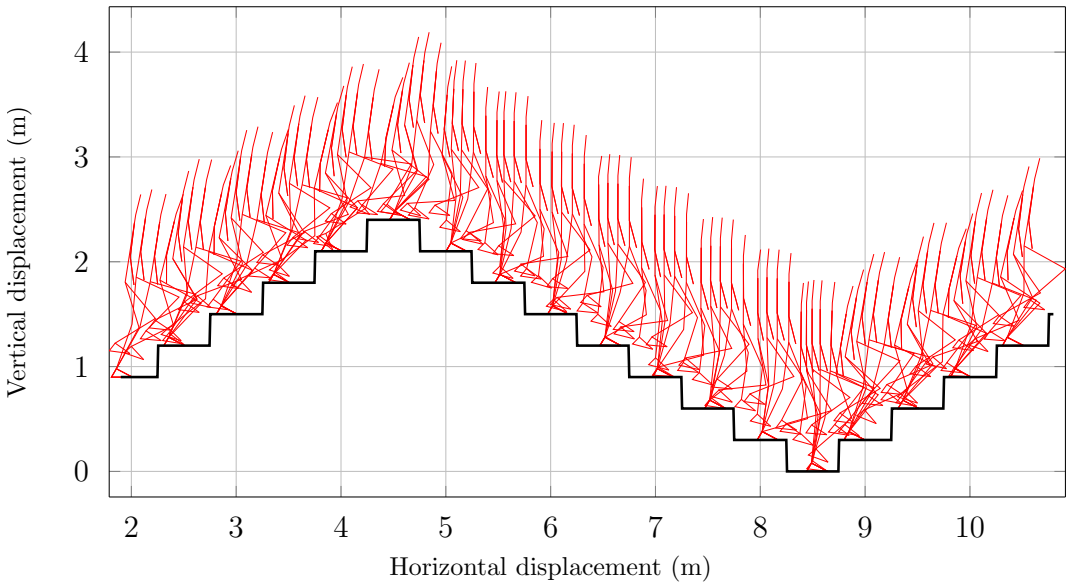

Figure 6.17: Stick plot @ 0.2 s corresponding to dynamic walking over level→up→down→up→level type staircase with $\tau_j = 0.5$m and $\rho_j = \pm 0.3$ m for V_{fc}=0.5 m/s

form stair walk can be perturbed by applying a forward push disturbance of f_{dy_7}=1 N along -$\overrightarrow{O_7Y_7}$ direction while the biped is steered with constant velocity along either ascending or descending stairs with constant parameters. However to analyse the contraction pattern starting from large initial trajectory dispersions, a computationally simpler approach is to study the self convergence, i.e. by plotting the norm of postural state error between consecutive toe strike events. The stability margins for various stair-walk sequences are shown in Fig 6.24 to Fig 6.26. The ascending dynamic walk over staircase with τ_j=0.4 m and ρ_j=0.3 m for V_{fc}=0.5 m/s is taken as the reference case for stability analysis. Out of all the contraction plots, only three are plotted based on perturbed trajectories generated by external force whereas others are plotted based on the self contraction of consecutive step errors. The latter method is able to bring out the contraction rate from large initial deviation with respect to the final orbit. Comparison of both methods when applied to the case with τ_j=0.4 m and ρ_j=-0.3 m are shown by dotted blue and dotted red plots. After the sixth step, both have the similar bounds, but dotted blue is able to show the convergence from large initial error during step-1 to step-4. Unlike uniform terrain dynamic walk, none of

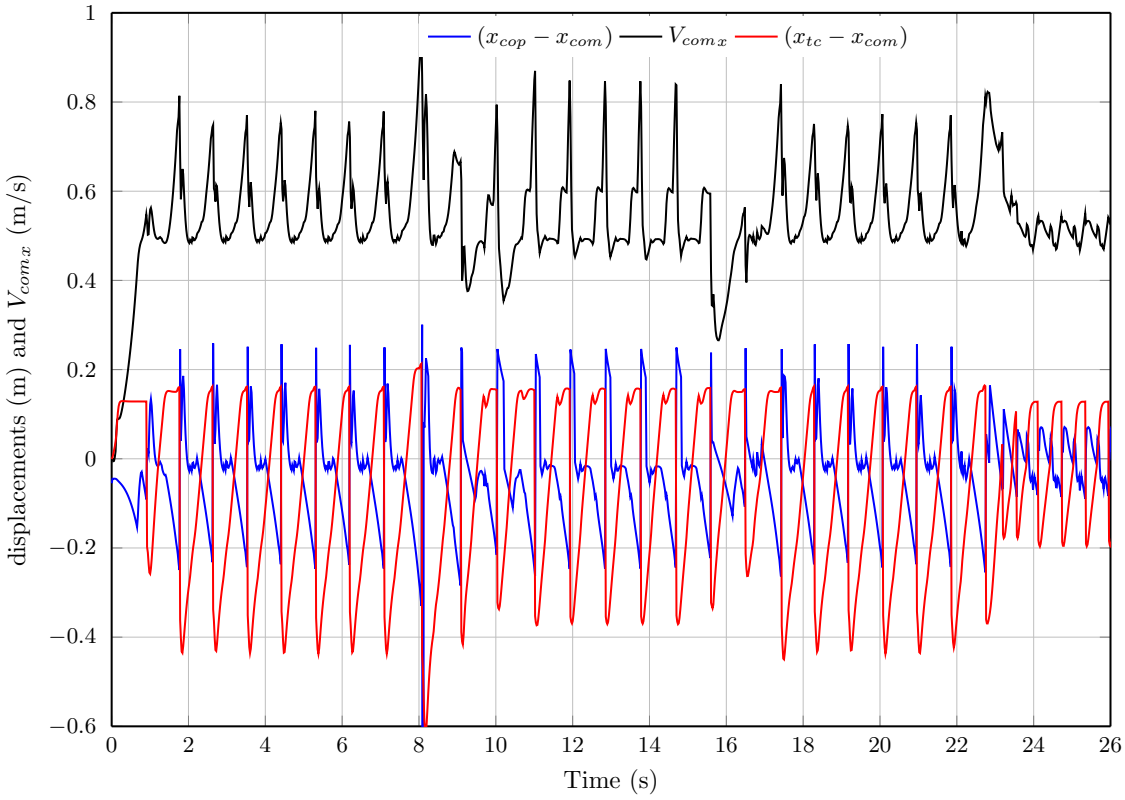

Figure 6.18: $(x_{cop} - x_{com})$, $(x_{tc} - x_{com})$, and V_{comx} corresponding to the level → up → down → up → level stair walk shown in Fig 6.17

the stair walk exhibit asymptotic contraction to a periodic orbit, rather exhibits EPS with finite value of $\mathcal{R}_C$. The cases shown in Fig 6.24 have an initial contraction factor of ρ_C=0.2 and the cases shown in Fig 6.25 - Fig 6.26 have ρ_C=0.1 as indicated by the thick magenta line. A general observation from Fig 6.24 is that descending stair-walk has less stability margin compared to ascending stair-walk. The stability margin decreases with increase in riser height, ρ_j.

The dependence of stability on the forward velocity of stair-walk is brought out in Fig 6.25 with respect to ascending stair-walk with τ_j=0.4 m and ρ_j=0.3 m. The radius of convergence, $\mathcal{R}_C$ for V_{fc}=0.1 m/s is 0.0215 and the same for V_{fc}=0.25 m/s is 0.0225 and are of the same order of $\mathcal{R}_C$=0.023 obtained for V_{fc}=0.5 m/s as seen from Fig 6.24. However, $\mathcal{R}_C$ increases to 0.15 for V_{fc}=0.75 m/s worsening the stability margin. The stability for V_{fc}=1 m/s looks to be better than for V_{fc}=0.75 m/s with $\mathcal{R}_C$=0.1. The reason for the reverse

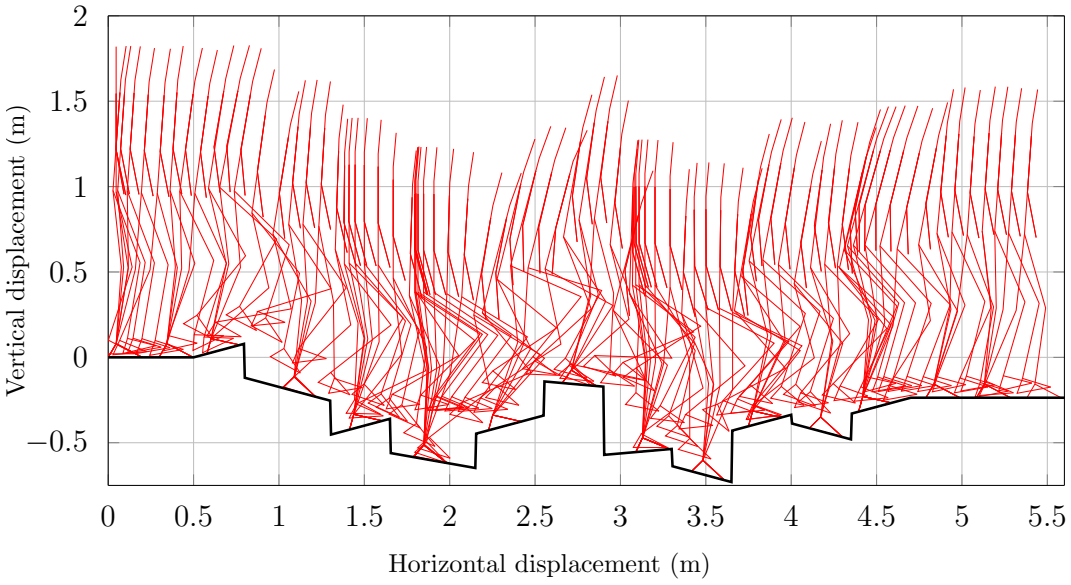

Figure 6.19: Stick plot @ 0.2 s corresponding to dynamic walking over randomly slopped non-uniform stairs with $\tau_j \in [0.3\,\text{m}, 0.5\,\text{m}]$, $\rho_j \in [0.05\,\text{m}, 0.4\,\text{m}]$ and $\sigma_j \in [-15, 15]$ deg for V_{fc}=0.4 m/s

trend is that the upper limit for stance knee torque, Γ_5 is increased from 500 N-m to 750 N-m and the normal contact force limit, f_{gy+} is increased from 1250 N to 2100 N for the latter case. Moreover, the actual forward velocity has not increased to 1 m/s as per the command to make a true judgement. The effect of step-slope perturbation by $\pm$ 5 deg and tread-depth perturbation by $\pm$ 0.025 m on $\mathcal{R}_C$ are also shown in Fig 6.25. The initial contraction rate for all the cases in Fig 6.25 are found to be ρ_C=0.1.

The stability under torso mass increase by 150% is analysed for the ascending stair-walk for the reference case and is shown by the solid red curve in Fig 6.26. The stability margin in terms of $\mathcal{R}_C$=0.016 seems to be even better than the corresponding nominal case shown Fig 6.24 with $\mathcal{R}_C$=0.0235. To achieve stable walking, f_{gy+} had to be increased from 1250 N to 2500 N and Γ_{5+} had to be increased from 500 N-m to 750 N-m to support for the additional mass increase by 60 kg. However, the stability for the case with torso mass increase by 10% without changing the force and torque limits, as shown by dotted blue curve in Fig 6.26, is inferior to the nominal case in terms of $\mathcal{R}_C$=0.2. The stability for riser height perturbation case by $\pm$0.025m for the reference case is also analysed and plotted by the solid blue curve in Fig 6.26. The radius of convergence, $\mathcal{R}_C$= 0.26 which is

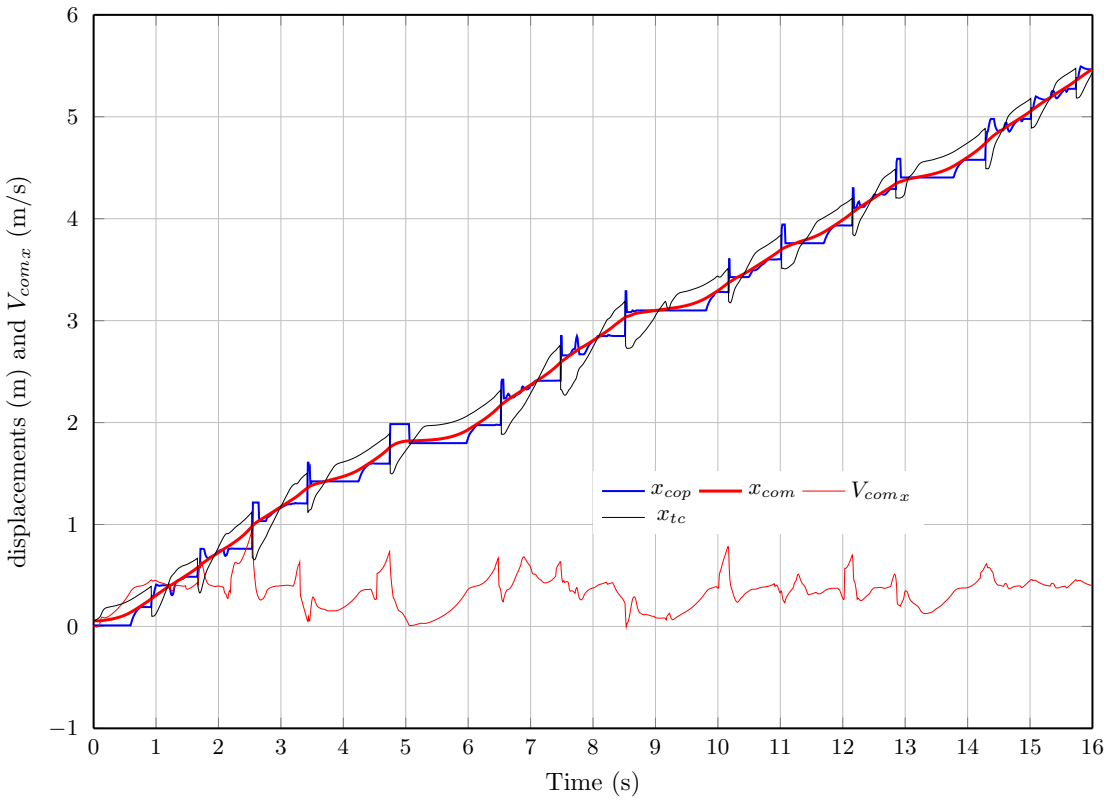

Figure 6.20: x_{cop}, x_{com}, x_{tc}, and V_{comx} corresponding to the randomly slopped non-uniform stair walk shown in Fig 6.19

much larger compared to the nominal value of 0.0235. However, the initial contraction rate for all the cases plotted in Fig 6.26 is found to be ρ_C=0.1. Finally the stability of compound staircase having the pattern *level*→*up*→*down*→ *up*→*level* is analysed as shown by the red dotted curve in Fig 6.26. The two peaks in δ_{AB} corresponds to up→down and down→ up stair transition zones as evident from velocity plot shown in Fig 6.18.

6.5 Chapter Summary

The present chapter has extended the hybrid state driven autonomous control concept to dynamic walking over generic non-uniform staircase. The non-uniform stairs under consideration have uneven distribution of tread-depth within the range of 0.3 m - 0.5 m, up-down step-rise within ± 0.4 m, and step-slope within ± 15 deg. The extended version of HyDAC for staircase locomotion was named as Stair-HyDAC. The distinctive requirement of Stair-

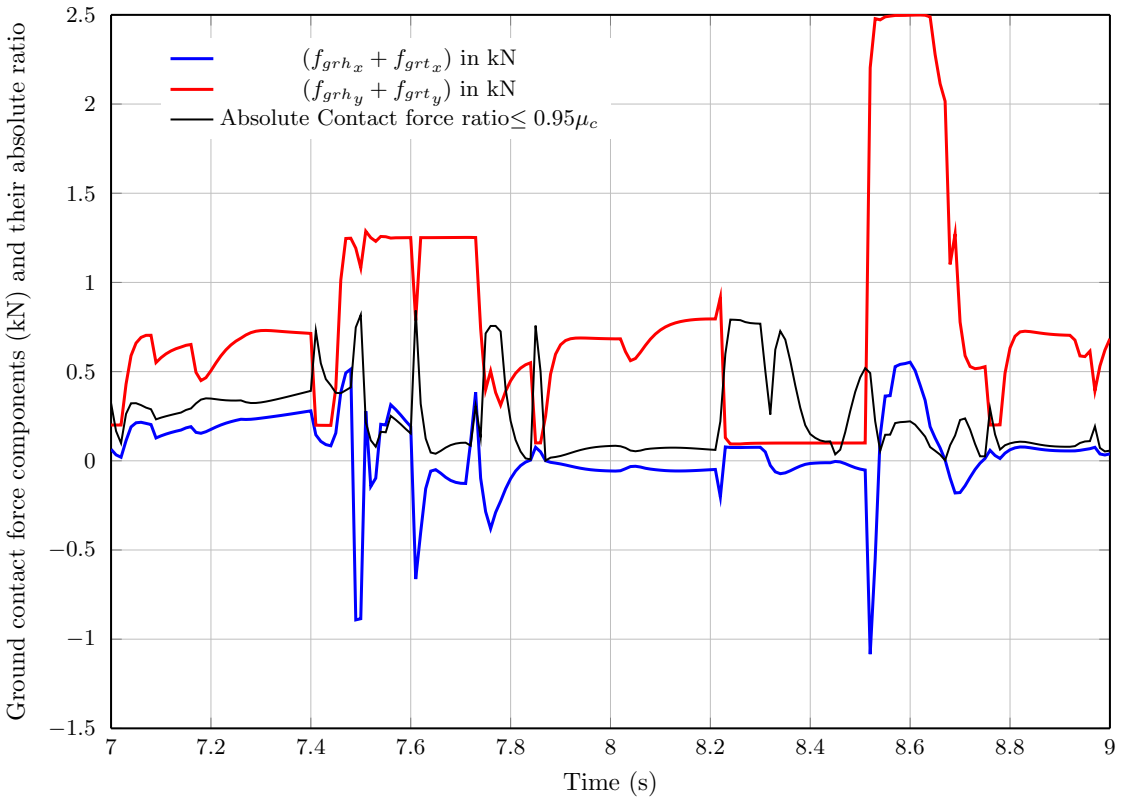

Figure 6.21: Tangential and normal components of ground contact force acting on reference foot along with their absolute ratio corresponding to the non-uniform stair walk shown in Fig 6.19

HyDAC is to place the transit foot in the specified feasible foothold on each step. Even though, this additional requirement limits the achievable forward velocity range compared to Normal-HyDAC, the proposed modifications in task level and supervisory level controls could achieve stable dynamic stair-walk upto a velocity range of 0.75 m/s.

The robustness of Stair-HyDAC control law with respect to payload mass was demonstrated by perturbing the torso mass as high as 2.5 times of nominal mass (additional mass of 60 kg over a nominal total mass of 84.5 kg of the biped). Similarly, the robustness of HyDAC with respect to unplanned actuator torque limit was demonstrated by externally limiting the torque commands to all lower limb joints. The reflex stability behaviour of Stair-HyDAC was demonstrated by the disturbance rejection response of stair-walk with respect to an external forward push force of 100 N applied at neck joint for a duration of 0.5 s. The agility of the control algorithm was demonstrated by steering the planar biped

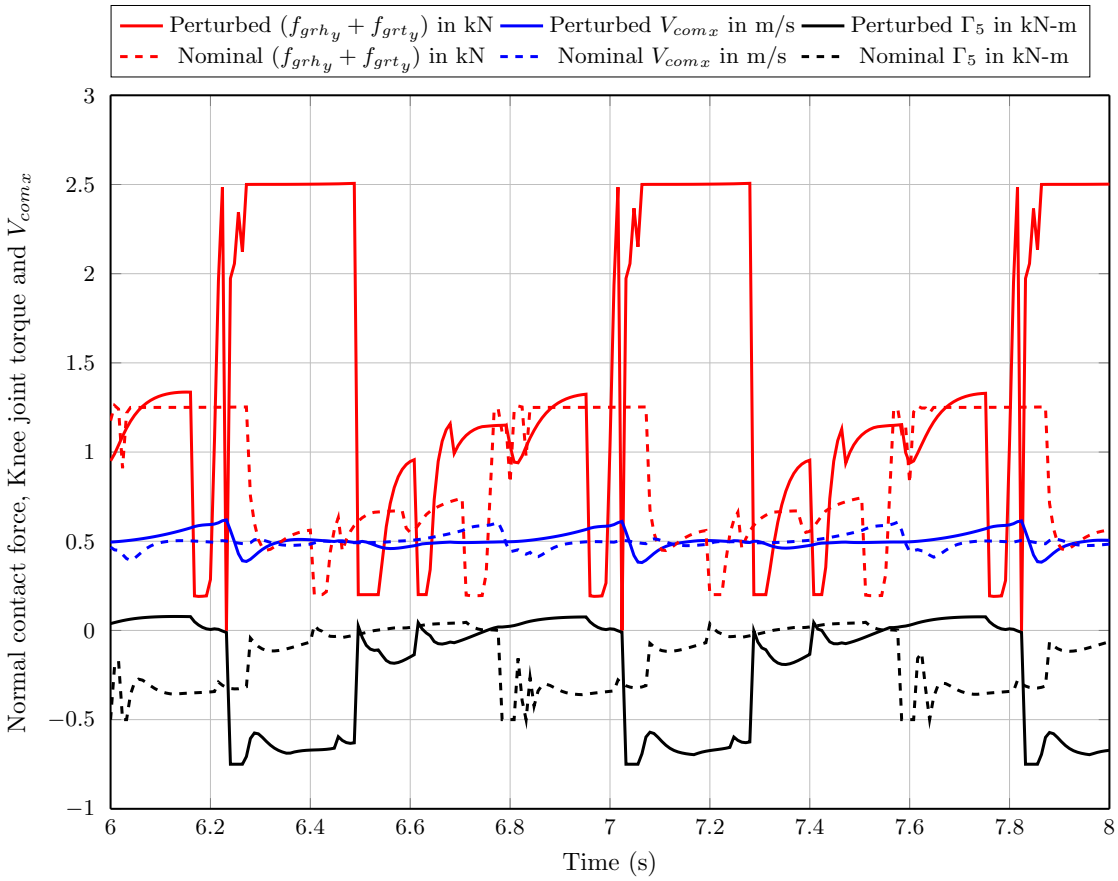

Figure 6.22: Comparison between nominal and perturbed cases with torso mass increased to 2.5 times for ascending stair walk with V_{fc}=0.5 m/s, τ_j=0.4 m and ρ_j=0.3 m

over different stair patterns including staircase with random distribution of tread depth, riser height and step slope.

Finally, the contraction stability theorem developed in Section 4.8 was used to quantitatively assess the stability margins of stair walk in terms of contraction factor, ρ_C and convergence radius, $\mathcal{R}_C$. Thus the contraction based stability was demonstrated as a more generic stability concept applicable for bipedal walk over uniform as well as uneven terrains.

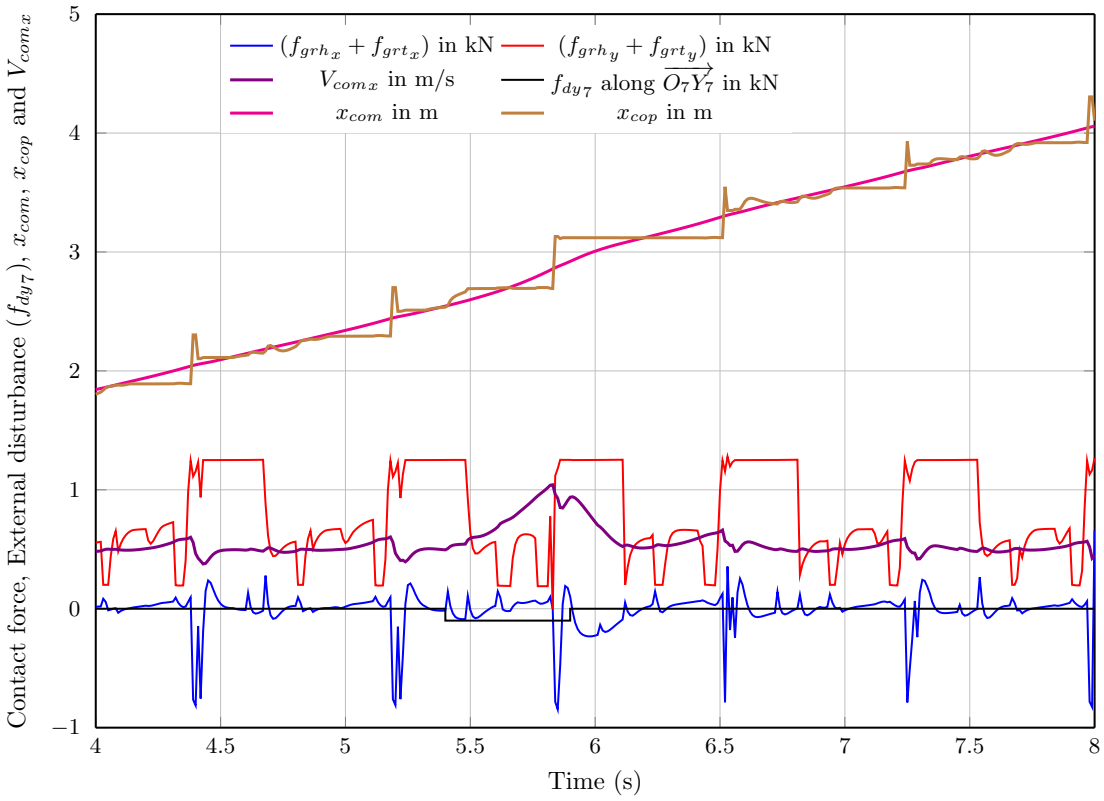

Figure 6.23: Effect of external force disturbance applied at 5.4 s for a duration of 0.5 s for ascending stair walk with V_{fc}=0.5 m/s, τ_j=0.4 m and ρ_j=0.3 m

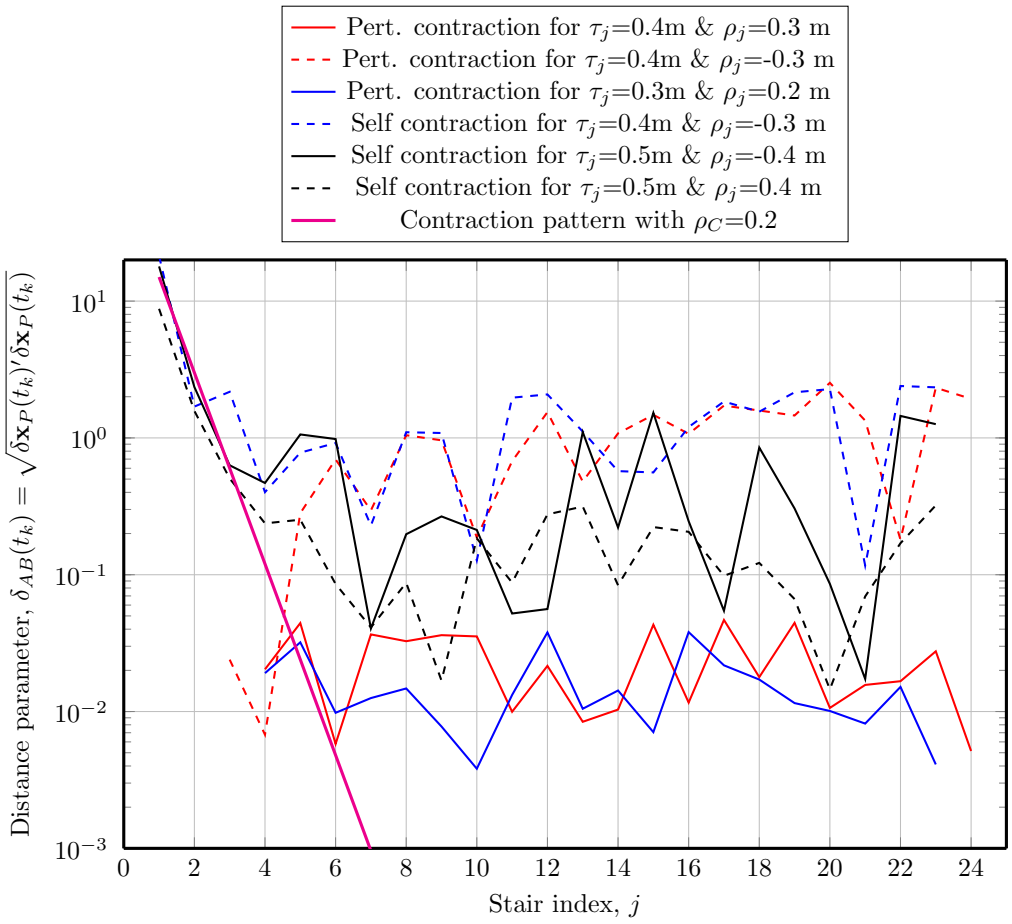

Figure 6.24: Contraction sequence for planar bipedal stair-walk with V_{fc}=0.5 m/s over uniform ascending and descending staircase with different tread and riser values

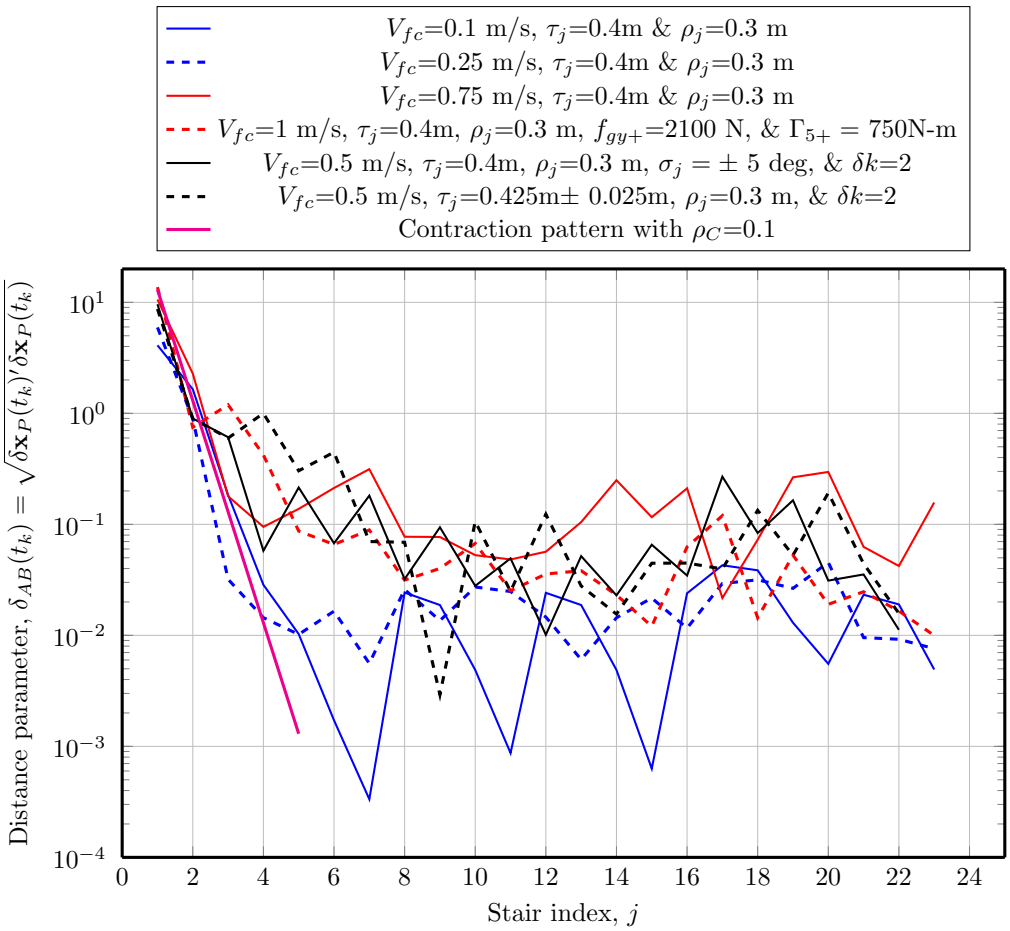

Figure 6.25: Self contraction sequence for planar bipedal stair-walk with V_{fc}=0.25 m/s to 1 m/s over uniform ascending staircase with τ_j=0.4 m & ρ_j=0.3 m and for V_{fc}= 0.5 m/s with tread and slope perturbations

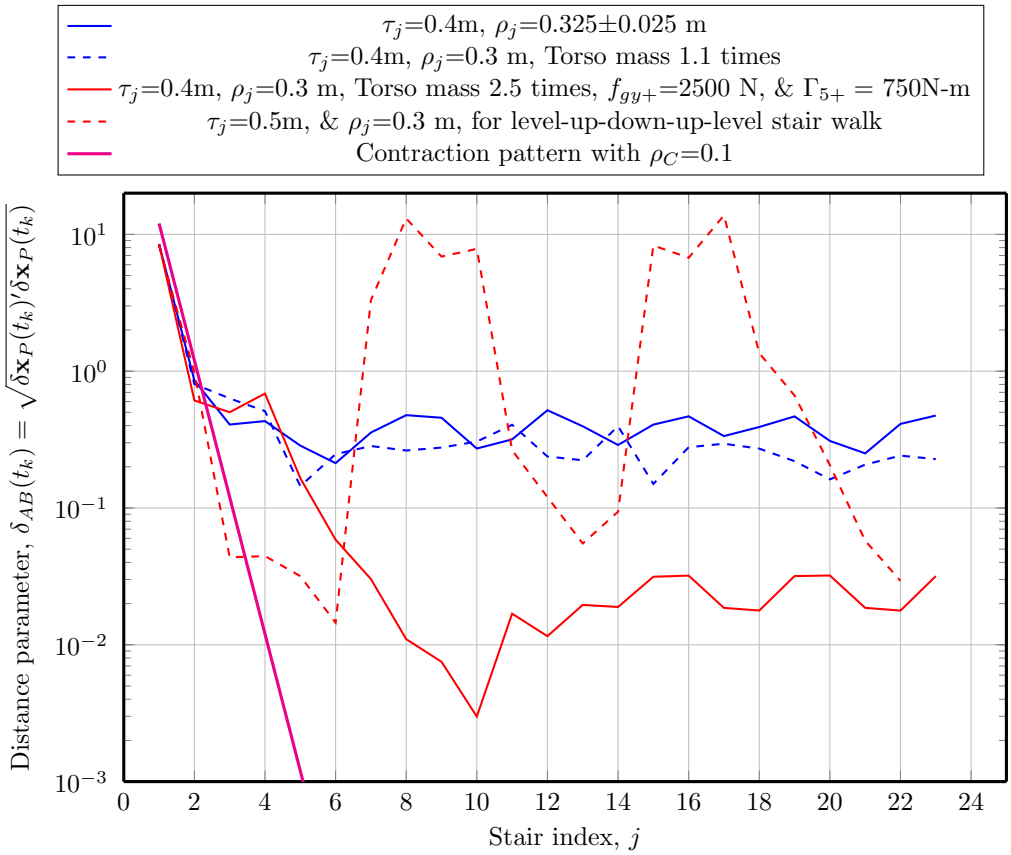

Figure 6.26: Self contraction sequence for planar bipedal stair-walk with V_{fc}=0.5 m/s over ascending staircase with riser perturbation, torso mass perturbations and for walking over compound staircase with V_{fc}=0.5 m/s

Chapter 7

Inferences, Contributions, and Future work

7.1 Inferences based on the Current Research

It was indeed a great experience to realize that how could a higher level intelligent behaviour evolve autonomously out of a dynamically coordinated set of low level behaviours when operated over an underactuated multi-degree of freedom robotic manipulator dynamics. If the manipulator were fully actuated, there would not have any room for the autonomous behaviour to evolve. The stability theory based on contraction mapping provides insight into the stability of evolved behaviour, if the underlying process is recurrent in nature. In fact the concept of HyDAC developed in the context of bipedal locomotion has shown how to realize a cyclic complex behaviour with quantifiable stability margins out of a temporally distributed sequence of dynamical behaviour primitives.

7.1.1 Benefits of Underactuation in bipeds

A fully actuated robotic manipulator with stable joint space control is a fully controllable multi-body system and any desired trajectory in the joint space, $q \in \mathcal{Q} \subset \mathbb{R}^n$ can be realized without any concern for global configuration stability within the kinematic and dynamic limits of joint actuators. However, they do lack an important characteristic of underactuated manipulators, namely the ability to reconfigure the link geometry to adapt with the environmental constraints. The legged robots are greatly blessed in this sense compared to wheeled robots. The inherent underactuation and redundancy enable the legged robots to adapt with the uneven terrain surface under the passive force of gravity without any need for a priori planning of joint trajectories. The additional redundancy of legged robots provides active suspension for the trunk isolating the motion induced disturbance over uneven terrain. The passive dynamics also play a vital role in locomotion to boost

up the energetic efficiency. For example, when we have to jump down over an unexpected step, we prefer to fall forward passively about the stance foot until the transit foot strikes the ground instead of controlled drooping on stance foot. After the foot impact, the CoM of the body rotates forward passively like an inverted pendulum making use of the residual kinetic energy until the forward velocity is controllable by manipulation of GCoP in the flat-foot state. As long as we are able to maintain the forward landing offset, λ_h or λ_t between the GCoM and transit foot within acceptable range, the dynamics of two consecutive passive rotation phases can compensate each other to bring back our posture to velocity controllable (or capturable) zone of next flat foot phase. The underactuated passive DoF has played two important roles during this process. One is enabling us to adapt with the unexpected step geometry and other is the effective utilization of potential energy drop for forward propulsion. Thus the underactuation of biped can be used effectively to ensure autonomous adaptation of feet with uneven ground, to boost up the locomotion efficiency utilizing the passive dynamics and to provide active suspension for torso.

7.1.2 Natural Choice of control approach for underactuated biped

Having realized the hidden virtues of underactuated dynamics of biped, the next question is regarding the natural choice of control approach to make use of these benefits. The efficiency of natural bipedal locomotion relies on making use of the autonomously evolved foot trajectory, under the controlled regulation of forward landing offset, λ_h during the passive forward rotation phase and regulation of GCoP during flat-foot phase. A control scheme built upon certain pre-planned foot trajectory under stiff closed loop control cannot make use of the benefits of inherent passive dynamics. Hence the requirement is to arrive at an online control scheme to indirectly manipulate the underactuated degrees of mechanical freedom so as to realize a stable locomotion without loosing the inherent benefits of biped morphology.

Despite the advantages, the floating base of bipeds put forth two major challenges to locomotion control, i.e. the constraints of unilaterality and friction cone with respect to ground contact force. In other words, the control law should be consistent with the unilateral and friction cone limits of ground contact force. As the ground contact force depends on joint kinematic variables, $(q, \dot{q}, \ddot{q})$ and joint torque variable, Γ, it is nearly impossible in a realistic locomotion environment to ensure constraint consistent ground contact force while the control law is only bothered to drive the joint variables along certain pre-planned trajectory in terms of $(q, \dot{q})$. The control action for correcting trajectory dispersion in

terms of $(\delta q, \delta \dot{q})$ can easily result in large enough values for $\ddot{q}$ violating the contact force constraints. Hence the right control variable for biped locomotion is the set of joint acceleration vector, $\ddot{q}$ and joint torque, Γ. Any requirement for controlling $(q, \dot{q})$ can be achieved equivalently through constraint consistent joint acceleration, $\ddot{q}$ which in turn can be realized through equivalent Γ_d based on inverse dynamics control law.

Another requirement during locomotion is the real-time coordination of upper body tasks such as manipulation of objects, movement of head or even multi-robot coordinated tasks. The joint redundancy of biped can be easily resolved in real-time to satisfy the simultaneous requirements of multiple tasks if joint acceleration is used as the basic control variable, without any replanning of joint trajectory. Thus the right selection of control scheme is *constraint consistent resolved joint acceleration based control* followed by implementation through joint torque command, Γ_d derived through *inverse dynamics* of biped.

7.2 Contributions of the Thesis

The contributions of the thesis can be grouped into four categories as listed below:

A) **Formulation of autonomous control framework for planar bipedal walking**

The true merit of bipedal walking relies on its agility and robustness over unplanned and non-smooth terrain. Hence the development of autonomous control framework is an important requirement of bipedal locomotion. The following are the major contributions of the thesis in this regard.

i) Stated the minimal set of control functional requirements ($\mathcal{CFR}$s) to precisely define the process of bipedal dynamic walking.

ii) Established the requirements for a two-level hierarchical control structure, called Hybrid-state driven autonomous control (HyDAC) for bipedal dynamic walking and defined the functional requirements for its supervisory level and task level controls (SLC and TLC).

iii) Developed a novel algorithm for regulating the forward velocity of biped-CoM by direct regulation of GCoP during flat foot state of stance foot.

iv) Formulated HyDAC control synthesis as a quadratic optimization problem with linear equality constraints with explicit analytic solution.

v) Formulated all behaviour primitives required for dynamic walk in the standard form of $H(q)\ddot{q} = B(q, \dot{q})$ for planar biped over uniform terrain.

vi) Derived empirical expression for all behaviour primitive parameters based on simulation based optimization.

vii) Carried out extensive simulation of planar bipedal walk over uniform terrain to demonstrate the agility and robustness of HyDAC for a wide range of forward velocity and terrain slope.

B) **Unified modelling framework for bipedal walking**

Another contribution of the thesis is the proposal of a unified mathematical model for the biped which facilitate the formulation of direct analytical expression for joint acceleration command. The following are the contributions in this regard.

i) Developed a unified model for planar biped applicable for all phases of biped like single point support, multipoint support and free floating phase.

ii) Incorporated the standard second degree differential form expression, $H(q)\ddot{q} = B(q, \dot{q})$ for all kinds of constraints as well as tasks in the unified model.

iii) Developed mathematical models for friction cone constraint, ground contact force constraints, and joint torque limit constraint, all in the standard form of $H(q)\ddot{q} = B(q, \dot{q})$.

iv) Incorporated a realistic assumption to simplify the velocity impact map in the unified model which will ensure the invariance of the ground contact state of pre-impact reference foot.

v) Incorporated the concept of *'solving from the null space of constraints'* to derive the least norm, least square solution for constraint consistent behaviours.

C) **Formulation of a control oriented stability theorem for realistic walking situations**

A viable stability definition for bipedal dynamic walk during realistic walking situations is an outstanding requirement of bipedal locomotion [58]. One of the major contributions of the thesis is to fulfil this requirement. The following are the research contributions in this regard.

i) Defined a control oriented postural configuration space, $\mathcal{C} := \{\mathbf{x}_{pc}\}$ to represent the essential postural features of biped relevant to locomotion dynamics and stability.

ii) Formulated a control oriented stability theorem called, Contraction Stability theorem by combining the Lyapunov asymptotic stability concept of periodic orbit, Poincaré theorem correlating the asymptotic stabilities of periodic orbit and the

corresponding fixed point and Contraction mapping theorem for the asymptotic stability of Poincaré return map for wide range of trajectory perturbation.

iii) Developed the concept of multi-phase goal seeking approach for meeting the contraction stability requirement.

iv) Extended the Contraction stability theorem to a class of non-periodic systems called *Event Periodic Systems* relevant for realistic bipedal walking.

v) Defined two normalized stability measures called, *Contraction factor,* ρ_C and *Radius of convergence,* $\mathcal{R}_C$ based on contraction stability theorem to quantify the relative stability of bipedal dynamic walk irrespective of the control framework and terrain condition.

D) **Extension of control algorithm for non-uniform staircase type terrain**

Bipedal locomotion over non-uniform staircase type terrain demands placing of the transit foot on the specified foothold during each step. The following are the contributions in this regard to meet this requirement.

i) Provided a general expression for non-uniform staircase type terrain with variable tread depth, riser height and tread slope and derived expressions for linear envelop segments to guide transit foot motion over staircase boundaries of different patterns.

ii) Modified control algorithms to suit for staircase type terrain in both SLC and TLC levels of HyDAC.

iii) Demonstrated the agility and robustness of Stair-HyDAC through extensive simulation studies.

In summary, the research objectives of the thesis as projected in Section 2.5 are fully accomplished.

7.3 Recommendations for Future work

The recommendations for future work along with brief description on their relevance are given below.

7.3.1 Extension of HyDAC to 3D biped

The current work is limited to sagittal plane of bipedal dynamic walk where the real forward motion takes place. However the real bipedal walk is a coupled 3-dimensional nonlinear control problem and hence it is essential to extend the postural stability concept to the other planes, i.e. the frontal as well as the transverse planes of biped. The versatile control framework of HyDAC along with the associated stability theorem are not expected to put forth any additional control challenge for realizing the 3D bipedal dynamic walk.

7.3.2 Extension of HyDAC to generic uneven terrain

One major assumptions of the thesis is the limiting of foot-ground contact point to either heel or toe or both heel and toe of the reference foot. This can be true only if the ground underneath the stance foot is perfectly planar. Under realistic walking situations, it is essential to relax this assumption by allowing in-between foot-ground contact points, minimum two for planar case and three four 3D case. This can be achieved by making the definitions of contact Jacobian more generic to accommodate any point on the foot sole as a ground contact point.

7.3.3 Inclusion of toe roll (TR) phase in HyDAC

The absence of TR phase (also known as toe-off phase) is the only noticeable difference between the human walk and the bipedal dynamic walk resulting from HyDAC. There are two basic prerequisites for including the human-like toe-off phase in HyDAC. One is the presence of an actuated toe joint to ensure a finite contact zone between foot and ground during the toe-off phase and to give the required forward push for initiating the subsequent swing phase. Another requirement is the extension of HyDAC algorithm to control the double-feet ground contact state during the heel-off phase. The planar biped model used in the thesis has no toe joint and forward rolling about the toe tip of stance foot is not a good postural phase in stability context.

7.3.4 Empirical expressions for motion control parameters

For a complex hybrid dynamical process like bipedal walk, simulation based optimization is one of the most successful tools to compute the optimal control parameters in supervisory as well as task levels. However, to avoid local optima and to accelerate the convergence during this process, it is essential to start at certain reasonably good initial estimates for

control parameters. Empirical expressions for control parameters, derived based on reduced order biped models which are valid locally during different phases of walking gait can be used for this purpose.

7.3.5 Online learning architecture

The elegant structure of HyDAC provides ample opportunity for adapting the control parameters in both SLC and TLC levels with respect to terrain and payload conditions. Many of the control parameters described in Chapter 5 and 6 are expressed as empirical functions of terrain parameters and forward velocity. However, there is further scope for refinement of these empirical expressions based on real-time performance evaluation and feedback correction.

7.3.6 Application in prosthesis

Since HyDAC makes use of human-like control architecture, it would be quite suitable for controlling prosthetic lower limbs under the supervisory control of the central nervous system (CNS) of the amputee.

List of Publications

Refereed Journals

1. Sam K. Zachariah and Thomas Kurian, “Hybrid-state driven autonomous control for planar bipedal locomotion”, Robotics and Autonomous systems, vol.83, pp.115-137, 2016

2. Sam K. Zachariah and Thomas Kurian, “Hybrid-state driven autonomous control for planar bipedal locomotion over randomly sloped non-uniform stairs”, Robotics and Autonomous systems, vol.97, pp.18-39, 2017

Bibliography

[1] M. H. Reibert, *Legged Robots That Balance*. Cambridge: The MIT Press, 1986.

[2] C. B. Cunningham, N. Schilling, C. Anders, and D. R. Carrie, "The influence of foot posture on the cost of transport in humans," *The Journal of Experimental Biology*, vol. 213, pp. 790–797, 2010.

[3] R. McNeill Alexander, *The Cambridge encyclopedia of human evolution*. Cambridge University Press, Cambridge, 1992, ch. Human locomotion, pp. 80–85.

[4] P. J. Steinhardt and N. Turok, "A Cyclic Model of the Universe," *SCIENCE*, vol. 296, pp. 1436–1438, 2002. [Online]. Available: https://www.sciencemag.org

[5] Cliff Hooker (Editor), *Handbook of the of Science Philosophy, Volume 10, Philosophy of Complex Systems*. North Holland: Elsevier, 2011.

[6] Christine Azevedo, Bernard Amblard, Bernard Espia, and Christine Assaiante, "A Synthesis of Bipedal Locomotion in Human and Robots," INRIA Sophia Antipolis, Sophia Antipolis Cedex ,France, Project DEMAR Report No. 5450, December 2004.

[7] Aristotle, *The Complete Works of Aristotle: the Revised Oxford Translation, volume 1 of Bollingen Series LXXI, chapter Progression of Animals*. Princeton University Press, 1984.

[8] M. Vukobratović, B. Borovac, D. Surla, and D. Stokic, *Bipedal Locomotion*. Berlin: Springer Verlag, 1990.

[9] M. Vukobratović and B. Borovac, "Zero-moment point - Thirty five years of its life," *International Journal of Humanoid Robotics*, vol. 1(1), pp. 157–173, 2004.

[10] E. R. Westervelt, J. W. Grizzle, C. Chevallereau, J. H. Choi, and B. Morris, *Feedback Control of Dynamic Bipedal Robot Locomotion*. Boca Raton: CRC Press, 2007.

[11] C. L. Vaughan, B. L. Davis, and J. C. O. Connor, *Dynamics of Human Gait*. Cape Town, South Africa: Kiboho Publishers, 1999.

[12] "Terminology of human walking," https://www.bostonoandp.com/Customer-Content/www/CMS/files/GaitTerminology.pdf, (Accessed on October 31, 2017).

[13] A. Goswami, "Postural stability of biped robots and the foot-rotation indicator (FRI) point," *International Journal of Robotic Research*, vol. 18(6), pp. 523–533, 1999.

[14] Hirai K., Hirose M.and Haikawa Y., and Takenaka T., "The development of Honda Humanoid robot," in *Proceedings of the 1998 IEEE International Conference on Robotics & Automation*, Leuven, Belgium, 1998.

[15] Yu Ogura, Hiroyuki Aikawa, Kazushi Shimomura, Hideki Kondo, Akitoshi Morishima, Hun-ok Lim, and Atsuo Takanishi, "Development of A Humanoid Robot WABIAN-2," in *Proceedings of the 2006 IEEE International Conference on Robotics & Automation*, Orlando,USA, May 2006.

[16] Thomas Buschmann, "Simulation and Control of Biped Walking Robots," Ph.D. dissertation, Technical University of Munich, Germany, 2010.

[17] R. Tedrake, S. Kuindersma, R. Deits, and K. Miura, "A closed-form solution for real-time ZMP gait generation and feedback stabilization," in *IEEE-RAS 15th International Conference on Humanoid Robots (Humanoids)*, Seoul, South Korea, Nov 3–5, 2015, pp. 936–940.

[18] J. Pratt, T. Koolen, T. de Boer, J. Rebula, S. Cotton, J. Carff, M. Johnson, and P. Neuhaus, "Capturability-based analysis and control of legged locomotion, Part 2: Application to M2V2, a lower-body humanoid," *The International Journal of Robotics Research*, vol. 31(10), pp. 1117–1133, 2012.

[19] J. E. Pratt and R. Tedrake, "Velocity-based stability margins for fast bipedal walking," in *Fast Motions in Biomechanics and Robotics*. Springer, 2006, pp. 299–324.

[20] Jonghoon Park and Youngil Youm, "General ZMP Preview Control for Bipedal Walking," in *IEEE International Conference on Robotics and Automation*, Roma, Italy, April 10–14, 2007, pp. 2682–2687.

[21] M. Popovic, A. Hofmann, and H. Herr, "Angular Momentum Regulation during Human Walking: Biomechanics and Control," in *Proceedings of the 2004 IEEE International conference on Robotics & Automation*, New Orleance, LA, April, 2004, pp. 2405–2411.

[22] S. KAJITA, F. KANEHIRO, K. KANEKO, K. FUJIWARA, K. HARADA, K. YOKOI, and H. HIRUKAWA, "Resolved Momentum Control: Humanoid Motion Planning based on the Linear and Angular Momentum," in *Proceedings of the 2003 IEEE/RSJ International Conference on Intelligent Robots and Systems*, Las Vegas, Nevada, October, 2003, pp. 1644–1650.

[23] S. KAJITA, F. KANEHIRO, K. KANEKO, K. FUJIWARA, K. HARADA, K. YOKOI, and H. HIR, "Biped Walking Pattern Generation by using Preview Control of Zero-Moment Point," in *Proceedings of the 2003 IEEE lnternational Conference on Robotics & Automation*, Taipei, Taiwan, September 14–19, 2003, pp. 4810–4817.

[24] T. McGeer, "Passive dynamic walking," *International Journal of Robotics Research*, vol. 9(2), pp. 62–82, 1990.

[25] S. H. Collins, A. Ruina, R. Tedrake, and M. Wisse, "Efficient bipedal robots based on passive dynamic walkers," *Science*, vol. 307, pp. 1082–1085, 2005.

[26] M. Wisse, "Essentials of dynamic walking : Analysis and design of two-legged robots," Ph.D. dissertation, Technical University, Delft, 2004.

[27] P. A. Bhounsule, J. Cortell, A. Grewal, B. Hendriksen, J. G. D. Karssen, C. Paul, and A. Ruina, "Low-bandwidth reflex-based control for lower power walking: 65 km on a single battery charge," *The International Journal of Robotics Research*, vol. 33(10), pp. 1305–1321, 2014.

[28] A. D. Kuo, "Stabilization of Lateral Motion in Passive Dynamic Walking," *The International Journal of Robotics Research*, vol. 18, pp. 917–930, September 1999.

[29] E. R. Westervelt, J. W. Grizzle, and D. E. Koditschek, "Hybrid Zero Dynamics of Planar Biped Walkers," *IEEE Transations on Automatic Control*, vol. Vol. 48, No. 1, pp. 42–56, Jan 2003.

[30] N. Sadati, G. A. Dumont, K. A. Hamed, and W. A. Gruver, *Hybrid control and motion planning of dynamical legged locomotion*. Hoboken, New Jersey: JohnWiely & Sons Inc. Publications, 2012.

[31] C. Chevallereau, D. Djoudi, and J. W. Grizzle, "Stable bipedal walking with foot rotation through direct regulation of the Zero Moment Point," *IEEE Transactions on Robotics*, vol. 24(2), pp. 390–401, 2008.

[32] T. Wang, C. Chevallereau, , and D. Tlalolini, "Stable walking control of a 3D biped robot with foot rotation," *Robotica*, vol. 32, pp. 551–570, 2014.

[33] A. D. Ames, K. Galloway, K. Sreenath, and J. W. Grizzle, "Rapidly Exponentially Stabilizing Control Lyapunov Functions and Hybrid Zero Dynamics," *IEEE Transations on Automatic Control*, vol. Vol. 59, No. 4, pp. 876–891, April 2014.

[34] M. J. Powell, H. Zhao, and A. D. Ames, "Motion primitives for human-inspired bipedal robotic locomotion: walking and stair climbing," in *Proc. 2012 IEEE International Conference on Robotics and Automation*, St. Paul, MN, USA, May 2016, pp. 543–549.

[35] B. Griffin and J. Grizzle, "Walking Gait Optimization for Accommodation of Unknown Terrain Height Variations," in *American Control Conference*, Palmer House Hilton , Chicago, IL, USA, July 2015, pp. 4810–4817.

[36] M. Scheint, M. Sobotka, and M. Buss, "Virtual holonomic constraint approach for planar bipedal walking robots extended to double support," in *Joint 48th IEEE Conference on Decision and Control and 28th Chinese Control Conference*, Shanghai, P. R. China, December 16-18, 2009, pp. 8180–8185.

[37] B. G. Buss, "Systematic controller design for Dynamic 3D Bipedal robot walking," Ph.D. dissertation, University of Michigan, Ann Arbor, MI, USA, May 2015.

[38] B. Griffin and J. Grizzle, "Walking Gait Optimization for Accommodation of Unknown Terrain Height Variations," in *2015 American Control Conference*, Palmer House Hilton Chicago, IL, USA, July 1–3 2015, pp. 4810–4817.

[39] B. Morris and J. W. Grizzle, "Hybrid invariant manifolds in systems with impulse effects with application to periodic locomotion in bipedal robots," *IEEE Trans. on Automatic Control*, vol. 54(8), pp. 1751–1764, 2009.

[40] I. R. Manchester, U. Mettin, F. Iida, and R. Tedrake, "Stable dynamic walking over uneven terrain," *The International Journal of Robotics Research*, vol. 30(3), pp. 265–279, 2011.

[41] S. K. Zachariah and T. Kurian, "Hybrid-state driven autonomous control for planar bipedal locomotion," *Robotics and Autonomous systems*, vol. 83, pp. 115–137, 2016.

[42] G. Wiedebach, S. Bertrand, T. Wu, L. Fiorio, S. McCrory, R. Griffin, F. Nori, and J. Pratt, "Walking on Partial Footholds Including Line Contacts with the Humanoid Robot Atlas," in *2016 IEEE-RAS 16th International Conference on Humanoid Robots (Humanoids)*, Cancun, Mexico.

[43] T. Sugihara, "Consistent Biped Step Control with COM - ZMP Oscillation Based on Successive Phase Estimation in Dynamics Morphing," in *IEEE International Conference on Robotics and Automation*, Anchorage Convention District, Anchorage, Alaska, USA, May 3-8, 2010, pp. 4224–4229.

[44] F. Tan, C. Fu, and K. Chen, "Biped Blind Walking on Changing Slope with Reflex Control System," in *IEEE International Conference on Robotics and Automation*, Anchorage Convention District, Anchorage, Alaska, USA, May 3-8, 2010, pp. 1709–1714.

[45] Jerry Pratt, Chee-Meng Chew, Ann Torres, Peter Dilworth, and Gill Pratt, "Virtual Model Control : An Intuitive Approach for Bipedal Locomotion," *The International Journal of Robotics Research*, vol. 20(2), pp. 129–143, 2001.

[46] JUNG-YUP KIM, ILL-WOO PARK, and JUN-HO OH, "Experimental realization of dynamic walking of the biped humanoid robot KHR-2 using zero moment point feedback and inertial measurement," *Advanced Robotics*, vol. 20(6), pp. 707–736, 2006.

[47] ——, "Walking Control Algorithm of Biped Humanoid Robot on Uneven and Inclined Floor," *Journal of Intelligent & Robotic Systems*, vol. 48(4), pp. 457–484, 2007.

[48] T. Erez and W. D. Smart, "Bipedal Walking on Rough Terrain Using Manifold Control," in *Proceedings of the 2007 IEEE/RSJ International Conference on Intelligent Robots and Systems*, San Diego, CA, USA, 2007.

[49] R. Deits and R. Tedrake, "Foot step planning on uneven terrain with mixed-integer convex optimization," in *Proceedings of the 2014 IEEE/RSJ International Conference on Humanoid Robots*, Madrid, Spain, 2014.

[50] M. B. Popovic, A. Goswami, and H. Herr, "Ground Reference Points in Legged Locomotion: Definitions, Biological Trajectories and Control Implications," *The International Journal of Robotics Research*, vol. 24(12), pp. 1013–1032, December 2005.

[51] T. Koolen, T. de Boer, J. Rebula, A. Goswami, and J. Pratt, "Capturability-based analysis and control of legged locomotion, Part 1: Theory and application to three simple gait models," *The International Journal of Robotics Research*, vol. 31(9), pp. 1094–1113, 2012.

[52] B. Griffin and J. Grizzle, "Walking Gait Optimization for Accommodation of Unknown Terrain Height Variations," in *American Control Conference*, Palmer House Hilton, Chicago, IL, USA, 2015, pp. 4810–4817.

[53] B. Siciliano, L. Sciavicco, L. Villani, and G. Oriolo, *Robotics- Modelling, Planning and Control*. Reading, MA: Springer-Verlag London Ltd, 2009.

[54] R. Featherstone, *Rigid Body Dynamics Algorithms*. LLC, The 2015 American Control Conference, July 1–3, Chicago, ILNew York: Springer Science + Business Media, 2008.

[55] M. W. Spong, S. Hutchinson, and M. Vidyasagar, *Robot Modeling and Control*. New Delhi: Wiley Student Edition, 2006.

[56] A. Jain, *Robot and Multibody Dynamics*. LLC,New York: Springer Science + Business Media, 2011.

[57] J. Peters, M. Mistry, F. Udwadia, J. Nakanishi, and S. Schall, "A unifying framework for robot control with redundant DOFs," *Autonomous Robot*, vol. 24, pp. 1–12, 2008.

[58] J. W. Grizzle, C. Chevallereau, R. W. Sinnet, and A. D. Ames, "Models, feedback control and open problems of 3D bipedal robotic walking," *Automatica*, vol. 50, pp. 1955–1988, 2014.

[59] L. Righetti, J. Buchli, M. Mistry, M. Kalakrishnan, and S. Schall, "Optimal distribution of contact forces with inverse dynamics control," *The International Journal of Robotics Research*, vol. 32(3), pp. 280–298, 2013.

[60] L. Righetti, J. Buchli, M. Mistry, and S. Schaal, "Inverse Dynamics Control of Floating-Base Robots with External Constraints : a Unified View," in *Proc. 2011 IEEE International Conference on Robotics and Automation*, Shanghai International Conference Centre, May 2011, pp. 1085–1090.

[61] Adi Ben-Israel and Thomas N. E. Greville, *Generalized Inverses - Theory and Applications*. Springer-Verlag, New York, Inc, 2003.

[62] B. Brogliato, *Nonsmooth mechanics: models, dynamics and control*. New York: Springer-Verlag, 1999.

[63] L. Sciavicco and B. Sicilliano, *Modelling and control of robot manipulators*. New York: McGraw-Hill, 1996.

[64] F. Plestan, J. W. Grizzle, E. R. Westervelt, and G. Abba, "Stable walking of a 7-DOF biped robot," *IEEE Trans. on Robotics and Automation*, vol. 19(4), pp. 653–668, 2003.

[65] X. Mu and Q. Wu, "On impact dynamics and contact events for biped robots via impact effects," *IEEE Trans. on System, Man and Cybernetics, Part B: Cybernetics*, vol. 36(6), pp. 1364–1372, 2006.

[66] S. Miossec and Y. Aoustin, "Dynamical synthesis of a walking cyclic gait for a biped with point feet," in *Fast Motions in Biomechanics and Robotics*. LNCIS Springer, 2006.

[67] Y. Hurmuzlu and D. B. Marghitu, "Rigid body collisions of planar kinematic chains with multiple contact points," *The International Journal of Robotic Research*, vol. 13(1), pp. 82–92, 1994.

[68] F. E. Udwadia and R. E. Kalaba, "What is the General Form of the Explicit Equations of Motion for Constrained Mechanical Systems ?" *Journal of Applied Mechanics*, vol. 69, pp. 335–339, 2002.

[69] M. Goulding, "Circuits controlling vertebrate locomotion: moving in a new direction," *NATURE REVIEWS|NEUROSCIENCE*, vol. 10, pp. 507–518, 2009.

[70] Auke Jan Ijspeert, "Central pattern generators for locomotion control in animals and robots: A review," *Neural Networks*, vol. 21, pp. 642–653, 2008.

[71] G. N. Orlovsky, T. C. Deliagina, and S. Grillner, *Neural control of locomotion. From mollusc to man*. New York: Oxford University Press, 1999.

[72] A. D. Ames, "Human-Inspired Control of Bipedal Walking Robots," *IEEE Transactions on Automatic Control*, vol. 59, pp. 1115–1130, 2014.

[73] J. Santos and A. Campo, "Biped locomotion control with evolved adaptive center-crossing continuous time recurrent neural networks," *Neurocomputing*, vol. 86, pp. 86–96, 2012.

[74] Kulić D. and Kragic D. and Krüger V., *Visual Analysis of Humans*. Springer, London, 2011, ch. Learning Action Primitives.

[75] S. H. Collins, M. Wisse, and A. Ruina, "A three dimensional passive-dynamic walking robot with two legs and knees," *International Journal of Robotics Research*, vol. 20(7), pp. 607–615, 2001.

[76] L. Sentis and O. Khatib, "Synthesis of whole body behaviors through hierarchical control of behavioral primitives," *International Journal of Humanoid robotics*, vol. 2(4), pp. 505–518, 2005.

[77] L. Sentis, "Synthesis and control of whole-body behaviors in humanoid systems," Ph.D. dissertation, Stanford University, USA, 2007.

[78] F. Flacco, A. D. Luca, and O. Khatib, "Prioritized multi-task motion control of redundant robot under hard joint constraints," in *2012 IEEE/RSJ International conference on Intelligent Robots and Systems*, Vilamoura, Portugal.

[79] B. Siciliano and J. J. E. Slotine, "A general framework for managing multiple tasks in highly redundant robotic systems," in *Proc.of 5th International Conference on Advanced Robotics, 1991*, 1991, pp. 1211–1216.

[80] S. K. Zachariah and T. Kurian, "Hybrid-state driven autonomous control for planar bipedal locomotion over randomly sloped non-uniform stairs," *Robotics and Autonomous systems*, vol. 97, pp. 18–39, 2017.

[81] B. Siciliano, "A closed-loop inverse kinematic scheme for on-line joint-based robot control," *Robotica*, vol. 8(03), pp. 231–243, 1990.

[82] W. M. Haddad and V. Chellaboina, *Nonlinear Dynamical Systems and Control*. New Jersey: Princeton University Press, 2008.

[83] H. K. Khalil, *Nonlinear systems*. New Jersey: Prentice Hall, 2002.

[84] T. Yang, E. R. Westervelt, A. Serrani, and J. P. Schmiedeler, "A framework for the control of stable aperiodic walking in underactuated planar bipeds," *Autonomous Robot*, vol. 27, pp. 277–290, 2009.

[85] Winfried Lohmiller and Jean-Jacques E Slotine, "On Contraction Analysis for Nonlinear Systems," *Automatica*, vol. 34, 1998.

[86] V. Chellaboina, S. P. Bhat, and W. M. Haddad, "An invariance principle for nonlinear hybrid and impulsive dynamical systems," *Nonlnear Analysis: Theory, Methods and Applications*, vol. 53(3-4), pp. 527–550, May 2003.

[87] S. G. Nersesov, V. Chellaboina, and W. M. Haddad, "A Generalization of Poincaré 's Theorem to Hybrid and Impulsive Dynamical Systems," *International Journal of Hybrid Systems*, vol. 2, pp. 35–51, 2002.

[88] S. G. Nersesov, "Nonlinear Impulsive and Hybrid Dynamical Systems," Ph.D. dissertation, Georgia Institute of Technology, USA, June 20057.

[89] R. Shorten, F. Wirth, O. Mason, K. Wulff, and C. King, "Stability Criteria for Switched and Hybrid Systems," *SIAM REVIEW*, vol. 49, pp. 545–592, 2007.

[90] Krzysztof P. Jankowski, *Inverse Dynamics Control - In Robotics Applications*. Victoria, British Columbia: Trafford Publishing Ltd., 2004.

[91] R. McNeill Alexander, *Locomotion of Animals*. Glasgow, London: Blackie & Son Limited, 1982.

[92] Navvab Kashiri et al., "An Overview on Principles for Energy Efficient Robot Locomotion," ***frontiers*** *in Roboics and AI*, vol. 5, pp. 1–13, December 2018.

[93] Zhibin Li and Bram Vanderborght and Nikos G. Tsagarakis and Darwin G. Caldwell, "Human-like walking with straightened knees, toe-off and heel-strike for the humanoid robot iCub," in *UKACC International Conference on Control*, Coventry, UK, 2010.

[94] D. L. Wight, E. G. Kubica, and D. W. L. Wang, "Introduction of the Foot Placement Estimator: A Dynamic Measure of Balance for Bipedal Robotics," *Journal of Computational and Nonlinear Dynamics, Transactions of the ASME*, vol. 3, pp. 011 009–1–011 009–10, January 2008.

[95] "Anthropometry and mass distribution for human analogues, Volume I: Military male aviators," Naval Biodynamics Laboratory, Tech. Rep. NBDL-87R003, March 1988.

[96] S. Cotton, A. P. Murray, and P. Fraisse, "Estimation of the Center of Mass: From Humanoid Robots to Human Beings," *IEEE/ASME Transactions on Mechatronics*, vol. 14, pp. 707–712, 2009.

[97] JUNG-YUP KIM, ILL-WOO PARK, and JUN-HO OH, "Experimental realization of dynamic stair climbing and descending of biped humanoid robot, HUBO," *International Journal of Humanoid Robotics*, vol. 6, pp. 205–240, 2009.

[98] R. W. Sinnet, M. J. Powell, S. Jiang, and A. D. Ames, "Compass Gait Revisited: A Human Data Perspective with Extensions to Three Dimensions," in *50^{th} IEEE Conference on Decision and Control and European Control Conference (CDC-ECC)*, Orlando, FL,USA, December 2011, pp. 682–689.

[99] A. D. Ames, "Human-inspired control of bipedal walking robots," *IEEE Transactions on Automatic Control*, vol. 59(5), pp. 1115–1130, 2014.

[100] A. Hereid, E. A. Cousineau, , C. M. Hubicki, and A. D. Ames, "3D dynamic walking with underactuated humanoid robots: A direct collocation framework for optimizing hybrid zero dynamics," in *Proc. 2016 IEEE International Conference on Robotics and Automation*, Stockholm, May 2016, pp. 1447–1454.

[101] Pet Christian Hansen, "The truncated SVD as a method for regularization," Computer Science Department , Stanford University, Stanford, California, Numerical Analysis Project Manuscript NA-86-36, 1986.